Developing *Dictyostelium discoideum* as a model to study the synthesis and metabolism of inositol pyrophosphates and inorganic polyphosphate

Thomas Miles Livermore

MRC Laboratory for Molecular Cell Biology

A thesis submitted to fulfil the requirements for the award of
Doctor of Philosophy in Biochemistry from
University College London

March 2016

I, Thomas Miles Livermore, confirm that the work presented in this thesis is my own. Where information has been derived from other sources, I confirm that this has been indicated in the thesis.

Work supported by the Medical Research Council

Acknowledgements

I have many people to acknowledge for their support and guidance during my PhD. First, of course, I must thank my supervisor Adolfo to whom I owe a great deal of gratitude for investing significant time and effort in my scientific training, both practical and methodological. His relentless interest and passion for the project was infectious and helped to motivate me throughout. Outside of my academic training, I must also thank Adolfo for allowing me to take 3 months away from the lab to follow my career aspirations. That I now have the job that I was striving for is in no small part due to his support.

I must also extend my thanks to my thesis committee of Buzz Baum, Shamshad Cockcroft, Geraint Thomas and, in particular, Jonathan Chubb. Jonathan's expertise and generosity with his time was invaluable.

Back in the Saiardi lab, I would like to thank those who helped create a fantastic and collaborative atmosphere. Cristina, for her unerring support, advice and willingness to discuss ideas, deserves special mention. In addition I owe Miranda huge thanks for her encouragement and enthusiasm as well as for her willingness to be distracted. I would also like to acknowledge the significant efforts of Francesca at the outset of this project, as well as Betty and Omar who were always willing to offer help when needed.

In the LMCB there are too many names to mention. A huge number of people have made it a special place to work, both academically and socially. In particular I would like to thank the core staff for their hard work, which makes our lives easier. I would also like to thank the students, past and present, with special nod to my year.

Finally I would like to thank Millie, my parents and my sis for their enduring support over the last four years. It's been a marathon, not a sprint. Thanks.

Publications

Wilson, M. S. C., T. M. Livermore and A. Saiardi (2013). Inositol pyrophosphates: between signalling and metabolism. Biochem J. **452:** 369-379.

Pisani, F., T. Livermore, G. Rose, J. R. Chubb, M. Gaspari and A. Saiardi (2014). Analysis of Dictyostelium discoideum inositol pyrophosphate metabolism by gel electrophoresis. PLoS ONE. **9:** e85533.

Azevedo, C., T. Livermore and A. Saiardi (2015). "Protein polyphosphorylation of lysine residues by inorganic polyphosphate." Molecular cell **58**(1): 71-82.

Livermore, T. M., J. R. Chubb and A. Saiardi (2016). Developmental accumulation of inorganic polyphosphate affects germination and energetic metabolism in Dictyostelium discoideum. Proc Natl Acad Sci USA. **113:** 996-1001.

Livermore, T. M., C. Azevedo, B. Kolozsvari, M. S. C. Wilson and A. Saiardi (2016). Phosphate, inositol and polyphosphates. Biochem Soc Trans. **44:** 253-259.

Abstract

Inositol pyrophosphates and inorganic polyphosphate (polyP) represent two of the most phosphate-rich molecules in the cell. However, the synthesis, metabolism and function of these “high-energy” molecules are not well understood. This work develops the amoeba, *Dictyostelium discoideum,* as a genetic model to study both classes of molecule. By applying improved polyacrylamide gel electrophoresis (PAGE) techniques, unlabelled inositol pyrophosphates and polyP extracted from *D. discoideum* have been visualised for the first time.

Deletion of a range of inositol phosphate kinases reveals a complex synthetic pathway of the inositol pyrophosphates in the amoeba. Surprisingly, strains lacking the majority of inositol pyrophosphates do not display a dramatic phenotype. However, these cells retain low levels of inositol pyrophosphates. In fact, this work identified at least four enzymes capable of synthesising inositol pyrophosphates in the amoeba, including the novel inositol phosphate kinases IPKA and IPKB. *In vitro,* both IPKA and IPKB act as specific IP_7 kinases. However, *in vivo* both enzymes are catalytically flexible and are able to phosphorylate other substrates.

In addition, PAGE technology allows the detection of polyP extracted from *D. discoideum*, revealing the unprecedented increase of polyP during development. Deletion of the Polyphosphate kinase (PPK)1 gene confirms this to be the only PPK in the amoeba. Deletion of PPK has a negative effect on the fitness of the amoeba, a phenotype underpinned by the ability of polyP to regulate primary metabolism. The *ppk1*-null strain fails to accumulate polyP during development and is defective in spore germination. Loss of polyP during the development of *ppk1* is partially compensated by an increase in inositol pyrophosphates. These observations support a model in which there is a functional interplay between inositol pyrophosphates, polyP and primary metabolism.

Table of Contents

Figures and Tables

Chapter 1

Chapter 2

Chapter 3

Chapter 4

Chapter 5

Chapter 7

Abbreviations

Abbreviation	Full name
A	Adenosine
Adar2	Adenosine deaminase acting on RNA 2
ADP	Adenosine diphosphate
AEC	Adenylate energy charge
AMP	Adenosine monophosphate
AP3B1	Adaptor-related protein complex 3, beta 1 subunit
ATP	Adenosine triphosphate
AX	Axenic
AX2	Axenic 2
BCL 2	B cell lymphoma 2
BHAM	Benzohydroxamate
BPB	Bromophenol blue
BSA	Bovine serum albumin
BSR	Blasticidin resistance
C	Cytosine
cAMP	Cyclic adenosine monophosphate
cDNA	Complementary deoxyribose nucleic acid
CHAPS	3-[(3- Cholamidopropyl)dimethylammonio]-1-propanesulfonate
cpm	Counts per minute
crac	Cytosolic regulator of adenylate cyclase
CSM	Complete synthetic media
CTP	Cytosine triphosphate
DAG	Di-acyl glycerol
DAPI	4',6-diamidino-2-phenylindole
Dd	*Dictyostelium discoideum*
DdPPK1	*Dictyostelium discoideum* polyphosphate kinase 1
DdPPK2	*Dictyostelium discoideum* polyphosphate kinase 2
DEPC	Diethylpyrocarbonate
DIPP	Diphosphoryl inositol polyphosphate phosphohydrolase
DMSO	Dimethyl sulfoxide
DNA	Deoxyribose nucleic acid
dNTP	Deoxynucleotide
DTT	Dithiothreitol
EDTA	Ethylenediaminetetraacetic acid
ER	Endoplasmic reticulum
ESR	Environmental stress response
FCCP	Carbonyl cyanide-4-(trifluoromethoxy)phenylhydrazone

FPLC	Fast protein liquid chromatography
FYVE	Fab 1, YOTB, Vac1, EEA1
G	Guanine
G protein	GTPase protein
GAPDH	Glyceraldehyde-3-Phosphate Dehydrogenase
GDP	Guanosine diphospahte
GPCR	G protein coupled receptor
GST	Glutathione sepharose transferase
GTP	Guanosine triphosphate
GWAS	Genome wide association study
HCl	Hydrochloric acid
HDAC	Histone deactylase
HEPES	4-(2-hydroxyethyl)-1-piperazineethanesulfonic acid
HPLC	High pressure liquid chromatography
Hs	*Homo sapiens*
IC50	Half maximal inhibitory concentration
IGF-1	Insulin-like growth factor 1
IPMA	Inositol monophosphatase
IP	Inositol phosphate
IP6K	Inositol hexakisphosphate kinase
IPK1	Inositol phosphate kinase 1
IPKA	Inositol phosphate kinase A
IPKB	Inositol phosphate kinase B
IPMK	Inositol phosphate multikinase
IPPK	Inositol-pentakisphosphate 2-kinase
IPS	Inositol-3-phosphate synthase
IPTG	Isopropyl β-D-1-thiogalactopyranosid
ITPK1	Inositol-tetrakisphosphate 1-kinase
IUPAC	International Union of Pure and Applied Chemistry
JMJD2C	Jumonji domain-containing 2C
KCN	Potassium cyanide
kDa	kilo Dalton
Km	Michaelis constant
LB	Luria broth
LETS	Lithium chloride, EDTA, Tris, SDS
M	Molar
m/z	mass/charge
mA	Milliampere
Mb	Megabase
MEF	Mouse embryonic fibroblast
MIPP	Multiple inositol-polyphosphate phosphatase
Mm	*Mus musculus*
mM	milli Molar

MOPS	3-(N-morpholino)propanesulfonic acid)
mPTP	Mitochondria permeability transition pore
mRNA	Messenger ribonucleic acid
mTORC2	Mammalian target of rapamycin 2
NAD	Nicotinamide adenine dinucleotide
NADP+	Nicotinamide adenine dinucleotide phosphate
NaF	Sodium fluoride
NC4	North Carolina 4
NEB	New England Biolabs
NLB	New lysis buffer
nm	nanometer
NMR	Nuclear magnetic resonance
NP40	Nonidet P-40
nt	Nucleotide
ORF	Open reading frame
PAGE	Polyacrylamide gel electrophoresis
PASK	Poly acidic, serine (S) and lysine (K)
PCR	Polymerase chain reaction
PDK1	Phosphoinositides dependent kinase 1
PH	Pleckstrin homology
PHB	Poly-(*R*)-3-hydroxybutryrate
Pi	Inorganic phosphate
PI	Phosphatidyl inositol
PI(3)K	Phosphatidyl inositol 3 kinase
PIKK	Phosphoinositides 3-kinase-related
PIP	Phosphatidyl inositol phosphate
PiUS	Inorganic phosphate uptake stimulator
PKC	Protein kinase C
PLC	Phospholipase C
PLD	Phospholipase D
polyP	Inorganic polyphosphate
PP-IPs	Inositol pyrophosphates
PPIP5K	Diphosphopentakisphosphate kinase
PPK	Polyphosphate kinase
PtdIns	Phosphatidyl inositol
PVDF	Polyvinylidene fluoride
PX	Phox Homology
RNA	Ribonucleic acid
RNAi	Ribonucleic acid interference
RPKM	Reads per kilobase per million mapped reads
RT	Room temperature
RTK	Receptor tyrosine kinase
SAX	Strong anion exchange

SC (media)	Synthetic complete media
SD	Standard deviation
SDS	Sodium dodecyl sulfate
SM	Slime mold
SSC	Saline Sodium Citrate
T	Thymine
TAE	Tris acetate EDTA buffer
TBE	Tris borate EDTA buffer
TBS	Tris buffered saline
TBST	Tris buffered saline tween
TE	Tris EDTA
TiO2	Titanium oxide
Top1	Topoisomerase 1
μM	micro Molar
V	Volts
VTC	Vacuolar transport complex
WT	Wild type
YPD	Yeast extract peptone dextrose

.1. Introduction

1.1 Inositol

The six-carbon inositol sugar is the key building block upon which a very large family of signalling molecules is based. The majority of inositol found in biological systems is in the *myo*-inositol form, in which the six-carbon ring is arranged in its chair formation. *Myo*-inositol has a single axis of symmetry through positions 2 and 5, making positions 1 and 3 as well as 4 and 6 enantiomeric (**Figure 1.1**). In its unphosphorylated state each carbon possesses a single hydroxyl group. The hydroxyl on position 2 is axial, perpendicular to the ring, whilst the remaining five hydroxyls are all equatorial, roughly in the same plain as the ring itself. Inositol is synthesised from glucose in a single isomerisation reaction conserved from archae to mammalian cells (Michell 2011)(**Figure 1.2**), forming a very stable, metabolically inert molecule. The stability of this molecule makes it an ideal canvas to be decorated with phosphates, generating the so-called inositol phosphates.

The unique stereochemical environment of each position allows an expansive repertoire of distinct inositol phosphates to be formed, with over 40 different soluble inositol phosphate species having been identified in living cells (Irvine and Schell 2001). The array of phospho-inositol species is further expanded by the phosphorylated inositol lipids, known as the phosphoinositides (Di Paolo and De Camilli 2006, Balla 2013). Greater complexity still is derived from the addition of more than one phosphate to a single carbon. These soluble molecules are characterised by their high phosphate content and the presence of one or more high-energy phospho-anhydride bonds. These molecules are termed diphosphoinositol phosphates although they are more commonly referred to as inositol pyrophosphates, as they will be referred to hereafter. Representatives of each inositol phosphate subfamily are depicted in **Figure1.3.**

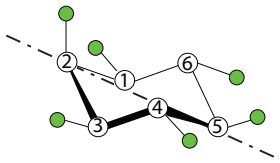

myo-inositol

Figure 1.1 Structure of *myo*-inositol

Myo-inositol exists in the chair formation. The hydroxyl group on position 2 is axial, whilst all others are equatorial. This gives *myo* inositol a single axis of symmetry, through carbons 2 and 5, making positions 1,3 and 4,6 enantiomeric.

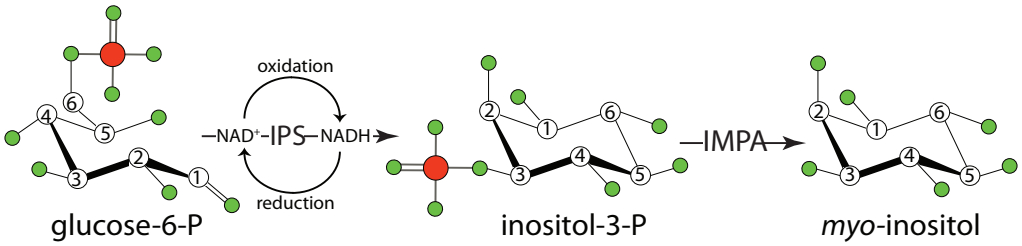

Figure 1.2 Enzymatic conversion of glucose-6P to inositol

Inositol is synthesised from glucose-6P by the inositol-3-phosphate synthase (IPS), which converts glucose-6P to inositol-3P. IPS requires NAD^+ and the rtwo-step eaction proceeds via oxidation followed by reduction. The so-called inositol monophosphatase (IMPase or IMPA) dephosphorylates inositol-3P to inositol. Carbon, white circle; phosphorus, red circle; and oxygen, green circle. Figure and figure legend adapted from (Livermore, Azevedo et al. 2016).

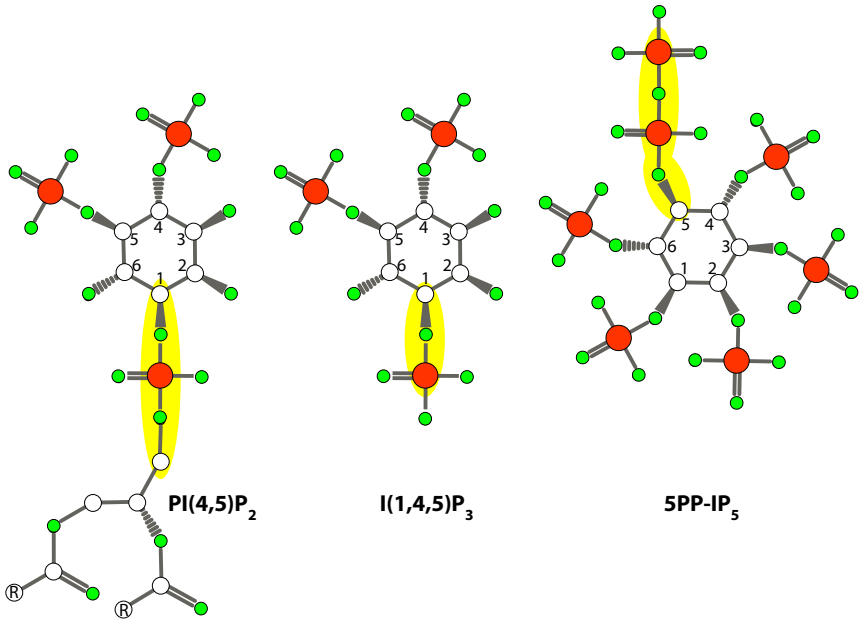

Figure 1.3 Illustrating representative members of three subfamilies of inositol phosphate-derived molecules

This figure represents (from left to right) the phosphoinositides, depicted by $PI(4,5)P_2$; the soluble inositol phosphates, depicted by $I(1,4,5)P_3$; and the inositol pyrophosphates, as depicted by IP_7 or 5PP-IP_5. Highlighted in yellow are the three distinct classes of phosphate bond, which are important for the function of each family of molecule. The phosphodiester bond (left) provides a structural link between the inositol phosphate head group and its diacyl glycerol anchor.. The phosphoester bond (centre) attaches the phosphate group to the inositol ring, providing the unique signalling properties of both the inositol phosphates and the phosphoinositides. The phosphoanhydride bond of the PP-IPs (right) provides these molecules with their 'high-energy' properties. This bond allows these molecules to partake in phosphotransfer reactions. Carbon, white circle; phosphorus, red circle; and oxygen, green circle. Figure and figure legend adapted from (Livermore, Azevedo et al. 2016).

1.1.1 Phosphoinositides

The best-characterised inositol phosphate species are without doubt the lipid bound or phosphoinositides. This family of molecules is linked through a phosphodiester bond on position 1 of the inositol ring to the diacyl glycerol group (**Figure 1.3, left**). The phosphoinositides are derived from the reversible phosphorylation of phosphatidyl inositol (PtdIns or PI)(see **Table 1.1**). This precursor molecule can be variably phosphorylated at positions 3,4 and 5 of the inositol ring, giving rise to a family of molecules that has eight members, including PI, in eukaryotic cells (Di Paolo and De Camilli 2006).

The phosphoinositides make up a very small proportion of the total lipids in the cell, approximately 10% of total lipids, of which the majority is PI (Balla 2013). Nevertheless, they are involved in, and indeed regulate, a huge array of cellular functions from membrane and vesicular trafficking to nuclear signalling (Balla 2013). The subcellular localisation of each individual member of this family is tightly controlled by activity of a range of kinases and phosphatases. Thus the identity of membranes is in part defined by their phosphoinositide composition. It is their presence throughout the membranes of the cell that allows these molecules to take part in such a wide array of cellular functions, a small number of which will be discussed below.

The negative charge of the phosphate group and distinct arrangements around the inositol ring allows proteins to recognise and discern between individual phosphoinositides and anchor themselves at particular membranes. A number of protein folds have been identified which specifically recognise the phosphoinositide family of lipids, including the PH, PX and FYVE domains (Balla 2013). The repertoire of protein modules described to interact with phosphoinositides is continuing to expand and now includes unstructured domains, which fold upon interaction with the head group. Consequently, the

range of functions in which phosphoinositides have been implicated is expanding too.

A phosphoinositide of particular importance is $PI(4,5)P_2$ (Figure 1.3). Primarily found at the plasma membrane, it is synthesised by the phosphorylation of PI(4)P and can be metabolised by dephosphorylation to either PI(4)P or PI(5)P, or by the cleavage by phospholipases, such as phospholipase C (PLC), in response to a stimulus. This cleavage of $PI(4,5)P_2$ yields another family of signalling molecules, the inositol phosphates, which will be covered in more detail later.

Alongside the role of $PI(4,5)P_2$ in transmitting a signal across the membrane, via the inositol phosphates, this lipid executes a pleiotropy of functions. The presence of $PI(4,5)P_2$ at the plasma membrane has been shown to be essential for the proper functioning of a range of ion channels (Hilgemann, Feng et al. 2001, Suh and Hille 2005). $PI(4,5)P_2$ regulates actin nucleation, organising cytoskeletal components (Rohatgi, Ho et al. 2000) and thus controlling cell shape and cell motility (Pollard and Borisy 2003). In addition many proteins regulating endocytosis possess domains which bind to $PI(4,5)P_2$, defining the role for this lipid in controlling membrane trafficking and specifically endocytic events (Godlee and Kaksonen 2013).

In addition to the actions briefly described above, $PI(4,5)P_2$ can also be phosphorylated by the phosphoinositides-(3)-kinases (PI(3)Ks) to form $PI(3,4,5)P_3$. This phosphorylation occurs transiently in response to growth factor stimulus, receptor tyrosine kinase (RTK) or G protein coupled receptor (GPCR) activation. $PI(3,4,5)P_3$ and can mediate a range of effects from chemotaxis to cell proliferation and survival.

In fact the localisation of PI(3,4,5)P_3 at the leading edge of the amoeba *D. discoideum* has been described to be responsible for polarised motility during chemotaxis (Iijima, Huang et al. 2002). However, the role of PI(3,4,5)P_3 in *D. discoideum* is controversial as genetic ablation of PI(3,4,5)P_3 signalling does not impair the ability of the amoeba to respond to chemoattractants (Hoeller and Kay 2007, Hoeller, Bolourani et al. 2013, Nichols, Veltman et al. 2015)**.**

Regardless of the controversy over the role of PI(3,4,5)P_3 in *D. discoideum* chemotaxis, in mammals this phosphoinositide plays a key role in signalling through the protein kinase Akt (Vanhaesebroeck, Stephens et al. 2012). Akt, also known as protein kinase B, is a serine, threonine kinase, which contains a PH domain with high affinity for both PI(3,4)P_2 and PI(3,4,5)P_3. The production of PI(3,4,5)P_3 at the plasma membrane in response to a stimulus results in the recruitment of Akt. Once recruited by PI(3,4,5)P_3, Akt can be phosphorylated and activated by phosphoinositides dependent kinase 1(PDK1) (Alessi, James et al. 1997, Stokoe, Stephens et al. 1997) and mammalian target of rapamycin (mTORC2)(Sarbassov, Guertin et al. 2005). Once activated, Akt phosphorylates a range of substrates including those involved in the insulin signalling pathway (glycogen synthase kinase 3), apoptotic pathway (BCL 2) and cell cycle regulators (p21 and p27) (Vanhaesebroeck, Stephens et al. 2012). Thus PI(3,4,5)P_3 is crucial to regulating these diverse process through its dual role in Akt activation, promoting its recruitment to the plasma membrane, as well as being required for the activity of the activating kinase PDK1 (Alessi, James et al. 1997), which phosphorylates Akt.

Aside from PI(4,5)P_2 and PI(3,4,5)P_3, other members of the phosphoinositides family have numerous and varied functions in other cellular compartments (Di Paolo and De Camilli 2006, Balla 2013). However, these molecules and the proteins that regulate them fall outside the scope of this work and will not be covered in further detail here. In addition, the nuclear signalling properties

displayed by the phosphoinositides (Blind, Suzawa et al. 2012, Shah, Jones et al. 2013) will not be covered in this work for the same reasons.

1.1.2 Inositol phosphates

While much research has elucidated the roles of inositol lipids in cellular processes, of which only a very small amount has been covered above, comparatively little is known about the functions of the much larger family of soluble inositol phosphates. There are, however, a number of well-studied examples, the most famed being the role of the second messenger $I(1,4,5)P_3$. $I(1,4,5)P_3$, abbreviated hereafter to IP_3, can be derived from the phospholipase C (PLC)-dependent cleavage of the lipid PIP_2. In 1983 it was first demonstrated that this cleavage of PIP_2 induces a transient increase in IP_3 resulting in Ca^{2+} release from internal stores (Streb, Irvine et al. 1983). In this classical example, IP_3 acts as the archetypal second messenger, acutely increasing in response to a stimulus, diffusing through the cytosol and binding to the IP_3Receptor to induce Ca^{2+} release from internal stores (Berridge 1993).

PLC, the enzyme that liberates IP_3 from its di-acyl glycerol (DAG) tail, comes in several flavours. These can be activated by either GPCR stimulation and heterotrimeric G proteins or by activated RTKs. Once activated the membrane associated enzyme cleaves PIP_2 at the plasma membrane, releasing two second messengers: IP_3 and DAG. The soluble IP_3 diffuses through the cytosol and binds to the large membrane protein IP_3Receptor. The IP_3Receptor, localised to the membrane of the endoplasmic reticulum (ER), has an IP_3 binding site in its N terminal region. Once bound by IP_3, the IP_3Receptor oligomerises, with four subunits coming together to form a Ca^{2+} channel, allowing the efflux of Ca^{2+} from the ER (Berridge 1993).

Whilst the soluble IP_3 diffuses through the cytosol, DAG, the other product of PIP_2 cleavage, diffuses through the plasma membrane. DAG, a second

messenger in its own right, is able to activate protein kinase C, leading to the phosphorylation of a wide range of substrates (Reyland 2009).

Since the initial description of IP_3 acting as a second messenger, much work focused on defining the pathways in which other inositol phosphates act. Whilst the levels of both I(1,3,4,5)P_4 and I(1,3,4)P_3 increase in response to stimulus, these are primarily metabolites of I(1,4,5)P_3 brought about by the phosphorylation by IP_3-3-Kinase (IP_3-3K) and subsequent dephosphorylation by a 5-phosphatase rather than signalling molecules in their own right (Irvine and Schell 2001).

In fact, the search for other inositol phosphate receptors has also largely been fruitless and it has been proposed that the only other member of this family that could be termed a second messenger is I(3,4,5,6)P_4 (Shears, Ganapathi et al. 2012). I(3,4,5,6)P_4 is a concentration-dependent inhibitor of Cl^- channels, in particular acting on the ClC3 channel (Mitchell, Wang et al. 2008). This species is increased in response to PLC activation in a manner dependent on the activity of another, unrelated, IP_3 kinase, ITPK1 (Shears 2009). I(3,4,5,6)P_4 is thereby able to influence a range of cellular processes dependent upon ClC3 channels, from neural development to inflammation (Shears 2009).

Whilst attention has been paid to the roles of inositol phosphates as second messengers, in particular focusing on IP_3, the most abundant forms of inositol phosphates in mammalian cells are in fact inositol pentakisphosphates, IP_5 and inositol hexakisphosphate, IP_6. Perhaps unsurprisingly these were the first inositol phosphate species to be identified. The accumulation of IP_6, also known as phytic acid, in seeds was the first description of the inositol phosphates almost a century ago (Posternak 1921). Subsequently, IP_5 was the first inositol phosphate to be described in animal cells, with its identification in chicken

erythrocytes (Johnson and Tate 1969). The synthetic pathway of these "higher" inositol phosphates is summarised in **Figure 1.4.**

The "higher" inositol" phosphates, whilst not considered classical second messengers, have been implicated in a wide range of cellular processes. IP_5 has, for example, been demonstrated to play a role in the oxygen affinity of haemoglobin (Coates 1975) and as a modulator of Wnt signalling (Gao and Wang 2007). The synthesis of IP_5 and IP_6 has also been shown to regulate neuronal development, with the intracellular ratio of these two molecules altering in response to stimulation in both differentiated PC12 cells and primary neurons (Loss, Wu et al. 2013). IP_6, meanwhile, has been implicated in processes including protein kinase C activation (Efanov, Zaitsev et al. 1997) and mRNA transport (York, Odom et al. 1999). An additional interesting role for IP_6 emerged with the surprise identification of a single IP_6 molecule deep within the structure of RNA editing enzyme Adar2 (Macbeth, Schubert et al. 2005). This raised the possibility that the highly charged IP_6 might function as a protein folding cofactor, independent of any classical signalling role. It is not clear how widespread this phenomenon is, nor whether other highly polar molecules might perform the same role *in vivo*, but it appears that Adar2 is not unique in its use of IP_6 as a protein folding cofactor (J.D. York personal communication).

1.2 Inositol pyrophosphates

Whilst IP_6 was for many years considered to the most highly phosphorylated form of inositol, two independent studies in *D. discoideum* and mammalian cells demonstrated otherwise in 1993 (Menniti, Miller et al. 1993, Stephens, Radenberg et al. 1993). It was noted that species more polar than IP_6 could be detected by high-pressure liquid chromatography (HPLC) analysis of radiolabelled ^{3}H-inositol. This indicated the existence of inositol phosphate species containing more than six phosphates. Given that the inositol sugar

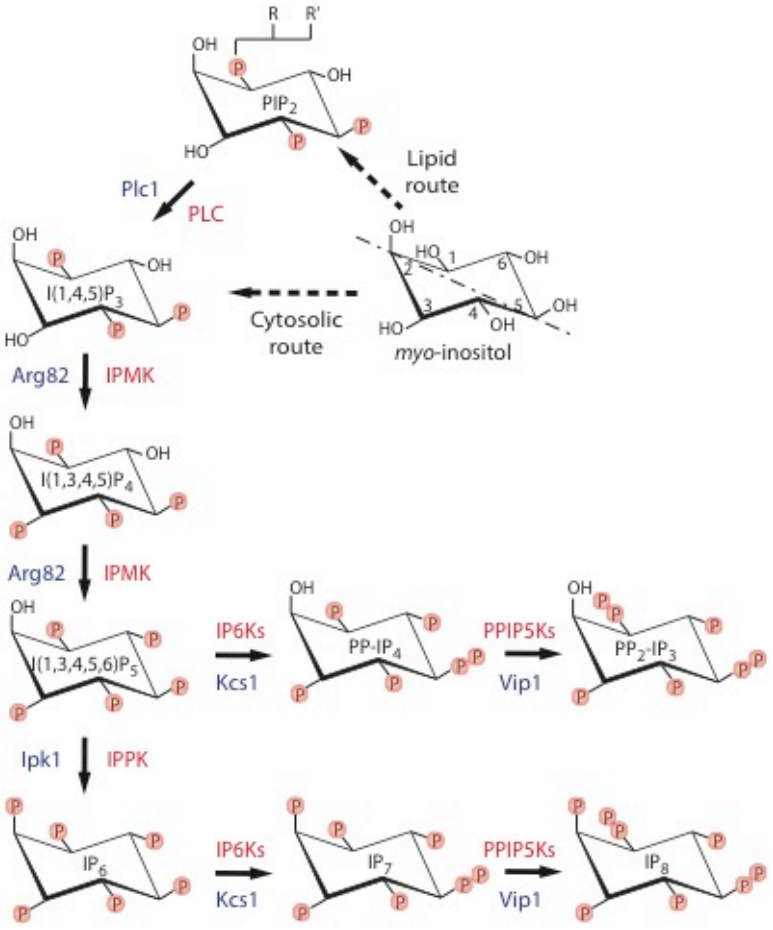

Figure 1.4 Simplified synthetic pathway of inositol pyrophosphates

This simplified pathway depicts the possible routes of inositol pyrophosphate synthesis in yeast (*S. cerevisiae*), amoeba (*D.discoideum*) and mammalian cells, starting from myo-inositol. *S. cerevisiae* exclusively synthesises inositol phosphates via the lipid pathway (York, Odom et al. 1999), whereas *D. discoideum* synthesises IP_6, via the cytosolic route (Stephens and Irvine 1990) The enzymology of this pathway is not well characterised. This figure highlights the major metabolic pathway as supported by yeast genetic studies (York, Odom et al. 1999, Saiardi, Sciambi et al. 2002, Seeds, Bastidas et al. 2005). Multiple PP-IP_4 isoforms can be synthesised *in vitro* by IP6K (5PP-IP_4 is shown here). P indicates a single phosphate (PO_4^{2-}) group; R and R′ represent fatty acid chains; dashed arrows represent multiple steps of modification that are not shown in detail; kinases catalysing each step are indicated in red (mammalian) and blue (*S. cerevisiae*). Figure and figure legend adapted from (Wilson, Livermore et al. 2013).

Table 1.1 Phosphoinositide and inositol phosphate nomenclature

Common name	IUPAC nomenclature	Alternative name	Common Isomeric forms
Lipid			
PI	PtdIns	-	
PIP	PtdInsP	-	PI(3)P PI(4)P PI(5)P
PIP_2	$PtdInsP_2$	-	$PI(4,5)P_2$ $PI(3,4)P_2$ $PI(3,5)P_2$
PIP_3	$PtdInsP_3$	-	$PI(3,4,5)P_2$
Soluble			
IP_3	Inositol trisphosphate ($InsP_3$)	-	$I(1,4,5)P_3$ $I(1,3,4)P_3$
IP_4	Inositol tetrakisphosphate ($InsP_4$)	-	$I(1,3,4,5)P_4$ $I(3,4,5,6)P_4$ $I(1,4,5,6)P_4$
IP_5	Inositol pentakisphosphate ($InsP_5$)	-	$I(1,3,4,5,6)P_5$
IP_6	Inositol hexakisphosphate ($InsP_6$)	Phytic acid	
IP_7/PP-IP_5	Diphosphoinositol pentakisphosphate (PP-$InsP_5$)	$InsP_7$	1 PP-IP_5 5 PP-IP_5
IP_8/$(PP)_2$-IP_4	Bisdiphosphoinositol tetrakisphosphate [$(PP)_2$-$InsP_4$]	$InsP_8$	1,5 PP-IP_4 (yeast, mammalian) 5,6 PP-IP_4 (*D. discoideum*)
PP-IP_4	Diphosphoinositol tetrakisphosphate	PP- $InsP_4$	(1/3)PP-IP_4 5 PP-IP_4
$(PP)_2$-IP_3	Bisdiphosphoinositol trisphosphate	$(PP)_2$-$InsP_3$	

contains six carbons itself, the arrangement of seven or more phosphates around the ring necessitates the formation of a high-energy phosphoanhydride bond linking a beta phosphate to the ring (**Figure 1.3**). In fact, it is this presence of at least one beta phosphate that characterises the so-called inositol pyrophosphates or, to use the correct IUPAC nomenclature, diphosphoinositol polyphosphates (see **Table 1.1** for disambiguation of nomenclature).

1.2.1 Inositol pyrophosphates: structure and synthesis

The most common form of inositol pyrophosphate in yeast and mammalian cells is the IP_6-derived PP-IP_5, hereafter referred to as IP_7 (see **Table 1.1**). Other members of this family include $(PP)_2$-IP_4, hereafter referred to as IP_8. Pyrophosphates can also be synthesised from IP_6 precursors such as IP_5 (**Figure 1.4**)(**Table 1.1**) and even less phosphorylated inositol species (Seeds, Bastidas et al. 2005). Whilst IP_6 is present at concentrations of up to 10-60 μM in mammalian cells, IP_7 usually exists at a concentration less than 10% of that, between 0.5 and 1.3 μM (Albert, Safrany et al. 1997, Shears 2001). The social amoeba *D. discoideum*, which will be the focus of this work, is exceptional in possessing extremely high levels of IP_6, up to 0.7 mM (Albert, Safrany et al. 1997). Furthermore the inositol pyrophosphates have also been described to increase up to ~1.5 mM during the starvation-induced development of this amoeba (Laussmann, Pikzack et al. 2000).

Two distinct classes of enzymes are able to synthesise inositol pyrophosphates by adding a beta phosphate to the inositol ring (**Figure 1.4**). These are the IP_6Kinases (IP6K) and the $PPIP_5$Kinases (PPIP5K). Each enzyme displays a specific activity towards a single position on the ring, with IP6Ks placing a pyrophosphate on position 5 (Draskovic, Saiardi et al. 2008) and PPIP5Ks placing a pyrophosphate on position 1 (Wang, Falck et al. 2012). These gene families are conserved from yeast (where they are called Kcs1 and Vip1 respectively) to mammals (**Figure 1.4**).

The IP6Ks are members of the inositol phosphate kinase family and possess the characteristic PxxxDxKxG inositol phosphate-binding motif (**Figure 7.1**). Yeast possess a single IP6K, Kcs1, whilst mammalian genomes encode three isoforms of IP6K, IP6K1-3. All of these kinases are able to phosphorylate IP_6 to IP_7 as well as IP_5 to PP-IP_4 *in vitro* (Saiardi, Erdjument-Bromage et al. 1999, Saiardi, Nagata et al. 2001, Draskovic, Saiardi et al. 2008). The substrate selectivity varies between isoforms and organism, for instance the mammalian IP6K1 has a five-fold higher affinity for IP_6 over IP_5, whilst the IP6K2 has a 20-fold higher affinity for IP_6 (Saiardi, Erdjument-Bromage et al. 1999). Kcs1 is a non-essential gene in yeast, although the *kcs1Δ* yeast does display a range of phenotypes affecting its general fitness (Saiardi, Caffrey et al. 2000). In mouse, each individual gene has been deleted in isolation to generate single knockouts *IP6K1-/-*, *IP6K 2-/-* and *IP6K3-/-* discussed in more detail later. Some of the phenotypes observed in yeast have been reproduced in these knockout mice, however all of these mice retain functional IP6K and likely IP_7. The close proximity of IP6K1 and IP6K2 on the same locus of the same arm of chromosome 9 in mice (chromosome 3 in humans) makes the generation of a double knockout mouse by traditional methods impractical.

The IP6Ks, in contrast to other members of the inositol phosphate kinase family, are notable for their very high K_m for ATP of between 1.0 and 1.4 mM, comparable to the intracellular concentration of ATP (Wundenberg and Mayr 2012, Wilson, Livermore et al. 2013). This makes these kinases exquisitely sensitive to changes in ATP concentration, the significance of which will be explored in more detail later.

Surprisingly, phylogenetic analysis suggests that the IP6Ks are in fact the most ancient members of the inositol phosphate kinase family (Bennett, Onnebo et al. 2006). This is counter intuitive considering that the synthesis of their preferred

substrate, IP_6, requires the activity of other inositol phosphate kinases, in particular IPMK (**Figure 1.4**). Nevertheless, this theory is supported by the recently published structure of the *E. histolytica* IP6K (Wang, DeRose et al. 2014). This enzyme displays hybrid kinase activity, phosphorylating not only IP_6 to IP_7 but also IP_3 to IP_4. The catalytic flexibility displayed by this evolutionarily ancient kinase is explained by the partial separation of the substrate binding determinants for IP_3 and IP_6. This separation was demonstrated by a 55° rotation of the smaller IP_3 in the active site. Based on these observations, single point mutations in the binding determinants of hsIP6K2, were shown to induce a 50-fold increase in IP_3K activity in hsIP6K2. Thus this evidence supports a model in which the IP6Ks were the first inositol phosphate kinases to arise and that subsequent mutations gave rise to first the flexible IPMK, then the more recently evolved and highly specific IP_3-3K.

The second class of enzyme capable of synthesising inositol pyrophosphates is PPIP5K. This enzyme was first characterised in yeast as Vip1 in 2007 (Mulugu, Bai et al. 2007). Yeast possess a single Vip1, whilst mammalian genomes encode two PPIP5Ks. These large enzymes (~130 kDa) are remarkable for their domain structure, which includes both a kinase domain and an acid-phosphatase domain. The kinase domain has a unique protein fold, unlike other inositol phosphate kinases, and is able to add a pyrophosphate moiety to position 1 on the ring(Wang, Falck et al. 2012). *In vitro* PPIP5K is able to phosphorylate both IP_6 and IP_7, however the physiological preference appears to be towards IP_7 generated by IP6K. In yeast, *kcs1Δ* possesses no detectable IP_7, whilst *vip1Δ* has increased levels of IP_7. The most likely explanation for this result is that Vip1 acts predominantly an IP_7 kinase *in vivo* and its deletion results in an increase in its substrate.

The deletion of Vip1 has relatively limited effect on the fitness of the *vip1Δ* mutant. This is in stark contrast to the severe effect in the *kcs1Δ,* adding further

to the hypothesis that PPIP5K/Vip1 is primarily an IP_7 kinase. However, deletion of Asp1, the *Schizosaccharomyces pombe* homologue to Vip1, renders the mutant temperature sensitive (Feoktistova, McCollum et al. 1999).

The structure of the PPIP5K kinase domain displays a number of unique properties. The addition of a further negative charge onto the already highly polar IP_7 is not an energetically favourable event. As such the positively charged residues in the binding site make numerous contacts with the substrate to neutralise the charge and facilitate the addition of an eighth phosphate to the already densely phosphorylated IP_7 (Wang, Falck et al. 2012). Furthermore, a second, less constrained binding site exists on the surface of PPIP5K (Wang, DeRose et al. 2014). This second binding pocket has been hypothesized to act as a substrate capture site, rather than having an allosteric effect. It is proposed that substrate transiently occupies the surface-binding site, before being flipped 100° into the active site where it is phosphorylated.

The PPIP5K enzymes are further complicated by the presence of an additional acidic-phosphatase domain. The phosphatase domain from the PPIP5K homologue (Asp1) of the fission yeast, *S. pombe*, has recently been shown to possess very specific activity towards pyrophosphate moieties at position 1 of the ring (Wang, Nair et al. 2015). Both the phosphatase domain alone and full-length protein were able to dephosphorylate (1PP) IP_7 and (1,5PP) IP_8, but not other isomeric forms of IP_7. This remarkable activity indicates that the product of the PPIP5K kinase domain is specifically destroyed by the phosphatase domain of the very same protein.

Aside from the PPIP5K phosphatase domain, additional inositol pyrophosphate phosphatases exist in the form of the DIPPs. These phosphatases also display a greater hydrolase activity towards position 1 of the inositol ring although they are able to dephosphorylate other positions on the ring. Four DIPPs have been

identified in mammals, whilst the yeast genome encodes a single homologue (Ddp1). These enzymes are members of the Nudix (nucleoside diphosphate linked moiety X) family of hydrolases and are highly promiscuous. They are able to cleave the phosphoanhydride bond of a wide range substrates, including nucleotide analogues such as Ap6A and, interestingly, for this work, inorganic polyphosphate (polyP), a property shared by both the mammalian and yeast homologues (Lonetti, Szijgyarto et al. 2011).

1.2.2 Inositol pyrophosphates: fluctuations and turnover

In most circumstances the steady state levels of the inositol pyrophosphates remain remarkably constant. Relatively few examples of modulation of the level of inositol pyrophosphates have been described. The most extreme example, as mentioned previously, is the increase in inositol pyrophosphates that occurs during the development of the social amoeba *D. discoideum*. Upon deprivation of nutrients the myxamoeba undergoes a 25-fold increase in the level of inositol pyrophosphates (Laussmann, Pikzack et al. 2000). This extreme event occurs over the course of 24 h or more and is a markedly different phenomena to the acute increase associated with second messengers. More rapid changes could be observed with direct treatment of pre-starved cells with cyclic AMP (cAMP), the key modulator of the developmental response in *D. discoideum* (Williams 2010). This treatment induced a rapid change in both IP_7 and IP_8 within 60 s. However, as well as being pre-starved, these cells had also been treated with caffeine and a PIKK (phosphoinositides 3-kinase-related) family inhibitor to supress endogenous cAMP production.

The pharmacological treatment of a variety of mammalian cells with NaF is also able to induce an increase in the level of inositol pyrophosphates. This treatment points to a rapid turnover of these molecules, with approximately 50% of the IP_6 and up to 20% of the IP_5 pool converted to inositol pyrophosphates each hour

(Menniti, Miller et al. 1993). This indicates that, whilst the concentration of these molecules does not vary dramatically, they are rapidly turned over. Thus maintaining their concentration requires significant investment of energy. Further evidence of this comes from primary hepatocytes where the IP_7 pool was shown to turnover ten times in a 40 min period. This can be compared to just 10% of the IP_6 pool in the same time period (Glennon and Shears 1993).

The physiological relevance of NaF-induced increases in inositol pyrophosphates is unclear. NaF is well known as a pan-phosphatase inhibitor, able to inhibit the action of DIPPs (although it's ability to inhibit the phosphatase domain of PPIP5K is not known) (Caffrey, Safrany et al. 2000). The effect of NaF may, therefore, be solely explained by its inhibitory action on phosphatases. However, the effect of NaF on levels of inositol pyrophosphates is not conserved in yeast, despite the fact that Ddp1p is also sensitive to NaF inhibition (Lonetti, Szijgyarto et al. 2011).

Physiological modulations of the level of inositol pyrophosphates during the cell cycle have been described in rat mammary tumour cells (Barker, Wright et al. 2004) and yeast (Banfic, Bedalov et al. 2012). In rat cells, IP_7 was reported to peak during G_1 phase, when the levels of inositol pyrophosphates doubled in comparison to any other stage of the cell cycle. Meanwhile in yeast, the peak in inositol pyrophosphates was found to occur during S phase. Neither the significance of these divergent results, nor the role of these fluctuations during the cell cycle, are well understood.

Alongside the effects described above, starvation has also been described to modulate the levels of inositol pyrophosphates in mammalian and yeast cells. Overnight serum starvation of mouse embryonic fibroblasts (MEFs) results in a depletion of the level of IP_7. This decrease can be reverted by treatment with insulin-like growth factor 1 (IGF-1) (Chakraborty, Koldobskiy et al. 2010).

Meanwhile, phosphate starvation has been reported to stimulate both an increase (Lee, Mulugu et al. 2007) and decrease (Boer, Crutchfield et al. 2010) in the levels of inositol pyrophosphates.

In plants, which possess homologues to PPIP5K, but not IP6K, jasmonate signalling can induce the synthesis of IP_8 (Laha, Johnen et al. 2015). Whilst the source of IP_7 in plants remains unclear, IP_8 is synthesised in a manner dependent upon the activity of the PPIP5K homologue, VIH2. Treatment of *Arabidopsis thaliana* with the plant hormone methyl jasmonate, a hormone involved in the plant pathogen response, induces a 2-fold increase in IP_8 (Laha, Johnen et al. 2015). This increase is dependent upon VIH2, disruption of this gene causes aberrant jasmonate perception and decreased resilience to pathogens.

That there are so few examples of fluctuations of the levels of inositol pyrophosphates suggests that these molecules are not classical second messengers and that they act in an alternative fashion. The rapid turnover and substantial energetic investment in a stable steady state concentration hints at a role in some kind of homeostatic control. In fact, of the few examples identified in which the level of inositol pyrophosphates change, most occur in response to some form of starvation, suggesting a potential link to metabolic homeostasis.

1.2.3 Roles of inositol pyrophosphates

The evolutionary conservation of these molecules indicates an important role in eukaryotic physiology. This view is further supported by the wide-ranging cellular processes in which the inositol pyrophosphates have been implicated. From vesicular trafficking to maintenance of telomere length and epigenetic control of transcription, the inositol pyrophosphates are exceptionally diverse in their influences.

A role in vesicular trafficking was first identified through the fragmented vacuole of the yeast *kcs1Δ* (Saiardi, Caffrey et al. 2000). The biogenesis of the yeast vacuole is dependent on both endocytic and Golgi trafficking, providing the first suggestions that vesicle fusion or trafficking might be regulated in some way by the presence of inositol pyrophosphates. Further genetic studies localised the trafficking defect to the endocytic pathway (Saiardi, Sciambi et al. 2002).

The role of inositol pyrophosphates in controlling telomere length was indicated by the altered telomere lengths in strains with aberrant levels of inositol pyrophosphates (Saiardi, Resnick et al. 2005, York, Armbruster et al. 2005). Cells synthesising increased levels of inositol pyrophosphates showed a decrease in length of telomeres, whilst cells lacking inositol pyrophosphates had longer telomeric regions (Saiardi, Resnick et al. 2005). This effect was mediated through the phosphoinositide 3-related-kinases Tel1 and possibly Mec1 pathways involved in DNA damage repair in yeast.

Further roles for the inositol pyrophosphates in the nucleus were indicated by the altered methylation of histones in mammalian cells lacking IP6K1 (Burton, Azevedo et al. 2013). A yeast two-hybrid screen identified IP6K1 as an interaction partner of the histone demethylase, Jumonji domain-containing 2C (JMJD2C). Investigation of this interaction in HeLa cells and *ip6k*-/- MEFs revealed that this interaction recruited IP6K1 to chromatin. Furthermore, synthesis of IP_7 by IP6K was able to regulate the activity of JMJD2C and thus the level of histone methylation. This effect is dependent on the catalytic activity of IP6K, but not due to direct effect of IP_7 on JMJD2C as IP_7 isomers are unable to alter JMJD2C demethylase activity in *in vitro* assays. Transcription of genes controlled by JMJD2C activity is altered by the presence or absence of IP6K1, indicating that inositol pyrophosphate signalling plays a role in transcription by acting on histone modifying enzymes via an as yet unidentified mechanism.

The role of inositol pyrophosphates in control of transcription is further demonstrated by the failure of yeast lacking inositol pyrophosphates to mount an environmental stress response (ESR) (Worley, Luo et al. 2013). The *kcs1Δvip1Δ* show defective transcriptional response to a range of stresses, manifesting in a failure to repress stress genes during logarithmic growth as well as a failure to induce stress genes upon osmotic, heat or oxidative stress. The effect of inositol pyrophosphates on the ESR response also occurs at the level of chromatin modification. Cells lacking inositol pyrophosphates are deficient in the activity of the histone deactelyase (HDAC) Rpd3L, leading to a failure to regulate transcriptional response downstream of the environmental stress pathway (Worley, Luo et al. 2013). The inhibition of Rpd3L by the inositol pyrophosphates has been suggested to be direct, due to the binding of inositol pyrophosphates to an IP_4 binding pocket previously identified in Rpd3L's human homologue, HDAC3 (Watson, Fairall et al. 2012).

Such a breadth of effects, across a disparate array of cellular processes suggests a more basic regulatory function of inositol pyrophosphates. One intuitive hypothesis postulates that the diverse influences of the inositol pyrophosphates are underpinned by an influence on primary metabolism (Bennett, Onnebo et al. 2006, Shears 2009).

In recent years evidence supporting this attractive hypothesis (detailed in **Figure 1.5**) has emerged from both yeast and mammalian models. In yeast, the *kcs1Δ* strain, which lacks detectable IP_7, is unable to grow on nonfermentable carbon sources and yet has three-fold higher levels of ATP (Szijgyarto, Garedew et al. 2011). This remarkable effect on energy homeostasis occurs in spite of the fact that the mitochondria of this strain are dysfunctional. Instead this increase in

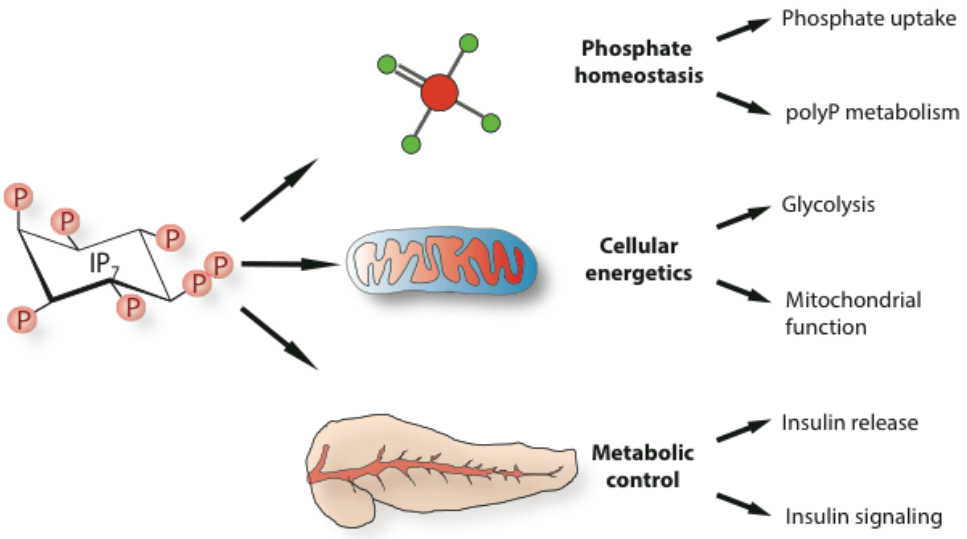

Figure 1.5 Influence of inositol pyrophosphates in primary metabolism

Primary metabolic influences exerted by inositol pyrophosphates (shown as IP_7). This figure shows three, probably connected, features that link inositol pyrophosphates to metabolism. This can be observed at the molecular level, through control of phosphate homoeostasis (Norbis, Boll et al. 1997, Illies, Gromada et al. 2007, Chakraborty, Koldobskiy et al. 2010, Lonetti, Szijgyarto et al. 2011); at a cellular level through an effect on primary metabolism (Szijgyarto, Garedew et al. 2011) and at the level of the organism, by regulating insulin signalling (Illies, Gromada et al. 2007, Chakraborty, Koldobskiy et al. 2010)levels. Figure and figure legend adapted from (Wilson, Livermore et al. 2013).

ATP stems from the dramatic shift to glycolytic ATP-production. Moreover, the adenylate energy charge (AEC), a measure of amount of metabolically available energy stored in the adenylate pool, of these cells is also increased. Overexpression of the human IP6K1 in this strain correspondingly reduces the level of ATP, indicating that this is a likely to be a direct effect of IP_7 rather than of Kcs1p itself. Mouse embryonic fibroblasts (MEFs) lacking the IP6K1 display a similar increase in the levels of ATP as well as defective mitochondria, indicating that this phenomenon is not specific to yeast.

The concept of inositol pyrophosphates as metabolic regulators gains support from the properties of the main synthesising enzyme, IP6K. IP6K has a K_m for ATP of between 1.0 and 1.4 mM (Voglmaier, Bembenek et al. 1996, Saiardi, Erdjument-Bromage et al. 1999, Saiardi, Caffrey et al. 2000), a value very close to that of intracellular concentrations of ATP. The other inositol phosphate kinases typically have a K_m for ATP between 20 and 100 μM (Wundenberg and Mayr 2012), making IP6Ks unusually sensitive to cellular ATP levels. This observation prompted the "energostat" model for inositol pyrophosphate control of metabolism (Wundenberg and Mayr 2012). This model postulates that any slight fluctuation in cellular ATP will be reflected by a subtle, but finely tuned change in IP6K activity and thus the level of IP_7. These subtle changes in the level of inositol pyrophosphates then exert their effects on a range of cellular functions as described above. This beautifully explains both remarkably constant steady state levels of inositol pyrophosphates and the extraordinary range of phenotypes with which they are associated. Importantly, the "energostat" model makes no assumptions regarding the mode of action, explored further below.

In light of this role as a regulator of basic cell metabolism, a range of phenotypic effects of can be explained. In the pathogenic yeast *Cryptococcus neoformans,* cells lacking inositol pyrophosphates are less able to sustain an infection than

their WT counterparts. This pathogenic defect is underpinned by the metabolic control exerted by the inositol pyrophosphates (Lev, Li et al. 2015). The *kcs1Δ* of *C. neoformans* displays a similar growth defect to the *S. cerevisiae* strain on non-fermentable carbon sources. In addition, the activity of Kcs1 was required for infection of mouse lungs, as infection with *kcs1Δ* strain resulted in a reduced fungal load. It is hypothesised that this infection defect was due to the observed metabolic defect of the *kcs1Δ* strain, impairing its proliferation in the low carbon environment of the lung and precluding its utilisation of alterative carbon sources (Lev, Li et al. 2015).

Considering the inositol pyrophosphates as metabolic regulators can also aid in the interpretation of the *IP6K1*-/- knockout mouse phenotype. This mouse displays a dramatic metabolic phenotype, with decreased insulin secretion (Bhandari, Juluri et al. 2008), hypersensitive to insulin and resistance to obesity even when fed a high fat diet (Chakraborty, Koldobskiy et al. 2010). This link to organismal energetic metabolism is consistent with the increase in insulin release by exocytosis from pancreatic beta cells overexpressing IP6K1 (Illies, Gromada et al. 2007). Similarly knock down of IP6K1 in these cells reduces their rate of exocytosis. These observations are all consistent with a link to metabolic homeostasis at the organismal level (**Figure 1.5**).

Conversely, the *IP6K2*-/- knockout mouse does not exhibit any metabolic phenotype or insulin sensitivity. Rather this mouse is resistant to ionising radiation and exhibits an upregulation of DNA-repair pathways (Morrison, Haney et al. 2009). Overexpression of IP6K2 in a range of cancer cell lines increases their susceptibility to cell stressors, including cisplatin and staurosporin (Nagata, Luo et al. 2005). Meanwhile RNAi of IP6K2, but neither IP6K1 nor IP6K3 diminishes staurosporin-induced apoptosis. The effect on apoptosis is IP6K2 specific and associated with the translocation of IP6K2 from the nucleus to the

mitochondria, although these localisation studies were performed with overexpressed, tagged IP6K2, not endogenous protein (Nagata, Luo et al. 2005).

Recently, characterisation of the *IP6K3*-/- knock out mouse has revealed a defect in coordination and motor function (Fu, Xu et al. 2015). IP6K3 is particularly abundant in the Purkinje cells of the cerebellum and its deletion results in a reduction in the number of synapses formed by these cells. However, this phenotype is dependent upon the kinase itself, rather than its inositol pyrophosphate products. IP6K3 interacts with components of the cytoskeleton, spectrin and adducin, independently of its kinase function. Deletion of IP6K3 abrogates the interaction between these cytoskeletal proteins, culminating in changes in cell morphology, reduced synapse formation and a coordination defect in the rotor rod (Fu, Xu et al. 2015).

1.2.4 Inositol pyrophosphates: mechanism of action

The inositol pyrophosphates are clearly influential in many cellular processes, however the molecular mechanism by which these influences are exerted is controversial. To date two modes of action have been proposed for the inositol pyrophosphates (**Figure 1.6**). The first, and most classical, is through binding of IP_7 to PH domain-containing proteins. This mechanism postulates that IP_7 competes with the normal ligand for the PH domain, PIP_3, and disrupts the membrane localisation of effector molecules. The first described example of this came from work in *D. discoideum* where IP_7 competes with PIP_3 for the PH domain of the cytosolic regulator of adenylate cyclase (crac) (Luo, Huang et al. 2003). Thus the presence of IP_7 has an inhibitory effect on the membrane localisation of crac. Deletion of the IP6K in these cells ablated IP_7. Expression of a GFP-tagged fusion protein of the crac PH domain (PH_{crac}) displays an increased membrane localisation in response to cAMP in mutant compared to WT cells. IP_7 is able to inhibit the localisation of the PH_{crac} to liposomes containing PIP_3 with an IC50 of 50 nM.

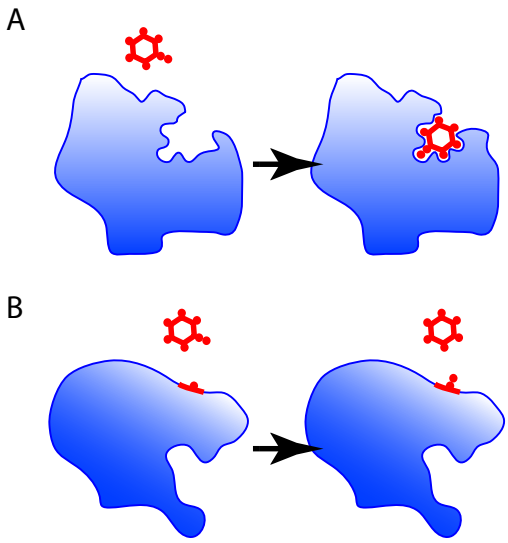

Figure 1.6 Mechanism of action of inositol pyrophosphates

The allosteric mechanism of action (A); where inositol pyrophosphates bind to an effector protein. This has been suggested for the *S. cerevisiae* protein Pho81 (Lee, Mulugu et al. 2007) as well as PH domains of the *D. discoideum* protein Crac (Luo, Huang et al. 2003) and the mammalian Akt (Chakraborty, Koldobskiy et al. 2010). Pyrophosphorylation of proteins (B); inositol pyrophosphates transfer their β-phosphate to target proteins (Saiardi, Bhandari et al. 2004). A pre-phosphorylated serine residue (Bhandari, Saiardi et al. 2007) in a negatively charged local environment (shown in red) can be pyrophosphorylated, in the presence of divalent cations. Figure and figure legend adapted from (Wilson, Livermore et al. 2013).

In fact IP_7 is able to competitively inhibit binding of mammalian PH domains to PIP_3, including the PH domain of Akt (PH_{Akt}) (Luo, Huang et al. 2003). In IP6K1 -/- MEFs there is an increased localisation of Akt to the membrane in response to IGF-1 treatment. Similarly, the proposed mechanism places IP_7 as a competitive inhibitor of PIP_3 for to the PH domain of Akt (Chakraborty, Koldobskiy et al. 2010). This study describes the inhibition of PDK1 phosphorylation of Akt by IP_7 with an IC50 of ~ 1μM in the presence of PIP_3 and 20 nM in the absence of PIP_3. However, since the cellular concentration of IP_7 in mammalian cells is typically 0.5 – 1.3 μM, it seems likely that Akt would be constitutively bound and inhibited by IP_7. This observation poses significant problems, as the membrane localisation of Akt upon PIP_3 production would require Akt to first release IP_7 before binding PIP_3 at the membrane.

In fact alternative studies of the PH domain of PDK1 measured its affinity for IP_7 to be less than that for IP_6 (Komander, Fairservice et al. 2004). Given that in most cells the concentration of IP_6 is far in excess of that of IP_7, it is unlikely that physiological concentrations of IP_7 will bind to PDK1. Finally, structural and spectral analysis of a PH domain bound to IP_3 suggests that positions 4 and 5 of the inositol ring are crucial to binding (Hyvönen, Macias et al. 1995). Therefore placing a pyrophosphate moiety at position 5, as is the case for the most commonly occurring form of IP_7 seems likely to disrupt the ability of the PH domain to bind IP_7.

The alternative mode of action for the inositol pyrophosphates depends more directly on the energy stored in the pyrophosphate moiety. Inositol pyrophosphates are able to take part in phosphotransfer reactions, donating their beta phosphate to target proteins (Saiardi, Bhandari et al. 2004). This process occurs in a non-enzymatic manner and involves the transfer of the beta phosphate onto a pre-phosphorylated serine located in acidic, serine-rich regions in a process termed pyrophosphorylation (Bhandari, Saiardi et al. 2007).

The evidence supporting this mode of action comes largely from the transfer of radioactivity from ^{32}P-labelled IP_7 (synthesised by incubating IP_6 with IP6k and ^{32}P ATP) to target proteins. Nsr1 was identified as the most abundant phosphoprotein in yeast extract treated with radio labelled IP_7. Nsr1, a ribosomal RNA processing enzyme, along with YGR130c, a protein of unknown function, are both phosphorylated by IP_7 *in vitro.* Both proteins contain a serine-rich, acidic region, a property shared by all targets of IP_7 phosphorylation to date.

Numerous targets have been identified, offering insight into the mechanism by which previously discussed roles of inositol pyrophosphates, including trafficking and primary metabolism, may be exerted. In mammalian cells, the β subunit of the AP-3 clathrin accessory protein (AP3B1) is a target of IP_7 mediated pyrophosphorylation (Azevedo, Burton et al. 2009). *In vitro* pyrophosphorylation of AP3B1 inhibits the interaction of the clathrin adaptor with its binding partner, motor protein KIF3a. By using release of Gag-containing vesicles as a measure of AP3B1-KIF3a trafficking, it was revealed that cells with reduced levels of IP_7 release more virus-like particles. The influence of AP3B1-KIF3a trafficking in cells indicates that the pyrophosphorylation-dependent inhibition of binding between these two proteins also occurs *in vivo*.

The metabolic phenotype of the *kcs1Δ* yeast, with dysfunctional mitochondria and yet elevated ATP, is dependent upon the upregulation of glycolytic genes, as shown by increased expression of GAPDH, PGK1 and alcohol dehydrogenase (ADH1) in this strain (Szijgyarto, Garedew et al. 2011). In fact the expression of these genes is regulated by inositol pyrophosphates via pyrophosphorylation. The expression of glycolytic genes in yeast is dependent upon the Gcr1, Gcr2 and Rap1 transcription factors. Gcr1 is pyrophosphorylated by IP_7, disrupting the interaction between Gcr1 and Gcr2 and inhibiting expression of glycolytic genes in WT cells. In *kcs1Δ* cells, lacking IP_7 there is more binding between Gcr1 and Gcr2, leading to increased

expression of glycolytic genes and elevated ATP (Szijgyarto, Garedew et al. 2011).

Despite the demonstration that numerous proteins, in a range of model organisms, can be modified in this way, direct biophysical evidence that this modification occurs *in vivo* remains absent.

1.2.5 Inositol pyrophosphates: concluding remarks

Regardless of their mode of action, the inositol pyrophosphates represent a fascinating and potentially rather large family of molecules. They exert an influence over a diverse array of cellular process and represent a substantial energetic investment from the cell. Nevertheless, much remains to be understood about how these molecules function and why they merit such investment. The work described here, which has sought to address these fundamental problems, has in no small part been informed by the yeast model. Whilst this model organism has proved exceptionally powerful, further analysis of the true physiological function and mode of action of these molecules will require additional models to supplement the pioneering work to date. The amoeba, *D. discoideum*, the organism in which the inositol pyrophosphates were discovered, offers an attractive system in which to probe these questions, as will be described in more detail in **section 1.5**

1.3 Inorganic polyphosphate (polyP)

1.3.1 PolyP: structure and synthesis

Inorganic polyphosphate (polyP) represents perhaps the simplest widely conserved polymer in biology (**Figure 1.7**). This molecule consists of chains of phosphate residues, ranging from tens to hundreds in length. Each phosphate is linked to the next by a “high-energy” phosphoanhydride bond, analogous to those found in ATP and inositol pyrophosphates (Kornberg 1995). Inorganic

polyphosphate has been identified across all kingdoms, from bacteria to mammals and, despite years of neglect, has recently begun to attract increased interest (Azevedo and Saiardi 2014).

The synthetic route from ATP to polyP has been elucidated in bacteria and some lower eukaryotes, however, the enzyme(s) responsible for its synthesis in mammalian cells remain elusive. Interestingly, polyP can also be synthesised in an abiotic manner, in conditions of extreme heat (Kulaev 1975). The fact that polyP can be synthesised in the absence of any organism has fuelled speculation that this molecule may have acted as a primitive energy source in prebiotic evolution. This proposed ancient role, although speculative, led to the coining of the faintly disparaging description of polyP as a “molecular fossil” (Kornberg 1995).

Regardless of the origins of polyP, four unrelated enzymes or enzyme complexes have been described to show polyphosphate kinase activity in modern organisms. The best characterised of these is the bacterial polyphosphate kinase (PPK), that is widely distributed across bacterial genomes. PPK1 was purified to homogeneity in 1990, revealing a 69 kDa protein functioning as part of a tetramer (Ahn and Kornberg 1990). Subsequent crystallisation of *E. coli* PPK1 refined this model to consist of a dimeric complex, in which each monomer possesses a positively charged channel that is predicted to interact with the elongating polyP chain (Zhu, Huang et al. 2005). Activation of PPK1 requires the autophosphorylation of histidine residues and, whilst PPK1 shows no structural similarities to other histidine kinases, it does share structural features with the eukaryotic enzyme phospholipase D (PLD), another enzyme activated by histidine phosphorylation (Kumble, Ahn et al. 1996, Zhu, Huang et al. 2005). Interestingly, the PPK1 enzyme can also be driven in reverse in conditions of high ADP and polyP, driving the synthesis of ATP, using polyP as a phosphate donor (Ahn and Kornberg 1990).

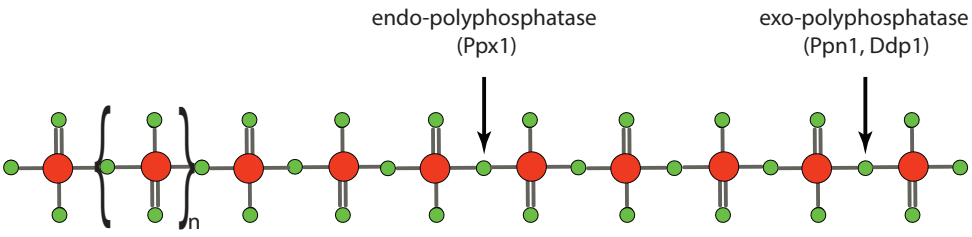

Figure 1.7 polyP structure and endo- and exo-polyphosphatase enzymatic site of action

This figure shows a schematic of the polyP polymer, where 'n' can range between tens and several hundreds. Endopolyphosphatases cleave internal polyP bonds, generating two shorter polyP chains. Exopolyphosphatases cleave the terminal phosphoanhydride bond, generating free phosphate and shortening the polymer by one phosphate at a time. Phosphorus, red circle; and oxygen, green circle. Figure and figure legend adapted from (Livermore, Azevedo et al. 2016).

A second polyphosphate kinase has been described in prokaryotic systems, the so-called PPK2 (Zhang, Ishige et al. 2002). This enzyme was identified by purification of activity found in lysates of *ppk1* null *P. aeruginosa.* Isolation of the protein by serial fractionation, followed by mass spectrometry revealed a 40.8 kDa protein. The protein, dubbed PPK2, is encoded by a 1074 bp gene widespread amongst prokaryotes. Characterisation of this protein reveals a number of differences in activity from PPK1. PPK2 is equally able to synthesise polyP using either ATP or GTP as substrate, in contrast to PPK1, which exclusively utilises ATP. This enzyme is also highly efficient in polyP-driven synthesis of GTP from GDP. Whilst this activity does not appear to extend to polyP-driven synthesis of ATP, the potency of GTP synthesis is far in excess of PPK2's polyP synthesising activity (75 fold)(Ishige, Zhang et al. 2002). Therefore, whilst this enzyme is capable of synthesising polyP it is possible that its physiological role is in fact to maintain cellular levels of GTP by utilising polyP. Homology searches have found this gene to be widely distributed in prokaryotic genomes, however no eukaryotic homologues have been identified (Zhang, Ishige et al. 2002).

In 2009 a eukaryotic polyphosphate kinase was identified in yeast (Hothorn, Neumann et al. 2009). This enzyme, Vtc4p, is part of the vacuolar transport chaperone (VTC) complex. This protein was identified when crystalisation of the VTC complex revealed a chain of electron density "winding through the tunnel domain" of the crystal. This VTC complex is predominantly located on the vacuolar membrane but can also be found on both the nuclear and plasma membrane. In each case the complex is orientated such that the catalytic domain faces the cytosol. The synthesis of polyP by this complex is coupled with its translocation across the membrane and in fact accumulation of polyP in the cytosol exerts a toxic effect on the cell (Gerasimaitė, Sharma et al. 2014).

Complexes homologous to the VTC complex have been identified in other simple eukaryotic systems, including the Trypanosome (Fang, Rohloff et al. 2007). Ablation of the TbVT1 protein, the trypanosome Vtc4 homologue, by RNAi results in a decrease in polyP in these cells. Despite the conservation of the VTC complex between yeast and trypanosomes, no such complex can be found in the genomes of multicellular higher eukaryotes. To date, although polyP has been widely reported in mammalian cells (Morrissey, Choi et al. 2012), no polyphosphate kinase has been identified.

One of the few other eukaryotes to possess an annotated polyphosphate kinase is the amoeba, *D. discoideum.* The genome of this amoeba encodes a bacterial-like PPK enzyme, known as DdPPK1. This gene, most likely acquired by horizontal gene transfer from bacteria, encodes a 1053 amino acid protein, which is homologous to the *E. coli* PPK1 (Zhang, Gómez-García et al. 2005). *D. discoideum* is also notable for the presence of a second polyphosphate kinase in its genome. This second enzyme complex, described as DdPPK2, is a tetrameric complex of three actin-related proteins (Gómez-García and Kornberg 2004). In a remarkably unique enzymatic process, this complex synthesises polyP as it polymerises itself to form actin-like fibrils. The conservation of homologous proteins in mammalian cells has led to some speculation that this enzymatic activity may be conserved in higher eukaryotes (Hooley, Whitehead et al. 2008). The synthesis of polyP in *D. discoideum* will be explored in more detail in **section 1.5** and **Chapter 5**.

PolyP is degraded by polyphosphatases, of which there are two classes, exopolyphosphatases, which degrade polyP by removing the terminal phosphate from the chain, and endopolyphosphatases, which cleave the internal bonds of the chain (**Figure 1.7**). The best-characterised exopolyphosphatase is the yeast protein Ppx1p, a member of the superfamily of phosphoesterases. This enzyme is able to processively cleave the terminal

phosphate from a polyP chain, degrading as far as the pyrophosphate moiety (Wurst and Kornberg 1994). Although the polyP kinase is yet to be identified in mammalian cells, a PPX homologue has been annotated in the form of h-Prune.

Endopolyphosphatases represent the second class of polyphosphatases. The yeast protein PPN1 is encoded by a 2025 bp gene, however the gene product must be proteolytically cleaved before it is active (Shi and Kornberg 2005). The catalytically active form of PPN1 resides in the vacuole and comprises a homotetramer of 35 kDa subunits. Each subunit is derived from the cleavage of the so-called prePPN1, a 78 kDa precursor protein (Shi and Kornberg 2005). The exact post translational processing required to generate an active PPN1 is unclear, hence comparatively little is known about this protein other than its cellular localisation to the vacuole. Despite being best known as an endopolyphosphatase it appears that in certain conditions, PPN1 can also act as an exopolyphosphatase(Andreeva, Trilisenko et al. 2015).

Whilst PPN1 is limited to yeast (Azevedo and Saiardi 2014), a second, more widespread, endopolyphosphatases has already been introduced in the form of the DIPPs and Ddp1. This enzyme has already been introduced for its ability to degrade the inositol pyrophosphates, however this highly promiscuous enzyme is also able to degrade polyP (Lonetti, Szijgyarto et al. 2011). As noted previously, DIPPs are widely conserved between yeast (Ddp1) and mammalian cells (DIPPS 1-4). The ability of a single enzyme to degrade both the inositol pyrophosphates and polyP is notable and the links between these phosphate-rich molecules will be explored in more detail later.

1.3.2 PolyP: fluctuations and turnover

PolyP is highly abundant in many bacteria as well as the yeast *S. cerevisiae,* where up to 20% of the dry mass is made up of polyP. Absolute quantification of polyP is challenging as the variable chain length of the polymer means that

concentration must be expressed in terms of free phosphate. By this measure, polyP is estimated to be in the millimolar range in both yeast and bacteria. Meanwhile the levels observed in mammalian cells are far lower, 20-120μM, with chain length of polymers also generally reduced (Kumble and Kornberg 1995). Nevertheless, several examples of accumulation of polyP have been described in bacteria. Nutrient starvation, osmotic stress and nitrogen starvation have all been shown to induce rapid accumulation of polyP in *E. coli* (Ault-Riché, Fraley et al. 1998). In yeast, phosphate starvation causes a rapid decrease in polyP, which can be restored upon addition of phosphate to the media (Trilisenko, Andreeva et al. 2003).

1.3.3 Roles of polyphosphate

Despite the unflattering term “molecular fossil”, polyP has been implicated in a wide range of cellular functions. There are several descriptions of enzymes that are able to utilise the energy stored in the phosphoanhydride bonds of polyP to drive biochemical processes. PPK for instance can be driven in reverse using polyP to reconstitute ATP by transferring a phosphate onto ADP (Ahn and Kornberg 1990). Furthermore, certain bacterial glucokinase enzymes are able to use polyP in place of ATP to phosphorylate glucose (Hsieh, Shenoy et al. 1993). More recently, the human mitochondrial protein C5orf33 has been shown to possess NAD kinase activity and is able to use both ATP and polyP to phosphorylate NAD, generating $NADP^+$ (Ohashi, Kawai et al. 2012).

In light of the large amounts of energy stored in a polyP polymer, its utility in both regenerating ATP and use by some enzymes to drive biochemical reactions, it is tempting to consider polyP as an energy source. In cells where polyP levels can exceed the steady state level of ATP, as is the case in the stationary phase of *E. coli* growth, this is a particularly attractive hypothesis. However, whilst there is no doubt that polyP is able to drive certain biochemical processes, in reality the turnover of ATP is so rapid that it could only be

sustained for a matter of seconds by physiological levels of polyP (Kornberg, Rao et al. 1999). Therefore, it does seem likely that in polyP acts as a major source of energy under most normal conditions.

Aside from acting as an energy source, another intuitive role of polyP is its ability to act as a reservoir of free phosphate (Pi) and thus a Pi buffer. The synthesis and degradation of polyP allows the rapid and tuneable regulation of free Pi. The availability of free phosphate is of upmost importance for primary metabolism and synthesis of ATP. The extremely anionic nature of polyP also makes it a strong chelator of divalent cations. In the cell this is primarily Mg^{2+}, however Ca^{2+} can be chelated with similar efficiency by polyP. Thus the synthesis or degradation of polyP can also have a dramatic effect on the cellular availability of these cations (Kornberg 1995).

This polymer has also been shown to play a role in more specific functions, including the virulence of numerous human pathogens. Deletion of PPK1 in the opportunistic pathogen *Pseudomonas aeruginosa* renders the bacteria unable to form biofilms. This *ppk* null strain is defective in production of virulence factors and less able to sustain infections (Rashid, Rumbaugh et al. 2000). In fact, numerous pathogenic bacteria with reduced levels of polyP, including *Salmonella* and *Shigella* species, have been shown to show similar reduction in pathogenicity (Moreno and Docampo 2013).

The effect of polyP on pathogenicity has also been documented in certain eukaryotic pathogens including *Trypanosoma brucei.* PolyP accumulates in an organelle known as the acidocalcisome in Trypanosomes. Acidocalcisomes are acidic, calcium and phosphate-rich organelles that were first described in Trypanosomes. Subsequently, orthologous compartments have been identified from bacteria to man (Docampo and Moreno 2011). Failure to accumulate polyP in the acidocalcisomes results in Trypanosomes with reduced pathogenicity

(Moreno and Docampo 2013). Despite conservation between prokaryotic or eukaryotic microorganisms the role of polyP in pathogenicity is not well understood.

In mammalian cells, the dense granules of platelets share many properties with the acidocalcisome. It is perhaps unsurprising therefore that the dense granule is also rich in polyphosphate (Ruiz, Lea et al. 2004). Patients displaying dense granule storage disorders, commonly associated with bleeding conditions, have lower levels of polyP in platelets (Hernández-Ruiz, Sáez-Benito et al. 2009).

Platelet activation induces the release of the contents of the dense granules, including polyP into the plasma. The release of polyP into the plasma has been shown to play an important role in the clotting cascade, directly activating plasma protease factor XII (Müller, Mutch et al. 2009). These and other studies have placed polyP as a potent modulator of platelet function and blood clotting, although the mechanism by which polyP exerts these effects is again unclear (Morrissey, Choi et al. 2012).

Whilst the molecular mechanism by which polyP exerts its influence on both virulence and blood clotting is unclear, some molecular interactions of polyP have been described. In fact, surprisingly, this highly charged polymer has also been implicated in the formation of membrane pores in both prokaryotic and eukaryotic cells.

The presence of non-proteic membrane channels is well documented in bacteria. These channels control cation membrane transport and are comprised of the polyester, poly-(*R*)-3-hydroxybutryrate (PHB) and polyP-Ca^{2+} (Azevedo and Saiardi 2014). In mammalian cells, polyP is associated with the membrane mitochondria permeability transition pore (mPTP) a multiprotein pore complex found in the inner leaflet of the mitochondrial membrane (Seidlmayer, Blatter et

al. 2012). The function of the mPTP is poorly understood, as is the role of polyP in its formation and maintenance. It is postulated that the presence of polyP is important for the ion conductance of these pores (Abramov, Fraley et al. 2007), indicating a further role for control of the cellular levels of ions by polyP.

In addition to its role in mitochondrial ion transport, polyP metabolism has been linked to primary metabolism by a genome-wide screen in yeast (Freimoser, Hürlimann et al. 2006). This screen found that in yeast, 225 genes were involved with the maintenance of polyP levels. In each case, deletion of the identified gene alters polyP levels. This was most commonly associated with alterations in primary metabolism (Freimoser, Hürlimann et al. 2006), offering further evidence linking polyP to the energy status of cells.

Recent work has illuminated some of the molecular interactions of polyP, potentially offering insight into how this polymer exerts its varied effects. In fact, polyP is able to act as a primordial protein-folding chaperone, showing an exceptional ability to protect protein folding in bacteria exposed to extreme denaturing conditions (Gray, Wholey et al. 2014). In response to treatment with protein unfolding stresses, for example hypochlorus acid (HOCl), *E. coli* accumulate polyP. The accumulation of polyP functions to prevent protein aggregation and protect against protein unfolding. Mutants with reduced polyP are less resistant to HOCl treatment and display higher levels of protein aggregation (Gray, Wholey et al. 2014). *In vitro,* polyP is able to act as a general molecular chaperone, stabilising the folding and thermal stability of numerous proteins, both prokaryotic and eukaryotic in origin. It is hypothesised that this remarkable property of polyP may be due to its ability to perform the role of molecular scaffold and stabilise secondary motifs. An alternative hypothesis is that the ionic interaction of the negatively charged phosphate residues, as well as the positive charge of associated cations, may exert a stabilising effect (Gray, Wholey et al. 2014).

This potentially universal property of polyP may offer insight into many of the functions described above. Whilst so far this role has only been described in prokaryotic cells, the simplicity and conservation of polyP structure is coherent with a similar role in eukaryotic cells.

In addition to its ability to act as a protein-folding chaperone, polyP is also able to post translationally modify proteins (Skorko 1989, Azevedo, Livermore et al. 2015). This process, termed polyphosphorylation, sees the addition of chains of polyphosphate to lysine residues attached in a non-enzymatic manner. Surprisingly this modification affects the pyrophosphorylation target Nsr1p as well as its interacting partner Top1p. The functionality of Top1p, its ability to relax supercoiled DNA, is negatively regulated by polyphosphorylation. Despite the non-enzymatic nature of this modification, regulation occurs via both the abundance of polyP and degradation of the modification. Polyphosphorylation of Nsr1p and Top1p varies according to the abundance of polyP and treatment with Ppx1 degrades the modification. Thus Ppx1 is not only an exopolyphosphatase, but also a protein polyphosphatase (Azevedo, Livermore et al. 2015).

Although no consensus sequence has been identified for this modification, both targets characterised to date are modified in a highly acidic region, enriched in serines and lysines. These domains, termed poly acidic, serine (S) and lysine (K) (PASK) domains are commonly found in nuclear proteins. It interesting to note, therefore that, contrary to previous reports, a large pool of polyP is located in the yeast nucleus, approximately 20% of the total amount. Thus, the abundance of effector (polyP) and potential targets (PASK domain containing proteins) in the nucleus could indicate that this modification represents a major regulatory mechanism in nuclear signalling (Azevedo, Livermore et al. 2015).

The results described above are indicative of a recent resurgence of interest in this molecule, which although ancient in origin is utterly contemporary in its biological significance. Once more, the yeast model has been an exceptionally powerful tool to study the polyP. In the absence of a mammalian polyP kinase to date, yeast represents one of very few genetic models to study polyP function in eukaryotic cells. Nevertheless, the VTC complex responsible for polyP synthesis in yeast is not conserved in higher eukaryotes and thus the development of additional genetic models will be essential to shed further light on the role of this fascinating molecule.

1.4 Links between inositol pyrophosphates and inorganic polyphosphate (polyP)

As introduced throughout this chapter thus far, numerous links exist between the structure, metabolism and functions of the inositol pyrophosphates and polyP. This should, perhaps, not come as a surprise given that they represent two of the most phosphate rich molecules in the cell. As a result, their involvement with phosphate metabolism and homeostasis is to be expected. A number of the concepts and phrasing introduced in this section draw from the recently published review “Phosphate, inositol and polyphosphates” (Livermore, Azevedo et al. 2016).

In yeast the cellular levels of inositol pyrophosphate and polyP are intimately coupled (Auesukaree, Tochio et al. 2005). The *kcs1Δ* yeast strain possesses almost undetectable levels of inositol pyrophosphates and a dramatically reduced level of polyP. Similarly the *vip1Δ* strain has elevated levels of IP_7 and correspondingly elevated levels of polyP (Lonetti, Szijgyarto et al. 2011). The mechanism by which this link is maintained is unknown.

In yeast, the Pho regulon represents a key pathway for phosphate sensing in *S. cerevisiae.* This regulon, consisting of numerous genes controls the transcription of hundreds of genes in response to phosphate abundance. A cyclin CDK complex, Pho80-Pho85 phosphorylates the Pho4 transcription factor (Kaffman, Herskowitz et al. 1994), causing its export from the nucleus (O'Neill, Kaffman et al. 1996). In conditions of phosphate starvation, the Pho80-Pho85 complex is inhibited by Pho81, resulting in the accumulation of Pho4 in the nucleus and a dramatic transcriptional response. Genetic perturbations to the Pho-regulon modulate levels of polyP, but do not affect the levels on inositol pyrophosphates. However, 1PP-IP_5, synthesised by Vip1p, is able to allosterically inhibit the Pho80-Pho85-Pho81 complex, altering the transcription of hundreds of genes (Lee, Mulugu et al. 2007). Whilst the Pho-regulon is restricted to *S. cerevisiae*, the interplay between inositol pyrophosphates and polyP metabolism is striking.

1.4.1 Phosphate metabolism

Phosphorus, present in its phosphate (PO_4^{3-}) form, is one of the most abundant elements in living cells. Its importance can be inferred from the range of molecules and functions with which it is associated. Phosphate plays a crucial structure role in the backbone of nucleic acids DNA and RNA. Its covalent attachment to proteins represents the most common signalling modality (Manning, Whyte et al. 2002), found from prokaryotic to eukaryotic cells. Furthermore, the energy stored in the phosphate-phosphate phosphoanhydride bond, present in ATP, inositol pyrophosphates and polyP, is the most common energy store in biology. Life as we know it depends upon phosphate (Elias, Wellner et al. 2012).

Thus, it is evident that the cellular abundance of Pi must be tightly controlled. A number of specific transporters regulate free phosphate uptake, controlling its

concentration in this way (Dick, Dos-Santos et al. 2014). However, both polyP and inositol pyrophosphates feed into this control.

As described above, the synthesis and degradation of polyP offers a rapid buffering system for free Pi. In turn the inositol pyrophosphates are able to regulate the level of polyP in yeast cells. In fact, links between phosphate metabolism and inositol pyrophosphates are conserved throughout biology. For example, IP6K2 was first identified as a regulator of phosphate uptake in *Xenopus laevis* oocytes before even IP6K was cloned. Injection of mammalian cDNA into the *Xenopus* oocyte was shown to induce the uptake of phosphate from the media, thus the gene was called Pi Uptake Stimulator (PiUS)(Norbis, Boll et al. 1997). It was noted at the time that this gene does not encode a transmembrane domain and therefore seemed unlikely to be a canonical phosphate transporter. Nevertheless, the mechanism by which phosphate uptake is achieved remains unknown. However, identification of PiUS as an enzyme, IP6K2 (Schell, Letcher et al. 1999), capable of synthesising IP_7 seems to suggest a role for the inositol pyrophosphates in the control of Pi uptake.

In addition, IP6K3 was one of only seven genes identified by genome-wide associated study (GWAS) to affect the level of phosphate in human blood serum (de Boer, Rue et al. 2009). Taken together these data point towards a strong relationship between inositol pyrophosphates and phosphate homeostasis at both the cellular and organismal level.

1.5 Inositol pyrophosphates and inorganic polyphosphate in *D. discoideum*

Having introduced, in a general way, the structure, synthesis and functions of the inositol pyrophosphates and polyP it is now necessary to examine the

current understanding of these molecules in the chosen model for this work, the social amoeba (myxamoeba) *D. discoideum.*

D. discoideum is a member of the *Dictystelid* family of social amoeba, so-called due to their fascinating ability to grow and divide in a unicellular, amoeboid manner in conditions of high nutrients. Upon deprivation of nutrients, these cells undergo a remarkable developmental process during which cells first aggregate in their thousands, forming a motile “slug” or “grex”, before culminating in a fruiting body (sporocarp) (**Figure 1.8**). The sporocarp consists of two major cell types, the spore cells, which are able to germinate upon availability of nutrients and the stalk cells, which perish during the formation of the fruiting body in an act of extraordinary cellular altruism.

D. discoideum was developed as a laboratory model in the 1930s, with much early work focusing on transition to multicellularity and cell fate determination (Williams 2010). Since then the amoeba has become an influential model in to study chemotaxis and many other cellular processes (Williams 2010).

The *D. discoideum* genome is haploid and approximately 35 Mb in length, comprising six chromosomes ranging between 4 and 8 Mb. At 78% A+T, the genome is remarkably A+T rich and has one of the highest A+T biases of any known organism. Introns are present in many, but not all, genes and are generally <100 base pairs in length. Few genes have more than 3 introns (Eichinger and Noegel 2003).

Wild, soil dwelling amoeba are only able to grow when provided with bacteria as a food source, thus the majority of the work in this organism has used the axenic (AX) strains. Axenic strains are able to grow in rich liquid media, either as adherent cells or in shaking culture. It is these axenic strains, most commonly AX2, that have been used to study many cellular processes, including

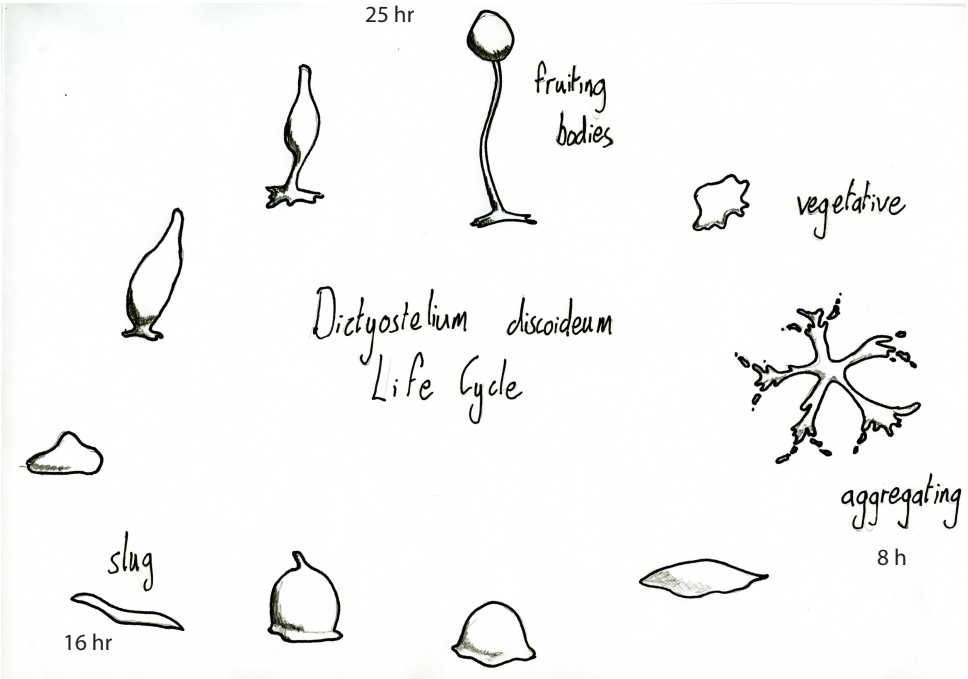

Figure 1.8 *D. discoideum* lifecycle

D. discoideum exist as unicellular amoeba during vegetative growth. Upon deprivation of nutrients, cells begin to aggregate in response to cAMP. Aggregating cells form multicellular mounds, which then develop into motile slugs, or “grex”, consisting of tens to hundreds of thousands of cells. These slugs ultimately mature, into fruiting bodies, consisting of spore cells (~80%) and stalk cells (~20%). Stalk cells die during the formation of the fruiting body, whilst spore cells are able to germinate into unicellular amoeba upon availability of nutrients (Williams 2010).

cell-fate determination (Kay, Flatman et al. 1999), chemotaxis (Kay, Langridge et al. 2008) and transcriptional regulation (Corrigan and Chubb 2014). It was the AX2 strain of *D. discoideum* that the inositol pyrophosphates were first identified in 1993 (Stephens, Radenberg et al. 1993).

1.5.1 Inositol pyrophosphates in *D. discoideum*

As described above this organism played an important role in the discovery of the inositol pyrophosphates. Both the discovery and dramatic physiologic accumulation of inositol pyrophosphates in *D. discoideum* have already been discussed. However, these do not represent the sole contributions of *D. discoideum* to field. In fact, it was in this organism that the direct, stepwise phosphorylation of *myo*-inositol to IP_6 was first described (Stephens and Irvine 1990). This study outlined the precise metabolic pathway leading to production of IP_6 in *D. discoideum,* progressing via phosphorylation on position 3, followed by position 6, then 4, then 1, then 5 and finally position 2. The presence of other isomers of IP_5, aside from the $I(1,3,4,5,6)P_5$ was shown to be due to rapid dephosphorylation of IP_6 rather than an alternative route of synthesis.

This work was corroborated by the observation that the deletion of the single PLC gene in the *D. discoideum* induced only a slight decrease in the level of $I(1,4,5)P_3$ detected (Drayer, Van der Kaay et al. 1994), suggesting that normal levels of inositol phosphates are obtained by a pathway independent of lipid phosphoinositides and PLC activity. In fact the $I(1,4,5)P_3$ is obtained by the dephosphorylation of the $I(1,3,4,5,6)P_5$ formed via the pathway described above (Dijken, Haas et al. 1995). This dephosphorylation activity could also be detected in a single enzyme purified from rat liver cells and attributed to an enzyme now known as MIPP (Dijken, Haas et al. 1995). These often overlooked data are in direct contrast to yeast, where the PLC1 gene is required for synthesis of higher inositol phosphates and *plc1Δ* yeast contain no detectable IP_6 (York, Odom et al. 1999). With at least 13 PLC genes encoded in mammalian

cells, it is not known whether a true *plc*-null mammalian cell would possess soluble inositol phosphates.

Another difference noted between structure and synthesis of inositol pyrophosphates between *D. discoideum* and *S. cerevisiae* is the isomeric form of IP_8 (**Table 1.1**). The *in vitro* activities of Kcs1p and Vip1p point towards yeast possessing the 1,5$(PP)_2$-IP_4 isomer of IP_8. However, NMR analysis of *D. discoideum* IP_8 defines this as the either the 4,5$(PP)_2$-IP_4 or 5,6$(PP)_2$-IP_4 isomer (Laussmann, Eujen et al. 1996, Albert, Safrany et al. 1997). This is to date, the only *in vivo* purified IP_8 that has been analysed by NMR. Nevertheless, the NMR data is validated by the presence of a very strong kinase activity towards 6PP-IP_5 in *D. discoideum* extract. The identity of this kinase is unclear, however, a partial purification was able to identify that a 40 kDa protein was responsible for this activity (Laussmann, Reddy et al. 1997).

It is possible that the recombinant *E. coli* purified kinases used to define the isomers synthesised by Kcs1p and Vip1p behave differently to their endogenously expressed counterparts. Alternatively, it may represent a genuine difference between the isomeric form of IP_8 found in the amoeba. The effect of such a difference to the physiology of these molecules would likely depend on the mode of action in which they are involved. Phosphotransfer reactions would be unlikely to be affected by placing the pyrophosphate on a different position on the ring, whilst allosteric interactions and receptor binding could be dramatically affected.

Finally, the most recent work on the inositol pyrophosphates in *D. discoideum*, now over ten years old, identified these molecules as regulators of the developmental response (Luo, Huang et al. 2003). An IP6K null strain, hereafter referred to as *ip6k** was generated in this study. This strain possesses no detectable inositol pyrophosphates, as determined by HPLC. The speed of

aggregation of this mutant strain is slightly increased. This increased speed of aggregation is due to the absence of IP_7-mediated inhibition of crac localisation to the membrane. IP_7 achieves this inhibition by competing for the binding of the PH-domain of crac with PIP_3 as described previously (Luo, Huang et al. 2003).

It is interesting to note once again, that genetic deletion of PIP_3 signalling does not impair the ability of *D. discoideum* to respond to cAMP (Hoeller and Kay 2007, Hoeller, Bolourani et al. 2013, Nichols, Veltman et al. 2015). This observation suggests PIP_3 plays a negligible role in directed chemotaxis in the amoeba and raises uncertainty about the mechanism of action of IP_7 proposed by Luo et al. (Luo, Huang et al. 2003)

1.5.2 PolyP in *D. discoideum*

The amoeba has also been influential as a model to study polyP. The first description of this polymer in *D. discoideum* was by Gezelius and colleagues in the 1970s (Gezelius 1974). This work described a low abundance of polyP in the amoeba, before undergoing a five-fold increase during development. The presence of polyP in the spore was later confirmed by ^{31}P NMR analysis, alongside substantial levels of IP_6 (Klein, Cotter et al. 1988).

D. discoideum was also the first eukaryotic organism in which a polyphosphate kinase was identified. As described in **section 1.3**, the amoeba possesses a bacterial-like PPK1 as well as a tetrameric complex known as DdPPK2, unrelated to the bacterial PPK2.

The PPK1 gene was likely acquired through a horizontal gene transfer event from the bacteria on which this amoeba feeds. The PPK1 enzyme shows 30% identity and 51% similarity to its *E. coli* counterpart (Zhang, Gómez-García et al. 2007), however the homology is limited to the C terminal portion of the amoeboid enzyme. The PPK1 gene encodes a 1050 amino acid protein,

compared to just 688 aa in *E. coli*. The N terminal portion of the PPK1 enzyme represents a novel protein fold with no clear homologues and no annotated function. It is, however, required for enzymatic activity (Zhang, Gómez-García et al. 2007).

A knock out strain of PPK1 has been generated previously (Zhang, Gómez-García et al. 2005). This strain was found to show defects in development, predation and cytokinesis. The mutant strain grows slower on bacterial lawns, but not in rich axenic media. This defect was shown to stem from a defect in phagocytosis as demonstrated by reduced uptake of bacteria. Furthermore, this mutant is slower to form fruiting bodies, but displays no defect in spore germination. The PPK1 mutant also displays a defect in cytokinesis, with significantly more multinucleate cells in the mutant compared to WT (Zhang, Gómez-García et al. 2007).

An additional, interesting link between polyP and predator-prey relationship was observed by examining the growth of the amoeba on an alternative bacterial substrate, *P. aeruginosa* (Zhang, Gómez-García et al. 2005). This bacterial strain does not support *D. discoideum* growth, however deletion of the PPK1 gene in the bacteria allows the amoeba, both WT and PPK1 null, to grow on this bacteria, suggesting polyP is important to the fitness of *P. aeruginosa*.

Despite genetic disruption of the PPK1 gene the amoeba strain generated by Zhang et al. retains approximately 5% of WT polyP kinase activity and residual levels of polyP, estimated at between 20-50% of WT (Zhang, Gómez-García et al. 2005). The presence of polyP in this strain can be attributed to the presence of additional polyP kinase, the PPK2 complex. This complex was purified from WT AX2M1 membranes (Gómez-García and Kornberg 2004). The polyP-synthesising properties of this actin-related complex are inhibited by addition of phalloidin and are concurrent with the formation of actin-like filaments. The

genes encoding this remarkable enzyme complex were not cloned, nor deleted, making it difficult to estimate the relative contribution of these enzymes to cellular polyP concentrations.

As in Trypanosomes, *D. discoideum* accumulates polyP in an organelle analogous to the acidocalcisome (Marchesini, Ruiz et al. 2002). Hyposmotic stress causes the interaction of this organelle with the contractile vacuole, indicating a functional linkage between the two organelles and a possible role for polyP in the osmotic regulation of the amoeba (Marchesini, Ruiz et al. 2002).

1.6 Rationale

Having outlined the current understanding of both inositol pyrophosphates and polyP, the aim of this project is to develop *D. discoideum* as a model to further study both these molecules. Whilst the amoeba is of great historical significance in the inositol pyrophosphate field it has been somewhat neglected in recent years in favour of the yeast model. Study of inositol pyrophosphates in yeast offers numerous advantages including ease of genetic manipulation and that cells can be readily labelled with ^{3}H-inositol. Consequently, this organism has been exceptionally informative and influential in the field to date.

However, the simplicity of the yeast model is not without its downsides. The yeast genome encodes just four inositol phosphate kinases (**Table 3.1**). Whilst these are well conserved in mammalian systems, the mammalian genome encodes additional inositol phosphate kinase, such as ITPK1, that do not feature in the yeast genome. The *D. discoideum* genome encodes seven inositol phosphate kinases, including a homologue to mammalian ITPK1 (**Table 3.1**).

Furthermore, in yeast, the synthesis of inositol phosphates (and therefore inositol pyrophosphates) is entirely dependent upon the phospholipase C-

medicated cleavage of PIP_2. It remains unclear if this is the case in higher eukaryotes, including mammals. Certainly in *D. discoideum* the situation is rather different. A direct, step-wise phosphorylation of inositol appears to be the primary route of synthesis in the amoeba as demonstrated by the lack of phenotype of the *plc1* strain. However, the enzymes responsible for these activities have not been identified.

Whilst the amoeba is evolutionarily distant from both yeast and mammalian cells, its genome size and conservation of kinases, positions it as an ideal intermediate between these two systems. Alongside these advantages, are numerous technical considerations making the amoeba an attractive model. Axenic strains can be grown in high quantities with ease, making biochemistry straightforward. Furthermore, the developmental life cycle allows the effect of these molecules on a robust and reproducible developmental process to be studied. Finally, the high rate of homologous recombination in *D. discoideum* allows the relatively simple deletion of genes (Williams 2010).

Perhaps the most important technical consideration, however, is the high level of inositol pyrophosphates and their precursor IP_6 in these cells. Whilst the amoeba is not readily labelled with ^{3}H-inositol (Saiardi lab observation), recent technological developments in PAGE technology have allowed the resolution and detection of unlabelled inositol pyrophosphates (Losito, Szijgyarto et al. 2009). This technique has been applied to *in vitro* studies, however the high levels of inositol phosphates in the amoeba offer the potential to analyse the inositol phosphate profile in unlabelled cell extracts for the first time (Pisani, Livermore et al. 2014)(See Chapter 3, **Figure 3.1**).

This improved PAGE technology also allows the resolution and detection of unlabelled polyP (Lonetti, Szijgyarto et al. 2011). As described above, *D. discoideum* is one of the few eukaryotic models in which a polyphosphate

kinase has been identified. Thus applying PAGE technology to polyP metabolism in *D. discoideum* is an equally attractive aim.

Together these characteristics make the amoeba an ideal model organism in which to study the synthesis and metabolism of the inositol pyrophosphates and polyP as well as the relationship between these phosphate-rich molecules. Therefore the aim of this project will be employ a genetic and biochemical approach to better characterise the synthesis, functions and interactions of these molecules in *D. discoideum*.

2. Materials and Methods

2.1 Bacteria

2.1.1 Bacterial growth media

E. coli was grown in LB (Luria-Bertani) media [1% Bacto-tryptone (Formedium^{TM}), 0.5% yeast extract (Formedium^{TM}), 10 mM NaCl] at 37°C, 220 rpm or on agar plates(LB media supplemented with 2%) agar. Transformed bacteria were selected on ampicillin at 100 μg/ml (stock 100 mg/ml in H_2O). Blue white screening of colonies was performed by supplementing LB agar plates with 20 μg/ml X-Gal (stock 20 mg/ml in DMF, stored at -20°C and protected from light) and 0.1 mM Isopropyl β-D-1-thiogalactopyranosid (IPTG) (stock 0.1 M in H_2O, filter sterilised). These plates will be referred to as IPTG, X-gal, Amp LB plates hereafter.

Glycerol stocks were prepared by mixing in a 1:1 ratio saturated bacterial culture, with 50% sterile glycerol. Stocks were stored at -80°C.

2.1.2 *E. coli* strains

E. coli

DH5α: F- endA1 glnV44 thi-1 relA1 gyrA96 deoR nupG lacZdeltaM15 hsdR17

DH5α: NEB® 5-alpha Competent E. coli (High Efficiency)

K. aerogenes

2.1.3 Competent cells

Chemical competent *E. coli* were prepared using a protocol modified from (Hanahan 1983). DH5α *E. coli* were streaked on an LB agar plate. A single colony was picked and grown overnight in LB media. The culture was diluted to an $O.D._{600}$ of 0.01 and incubated at 37°C, 220 rpm until an $O.D._{600}$ of 0.6 was reached. The bacteria were placed on ice for 15 min and collected by centrifugation at 2800 rpm for 10 min. Bacteria were resuspended in 0.4 vol of

ice cold TfbI and incubated on ice for an additional 15 min. Cells were collected by centrifugation (as above) and resuspended in 0.04 volumes of ice cold TfbII. Aliquots of 200 μl were frozen in dry ice and ethanol bath, then stored at -80°C.

TfbI

Compound	**Final Concentration**
Potassium Acetate	30 mM
Rubidium chloride	100 mM
Calcium chloride	10 mM
Manganese chloride	50 mM
Glycerol	15% (v/v)

The pH was adjusted to 5.8 using dilute acetic acid. The buffer was filter sterilised and stored at 4°C.

TfbII

Compound	**Final Concentration**
MOPS	10 mM
Rubidium chloride	10 mM
Calcium chloride	75 mM
Glycerol	1% (v/v)

The pH was adjusted to 6.5 using dilute sodium hydroxide. The buffer was filter sterilised and stored at 4°C.

2.1.4 *E. coli* transformation

100 μl chemical competent cells were mixed with 100 ng plasmid DNA or 7μg ligation mixture. Cells were incubated on ice for 30 min before heat shock at 42°C for 45 s. Cells were then chilled on ice before incubation at 37°C, 220 rpm

for 45 min in pre-warmed LB media. Transformants were selected on LB agar plates containing 100 μg/ml ampicillin overnight.
Ligations using Promega Ltd., PGEM T- easy cloning vectors vector were selected using IPTG, X-gal, Amp LB plates.

2.2 Manipulation of nucleic acids

All routine nucleic acid manipulations were performed using either Qiagen Ltd. or Promega Ltd. kits according to manufacturer's instructions. Restriction enzymes were purchased from New England Biolabs, Inc (NEB). T4 DNA ligase was purchased from either Roche Diagnostics or TaKaRa Co., Ltd. Small scale DNA purification were made using Qiagen Ltd. Mini kits, according to manufacturer's instructions. Large scale DNA purifications were performed using Promega Ltd. PureYield™ plasmid Midiprep kit according to manufacturer's instructions. Qiagen Qiaquick™ Gel Extraction Kit and Qiaquick™ PCR Purification Kits were used for purification of DNA from agarose gels and PCR product respectively.

2.2.1 Agarose gel electrophoresis

DNA fragments were resolved in 0.7-1% agarose gels containing 1x TAE buffer (40 mM Tris Acetate, 1 mM EDTA) and 0.1 μg/ml ethidium bromide. Gels were run in 1x TAE buffer at 30-90 V. A 1 kb DNA ladder (NEB) was loaded as a size marker. DNA samples were mixed with 6x DNA loading buffer (either: 10 mM Tris-HCl pH 8.0, 1 mM EDTA pH 8.0, 50% (vol/vol) glycerol and 0.005% orange G or 10 mM Tris-HCl pH 8.0, 1 mM EDTA pH 8.0, 50% (vol/vol) glycerol and 0.005% bromophenol blue) prior to loading.
RNA fragments were resolved in 1% agarose gels containing 1% MOPS, made with DEPC treated water. These gels were supplemented with 5% (vol/vol) 37% formaldehyde. Gels were run in 1x MOPS at 60 V. RNA samples were mixed with an equal volume of RNA loading buffer (75% (vol/vol) formamide, 20% (vol/vol) 37% formaldehyde and 5% DNA and 0.001% ethidium bromide), they were then boiled for 5 min, before loading on the gel.

2.2.2 Restriction enzymes

Restriction digests were performed according to manufacturer's instructions. Typically reactions were performed in 40 μl volumes, including 4 μl 10x buffer (NEB), 10-20 units of enzyme (NEB) and 1-3 μg DNA. Reactions were incubated at 37°C from 2-4 h.

2.2.3 DNA ligations

Digested plasmid vectors (typically 50 ng) were mixed with inserts at a 1:3 molar ratio in a reaction volume of 10-15 μl, containing 5 units of DNA ligase (Roche/TaKaRa). Reactions were incubated at 16°C overnight or for 1 h at room temperature (RT).

PCR products were ligated into Promega Ltd., PGEM T- easy cloning vectors without prior digestion using a Promega Ltd., T4 DNA ligase.

2.2.4 Polymerase Chain Reaction (PCR)

Oligonucleotide primers were purchased from Integrated DNA Technologies, Inc. and resuspended in nuclease free water at a concentration of 100 picomoles/μl. TaKaRa Ex Taq DNA polymerase was used to amplify DNA for both cloning purposes and for colony PCR. Reactions were performed in a PTC-200 DNA Engine (MJ Research).

PCR reaction mixtures were optimised for each reaction, but a typical 50 μl reaction mix was as follows:

Reaction Component	Volume (μl)	Final Concentration
Template (genomic DNA)	0.1	-
10 x Reaction Buffer (TaKaRa)	5	1x
dNTPs	4	800 μM
Primer (forward) 10 pM/μl	1	1 pM/μl
Primer (reverse) 10 pM/μl	1	1 pM/μl
Enzyme	0.5	0.1 U/μl
H_2O	38.4	-

PCR cycling conditions were optimised for each reaction, but a cycle was as follows:

1. Denaturing: 95°C, 5 min
2. Denaturing: 95°, 30 s
3. Annealing: at T_m of primers, -3-5°C (approximately 68°C), 30 s
4. Extension: 72°C, 1 min per kb
5. Repeat steps 2-4, 30 times
6. Final extension: 72°C, 10 min

2.2.5 Colony PCR

- Bacterial

Colony PCR was used to identify bacterial clones containing recombinant plasmids after ligation. Where possible, one primer was specific to the insert. Individual bacterial clones were picked from agar plates in 20 μl sterile H_2O and 1 μl was used in 10 μl reactions. A standard 10 μl reaction mix was as follows:

Reaction Component	Volume (μl)	Final Concentration
Template (Cells)	1	-
10 x Reaction Buffer (TaKaRa)	1	1x
DNTPs	0.8	800 μM
Primer (forward) 10 pM/μl	0.05	1 pM/μl
Primer (reverse) 10 pM/μl	0.05	1 pM/μl
TaKaRa Ex Taq	0.05	0.1 U/μl
H_2O	7.05	-

- *D. discoideum*

Crude genomic preparation of individual *D. discoideum* clones were prepared by scraping a p2 tip through a colony and placing in 20 μl crude genomic extraction buffer for 5 min.

Reaction Component	Volume (μl)	Final Concentration
10 x Reaction Buffer (TaKaRa)	2	1x
10% NP-40	1	1 pM/μl
Proteinase K	0.1	0.1 U/μl
H_2O	17	-

Genomic preparations were incubated at:

1. 55°C for 45 min
2. 95°C for 10 min

Crude genomic DNA was then used as a template in 10 μl PCR reactions to identify clones in which homologous recombination had occurred. Reactions included either one primer within the inserted resistance gene or within the region to excised by recombination. A typical 10 μl reaction was as follows:

Reaction Component	Volume (μl)	Final Concentration
Template (Crude genomic DNA)	1	-
10 x Reaction Buffer (TaKaRa)	1	1x
dNTPs	0.8	800 μM
Primer (forward) 10 pM/μl	0.05	1 pM/μl
Primer (reverse) 10 pM/μl	0.05	1 pM/μl
TaKaRa Ex Taq	0.05	0.1 U/μl
H_2O	7.05	-

2.2.6 DNA sequencing

DNA samples were sent for sequencing by MWG Eurofins.

2.2.7 DNA extraction from *D. discoideum*

D. discoideum pellets from 2 x 10^7 cells from vegetative cultures were resuspended in 1 ml cold RLB. Samples were spun at 5 k x g for 5 min at 4°C. The pellet was then resuspended in 50 μl RLB, before adding 350 μl GPA, mixing by pipette and then GPB 350 μl GPB. Finally, 3 μl of 20 mg/ml Proteinase K was added and samples were incubated overnight at 55°C. 500 μl of phenol (pH 8.0) was then added, samples were mixed by pipette and spun at 16k x g for 10 min. The aqueous upper phase was transferred to a fresh tube and an additional 500 μl phenol (pH 8.0) added. Samples were mixed and centrifuged as before. The aqueous phase was then transferred to a fresh tube and mixed with 2 vol of 100% ice cold ethanol and 0.1 vol 3 M sodium acetate. Samples were incubated at -20°C for > 4 h, before being centrifuged for 10 min at 16k x g. Pellets were washed in 70% ethanol, centrifuged again and then resuspended in 50-100 μl TE (10 mM TrisHCl pH 7.4, 1 mM EDTA) depending on pellet size.

RLB

Compound	Final Concentration
Sucrose	0.32 M
TrisHCl pH 7.4	10 mM
Magnesium chloride	5 mM
Triton X-100	1%

GPA

Compound	Final Concentration
TrisHCl pH 7.4	10 mM
EDTA	10 mM

GPB

Compound	Final Concentration
TrisHCl pH 7.4	10 mM
SDS	0.7%

2.2.8 RNA extraction from *D. discoideum*

Pellets of 2 x 10^7 cells from vegetative cultures were harvested and washed in 1 ml 20 mM Potassium phosphate buffer pH 6.2 (KK2). Cell pellets were resuspended in 500 μl RNA lysis buffer, before adding 500 μl phenol (pH 4.3). Mixtures were incubated at RT on a rotary shaker for 20 min. Samples were centrifuged in a benchtop microcentrifuge at 16k x g for 5 min. The upper, aqueous phase was transferred to a fresh microcentrifuge tube before adding 200 μl chloroform. Samples were centrifuged at 16k x g for 5 min. The upper, aqueous phase was again transferred to a fresh tube, before adding 1 ml of 100% ethanol. Samples were incubated at -20°C for 20 min and then centrifuged at 16k x g for 5 min. Supernatant was removed and RNA pellets were resuspended in RNase free H_2O.

RNA Lysis Buffer

Compound	**Final Concentration**
Tris HCl pH 7.4	50 mM
Sodium chloride	100 mM
Sodium dodecyl sulfate (SDS)	1%
EDTA	10 mM
DEPC H_2O	

2.2.9 cDNA synthesis

RNA was diluted to 1 μg/μl and mixed with 50 ng/μl random hexamers (pdN6), 10 mM dNTP mix in a final volume of 13.75 μl. Samples were incubated at 65°C for 5 min, then on ice for 2 min. 4 μl of 5x first strand buffer (Invitrogen™), 1 μl 0.1 M DTT and 1 μl RNaseOUT™ were added along with 0.25 μl Superscript III reverse transcriptase (Invitrogen™). Samples were then incubated at 25°C for 5 min and 50°C for 1 h, before inactivating the reverse transcriptase at 70°C for 15 min.

2.2.10 Southern blotting

Genomic DNA was purified from *D. discoideum* cells as described above. DNA was digested with 10-20 units restriction enzymes (NEB) in 40 μl reactions containing 4 μl 10 x buffer (NEB), 5-10 μg of gDNA overnight at 37°C. Digested DNA was run on 0.7 % agarose gel at 30 V. The gel was then treated in 0.125 M HCl solution for 10 min, before neutralisation in 1.5 M NaCl, 0.5M NaOH for 30 min. Finally the gel was incubated in 1.5 M NaCl, 0.5 M TrisHCl 7.5 for 60 min. DNA was then transferred overnight onto Hybond membrane (Amersham) using 10 x SSC (1.5 M NaCl, 0.15 M tri Sodium citrate). Radiolabelled probe was generated using fragments of DNA digested from the deletion construct, labelled using HiPrime labelling kit (Roche Diagnostics) and $dCTP^{32}$ from Perkin Elmer. Membranes were incubated with probe overnight at 65°C in Church

phosphate buffer (0.5 M $NaPO_3$ pH 7.2, 7% SDS, 1 mM EDTA). The membrane was then washed for 15 min with 1x SSC and 0.1% SDS and then for another 15 min with 0.1x SSC and 0.1% SDS. The membrane was then exposed to photographic film overnight at -80°C.

2.2.11 Northern blotting

RNA was purified from cells and resolved by agarose electrophoresis as described above. RNA was transferred onto membrane as described for Southern blotting. Probes to the coding region of were synthesised as for Southern blotting using HiPrime labelling kit (Roche Diagnostics) and $dCTP^{32}$ from Perkin Elmer to label double stranded DNA. Hybridisation of the probe with membrane was performed overnight at 65°C in 1 % BSA, 0.5 M NaPO4 pH 7.2, 1 mM EDTA, 7% SDS. The membrane was then washed twice for 30 min with 40 mM NaPO4 pH 7.2, 1 mM EDTA and 5% SDS. Finally the membrane was washed a further two times for 30 min each with 40 mM NaPO4 pH 7.2, 1 mM EDTA, 1% SDS, 30-60. All washes were at 65°C. The membrane was then exposed to photographic film overnight.

2.3 *D. discoideum*

2.3.1 Media

D. discoideum was grown in HL5 media for all purposes except where noted. HL5 media was composed of:

HL5

Compound	**Final concentration (g/L)**
Glucose	14
Yeast extract (Formedium™)	7
Proteose peptone No 2 (Bacto™)	14
Sodium phosphate (dibasic) anhydrous	0.5
Potassium phosphate (monobasic) anhydrous	0.5

HL5 was adjusted to pH 6.5 with phosphoric acid.
HL5 was supplemented with penicillin/streptomycin at a working concentration of 10 U/ml and 10 μg/ml respectively. Transformant cells were selected with either Blasticidin (10 μg/ml)(Calbiochem) or G418 (5-20 μg/ml)(InvivoGen).
HL5 was also supplemented with 0.2 M sorbitol where indicated (spore germination experiments).

For certain purposes, including clonal selection, *D. discoideum* was grown on bacterial (*K. aerogenes*) lawn. These bacteria were grown on slime mould (SM) plates.

- SM

Compound	Final Concentration (g/L)
Glucose	10 g/L
Yeast extract (Formedium™)	5 g/L
Proteose peptone No 2 (Bacto™)	10 g/L
Potassium phosphate (monobasic) anhydrous	1
Potassium phosphate (dibasic) anhydrous	1.9
Magnesium sulfate, heptahydrate	1

All other media were obtained from Formedium™, including SIH and SIH without potassium phosphate.

2.3.2 Buffers

- KK2

20 mM potassium phosphate pH 6.2.

2.3.3 *D. discoideum* strains

AX2 Axenic strain

NC4 wild isolate strain

2.3.4 Axenic strains growth

Axenic strains were grown at 22°C in HL5 media either adherent to uncoated Nunclon™ 92 mm dishes or in shaking (120 rpm) flasks. Cells grown in shaking culture were diluted every 1-2 days such that cell density did not exceed 5 x 10^6 cells per ml. For clonal selection AX2 strain were grown on SM plates on *K. aerogenes. D. discoideum* were diluted to a density of ~1 x 10^3 cells/ml and mixed with ~100 μl of saturated *K. aerogenes* culture.

Stocks of cells were made from vegetative cultures (density ~2 x 10^6 cells/ml), that were centrifuged at 2 k rpm for 2 min. Pellets were cooled on ice for 5 min before resuspending in ice cold HL5. An equal volume of ice cold HL5 supplemented with 20% DMSO was then added, giving a final concentration of 10% DMSO. Cells were frozen at -20°C for 1-2 h, before transfer to -80°C.

2.3.5 Wild isolate growth

NC4 cells were grown on SM plates and *K. aerogenes* as described above.

2.3.6 Mutant construction

Mutants were constructed using the TMO1 deletion vector (Muramoto, Cannon et al. 2012).

Regions of DNA flanking the gene of interest were amplified by PCR from AX2 genomic DNA as described above. **Table 2.1** indicates the primers used to amplify targeting arms.

Knockout plasmids TMO1-IP6K-Bsr, TMO1-PPIP5K-Bsr, TMO1-IPMK-Bsr, TMO1-PPK1-Bsr were generated by inserting these sequences into the plasmid TMO1, with the 5' sequence inserted between the NotI and EcoRI sites and the 3' sequence between the HindIII and KpnI sites. The resultant plasmids were then digested using BssHII and used to transform AX2 cells by electroporation, see below.

Table 2.1 Primers for deletion constructs

Gene	Primer	Primer sequence	Product length	Restriction site
IP6K	5' arm Forward	GCAGCGGCCGCCTCAATCCACCCACACTCAC	1050	NotI
	5' arm Reverse	GCAGAATTCGTTGTTGTTGGGCTTCTTGG		EcoRI
	3' arm Forward	GCGAAGCTTGCGGTAGTAAACCTCAACCTTC	835	HindIII
	3' arm Reverse	GCAGGTACCCTCTTCACTGGTGACACCTATGC		KpnI
PPIP 5K	5' arm Forward	GCAGCGGCCGCGTAGTCAGCAAATTTACCAC	1069	NotI
	5' arm Reverse	GCAGAATTCCTATCTACAATTGGCCATTC		EcoRI
	3' arm Forward	GCGAAGCTTGATATATTACGTGTTAATGG	832	HindIII
	3' arm Reverse	GCAGGTACCTCAAATGGTCAAATTGCTGG		KpnI
IPMK	5' arm Forward	GCAGCGGCCGCTTACCACCAGCCAATAAGGC	901	NotI
	5' arm Reverse	GCAGAATTCAATTCTAATTCTTTACCACC		EcoRI
	3' arm Forward	GCGAAGCTTGATAGAATCTATGAAGATGG	749	HindIII
	3' arm Reverse	GCAGGTACCTTAACCAATTTGAAACTATG		KpnI
PPK	5' arm Forward	GCAGCGGCCGCGACAAACCCCCCAGACAATGG	1042	NotI
	5' arm Reverse	GCAGAATTCCATTTGCTAATGGTGGTGCATC		EcoRI
	3' arm Forward	GCGAAGCTTCGTCGTGTCGAAGTAATGGTTCC	925	HindIII
	3' arm Reverse	GCAGGTACCGGACGCCACCTTTAACTCG		KpnI

2.3.7 Blasticidin Resistance excision

The Blasticidin Resistance gene was excised from the *ppip5k* strain using the pDex-Cre-NLS plasmid (dictybase stock centre, **dictybase.org**). This extrachromasomal vector was introduced into *ppip5k* by H50 electroporation as described below. The overexpression of a nuclear targeted Cre recombinase cleaved the loxP sites engineered into the TMO1 vector either side of the BSR gene, excising it from the genome. Cells were selected under G418 (described below) and scored for sensitivity to Blasticidin.

2.3.8 Electroporation

D. discoideum were electroporated by two methods, E-buffer protocol and H50 protocol

- E-buffer

Each electroporation required $2x10^7$ from vegetative cultures. These were centrifuged at 2 k rpm for 2 min before resuspension in 5 ml ice cold E-Buffer. Cells were centrifuged again and resuspended in 1 ml of E buffer per electroporation. 10-25 μg digested DNA (deletion construct) was added per electroporation and mixed by inversion. Cells were transferred to ice-cold 0.2 cm electroporation cuvettes (Bio-rad Laboratories, Inc.) and placed in a Bio-rad Inc. genepulser and exposed to a single pulse of 0.65 kV at 25 μF. Cuvettes were then placed on ice before transferal of cells into a 92 mm dish and mixing with 16 μl Healing Solution. After 15 min, 12 ml of room temperature HL5 was added. Cells were allowed to grow overnight without selection. Transformant cells were selected by addition of 10 μg/ml Blasticidin (Calbiochem). Cells were selected for 6-9 days and media changed every 2-3 days.

E buffer

Component	Final concentration
Sucrose	50 mM
Potassium phosphate pH 6.1	10 mM

Healing buffer

Component	Final concentration
Magnesium chloride	100 mM
Calcium chloride	100 mM

- H50

Cells were centrifuged at 2 k rpm for 2 min and washed twice in cold H50 buffer. Cells were resuspended in H50 buffer at a concentration of $5x10^7$ cells per ml and incubated on ice for 5 min before transferral to an ice cold 0.1 cm electroporation cuvettes (Bio-rad Laboratories, Inc.) and electroporated with two pulses, with 5 s in between pulses. Each pulse was 0.85 kV and 25 μF. Cells were then iced for 5 min and allowed to recover in HL5 in a 92 mm dish overnight. G418 selection (5-20 μg/ml) was added the following day. Cells were selected for 4-6 days and media changed every 2-3 days.

H50

Component	Final concentration
HEPES	20 mM
Potassium chloride	50 mM
Sodium chloride	10 mM
Magnesium sulfate	1 mM
Sodium bicarbonate	5 mM
Sodium phosphate (monobasic)	1 mM

2.3.9 Clonal selection

After 6-9 days selection (Blasticidin) or 4-6 days selection (G418) cells were transferred from 92 mm dishes and diluted to $1x10^3$ cells per ml. 5-50 μl of this dilution was then plated on SM plates along with 100 μl saturated *K. aerogenes* culture. These plates were allowed to grow at 22°C for 4- 5 days until individual colonies of *D. discoideum* had cleared plaques in the bacterial lawn. Clones were then selected for either screening or amplification with a P2 tip (see above, **Section 2.2**).

2.3.10 Starvation

Cells were starved by transferring cells from vegetative cultures onto KK2 2% agar plates in either 35 or 92 mm dishes. $1x\ 10^7$ cells were plated on a 35 mm plate, whilst $8x10^7$ cells were plated on a 92 mm plate. Cells were allowed to develop for between 1 and 48 h on KK2 agar plates. Cells were collected after 1 h, ~8 h when cells were beginning to aggregate, 16 h, when cells had coalesced to form slugs and after >24 h when fruiting bodies were fully formed. Cells were harvested either by dislodging with KK2 and a P100 pipette or, at later time points, with a plastic scraper.

2.3.11 Cell extract preparation

$3x\ 10^7$ cells from vegetative cultures were centrifuged at 2k rpm for 2 min. Cells were washed once in KK2, then transferred to a 1.5 ml microcentrifuge tube. Cells were centrifuged again at 2k rpm for 1 min and resuspended in 80 μl ice-cold Cell Lysis Buffer. Samples were transferred to a 100 μl volume dounce homogenizer (on ice). Cells were agitated with ten strokes in the dounce and incubated on ice for 5 min. Lysates were then transferred to a fresh tube and centrifuged in a refrigerated centrifuge at 4°C at 16k rpm for 15 min. Supernatant was collected and protein concentration measured using Bio-rad DC protein assay. Extracts were stored on ice and used in *in vitro* assays immediately.

Cell Lysis Buffer

Component	**Final concentration**
Tris HCl pH 7.0	20 mM
Sodium chloride	150 mM
EGTA	1 mM
EDTA	1 mM
CHAPS	0.1%
DTT (added fresh)	5mM
Mammalian Protease Inhibitor Cocktail (Sigma P8340) (added fresh)	1x

2.3.12 Potassium cyanide and BHAM treatment

Cells from vegetative cultures were transferred to 92 mm dishes and allowed to adhere, at a confluence of ~50%. Once cells were adherent, media were replaced with fresh HL5, supplemented with 100 μM potassium cyanide (KCN) and 20 μM benzohydroxamate (BHAM). Cells were harvested at indicated time points.

2.3.13 Fruiting body images

Cells were allowed to develop and form fruiting bodies on KK2 agar plates for 48 h. Images were then taken on an camera mounted on an adjustable zoom dissecting microscope. Images were taken at the same magnification.

2.3.14 Spore preparation

Cells were developed for 48 h on KK2 agar plates as described above. Spores were obtained using protocols adapted from (Chiew, Reimers et al. 1985, Dynes, Clark et al. 1994). Fruiting bodies were harvested by scraping cells from plates and then incubated in 0.5 % NP40 for 3 min before spinning and washing three times in either KK2 or H_2O. If used for spore germination or whole fruiting

body extraction these cells were pelleted and resuspended in KK2, counted and either inoculated at indicated spore concentration or used in phenol chloroform extraction as described. Pure spore preparations were obtained by passing fruiting body preparations through 114 grade Whatman filter paper after washes to remove stalk cells. Spore cells were then collected and resuspended in KK2, counted and used for phenol chloroform extraction.

2.3.15 Spore germination

Spore germination was assayed using a protocol adapted from (Van Dijken and Van Haastert 2001). Spores were prepared as described above, counted and diluted at a density of 1.5 x 10^6 spores/ml in either HL5, HL5 supplemented with 0.2 M sorbitol or SIH without phosphate. Cells were then counted and scored as either spore, swollen spore or amoeba at indicated time points.

2.3.16 Immunofluorescence

Cells from vegetative cultures were transferred to 4 well plates and allowed to adhere to 13 mm glass coverslips. Cells were either allowed to recover in HL5, or media removed and replaced with KK2 for 1-5 h. Cells were fixed with either ice-cold methanol of formaldehyde:

- Methanol

Media was replaced with ice-cold methanol for 15 min. Methanol was then removed and cells were washed three times in KK2.

- Formaldehyde

Media was replaced with 4% formaldehyde. Formaldehyde was then removed and cells were washed three times in KK2.

Coverslips were stained by either:

- DAPI staining

Inverted on a solution of 2 mg/ml DAPI in KK2 for 10 min. Coverslips were washed in KK2 and mounted on a slide using ProLong Gold Mounting Media (ThermoFisher). Coverslips were then imaged on a 2012 model Leica TCS SPE confocal microscope mounted on a semi-automated, inverted Leica DMI4000 stand. Samples were imaged using a 408 nm laser and emission measured between 440-480 nm.

- PolyP binding domain (PPBD)

Coverslips were blocked for 10 min at room temperature with 1% BSA, 1 mM EDTA and 1 mM EGTA. Coverslips were inverted on 20 μl of 100 μg/ml PPBD in KK2, with 1% BSA overnight. Coverslips were then washed in 0.05% Triton X 100, KK2 and again in KK2. After washes, coverslips were incubated with 7.5 μg/ml anti Xpress (Invitrogen™) with 1% BSA in KK2 overnight. Coverslips were then washed in 0.05% Triton X 100, KK2 and again in KK2. After washes, coverslips were incubated with α-mouse (goat) conjugated to alexa 488 at 1:5,000, KK2 with 1% BSA plus 1:2,500 Hoechst for 4 h. Coverslips were then washed in 0.05% Triton X 100, KK2, then in KK2 and finally in H_2O, before being mounted using ProLong Gold Mounting Media (ThermoFisher). Coverslips were then imaged on a 2012 model Leica TCS SPE confocal microscope mounted on a semi-automated, inverted Leica DMI4000 stand.

2.3.17 Electron microscopy

Spores were prepared as described above. Spore pellets were then fixed in 2% glutaraldehyde/2% Paraformaldehyde (both EM grade) in 0.1 M Sodium cacodylate at room temperature for 30 min. Cells were centrifuged and washed in 0.1 M Sodium cacodylate. Spores were centrifuged and resuspended in 0.7% low gelling point agarose in 0.1 M Sodium cacodylate. Pellets were incubated on ice for 10 min to allow agarose to set. The pellet was then cut from tube and cut into smaller blocks (1-2mm x 1-2mm) to increase surface area to volume ratio and assist infiltration. The cut pellet was then washed twice in 0.1 M Sodium cacodylate. Samples were subjected to a secondary fix in 1% osmium

tetroxide/1.5% Potassium ferricyanide at 4°C for 1 h. Samples were washed three times in 0.1 M Sodium cacodylate and incubated in 1% tannic acid in 0.05 M Sodium cacodylate for 45 min at room temperature. Samples were washed twice in 0.05 M Sodium cacodylate and then once in ddH_2O. Samples were sequentially dehydrated in increasing EtOH concentrations, for 5 min in 70%, 5 min in 90% and 2 x 10 min in 100%.

Samples were incubated in 1:1 mix of propylene oxide:Epon resin for 90 min on rotary mixer, before an overnight incubation in 100% Epon on rotary mixer at room temp. Finally, samples were incubated in fresh 100% Epon for 2 h and transferred to embedding moulds in fresh Epon and baked overnight at 60 degrees to polymerise resin.

Samples were cut into 70 nm thick “ultrathin” sections were cut on a Leica UC7 ultramicrotome using a Diatome ultra 45 degree diamond knife, and transferred onto formvar coated slot grids. Sections were stained on grids using Reynolds lead citrate for 10 min, before washing five times in ddH_2O.

- **Imaging**

Samples were imaged on an FEI Tecnai G2 Spirit 120kv transmission electron microscope, using an Olympus SIS Morada CCD camera.

2.4 *S. cerevisiae*

2.4.1 Media

Growth without selection was performed in either YPD (Formedium^{TM}) or SC (see below). Selection was performed in SC URA^-.

- **YPD**

YPB Broth (Formedium™)

- **YPD agar**

YPB Broth (Formedium™)

Agar 20 g/L

- **SC media**

Compound	**Final Concentration (g/L)**
Glucose	10 g/L
Yeast Nitrogen Base without amino acids (Sigma)	6.9 g/L
Complete Synthetic Media (CSM) (MPBiomedicals)	0.79 g/L

- **SC media URA$^-$**

Compound	**Final Concentration (g/L)**
Glucose	10 g/L
Yeast Nitrogen Base without amino acids (Sigma)	6.9 g/L
CSM-URA amino acid (MPBiomedicals)	0.77 g/L

- **SC media URA$^-$ agar**

Compound	**Final Concentration (g/L)**
Glucose	10 g/L
Yeast Nitrogen Base without amino acids (Sigma)	6.9 g/L
CSM-URA amino acid (MPBiomedicals)	0.77 g/L
Agar	20 g/L

2.4.2 Strains

DDY1810: MATa, leu, ura3-52, trp1, prb1-1122, pep4-3, pre1-451

2.4.3 Transformation

- High efficiency

Yeast colonies were inoculated in 10 ml YPD media and grown overnight at 30°C, 200 rpm shaking to an OD^{600} of ~0.4-0.8. Cells were centrifuged at 2000 rpm for 3 min and washed once in sterile water. Cell pellets were resuspended in 100 μl TE/LiAc (10 mM TrisHCl pH 7.6, 1 mM EDTA, 100 mM lithium acetate). 0.1 μg of plasmid DNA and 0.1 mg pre-boiled salmon sperm carrier DNA. 600 μl of PEG/LiAc was added (40% PEG 3350, 100 mM lithium acetate, 10 mM Tris-HCl pH 7.6, 1 mM EDTA). Cells were vortexed for 10 sec and incubated at 30°C, 200 rpm for 30 min. 70 μl DMSO was added and cells heat shocked at 42°C for 15 min. Cells were then incubated on ice for 2 min and resuspended in 300 μl sterile water. 120 μl of yeast were transferred to URA^- agar plates and incubated for 3-4 days.

- Quick transformation

Cells were picked from YPD agar plates and transferred to 1 ml sterile water. Cells ere centrifuges at 3 k rpm for 2 min and resuspended in 33% PEG (w/v), 100 mM LiAc and 0.1 mg pre-boiled salmon sperm carrier DNA. 0.1 μg of plasmid DNA was added to each transformation and vortexed. Cells were incubated at 42°C for 30 min before centrifugation at 2 k rpm, 3 min. Cells were resuspended in 400 μl sterile water. 200 μl of mixture was URA^- agar plates and incubated for 3-4 days.

2.4.4 Growth rescue

Yeast cells were grown to an OD^{600} of 0.8, and then serial dilutions were prepared in sterile H_2O and 10 μl dropped onto URA^- minimal media plates. Plates were incubated at 30°C for 3-4 days.

2.4.5 Protein extraction

Yeast cells were grown to an OD^{600} of 0.8, centrifuged at 2000 rpm for 3 min, washed once in ice-cold water and resuspended in New Lysis Buffer (NLB). 1/3 vol of glass beads were added and samples were vortexed for 5 min at 4°C. Extracts were centrifuged at 16 k x g at 4°C and supernatant was transferred to new tube for further use.

NLB

Component	**Final concentration**
Tris pH8.0	50 mM
Sodium chloride	10 mM
EDTA	7 mM
DTT	5 mM
Protease inhibitor cocktail (Sigma P8215)	1x

2.5 Molecular biology: Proteins

2.5.1 SDS-PAGE

The NuPAGE™ (Invitrogen™) system was used with 4-12% Bis-tris gels (Invitrogen™) in MOPS SDS running buffer (Invitrogen™). Molecular weight marker (PAGE ruler™)(ThermoFisher) was used. Gels were run at 120-180 mV according to manufacturers instructions.

2.5.2 Immunoblot analysis

Proteins were transferred to Polyvinylidene Fluoride (PVDF) membrane (Bio-Rad) that had been equilibrated in methanol. Transfer was in 1 x Tris-Glycine transfer buffer (25 mM Tris, 192 mM glycine), using the Invitrogen™ transfer cell for 90 min at 100 mV at 4°C. PVDF membranes were blocked in 5 % (w/v) skimmed

milk powder in Tris-buffered saline-Tween 20 (TBST; 137 mM NaCl, 2.7 mM KCl, 19 mM Tris base, 0.1% Tween 20) for 30 min – 1 h at room temperature. Membranes were incubated with primary antibody (**Table 2.2**), α-GST (rabbit) at 1:7000 in 3% skimmed milk in TBST for 1 h at room temperature or overnight at 4°C with rotation. Membranes were washed three times in TBST from 10 min before incubation with secondary antibody **Table 2.2**), α-rabbit (mouse), at 1:100,000 in 3% skimmed milk in TBST for 1 h at room temperature with rotation. Membranes were washed three times in TBST for 10 min. Membranes were incubated with Luminata™ Crescendo Western HRP Substrate (Millipore™) as per manufacturer's instructions. Luminescence was detected by exposing membranes to photographic film (GE Healthcare).

2.5.3 Glutathione Sepharose Transferase (GST) pull down

GST tagged proteins were pulled down from yeast cell extract prepared from ~ 1 L of cells at an OD^{600} of ~1.7. Cells were centrifuged at 2.5k rpm for 5 min and washed once in ice-cold water. Cell pellets were resuspended in one vol. NLB (supplemented with 1x yeast PIC and 5 mM DTT). Cells were lysed in a Bead Beater™ homogeniser (Bio Spec Products Ltd.) with acid washed glass beads for 5 min. Extracts were kept ice-cold throughout. Cell extract was recovered and beads washed once with 0.5 vol NLB. Extract was then centrifuged at 16k x g at 4°C for 10 min. GST beads Glutathione Sepharose High Performance beads (GE healthcare) were equilibrated in NLB (plus 1x yeast PIC; 5 mM DTT) and at a ratio of 1:3. 500 μl of GST bead preparation (125 μl beads, 375 μl NLB) was added to cell extract and rotated at 4°C for 1.5 h. Samples were centrifuged at 1 k rpm for 30 sec and cell extract was removed. GST beads were washed three times with NLB supplemented with 1x yeast PIC; 5 mM DTT and 0.5% Triton X. GST beads were washed once in NLB supplemented with 1x yeast PIC and 5 mM DTT and then resuspended in 375 μl NLB supplemented with 1x yeast PIC and 5 mM DTT. GST beads were stored at 4°C for up to 3 days.

2.5.4 Silver Stain

Proteins were resolved by SDS PAGE as described above. Gels were then fixed in fixative 1 (40 % methanol, 10 % acetic acid) for 30 min. Gels were then transferred to fixative 2 (10% ethanol, 5% acetic acid) for 15 min, after which fixative 2 was replaced for an additional 15 min incubation. Gels were transferred to Oxidizer solution (3.4 mM potassium dichromate, 3.2 mM nitric acid). Gels were then washed 3-4 times in milliQ water until the yellow colour of the gel had been removed. Subsequently gels were incubated in 12 mM Silver nitrate solution for 20 min. Gels were washed once in milliQ before addition of developer solution (0.28 M sodium carbonate, 0.05% formaldehyde) for 5 min. Developer solution was replaced once before transfer of gel to stop solution (5% acetic acid) for 5 min.

2.5.5 *In vitro* assays

- Cell extract

Cell extract was prepared as described above. Cell extract activity assays were performed in either 25 μl or 40 μl volumes, rotating, for between 30 min and 3 h at 37°C.

- 10x Reaction Buffer

Component	**Final concentration**
HEPES pH6.8	200 mM
Potassium chloride	1 M
Magnesium chloride	60 mM
DTT	10 mM

A typical 40 μl reaction mixture was as follows:

Reaction Component	Volume (μl)	Final Concentration
Cell extract	5	-
10x Buffer	4	1x
Substrate 10 mM $IP_3/IP_5/IP_6/IP_7$	1.5	400 μM
Sodium fluoride (10mM)	4	1 mM
ATP, Mg salt (10 mM)	6	1.5 mM
Phosphocreatine (100mM)	1	2.5 mM
Creatine phosphokinase 500 U/ml	1	12.5 U/ml

- GST tagged enzymes

GST tagged enzymes were pulled down on GST beads as described above. Enzyme activity assays were performed in 40 μl volumes, rotating for 3 h at 37°C. A typical 40 μl reaction mixture was as follows:

Reaction Component	Volume (μl)	Final Concentration
GST beads (1:3 beads: buffer)	20	-
10x Buffer	4	1x
Substrate 10 mM $IP_3/IP_5/IP_6/IP_7$	1.5	400 μM
Sodium fluoride (10mM)	4	1 mM
ATP, Mg salt (10 mM)	6	1.5 mM
Phosphocreatine (100mM)	1	2.5 mM
Creatine phosphokinase 500 U/ml	1	12.5 U/ml

2.5.6 Fast Protein Liquid Chromatography (FPLC)

Cell extracts were prepared as described above from 1.5 x10^8 cells in 500 µl lysis buffer in a 2 ml dounce. Cell extract was then loaded on an AKTA FPLC system and fractionated by either Heparin column or DEAE column.

- HiTrap™ Heparin HP, 1 ml (GE Healthcare)

After loading, column was washed with wash buffer (25 mM HEPES, 50 mM KCl, 1 mM EDTA, 0.05% CHAPS). A 10 min gradient with elution buffer (25 mM HEPES, 1.5 M KCl, 1 mM EDTA and 0.05% CHAPS). 0.5 ml extracts were collected and used in *in vitro* reactions as described.

- HiTrap™ DEAE FF, 1 ml (GE Healthcare)

After loading, column was washed with wash buffer (25 mM HEPES, 50 mM KCl, 1 mM EDTA, 0.05% CHAPS). A 10 min gradient with elution buffer (25 mM HEPES, 1.5 M KCl, 1 mM EDTA and 0.05% CHAPS). 0.5 ml extracts were collected and used in *in vitro* reactions as described.

2.6 Molecular biology: Phosphate

2.6.1 Perchloric acid extraction

- *D. discoideum*

The inositol polyphosphate extraction procedure was adapted from the yeast protocol previously described (Azevedo and Saiardi 2006) and as described by Pisani et al. (Pisani, Livermore et al. 2014). *D. discoideum* cells were collected during the vegetative growth phase (1-2x10^6cells/ml), washed twice with KK2 and centrifuged at 2 k rpm on a Sorval RC-3C centrifuge for 2 min. The cell pellets were transferred to 1.5 ml tubes, resuspended in 1 M Perchloric acid, vortexed for 5 min at 4°C and centrifuged at 16 k g at 4°C for 10 min. The supernatants were transferred to a new tube and neutralised using 1 M Potassium Carbonate containing 3 mM EDTA. The samples were placed on ice for 2–3 hours and subsequently centrifuges for 10 min. The supernatants were transferred to new tubes and stored at 4°C.

- *S. cerevisiae*

The inositol polyphosphate extraction procedure was as previously described (Azevedo and Saiardi 2006). Exponentially growing *S. cerevisae* cells were harvested by centrifugation at 2 k g for 2 min. Cells were washed twice in ice-cold water and then resuspended in 1 M Perchloric acid, 1 volume of acid washed beads was added and cells were vortexed for 5 min at 4°C and centrifuged at 16 k g at 4°C for 10 min. Supernatants were transferred to a fresh tube and neutralised as above.

2.6.2 Phenol chloroform extraction

- *D. discoideum*

PolyP was extracted by phenol-chloroform extraction. Cells were harvested at indicated time points or growth conditions. Pellets were resuspended in one volume of LETS buffer (100 mM LiCl, 10 mM EDTA, 10 mM TrisHCl pH 8.0, 0.5% SDS), one volume of acidic phenol (pH 4.0) was added and samples were vortexed at 4°C for 5 min. Samples were centrifuged at 16 k g at 4°C and aqueous upper phase was recovered. 2 volumes of chloroform were added and samples were again vortexed at 4°C for 5 min before being centrifuged at 5k g for 5 min. Aqueous phase was collected and precipitated by adding 2.5 vol of ethanol and incubating at -80°C for 1-2 h. After centrifugation at 14 k g for 10 min, pellets were washed once in 70% ethanol, then resuspended in 10 mM TrisHCl pH 7.4, 1 mM EDTA and 0.1 % SDS. RNA concentration was measured by nanodrop and used to normalise samples prior to loading on PAGE

- *S. cerevisiae*

Exponentially growing *S. cerevisae* cells were harvested by centrifugation at 2 k g for 2 min. Cells were resuspended in one vol of LETS (as above). One volume of acidic phenol (pH 4.0) was added alongside 1.5 volume of acid washed glass beads. Samples were then vortexed at 4°C for 5 min. Aqueous phase was collected and samples were treated as above.

2.6.3 Enzymatic treatments

D. discoideum phenol-chloroform extracts were incubated in 45 μl enzymatic reactions and incubated with either DNaseI, RNase A and RNase T1, phytase (Sigma P1259) or Ddp1 and PPX recombinant protein purified as previously described (Losito, Szijgyarto et al. 2009). Reactions were conducted in either relevant commercially supplied buffer, RNase buffer (300 mM NaCl, 10mM Tris HCl (pH7.4), 5mM EDTA or 1x phosphatase buffer (100 mM KCl, 20 mM HEPES, 6 mM $MgSO_4$, 1 mM DTT) for 1.5 h at 37°C.

2.6.4 Polyacrylamide Gel Electrophoresis (PAGE)

20%-35.5% polyacrylamide gels, as indicated were, prepared using 24 x 16 x 0.1 cm glass plates, 40 polyacrylamide (national diagnostics) in 1x TBE. Samples were mixed in with 6 x Dye (0.01 % Orange G or Bromophenol blue ((BBF); 30 % glycerol; 10 mM TrisHCl pH 7.4; 1 mM EDTA). Gels were pre run for 30 min at 300 V and run overnight at 4 °C at 450 V and 3 mA for 20% gels and 700 V and 5 mA for 35 % gels in 1x TBE running buffer. Gels were stained with either DAPI or Toluidine Blue as previously described (Pisani, Livermore et al. 2014).

- DAPI

Gels were stained by gently agitating in DAPI staining solution (20 mM Tris Base; 20% Methanol; 2% glycerol; 20 mg/ml DAPI) under a daylight bulb for 45 min at room temperature. Gels were then destained in the same buffer in the absence of DAPI. Inositol pyrophosphates or polyP species were visualised using a UV transilluminator at 360 nM, gels were exposed for 2-10 min to allow photobleaching to occur

- Toluidine Blue

Gels were gently agitated for 30 min at room temperature in a staining solution (20% methanol; 2% glycerol; 0.05% Toluidine Blue), then destained for 30 min – 2 h in 20 % methanol with several changes. Gels were then scanned using a conventional Epsom scanner.

10x TBE

Component	**Final concentration**
Tris Base	121.1 g/L
Boric Acid	61.8 g/L
EDTA	2 mM

- Densitometry

Inositol pyrophosphates were quantified by densitometry using ImageJ software as previously described (Pisani, Livermore et al. 2014). After scanning, the Tiff format file, band densitometry was performed using ImageJ software (http://rsbweb.nih.gov/ij/). Ratios between densitometry of bands were calculated as indicated.

2.6.4 Strong anion exchange High Pressure Liquid Chromatography (SAX HPLC)

SAX HPLC was conducted as previously described by Azevedo et al. (Azevedo and Saiardi 2006). Cells were labelled with [^{3}H] inositol, either by:

- *S. cerevisiae*, cells were grown overnight in URA$^-$ minimal media. This was diluted to an OD^{600} of 0.005-0.01 in inositol free, synthetic media, supplemented with 5 μCi /ml of [^{3}H] inositol. Cells were grown at 30°C, shaking at 200 rpm overnight.
- Vegetative cultures of *D. discoideum,* were diluted to a density of 2 x 10^5 cells/ml in inositol free synthetic media (SIH minus inositol, Formedium™). Cells were grown at 22°C shaking at 120 rpm for 2-3 days.

Inositol phosphates were extracted as described above. Neutralised extracts were resolved by SAX-HPLC using a 4.6x125 mm PartiPhere SAX column (Whatman). Elution was performed with a gradient of Buffer A (1 mM EDTA) and Buffer B (1. 3M $(NH_4)_2HPO_4$) and 1 mM EDTA, pH to 3.8 with phosphoric acid). The gradient was as follows, 0-5 min, 0% Buffer B; 5-10 min 0-30% Buffer B;

10-60 min 30-100% Buffer B; 60-80 min 100% Buffer B. 1 ml fractions were collected and counted using 4 ml Ultima-Flo AP LCS-cocktail (Perkin Elmer).

2.6.5 ATP quantification

ATP was extracted from cell pellets by phenol-chloroform extraction as previously described, however after chloroform step samples were not ethanol precipitated. Instead aqueous phase was collected and immediately used in a luciferase assay using the Molecular Probes ATP Determination Kit according to manufacturers instructions.

2.6.6 Gel filtration

PolyP was fractionated according to size by FPLC with a gel filtration column (Superdex^{TM} peptide 10/300GL; GE Healthcare -17-5176-01). PolyP was extracted by phenol chloroform extraction (as described above) from either fruiting bodies or cells from vegetative cultures, as indicated. After ethanol precipitation samples were resuspended in 1 ml Buffer C (10 mM Tris-pH7.4, 1 mM EDTA, 25 mM NaCl) at a concentration of ~2-8 mg/ml RNA. 200-700 μl of sample (500 μg – 6 mg of RNA) was injected into the FPLC and fractionated at a constant flow rate of 0.2 ml/min in. 52 fractions of 0.5 ml were collected.

2.6.7 Acid degradation

Acid degradation of both inositol pyrophosphates and polyP was conducted by incubating samples at 100°C for 30 min in the presence of 1 M perchloric acid. Acid-treated samples were neutralised using 1 M K_2CO_3 and 3 mM EDTA before loading.

2.7 Statistical analysis

Statistical analysis was performed using GraphPad Prism software. Comparison between strains was conducted by unpaired t-tests of experimental values obtained from 3 or more independent experiments. Analysis of spore

germination compared each time point separately by unpaired t-test. Difference in growth rate between WT and mutant strains was assessed by comparing cell density at indicated time points by multiple t test. Accumulation of inositol pyrophosphates was analysed by One-way ANOVA multiple comparisons, where each time point was compared to the level of inositol pyrophosphates in the vegetative state. Significant differences were indicated where (*$p < 0.05$), (**$p < 0.01$) and (***$p < 0.0001$).

2.8 Antibodies

Table 2.2 Antibodies

Name	Company	Cat. Number	Application	Dilution
Primary				
Rabbit α-GST	Sigma	G7781	Western Blotting	1:7,000
Secondary				
α-rabbit IgG peroxidase conjugate	Sigma	A1949	Western Blotting	1:100,000
Mouse anti Xpress mouse	Invitrogen	46-0528	Immunofluoresence	7.5 μg/μl
α-mouse IgG alexa fluor^{R} 488	Invitrogen	A11001	Immunofluoresence	1:5,000

2.9 Plasmid DNA constructs

Table 2.3 Plasmid Vectors

Vector	Origin	Application
pGEM^{R} T Easy	Promega	TA cloning
pADH-GST	(Draskovic, Saiardi et al. 2008)	Protein expression in yeast
TMO1	(Muramoto, Cannon et al. 2012)	*D. discoideum* deletion construct
pDEX NLS Cre	(Faix, Kreppel et al. 2004)	Blasticidin Resistance excision

Table 2.4 Deletion constructs

Vector	5' Insert	5'	3'	Insert origin	3' Insert	5'	3'	Insert origin
TMO1	IP6K 5A	NotI	EcoRI	PCR gDNA	IP6K 3A	HindIII	KpnI	PCR from gDNA
TMO1	PPIP5K 5A	NotI	EcoRI	PCR gDNA	PPIP5K 3A	HindIII	KpnI	PCR from gDNA
TMO1	IPMK 5A	NotI	EcoRI	PCR gDNA	IPMK 3A	HindIII	KpnI	PCR from gDNA
TMO1	IPKA 5A	NotI	EcoRI	PCR gDNA	IPKA 3A	HindIII	KpnI	PCR from gDNA
TMO1	IPKA 5A_2	NotI	EcoRI	PCR gDNA	IPKA 3A_2	NdeI	KpnI	PCR from gDNA
TMO1	IPKB 5A	NotI	EcoRI	PCR gDNA	IPKB 3A	HindIII	KpnI	PCR from gDNA
TMO1	PPK 5A	NotI	EcoRI	PCR gDNA	PPKA 3A	HindIII	KpnI	PCR from gDNA

Table 2.5 Overexpression constructs

Vector	5' digest	3' digest	Insert	5' digest	3' digest	Insert origin
pADH-GST	BamHI	EcoRI	IPKA	BglII	EcoRI	PCR from cDNA
pADH-GST	BamHI	EcoRI	IPKB	BglII	EcoRI	PCR from cDNA

3. Inositol pyrophosphates: *D. discoideum* as a genetic model

3.1 Introduction

3.1.1 Background

The inositol pyrophosphates were first described in two independent studies in 1993, in mammalian cells (Menniti, Miller et al. 1993) and the social amoeba *D. discoideum* (Stephens, Radenberg et al. 1993). Since then these molecules have been observed in all eukaryotic organisms tested (Wilson, Livermore et al. 2013). In recent years the budding yeast *S. cerevisiae* has been the preferred model in which to study the structure and synthesis of the inositol pyrophosphates. Research in yeast has revealed the identity of a number of the key enzymes responsible for the synthesis of the inositol pyrophosphates, allowing their homologues to be identified in mammalian cells.

However, due to their relatively low abundance, study of these molecules in yeast requires the use of radiolabelled [^{3}H] inositol and HPLC. These techniques, although powerful, are laborious and inaccessible for a large number of cell biology laboratories. Recent improvements in the use of polyacrylamide gel electrophoresis (PAGE) techniques coupled with Toluidine staining has allowed the resolution and visualisation of these molecules. In fact this approach suggests that HPLC techniques may in fact underestimate the true abundance of the inositol pyrophosphates (Pisani, Livermore et al. 2014). Consequently the aim of this project is to make use of these techniques and return to the amoeba *D. discoideum* as a model to study the inositol pyrophosphates. In fact, this approach has already yielded the first detection of unlabelled inositol pyrophosphates extracted directly from cells (Pisani, Livermore et al. 2014).

The analysis of neutralised perchloric acid extract from 1 x 10^6 WT AX2 *D. discoideum* cells by 35.5% PAGE and Toluidine Blue staining reveals three distinct bands (Pisani, Livermore et al. 2014) (**Fig 3.1 A**). Toluidine Blue is a metachromatic dye that stains acidic phosphate-rich molecules. The strong staining of these bands indicates that they represent highly phosphorylated species. The fastest migrating of these bands co-migrates with IP_6 standard. Together these results suggest that the likely identity of this fastest migrating band is IP_6 and that the slower migrating bands are likely higher molecular weight inositol phosphates. Analysis of extract from the previously generated *ip6k* strain (Luo, Huang et al. 2003) revealed that only the putative IP_6 band can be detected by Toluidine Blue staining (**Figure 3.1**). This genetic evidence supports the notion that this band is IP_6 and the slower migrating bands are inositol pyrophosphates, most likely IP_7 and IP_8.

In accordance with previous work (Stephens and Irvine 1990, Drayer, Van der Kaay et al. 1994) analysis of a *plc* strain reveals the same three major bands, as in WT, with no detectable decrease in the staining. This method corroborates previous suggestions that IP_6 and inositol pyrophosphates are synthesised in a lipid-independent manner in *D. discoideum*.

In addition, analysis of *D. discoideum* cell extract by PAGE and DAPI staining reveals the enhanced photo bleaching properties of the slower migrating bands (**Figure 3.1 B**), a property associated with the phosphoanhydride bond present in inositol pyrophosphates (Losito, Szijgyarto et al. 2009). The increased sensitivity of DAPI staining also reveals the presence of an additional band, migrating still slower than the putative IP_8 band in both WT and *plc null* strains (**Figure 3.1 B**). The photo bleaching of this band suggests that it too is an inositol pyrophosphate species, probably possessing even more phosphates and most likely IP_9, the first detection of such a species *in vivo*.

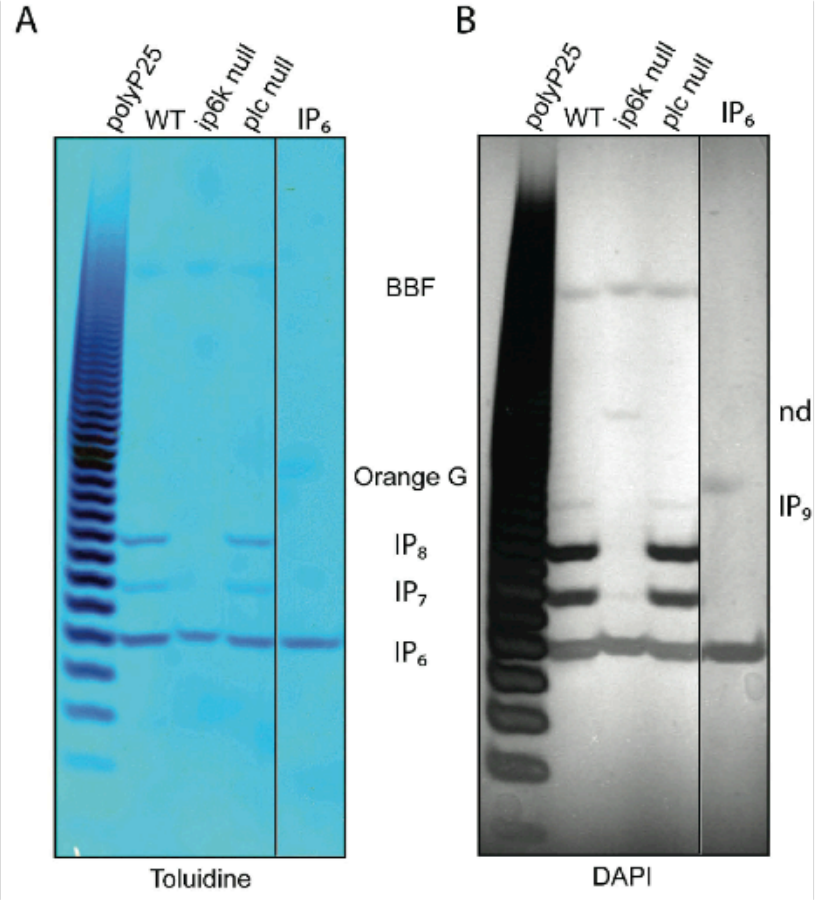

Figure 3.1 PAGE analysis of *D. discoideum* extract.

Perchloric acid extracts from 10 ml culture growth of wild type (WT) *D. discoideum* (AX2 strain) and the IP6-Kinase (*ip6k**) and phospholipase C mutant (*plc*) grown at a density of 2–4x10^6. Approximately 30–40 μl of neutralised cell extract (5% of total extract volume) was analysed by 35.5% PAGE. Inositol pyrophosphates were visualised with Toluidine blue (A) and DAPI staining (B), revealing three distinct bands. The figure shows a representative result of an experiment performed more than three times. Figure and figure legend adapted from (Pisani, Livermore et al. 2014), experiment performed by F. Pisani.

Treatment of this extract with phytase, which sequentially removes phosphate moieties from the inositol ring, degrades all three of these bands, confirming that they are indeed inositol phosphate species (**Fig 3.2 A**). Treatment of the extract with the pyrophosphatase Ddp1 (Lonetti, Szijgyarto et al. 2011) causes the putative IP_7 and IP_8 bands to collapse on to the fastest migrating IP_6 band (**Fig 3.2 B**). Finally, treatment of this extract with acid also ablates the slower migrating, IP_7 and IP_8 bands. Following acid treatment there is stronger staining of the fastest migrating band indicating that acid degradation of the slower migrating bands yielded more of this material (**Fig 3.2 C**). However, three further bands that migrate faster than this band also appear after acid treatment.

The sensitivity to phytase, but not Ddp1 nor acid, as well as co-migration with IP_6 standard (**Figure 3.2**) confirms that the fastest migrating band of these three is in fact IP_6 and the slower two migrating bands are IP_7 and IP_8. However, the appearance of three faster migrating bands, most likely isomers of IP_5, after acid treatment indicates that there may also be IP_5-derived inositol pyrophosphates present in this extract. Given that speed of migration is related to the number of phosphates, it is likely that these IP_5-derived inositol pyrophosphates co-migrate with the "conventional" IP_6-derived inositol pyrophosphates (e.g. $(PP)_2$-IP_3 and PP-IP_5). This precludes the resolution of distinct IP_5-derived inositol pyrophosphate such PP-IP_4 bands in untreated extract.

Analysis of gel-purified putative IP_7 and IP_8 bands (**Figure 3.3 A**) by mass spectrometry confirms the identity of these bands. The "IP_7" band reveals two peaks in the 500-1000 m/z range, one at 738.822 m/z and another at 760.793 m/z, representing the theoretical mass of deprotonated IP_7 and the sodium adduct of deprotonated IP_7 respectively (**Figure 3.3 B**). Similarly, analysis of the putative IP_8 band reveals two peaks, one at 818.627 m/z and the other at 840.590 m/z, representing deprotonated IP_8 and its sodium adduct, respectively (**Figure 3.3 C**). These analyses confirm the identity of the three detectable bands

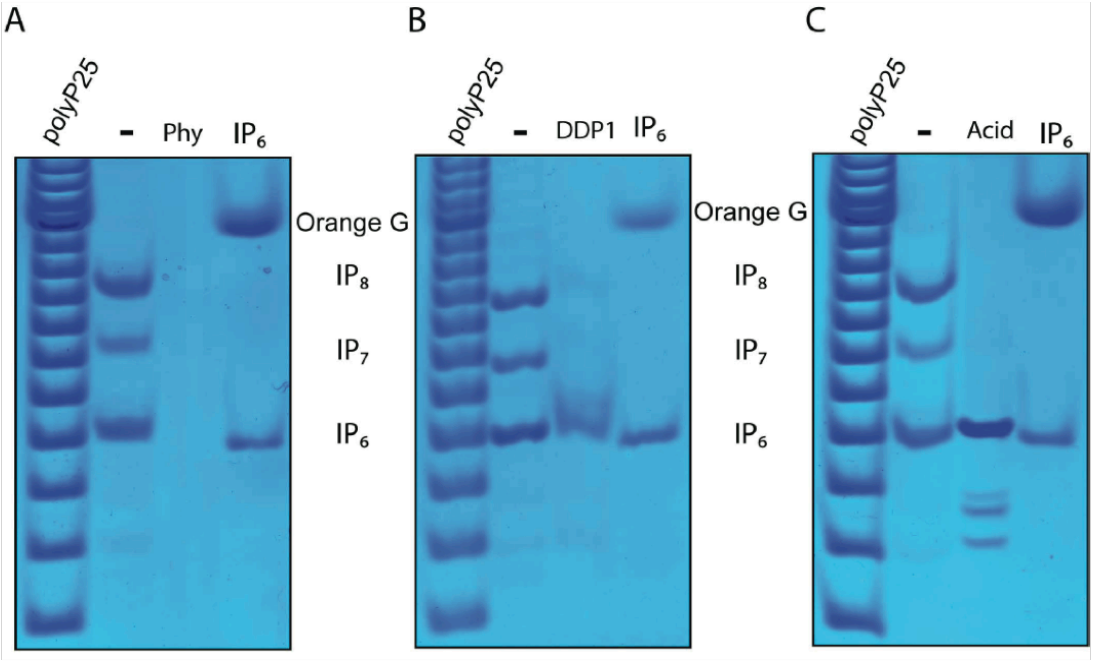

Figure 3.2 Enzymatic treatments of *D. discoideum* extract confirms identity of IP_6, IP_7 and IP_8.

Untreated WT *D. discoideum* cell extract (-) was incubated with phytase (Phy) (A), recombinant diphosphoinositol polyphosphate phosphohydrolase (DDP1) (B) or boiled in 1 M acid (C). Phytase degradation of extract (A) confirms these bands are inositol phosphates. DDP1 degradation of the two slower migrating bands confirms their identity as inositol pyrophosphates (B). Sensitivity to acid hydrolysis further confirms the pyrophosphate nature of these bands (C). The figure shows a representative result of an experiment performed more than three times. Figure and figure legend adapted from (Pisani, Livermore et al. 2014), experiment performed by F. Pisani.

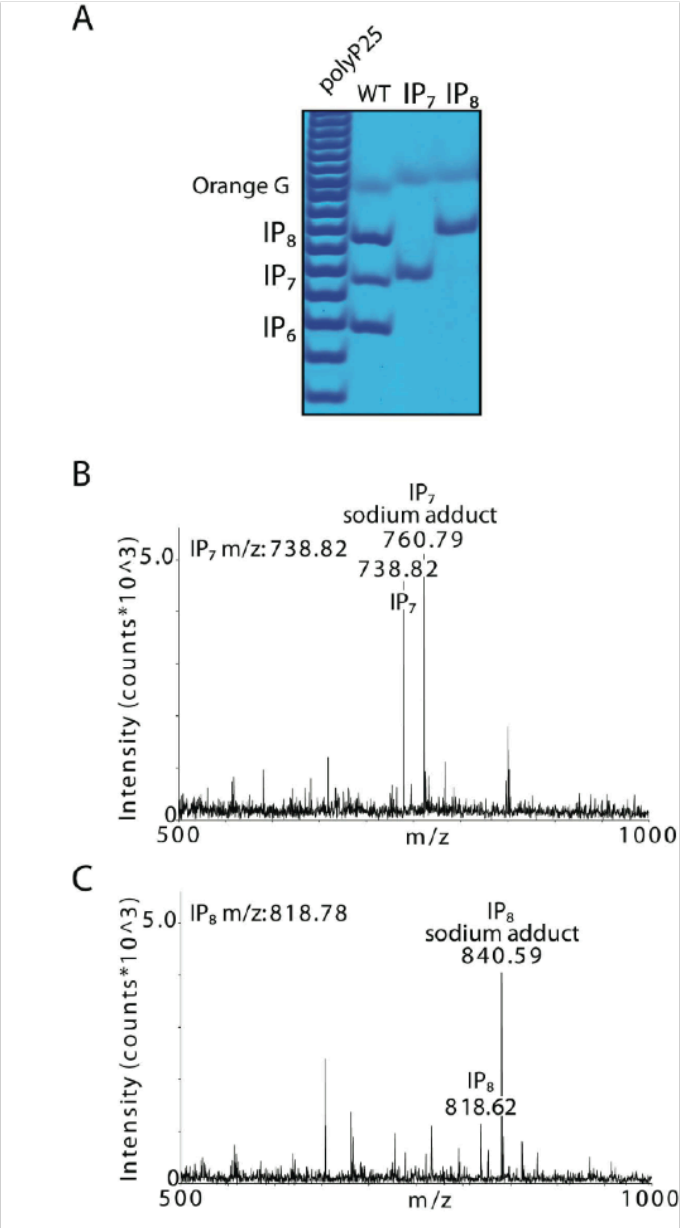

Figure 3.3 Mass spectrometry analysis of inositol pyrophosphates purified from *D. discoideum*.

Inositol pyrophosphates purified from gels (A) were analysed by mass spectrometry (B, C). The m/z spectrum of the IP_7 band (B) and IP_8 band (C) is shown. The peaks in the spectra describing inositol pyrophosphates are consistent with the theoretical values for molecular weight of 738.82 Da and 818.78 Da respectively. Figure and figure legend adapted from (Pisani, Livermore et al. 2014), experiment performed by F. Pisani.

seen by PAGE analysis of WT extract as IP_6, IP_7 and IP_8. Whilst the slowest migrating band detected by DAPI (**Figure 3.1 B**) has not been analysed by mass spectrometry, it seems highly likely that this band is IP_9, thus representing the first detection of this molecule in cell extracts.

Toluidine staining intensity reflects the number of phosphates present in a given molecule (Pisani, Livermore et al. 2014), allowing the concentration of IP_6, IP_7 and IP_8 to be estimated. Resolving acid treated IP_8, along with the corresponding amount of untreated IP_8 allows the comparison of the relative staining efficiencies of these two samples by densitometry, revealing that on average IP_8 is stained 1.27 +/- 0.08 more efficiently than the corresponding amount of IP_6. This fits well with the theoretical value based on number of phosphates of 8/6 or 1.33. Thus, the concentration of IP_6, IP_7 and IP_8 during the vegetative state can be estimated at 520 μM, 60 μM and 180 μM respectively. The calculated value for IP_6 concentration is consistent with previous estimates (Stephens and Irvine 1990, Letcher, Schell et al. 2008). However, the levels of IP_7 and IP_8 were much higher than suggested by some earlier work, which measured the vegetative levels of IP_8 to represent approximately 5% of the level of IP_6 (Laussmann, Pikzack et al. 2000). This analysis clearly revealed that the levels of inositol pyrophosphates during the vegetative state are much higher than estimated by Laussmann et al.. It is also interesting to note that, unlike yeast and mammalian cells, the level of IP_8 exceeds that of IP_7, possibly indicating that the conversion of IP_7 to IP_8 occurs more rapidly than the conversion of IP_6 to IP_7.

The ease of analysis of unlabelled inositol phosphates by PAGE and Toluidine staining or DAPI staining makes this model a technically attractive system in which to study the synthesis and metabolism of the inositol pyrophosphates. The ability to analyse the inositol pyrophosphates in this way has a number of benefits. This method allows the processing and analysis of numerous samples at once. A single poly acrylamide gel can be run overnight and can

accommodate more than ten samples. This is compared to HPLC, where each sample must be run and counted separately. The second benefit of this technique is that it does not require the use of radioactive material. This not only makes the technique more amenable, but more importantly, removes the need for labelling. Depending on the generation time and labelling efficiency, cells must be labelled for between overnight (yeast) and up to five days (mammalian cells) in order to reach equilibrium. The duration of labelling is a perennial problem for the study of inositol phosphates, removal of this step can not only drastically reduce the time required to generate samples, but also address any uncertainty associated with not reaching equilibrium labelling. In addition, this method allows the detection of metabolically inactive pools of inositol phosphates.

3.1.2 Enzymology

The technical advantages of working with this organism are clearly demonstrated in the work described above (Pisani, Livermore et al. 2014). In addition to the technical advantages of working with this organism, the *D. discoideum* genome encodes seven inositol phosphate kinases compared to just four in yeast (**Table 3.1**). This includes homologues to the two pyrophosphate synthesising enzymes, IP6K and PPIP5K. The IP6K gene, annotated I6Ka (ID: DDB_G0278739), encodes an 81 kDa protein, compared to the mammalian IP6K1 at ~52 kDa and the yeast Kcs1p at ~120 kDa (**Figure 7.1**).

The PPIP5K (ID: DDB_G0284617) homologue in *D. discoideum* encodes a 56 kDa protein, compared to the 130 kDa yeast protein and ~150 kDa in mammalian cells. As described previously this remarkable enzyme possesses both a kinase domain and a phosphatase domain in yeast and mammalian cells.

Table 3.1 Inositol phosphate kinases in *D. discoideum*

Gene ID	Annotated Gene name	Chromo-some	Annotated gene product	kDa	Gene name	Yeast Homo-logue	Mammalian Homo-logue
DDB_G0278739	I6KA	3	inositol phosphate kinase	81	Ip6k	Kcs1	IP6K 1-3
DDB_G0284617	na	4	na	56	Ppip5k	Vip1	PPIP5K 1-2
DDB_G0281737	na	3	inositol polyphosphate multikinase	33	Ipmk	Arg82	IPMK
DDB_G0288351	ipkA1	2	inositol polyphosphate multikinase	36	Ipka	na	?
DDB_G0283863	na	4	inositol hexakisphosphate kinase	70	Ipkb	na	?
DDB_G0288351	na	5	Inositol pentakisphosphate 2 kinase	59	Ipk1	Ipk1	IPPK
DDB_G0269746	itpk1	1	inositol-tetrakisphosphate 1-kinase	38	Itpk1	na	ITPK1

Interestingly the *D. discoideum* gene encodes a much smaller enzyme, which completely lacks the phosphatase domain (**Figure 7.2**). The absence of this phosphatase domain in the amoeba abolishes the futile cycle demonstrated by the yeast enzymes (Wang, Nair et al. 2015) simplifying the activity of this protein and possibly suggesting a more prominent role for the product of this enzyme, IP_8. It might also provide some clues as to why the levels of IP_8 exceed IP_7 in this organism.

Alongside IP6K and PPIP5K are five additional inositol phosphate kinases. An IPMK homologue (ID DDB_G0281737) (Arg82 in yeast) encodes a 32 kDa protein (**Figure 7.3**). This enzyme, which phosphorylates I(1,4,5)P_3 to I(1,3,4,5,6)P_5 in yeast has also been described to possess the ability to synthesise inositol pyrophosphates *in vitro* (Saiardi, Nagata et al. 2001). The catalytic flexibility of this enzyme is demonstrated still further by its ability to phosphorylate phosphoinositides, forming PIP_3 *in vitro* (Resnick, Snowman et al. 2005). IPMK is a member of the inositol phosphate kinase family of proteins and is likely an evolutionary descendent of an ancient IP6K-like enzyme (Bennett, Onnebo et al. 2006, Wang, DeRose et al. 2014).

In addition the *D. discoideum* genome encodes two further members of the inositol phosphate kinase family, termed here IPKA (ID: DDB_G0288351) and IPKB (ID: DDB_G0283863). These genes have been annotated respectively as an IPMK and an IP6K, however both show some divergence from the anticipated sequence (**Figures 7.4 and 7.5**). The gene referred to here as Ipka encodes a 36 kDa protein and has previously been termed ipkA1 and annotated as and IPMK. This gene has been cloned and overexpressed in *D. discoideum* cells lacking the phosphatase MIPP (King, Keim et al. 2010). Overexpression of IPKA was shown to confer resistance to Li^+-mediated inhibition of chemotaxis. It was postulated that resistance was caused by the synthesis of IP_5 by IPKA, however this was not confirmed by measurement of IP_5 production.

The gene referred to here as Ipkb has been annotated as an additional Ip6k. This is based on homology and has not been experimentally tested. Sequence alignment (**Figure 7.5**) supports this annotation, however the observed phenotype of the *ip6k** null mutant (Luo, Huang et al. 2003) suggests that the IPKB enzyme is not the major source of IP_7 in *D. discoideum in* the vegetative state.

Alongside these five kinases (four members of inositol phosphate kinase family and Ppip5k) the *D. discoideum* genome encodes two additional enzymes likely to be involved in the synthesis of inositol phosphates. Sequence alignment reveals a homologue to the yeast Ipk1 and mammalian Ippk in the amoeba genome (ID: DDB_G0288351), referred to here as Ippk. This gene has yet to be characterised, however homology suggest it is an inositol pentakisphosphates-2-kinase (**Figure 7.6**). This enzyme represents a different fold to the inositol phosphate kinase family and is the only enzyme described to phosphorylate the axial position 2 of the inositol ring.

The final inositol phosphate kinase identified in the *D. discoideum* genome is the inositol-tetrakisphosphate 1-kinase (Itpk1) (ID: DDB_G0269746). This gene product again has not been characterised, however it can be identified as an ITPK1 by sequence alignment (**Figure 7.7**). The mammalian homologue ITPK1 has been described to phosphorylate the isomer $I(1,3,4)P_3$ to $I(1,3,4,5,6)P_5$ by placing a phosphate on positions 5 and 6 of the inositol ring (Zhang, Majerus et al. 2012). Yeast do not possess a homologue for this gene (nor, intriguingly, do Drosophila (Seeds, Sandquist et al. 2004)), thus its presence in the *D. discoideum* genome suggests a complexity of synthesis of inositol phosphates more akin to mammalian cells than that seen in yeast.

3.1.3 Expression

The expression profiles of these genes as reported by DictyExpress database (https:// dictyexpress.research.bcm.edu/landing/) reveals that many of these genes are developmentally regulated (**Figure 3.4**). In the vegetative state (0 h post starvation) Ip6k, Ppi5k and Ipmk all show fairly low levels of expression, approximately 10 Reads per Kilobase per Million Mapped Reads (RPKM) (**Figure 3.4, top panel**). Upon the onset of starvation the expression of all of these genes is increased. Both Ip6k and Ipmk mRNA levels show a rapid induction after just 4 hours, before either levelling off, in the case of Ipmk or dropping slightly, as in Ip6k. Expression of Ipmk reaches a peak of ~80 RPKM after 16 hours of starvation. Meanwhile Ip6k, after dropping between 4 and 16 h, reaches its highest levels of expression after 24 h of starvation, at ~50 RPKM. The expression of Ppip5k does not increase as rapidly as either Ipmk or Ip6k, however expression does increase after a slight delay, ultimately rising to well over 100 RPKM at 12 h and 20 h post starvation.

The expression profiles of both Ipka and Ipkb are also both developmentally regulated (**Figure 3.4, middle panel**). Ipka is expressed at very low levels during the vegetative state and undergoes a rapid increase in expression upon the onset of the starvation response. The expression of Ipka peaks at 16 h, with a read count of ~60 RPKM. Meanwhile Ipkb is more highly expressed during the vegetative state, before steadily increasing during the starvation response to 65 RPKM after 24 h.

Finally, neither Ippk, nor Itpk1 are developmentally regulated. In fact, neither gene is highly expressed at any stage of development, with read counts failing to exceed 5 RPKM for either gene (**Figure 3.4, bottom panel**).

3.1.4 Concluding remarks

This short introduction to the technical advantages of the amoeba, *D. discoideum*, alongside the enzymology of inositol phosphate synthesis presents the amoeba as an ideal model to investigate inositol phosphate metabolism. The breadth of enzymes encoded in the *D. discoideum* genome suggests a more complex synthetic pathway than that described in yeast and possibly more analogous to mammalian cells. The presence of the Itpk1 in particular, invites speculation that the synthesis of inositol phosphates in this amoeba may offer insights into the mammalian system that the yeast model could not. The aim, therefore, of the work presented in the following results was to generate a panel of mutant strains in which the enzymes described above were deleted. Generation of a genetic model will provide insight into the synthesis of the inositol pyrophosphates and their precursors in *D. discoideum*, complementing the yeast model and potentially offering additional clues into the synthetic pathway of inositol pyrophosphates in mammalian cells.

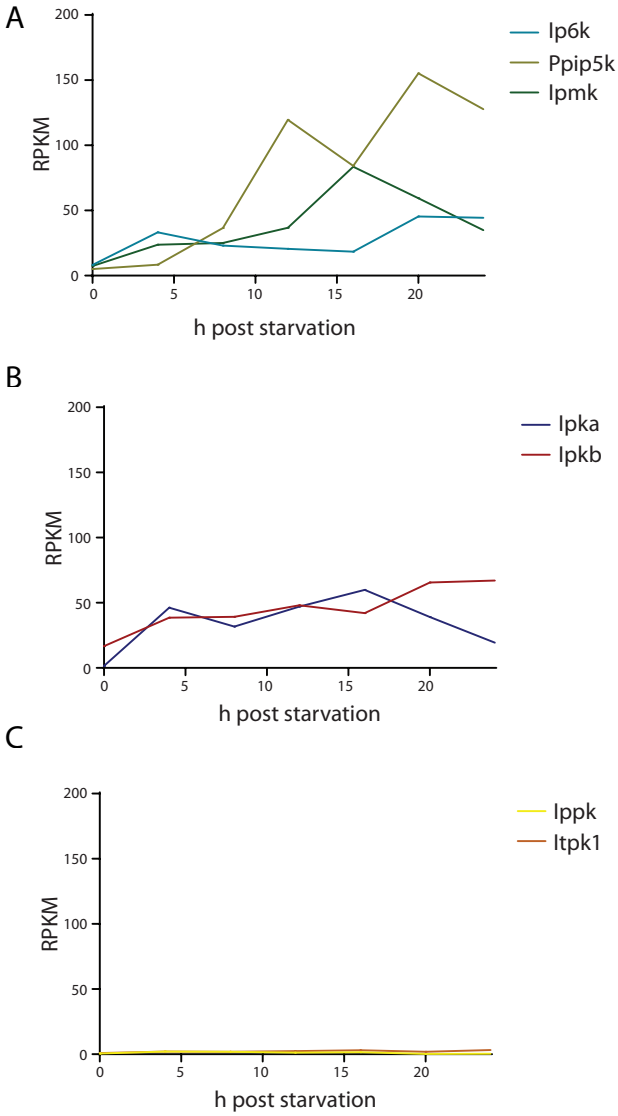

Figure 3.4 Developmental expression profiles of inositol phosphate kinases. Expression profiles all seven inositol phosphate kinases during 24 hours of development. RNA copy number expressed as reads per kilobase per million mapped reads (RPKM). Expression of Ip6k (cyan line) Ppip5k (olive line) and Ipmk (green line) increase after the onset of starvation (**A**). Expression profiles of Ipka (blue line) Ipkb (red line) increase after the onset of starvation (**B**). Expression of Ippk (yellow line) and Itpk1 (orange line) are very low at all stages of development (**C**). All data from DictyExpress database (https://dictyexpress.research.bcm.edu/landing/).

3.2 Results

3.2.1 Generation of knockouts

A genetic approach was employed to investigate the synthetic pathway of the inositol pyrophosphates in *D. discoideum*. Deletion constructs were designed and cloned for each of the seven inositol phosphates kinases described above. Not all genes were successfully deleted by this approach, but a number of mutant strains were generated and these will be discussed below.

A commonly used homologous recombination approach was used to generate knock out cell lines in *D. discoideum* (Gaudet, Pilcher et al. 2007). This approach involved cloning of two regions flanking (or slightly overlapping) the target gene and inserting them either side of a Blasticidin resistance marker gene in the TMO1 plasmid (**materials and methods, 2.3.6**)(Muramoto, Cannon et al. 2012). The strategy for deletion of the Ppip5k involved cloning 1.1 kb of genomic sequence overlapping slightly with the 5' region of the gene and 0.8 kb 3' of the gene (**Figure 3.5 A**). Homologous recombination using this construct deleted 44 % of the coding sequence of the gene. Recombinant strains were initially screened by PCR (not shown) and confirmed by Southern blot (**Figure 3.5 B**) and Northern blot (**Figure 3.5 C**). This strain is hereafter referred to as *ppip5k*.

Although the Ip6k gene has previously been deleted (Luo, Huang et al. 2003), this strain was generated again from the WT background used in this study. It was reasoned that any attempt to analyse the metabolic phenotype of the *ip6k* mutant should compare directly to a parental WT strain. Thus, deletion of the Ip6k gene followed a similar strategy, cloning a 5' sequence of 1 kb and a 3' sequence of 0.8 kb (**Figure 3.6 A**). Homologous recombinants had 56% of the coding sequence deleted and were screened by PCR (not shown). This strain is hereafter referred to as *ip6k*.

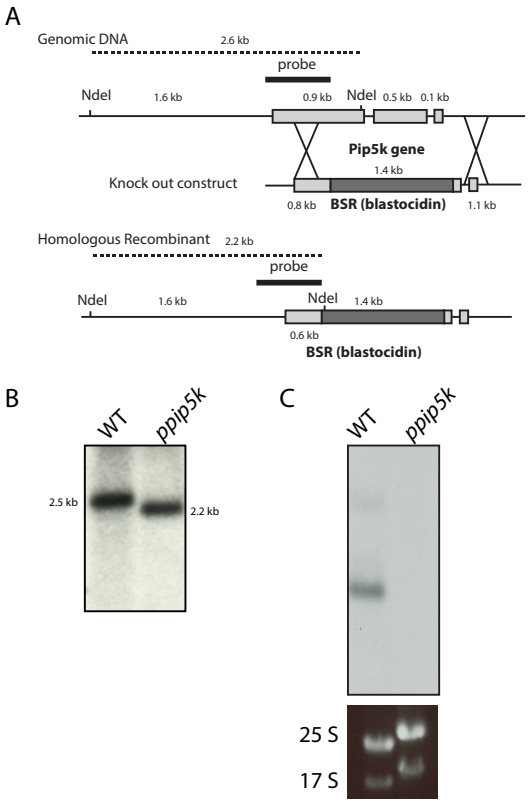

Figure 3.5 Deletion of PPIP5K by Homologous Recombination.

Schematic of deletion strategy, deletion construct contained a 5' targeting arm of 1069 bp and a 3' targeting arm of 832 bp (A). Southern blot revealed that digestion with NdeI generated a fragment of 2.5 kb in WT genomic DNA and 2.2 kb in *ppip5k* genomic DNA (B). Northern blot identified PPIP5K transcript in WT cells, but not *ppip5k* (B, upper panel), rRNA fragments revealed equal loading (C, lower panel).

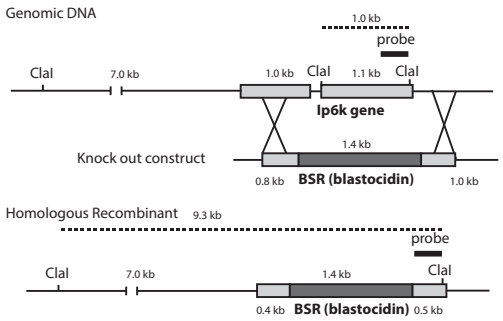

Figure 3.6 Deletion of IP6K by Homologous Recombination.

Schematic of deletion strategy, deletion construct contained a 5’ targeting arm of 1050 bp and a 3’ targeting arm of 835 bp .

Double mutants, in which both ppip5k and ip6k genes were disrupted, were generated using the same deletion constructs. Using the *ppip5k* strain described above the Blasticidin resistance gene (BSR) was excised by overexpressing a recombinant Cre with a nuclear localisation signal (pDex Cre NLS) (**materials and methods, 2.3.7**). The loxP sites located either side of the BSR gene were cleaved and the resistance gene excised. The Ip6k gene was then disrupted as described above to generate the *ip6k*/*ppip5k* strain. These mutants were screened by PCR (not shown).

Perchloric acid extracts of these mutants were analysed by PAGE to investigate the relative contributions of these genes to the pool of inositol pyrophosphates (**Figure 3.7**). For added sensitivity the gel was stained with DAPI. As described above an additional, slower migrating band, most likely IP_9 is faintly visible in WT extracts stained with DAPI (**Figure 3.7**).

Disruption of the ip6k gene completely ablated the level of IP_8 and almost completely ablated the level of IP_7. Some IP_7 remained detectable by DAPI, however this is band was not visible by Toluidine staining (not shown). These results recapitulated those from the previously generated *ip6k** mutant (Luo, Huang et al. 2003, Pisani, Livermore et al. 2014)(**Figure 3.1**), confirming that IP6K is the main, but not the only, source of IP_7 in *D. discoideum.*

Surprisingly, deletion of the ppip5k gene failed to ablate the IP_8 band. Both IP_7 and IP_8 were detectable in the *ppip5k* mutant. DAPI staining cannot be used to quantitatively assess the levels of inositol pyrophosphates, however, both IP_8 and IP_7 seemed to be less abundant than in WT (**Figure 3.7**), IP_6 was unaltered.

Cells lacking both IP6K and PPIP5K enzymes also possessed residual levels of IP7, as detected in the ip6k mutant (Figure 3.7). This suggested that PPIP5K

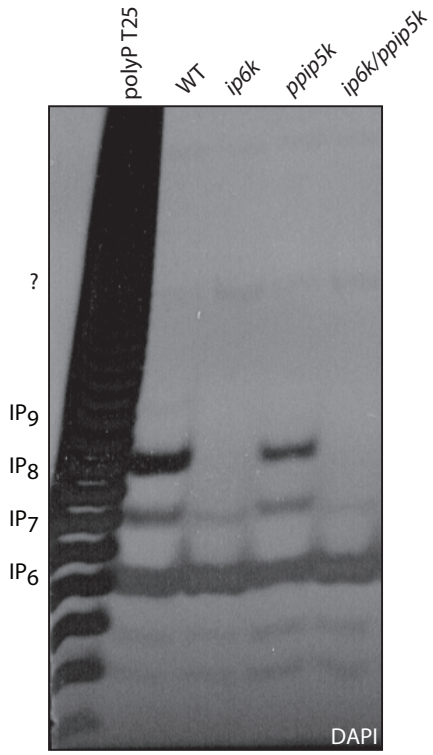

Figure 3.7 PAGE analysis of panel of *D. discoideum* extract.

Perchloric acid extracts of WT, *ip6k, ppip5k, ip6k/ppip5k* were analysed by 35.5% PAGE and DAPI staining. Samples were normalised by protein. The figure shows a representative result of an experiment performed more than three times.

was not the enzyme responsible for synthesis of the IP_7 detectable in *ip6k* and that an additional enzyme (or enzymes) were capable of synthesising inositol pyrophosphates in this amoeba. Nevertheless, these results confirmed that IP6K was the primary source of IP_7 in the vegetative state in *D. discoideum.* Neither the presence of PPIP5K, nor the additional unidentified kinase(s), was able to compensate for the loss of IP6K.

In order to better quantify the levels of inositol pyrophosphates in *ppip5k* mutant cells, perchloric acid extracts of two independent clones were analysed by PAGE and stained with Toluidine (**Figure 3.8**). Samples were normalised by cell number, with extract from 1.08 x 10^6 cells loaded in each lane. Toluidine staining confirmed that the levels of both IP_8 and IP_7 were reduced in absolute terms.

Further analysis of the levels of inositol pyrophosphates in these figures, and all further figures, used IP_6 as an internal control within each lane. Whilst this did not account for the differing staining intensity of IP_8, IP_7 and IP_6 nor any changes in the level of IP_6 in between strains, it allowed a more consistent measure of the ratio between IP_8 or IP_7 and IP_6 in each experiment. It also allowed each lane of the gel to be internally normalised thereby allowing comparison of the ratio between samples run on different gels. Densitometry analysis of multiple gels stained with Toluidine was performed using Image J software (**materials and methods, 2.6.4**). The relative strength of each band was assessed and the average ratio of IP_7:IP_6 and IP_8:IP_6 calculated. Comparison of these ratios revealed that the level of IP_7 (compared to IP_6) was reduced by approximately 40% in *ppip5k* extracts (**Figure 3.8 B**). Meanwhile, the level of IP_8 (compared to IP_6) was reduced by almost 70% in *ppip5k* extracts (**Figure 3.8 C**).

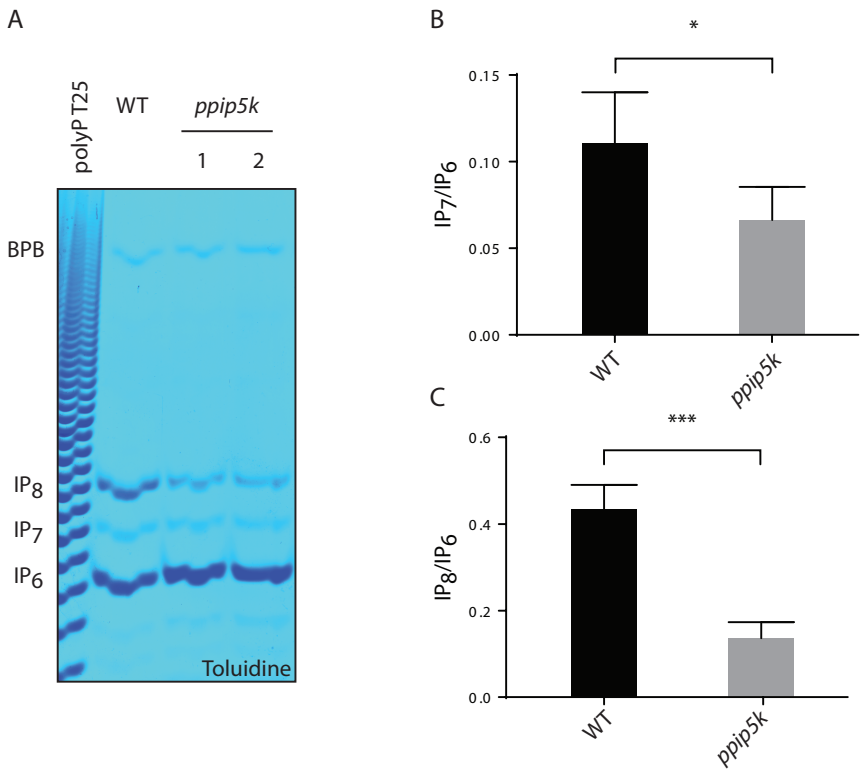

Figure 3.8 Quantification of inositol pyrophosphates in *ppip5k.*

Perchloric acid extracts of WT and two independent clones of *ppip5k* were analysed by 35.5% PAGE and Toluidine staining (A). Densitometry analysis of the level of IP_7 compared to IP_6 (B) and the level of IP_8 compared to IP_6 (C). Average values +/-SD determined from three independent experiments. Significant differences were indicated where (*$p < 0.05$) and (***$p < 0.0001$).

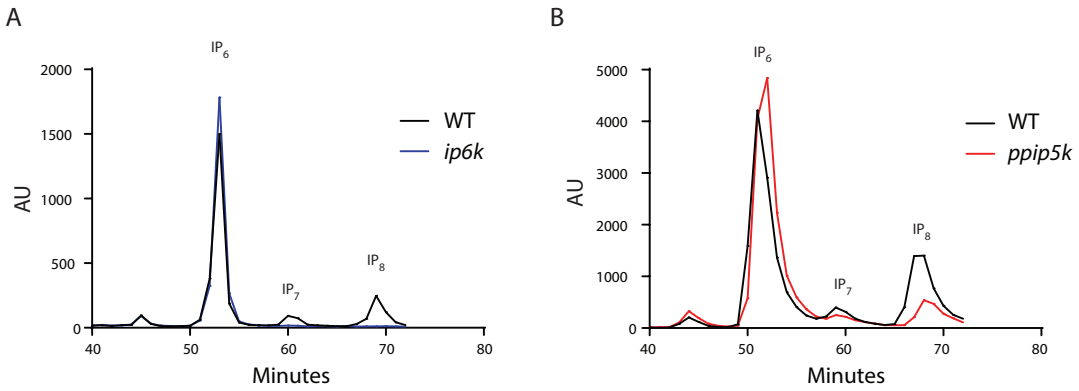

Figure 3.9 HPLC analysis of *D. discoideum* extract.

D. discoideum was labelled with [^{3}H] inositol for 3-4 days. Perchloric acid extracts were analysed by HPLC and radioactivity contained in fractions counted. WT extract was compared to *ip6k* extract (A) and WT extract was compared to *ppip5k* extract (B). Traces shown on the same graph represent experiments conducted in parallel.

3.2.2 HPLC analysis of inositol phosphates in *D. discoideum* mutants

To confirm the results obtained by PAGE analysis, WT, *ip6k* and *ppip5k* cells were labelled with [^{3}H] inositol. Cells were grown in inositol-free media for 3-4 days, supplemented with 50 μCi/ml [^{3}H] inositol. Neutralised perchloric acid extracts were then analysed by HPLC (Azevedo and Saiardi 2006) (**materials and methods, 2.3.1**). HPLC traces of WT extract revealed three peaks corresponding to IP_6, IP_7 and IP_8 (**Figure 3.9**). Both the IP_7 and IP_8 were completely absent from the *ip6k* extract (**Figure 3.9 A)**. In separate experiments the levels of inositol pyrophosphates were compared between WT and *ppip5k* (**Figure 3.9 B**). The peaks of both IP_7 and IP_8 were both reduced in *ppip5k* extract, corroborating the results obtained by PAGE and Toluidine staining.

Labelling of *D. discoideum* was very poor, making these experiments challenging. In addition, the HPLC traces obtained in these experiments indicated that the use of DAPI and PAGE was more sensitive for detection of inositol pyrophosphates in *D. discoideum*. As noted previously (Pisani, Livermore et al. 2014), the level of inositol pyrophosphates is underestimated by detection with HPLC compared to PAGE. This was demonstrated by the failure to detect the residual IP_7 in the *ip6k* strain by HPLC (**Figure 3.9 A**). Due to this combination of factors, all further analysis of inositol pyrophosphates in *D. discoideum* was performed by PAGE.

3.2.3 PPIP5K synthesises bis-diphosphoinositol phosphate species

PPIP5K has been described to possess activity towards both IP_6 and IP_7 *in vitro* (Wang, Falck et al. 2012). However, *in vivo* evidence from yeast (Onnebo and Saiardi 2009) and mammalian cells (personal communication M. Wilson) indicates that this enzyme contributes very little towards the steady state level of IP_7 and is almost exclusively an IP_7 kinase (hence PPIP5K). Conversely, the *ppip5k* strain generated in these experiments displayed decreased levels of both IP_7 and IP_8, as confirmed by both PAGE and HPLC. There are several

explanations for this, the first being that PPIP5K is both an IP_6 and IP_7 kinase in *D. discoideum.* The lack of the phosphatase domain in the amoeba PPIP5K could explain such a discrepancy in activity. Alternatively, it may be that the apparent IP_7 band is comprised of other co-migrating species inositol pyrophosphate species derived from IP_5, as suggested previously (**Figure 3.2 C**)(Pisani, Livermore et al. 2014). A bis-diphosphoinositol species derived from IP_5 ($(PP)_2$-IP_3) would be indistinguishable from IP_7 (PP-IP_5) by mass spectrometry. If these species are generated by PPIP5K, then the deletion of this gene may reduce their synthesis and be manifested by a reduction in the strength of the "IP_7" band.

To investigate this possibility, several isomers of IP_5 were incubated with mammalian IP6K1. Mammalian IP6K1 is known to show activity towards IP_5 (Saiardi, Nagata et al. 2001) and was readily available in the lab hence it was used as a reliable means of assessing the migration of PP-IP_4. As anticipated, mammalian IP6K was capable of utilising IP_5 as a substrate as demonstrated by the appearance of two further, slower migrating bands when the I(2,3,4,5,6)P_5 was treated with IP6K (**Figure 3.10 A)**. These two bands did not perfectly co-migrate with those seen in the WT extract, however, the migration of different isomeric forms can vary (as seen by the differences in migration between the IP_5 isomers used as substrate). This data indicated that IP_5-derived inositol pyrophosphates might co-migrate with IP_6 and IP_7 bands in WT extract.

This hypothesis was explored by treatment of both WT and *ppip5k* extracts with acid at high temperature. Boiling of inositol pyrophosphates in acid hydrolyses the phosphoanhydride bond linking the beta-phosphate to the ring. Phosphoester bonds, which link alpha phosphates to the ring, are not degraded, although this treatment can induce their rearrangement around the inositol ring (Pisani, Livermore et al. 2014). Thus inositol pyrophosphates are degraded to their precursor form by acid hydrolysis. Acid hydrolysis of WT extract almost

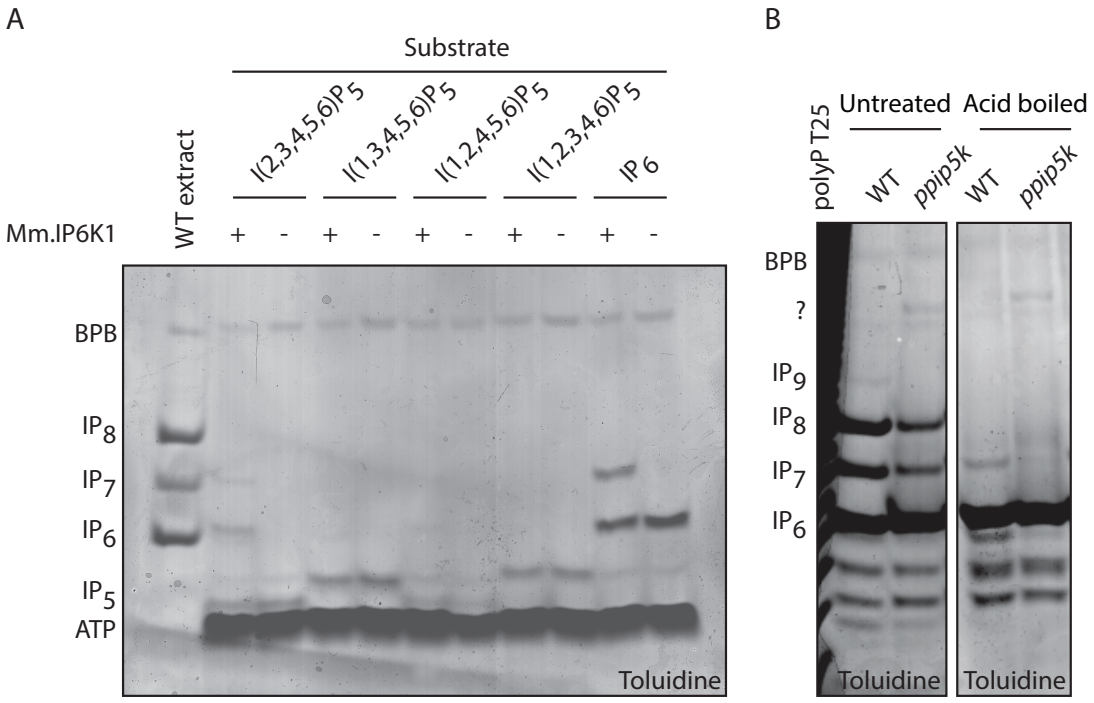

Figure 3.10 Inositol pyrophosphates derived from IP_5 can co-migrate with those derived from IP_6.

Four isomers of IP_5 were treated with myc tagged mouse IP6K (Mm.IP6K1). Migration of products was compared to *D. discoideum* extract and IP_6 treated with MmIP6K1 (A). Migration of untreated and acid treated extracts from WT and *ppip5k D. discoideum* extract revealed the formation of species that migrated faster than IP_6 (B). All samples analysed by 35.5% PAGE and stained with Toluidine Blue.

completely ablated the presence of the IP_7 and IP_8 bands (**Figure 3.10 B, right panel)**. Furthermore, there was a clear increase in the intensity of the IP_6 band, indicating that most of this material was degraded to IP_6. However, there was also a clear increase in the staining of three bands that migrated faster than IP_6. Whilst IP_5 migrates with these characteristics, nucleotides including ATP and GTP also migrate in this region (Losito, Szijgyarto et al. 2009)(**Figure 3.10 A**). The phosphoanhydride bonds in both ATP and GTP are also degraded by acid hydrolysis. Thus it seems most likely that the increase in strength of these bands was due to a release of IP_5 by acid hydrolysis.

Two of these bands clearly increased after acid hydrolysis of *ppip5k* extract, although the slowest migrating of the three did not. Nevertheless, acid hydrolysis of both WT and *ppip5k* extract revealed an increase in both IP_6 and IP_5, indicating that IP_5-derived inositol pyrophosphates were present in *D. discoideum* extract. Thus it seems most likely that the observed decrease in the IP_7 band in *ppip5k* (**Figure 3.8-3.10**) was due to a decrease in the bisdiphosphoinositol species derived from IP_5 ($(PP)_2$-IP_3) and not PPIP5K acting as an *in vivo* IP_6 kinase.

3.2.4 Growth of mutant strains reveals no major fitness defect

To investigate the effect of the altered inositol pyrophosphate metabolism on general fitness, the growth of the WT strain was compared to *ip6k, ppip5k* and the *ip6k*/*ppip5k* mutants. Cells were grown over 48 hours in rich (HL5) media (**materials and methods, 2.3.1**)(**Figure 3.11**). All three mutants displayed very slight growth defects. Only *ppip5k* appeared to grow significantly more slowly from WT. The mean generation time increased from 11 h in WT to ~ 12 h in *ip6k, and ip6k*/*ppip5k*, rising to >12 h in *ppip5k*. Thus the effect on growth did not completely correlate with the presence of inositol pyrophosphates, as the *ppip5k* mutant, which grew slowest possessed substantial levels of inositol pyrophosphates, in contrast to both *ip6k* and the double mutant (**Figure 3.7**).

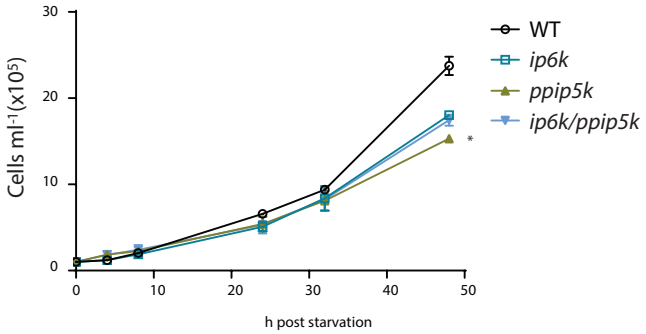

Figure 3.11 Comparison of growth curves of panel of *D. discoideum* mutants.

WT, *ip6k, ppip5k* and *ip6k/ppip5k* were grown for 48 h in HL5 media starting at a density of 1 x 10^5 cells per ml. After 48 h, the cell density of *ip6k, ppip5k* and *ip6k/ppip5k* were lower than WT. The figure shows averages +/- SD from three independent experiments. Differences in growth rate between WT and mutants were evaluated by multiple t tests (**materials and methods, 2.7**), significant differences were indicated where (*$p < 0.05$).

3.2.5 Inositol pyrophosphate accumulation during development

Upon deprivation of nutrients, *D. discoideum* undergoes a developmental process in which the unicellular amoeboid cells aggregate, form motile "slugs" and culminate in the formation fruiting bodies, comprised of spore cells and stalk cells (**Figure 1.8**). This process is one of the few physiological examples of fluctuations in the levels of inositol pyrophosphates (Laussmann, Pikzack et al. 2000). It has also been previously noted that the *ip6k* strain undergoes the early stages of this process more rapidly than WT cells (Luo, Huang et al. 2003).

Consequently the level of inositol pyrophosphates during this process were investigated by PAGE both in WT and mutants to determine the relative contribution of each enzyme (**Figure 3.12**). Densitometry analysis of WT extracts taken at five time points during development revealed a 2.5-fold increase in IP_8 in comparison to IP_6 (**Figure 3.12 A**). This value was dramatically less than the previously reported value of a 25 fold increase in inositol pyrophosphates (Laussmann, Pikzack et al. 2000). This discrepancy is most likely due to the underestimate of the level of IP_8 in the vegetative state by previous work (Laussmann, Pikzack et al. 2000). It should be recognised, that this analysis does not account for fluctuations in the level of IP_6, which was deemed to be relatively constant (**Figure 3.12**).

During the development of *ip6k* no accumulation of inositol pyrophosphates was observed **(Figure 3.12 B)**. Interestingly *ppip5k* (**Figure 3.12 C**) did show a developmental increase in the level of inositol pyrophosphates, although it did not reach siginificance. As previously discussed the level of IP_8 (expressed as a ratio of IP_6) was around 40% of that of WT, however an increase in the level of IP_8 could be observed after 8 hours of starvation. Quantification of this increase indicated that IP_8 did not increase to quite the same level as observed in WT, although it there was a substantial increase during development. Calculating

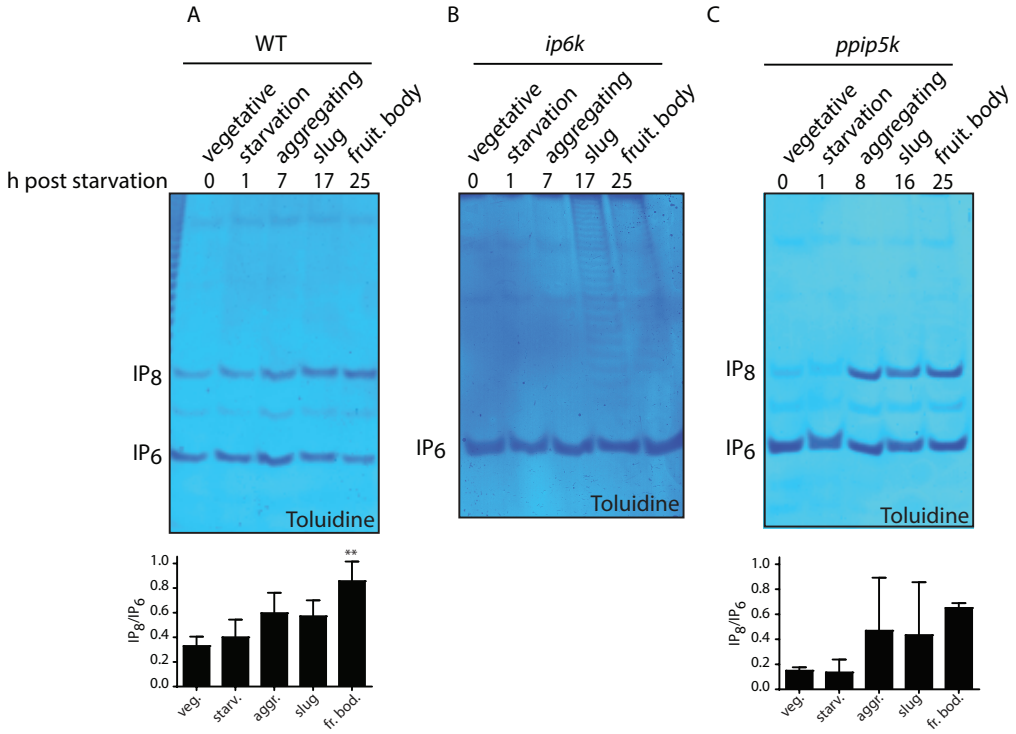

Figure 3.12 Accumulation of inositol pyrophosphates during development. Cells were starved as described in (**materials and methods, 2.3.10**). The inositol phosphates extracted at the indicated time points were resolved on 35.5% PAGE and visualised with Toluidine. The analysis of WT developmental program revealed a 2-fold increase in the IP_8/IP_6 ratio in fruiting bodies as quantified by densitometry quantified (Bottom), average +/- SD of four independent experiments Panel adapted from (Pisani, Livermore et al. 2014), (A). Analysis of *ip6k* extract failed to detect any accumulation of inositol pyrophosphates during development. The figure shows the result of a representative experiment that was repeated at least twice for *ip6k* (B). Analysis of *ppip5k* extract revealed a developmental increase in the level of IP_8, quantification by densitometry (bottom) average +/- SD of two independent experiments (C). Increases in inositol pyrophosphates during development were evaluated according One-way ANOVA, multiple comparisons (**materials and methods, 2.7**). Significant differences were indicated where (**$p < 0.01$).

the increase during development reveals a slightly higher fold change during development of ~ 3.5 times. However, the lower levels of IP_8 in the vegetative state can explain this observation. These results indicated that the accumulation of inositol pyrophosphates during development occurred despite the disruption of PPIP5K and an alternative enzyme able to synthesis IP_8 was likely to be developmentally regulated.

The speed of *D. discoideum* development showed slight variation between experiments (data not shown). WT cells began to aggregate after between 7 and 12 h of starvation. The speed of aggregation of *ip6k* cells appeared slightly faster, ranging between 6 and 8 hours, confirming previous observations (Luo, Huang et al. 2003), although this was not the focus of detailed investigation. No substantial alteration in speed of aggregation was observed in *ppip5k*. All strains tested formed fruiting bodies as normal.

3.2.6 Inositol pyrophosphates and primary metabolism

Previous experiments in the Saiardi lab have identified the inositol pyrophosphates to be key regulators of the cell's energetic metabolism (Szijgyarto, Garedew et al. 2011). Yeast and mammalian cells lacking inositol pyrophosphates display dramatic increases in the level of ATP. In order to investigate the conservation of this link, the level of ATP in *ip6k* cells was compared to WT. This analysis revealed that the level of ATP was not dramatically affected by disruption of the Ip6k gene (**Figure 3.13**).

This result suggested that the link between inositol pyrophosphates and energetic metabolism might not be conserved in *D. discoideum.* However, it is possible to speculate that the residual level of IP_7 detectable in the *ip6k* mutant was sufficient to fulfil the regulatory role over energetic metabolism.

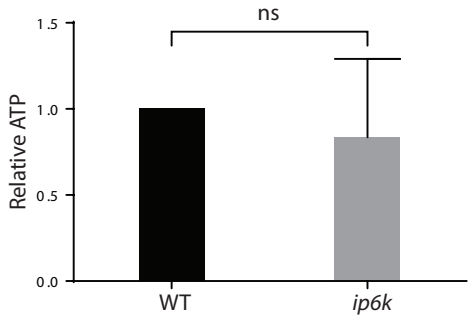

Figure 3.13 No significant difference between primary metabolism of WT and *ip6k*.

ATP was quantified as described in (**materials and methods, 2.6.5**) from phenol-chloroform extracts of both WT and *ip6k*. Samples were normalised by RNA and results shown are average +/- SD of three independent experiments, where the relative level of ATP was calculated by comparing to WT in each experiment.

3.2.7 Generation of an *ipmk* knock out strain

The results described above illustrate a number of divergences in the synthetic pathway of inositol pyrophosphates between yeast and *D. discoideum*. Whilst IP6K was evidently the primary source of inositol pyrophosphates in these cells, both *ip6k* and *ip6k*/*ppip5k* retained low levels of IP_7. However, IP6K and PPIP5K are not the only enzymes that have been described to possess activity capable of synthesising inositol pyrophosphates. As noted previously IPMK (Arg82 in yeast) has also been shown to be capable of producing inositol pyrophosphates *in vitro* (Saiardi, Nagata et al. 2001). In order to investigate the role of this enzyme and the possibility that it may be synthesising inositol pyrophosphates, the Ipmk gene was disrupted as detailed in (**Figure 3.14 A**). Homologous recombination was confirmed by Southern blot (**Figure 3.14 B**), whilst Northern Blot confirmed absence of expression (**Figure 3.14 C**). This strain is hereafter referred to as *ipmk*.

Interestingly, Northern blot analysis with a probe for IPMK revealed two major bands and a third faint band in the WT strain (**Figure 3.14 C**). The fastest migrating of these bands was most consistent with the anticipated size of Ipmk mRNA. It is possible that the slower migrating bands were caused by non-specific binding, perhaps to ribosomal RNA. However, these bands were not present in the *ipmk* knockout sample, suggesting that these bands may due to transcript variants of Ipmk. It is worthy of note that the mammalian Ipmk transcript possesses a particularly long 3' UTR sequence of 4127 nt (Saiardi, Nagata et al. 2001). This observation was not explored in further detail due to time constraints.

The level of inositol pyrophosphates found in the vegetative state of *ipmk* was analysed by 35.5% PAGE and densitometry. These experiments demonstrated that the levels of inositol pyrophosphates in *ipmk* were unchanged compared to

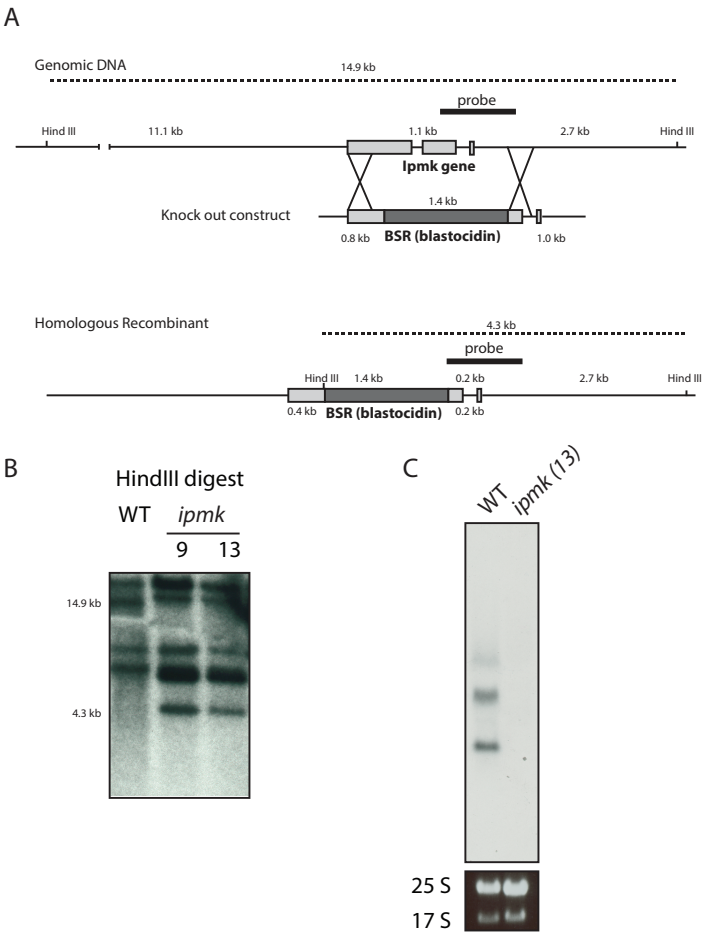

Figure 3.14 Deletion of IPMK by Homologous Recombination.

Schematic of deletion strategy, deletion construct contained a 5' targeting arm of 901 bp and a 3' targeting arm of 749 bp (A). Southern blot revealed that digestion with HindIII generated a fragment of 14.9 kb in WT genomic DNA and 4.3 kb in *ipmk* genomic DNA (B). Northern blot identified three IPMK transcript in WT cells, but none *ipmk* (B, upper panel), rRNA fragments revealed equal loading (C, lower panel).

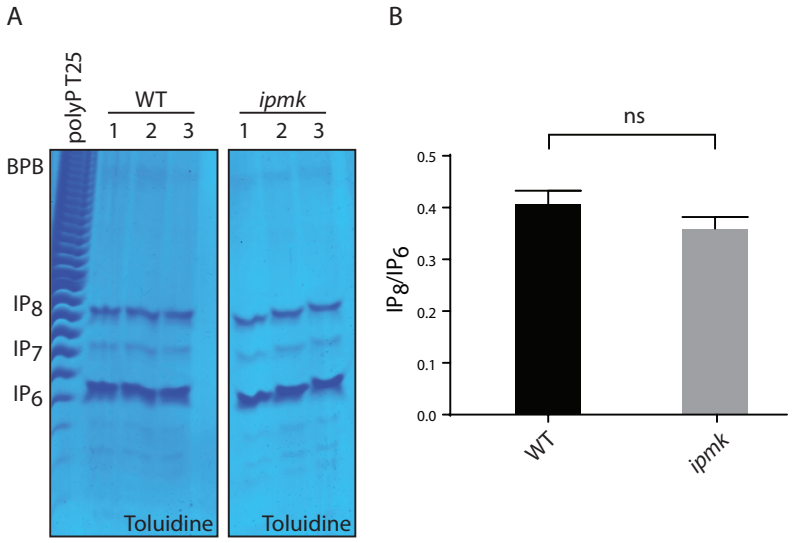

Figure 3.15 Quantification of inositol pyrophosphates in *ipmk*.

Perchloric acid extracts of WT and *ipmk* were analysed by 35.5% PAGE and Toluidine staining (A). Densitometry analysis of the level of IP_8 compared to IP_6 (B) revealed no significant difference between WT and *ipmk*. Average values +/- SD determined from three independent extractions analysed on a single gel.

WT (**Figure 3.15**). This result is again divergent from that obtained in the yeast *arg82Δ* mutant, which lacks higher inositol phosphates (Saiardi, Sciambi et al. 2002).

Whilst IPMK did not play a major role in the synthesis of inositol pyrophosphates in the vegetative state it may play a more prominent role at different stages of the life cycle. In order to test this hypothesis the accumulation of inositol pyrophosphates was examined in the *ipmk* strain (**Figure 3.16**). As in the vegetative state, *ipmk* showed no dramatic difference compared to WT. The level of IP_8 increased to a level comparable to WT, suggesting that IPMK is not the enzyme responsible for the production of inositol pyrophosphates during development, nor the primary source of higher inositol phosphates at any point in the *D. discoideum* lifecycle.

3.2.8 IP_5 kinase activity in cell extract

The results described above failed to identify the role of IPMK and were dramatically different from other model systems. In order to better characterise the *ipmk* mutant a series of cell-free experiments were conducted to assay whether this cell line lacked any activity that could be detected in WT. If the lack of phenotype in *ipmk* was due to redundancy in the pathway then it was possible that, whilst the overall synthesis of IP_6 and beyond was unaffected, specific enzymatic activities may be absent from this strain. As described above, IPMK is best known as a 3-, 6- kinase using I(1,4,5)P_3 as substrate, however conversion of IP_3 to IP_4 or IP_5 is hard to assess by PAGE due to poor staining of lower inositol phosphates by Toluidine. Therefore the cell extracts of both WT and *ipmk* were assayed for their ability to metabolise IP_5 isomers to IP_6 (or PP-IP_4) (**Figure 3.17**). For reference the endogenous inositol phosphates present in the same volume of cell extract used to treat IP_5 could be detected in lanes 10 and 11.

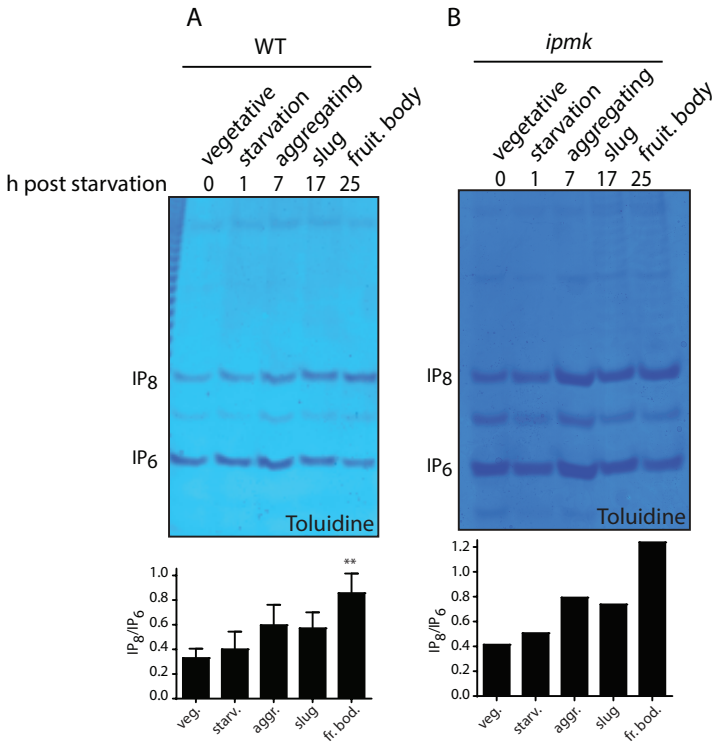

Figure 3.16 Accumulation of inositol pyrophosphates during development in *ipmk*.

Cells were starved as described in (**materials and methods, 2.3.10**). The inositol phosphates extracted at the indicated time points were resolved on 35.5% PAGE and visualised with Toluidine. As shown in **Figure 3.12**, the analysis of WT revealed a 2-fold increase in the IP_8/IP_6 ratio during development as quantified by densitometry quantified (Bottom), average +/- SD of four independent experiments (A), panel adapted from (Pisani, Livermore et al. 2014), and **Figure 3.12**. Analysis of *ipmk* revealed a developmental increase in inositol pyrophosphates, quantified by densitometry (below) (B). Results for *ipmk* were not repeated and quantification was from the gel shown. Statistical differences were evaluated according One-way ANOVA, multiple comparisons. Significant differences were indicated where (**$p < 0.01$).

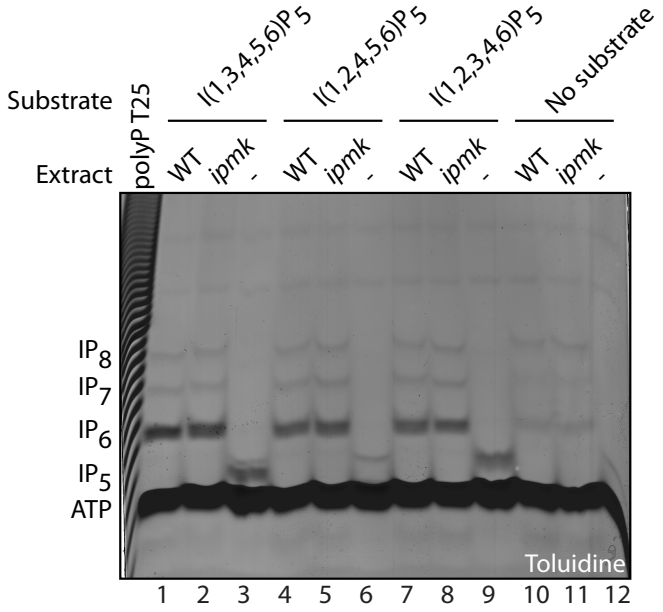

Figure 3.17 IP_5 kinase activity in cell extract.

Cell extracts were prepared as described in (**materials and methods, 2.3.11**) from vegetative cultures of WT and *ipmk* cells. Three isomers of IP_5 were treated with extract and formation of IP_6 was detected by PAGE analysis and Toluidine blue staining. This result is representative of an experiment was performed twice.

Phosphorylation of IP_5 to either IP_6 or PP-IP_4 was observed by both the diminished strength of the IP_5 band compared to untreated substrate (lanes 3, 6 and 9) and the accumulation of IP_6 or PP-IP_4 in lanes 1,2,4,5,7 and 8. This experiment revealed strong activities towards the three tested isomers of IP_5, the presence of which had all been previously described in *D. discoideum* (Stephens and Irvine 1990). All observed activities were present in both WT and *ipmk* extracts.

Whilst a full panel IPMK substrates was not tested, this experiment once more failed to identify any difference between WT and *ipmk.* Nevertheless it should be noted that it is not possible to attribute this activity to any particular enzyme, nor is it possible to distinguish between synthesis of IP_6 and PP-IP_4 by the experiments described. Further experiments would be required to ascertain the precise identity of this band however these were not performed in this work.

3.3 Discussion

3.3.1 Synthesis of inositol pyrophosphates

The work described in this chapter demonstrates that the synthesis of the inositol pyrophosphates is more complex than anticipated in the myxamoeba *D. discoideum*. It also highlights further differences between the synthetic pathway of IP_7 and IP_8 between *D. discoideum* and *S. cerevisiae.* This should perhaps not come as a surprise given the previously noted discrepancies between the synthesis of inositol phosphates in yeast and *D. discoideum.* Inositol phosphates are synthesised independently of the lipid route in *D. discoideum* (Stephens and Irvine 1990), as confirmed by PAGE (**Figure 3.1,** (Pisani, Livermore et al. 2014)) unlike in *S. cerevisiae* in which the *plc1Δ* lacks the higher soluble inositol phosphates (York, Odom et al. 1999).

As previously noted the deletion of Ip6k results in a strain lacking almost all IP_7 and IP_8. However, residual levels of IP_7 could still be detected in this strain (Pisani, Livermore et al. 2014)(**Figure 3.7**). This finding was in contrast to the *kcs1Δ* yeast strain, in which IP_7 is undetectable (Saiardi, Sciambi et al. 2002). In addition the generation of the *ppip5k* mutant reveals further, striking differences to the synthesis of IP_8 compared to yeast. Whilst the levels of IP_8 are dramatically reduced (**Figure 3.8 and 3.9**), readily detectable levels of IP_8 remain. This suggests that the PPIP5K enzyme is not the only IP_7 kinase in the *D. discoideum* genome. These results are in stark contrast to those from the *vip1Δ* yeast strain, in which there is no detectable IP_8 and an increase in the level of IP_7 compared to WT yeast (Onnebo and Saiardi 2009).

In fact, the *ppip5k* strain differs from *vip1Δ*, not only in the presence of IP_8, but that rather than increasing, the band identified as IP_7 actually decreases. Given that IP_7 is predicted to be the substrate of the PPIP5K enzyme, it was counterintuitive that its deletion should result in a decrease in the substrate. In

fact, further investigation revealed that this was most likely due to the fact that the band identified as IP_7 is comprised of two co-migrating species; the classical IP_7 (PP-IP_5) consisting of a fully phosphorylated inositol ring and a single pyrophosphate moiety, as well as an IP_5-derived inositol pyrophosphate ($(PP)_2$-IP_3) species hosting two pyrophosphate moieties. This is consistent with previous findings that the amoeba, *D.* discoideum, possesses significant levels of IP_5-derived inositol pyrophosphates (Pisani, Livermore et al. 2014). Considering the loss of "IP_7" staining in the *ppip5k* strain, as seen in **Figure 3.8 A,** and quantified in **Figure 3.8 B**, it seems probable that PPIP5K products include IP_5-derived inositol pyrophosphates ($(PP)_2$-IP_3).

Furthermore, the generation of a double knockout strain in which both IP6K and PPIP5K were deleted, *ip6k/ppip5k,* revealed additional complexity. This strain, which lacks the two conventional inositol pyrophosphate-synthesising enzymes, retains low, but detectable levels of inositol pyrophosphates (**Figure 3.7**). The presence of IP_8 in the *ppip5k* strain is suggestive of another inositol pyrophosphate-synthesising enzyme. While it cannot be excluded that the *D. discoideum* IP6K is a hybrid kinase, capable of phosphorylating both IP_6 and IP_7, the presence of IP_7 in the *ip6k/ppip5k* strain confirms the presence of additional enzyme(s) capable of synthesising inositol pyrophosphates in the amoeba.

These data demonstrate that IP6K is the primary source of IP_7 in the amoeba *D. discoideum*. Whilst other enzymes are clearly capable of synthesising IP_7 they are not able to compensate for the loss of IP6K. The presence of residual IP_7 in the *ip6k/ppip5k* double mutant indicated that there is an additional enzyme capable of synthesising inositol pyrophosphates, however the low abundance of IP_7 in this strain suggests that it's activity towards IP_6 is low. The presence of IP_8 in the *ppip5k* strain also indicates that PPIP5K is not the only enzyme capable of synthesising IP_8 in this amoeba. It is possible that the same enzyme catalyses both of these activities.

It should perhaps not be surprising that the synthesis of IP_8 in *D. discoideum* is more complex than in yeast. The amoeba is peculiar amongst all organisms examined for its increased abundance of IP_8 over IP_7. The accumulation of IP_8 to high levels is an unusual feature, normally associated with particular treatments, such as NaF in mammalian cells (Menniti, Miller et al. 1993). However, IP_8 is the most abundant form of inositol pyrophosphate in the amoeba, approximately three-times the abundance of IP_7 (Pisani, Livermore et al. 2014).

As noted previously, the amoeba's PPIP5K enzyme lacks the phosphatase domain found in Vip1 and HsPPIP5K (**Figure 7.2**). Given the specific activity of this phosphatase domain towards the product of the attached kinase domain (Wang, Nair et al. 2015), one possible hypothesis for the accumulation of IP_8 could be the unmasking of PPIP5K activity by the removal of its own remarkable futile cycle. However, the genetic evidence described above indicates that this alone cannot explain the extraordinary abundance of IP_8.

3.3.2 Effect on general fitness

Analysis of the general fitness of the *ip6k*, *ppip5k* and *ip6k*/*ppip5k* mutant strains failed to detect any major phenotypes associated with reduced levels of inositol pyrophosphates. Growth rate was mildly affected in three strains showing defective synthesis of inositol pyrophosphates. This was once again markedly different from yeast in which *kcs1Δ* displays a major growth defect (Saiardi, Erdjument-Bromage et al. 1999). However, it should be noted that these experiments were performed in rich (HL5) media. Analysis of the growth of *kcs1Δ* yeast on a range of carbon sources reveals that this growth phenotype is exacerbated by growth on different media (Szijgyarto, Garedew et al. 2011). The growth of the *ip6k* mutant was assayed in rich media and on bacterial lawns (not shown), revealing no major growth defects. Both HL5 and bacteria represent rich sources of nutrient and it is possible that faced with the additional challenge

of minimal or sub-optimal media, a more substantial fitness defect may have emerged. It would be interesting to test this possibility more rigorously in further work.

3.3.3 Developmental accumulation of inositol pyrophosphates

It was previously noted that IP_8 increases 25 fold during the developmental response (Laussmann, Pikzack et al. 2000). However, this analysis reveals that, whilst there was a dramatic increase in the level of IP_8 during development, it was not of the scale described (**Figure 3.12**). A more modest 2.5 fold increase in the level of IP_8 was detected in these experiments. This figure was calculated relative to the level of IP_6, which was considered to be broadly consistent throughout the developmental time course. This discrepancy with previously published data is due to the much higher levels of inositol pyrophosphates detected in the vegetative state (**Figure 3.1**). Meanwhile this analysis, which reveals the level to which IP_8 accumulates in the fruiting bodies (**Figure 3.12 A**) is consistent with previous calculations (Laussmann, Pikzack et al. 2000). It is seems likely that the discrepancy between the levels of inositol pyrophosphates detected during the vegetative state were due to methodological differences, not genuine physiological differences.

Analysis of the developmental accumulation of inositol pyrophosphates of the mutants generated reveals once more, that IP6K is the primary source of IP_7 in this amoeba at all stages of development. The *ip6k* mutant completely fails to accumulate any inositol pyrophosphates during fruiting body formation. Meanwhile, the *ppip5k* mutant undergoes a developmental increase in the level of inositol pyrophosphates. This accumulation is evident from 8 h after onset of starvation. Averaging of two experiments reveals that the level of IP_8 does not quite reach the level obtained in WT cells, with levels of IP_8 rising to approximately 70% of IP_6. This result indicates that, despite its dramatic developmental increase in expression (**Figure 3.4**), PPIP5K is not solely

responsible for the increase in inositol pyrophosphates during the starvation response. It seems likely, therefore, that the enzyme responsible for the increase in IP_8 is developmentally regulated. It appears that this enzyme(s) has a strong preference in substrate for IP_7 over IP_6 as it is not able to induce a developmental increase of IP_7 in the *ip6k* mutant.

Despite the alterations in the accumulation of inositol pyrophosphates during development, neither mutant strain analysed in this way exhibits significant defects in developmental progression or timing. The *ip6k* strain showed a slight increase in aggregation speed, but both *ip6k* and *ppip5k* formed fruiting bodies as normal. The spores of both strains also appeared to germinate as normal (data not shown). These observations were somewhat surprising given the substantial amounts of energy invested in to the accumulation of these molecules during a period of starvation. It might, therefore, be reasonable to expect that the complete failure to accumulate these molecules would result in a more dramatic phenotype.

3.3.4 Link between inositol pyrophosphates and primary metabolism?

Given the conserved link between inositol pyrophosphates and energetic metabolism in yeast and mammalian cells, it is also surprising that no such link was detected in the amoeba in these experiments (**Figure 3.13**). There was no significant difference between the levels of ATP measured from WT or *ip6k* cells.

3.3.5 A role for inositol pyrophosphates in *D. discoideum*?

Given the apparent absence of dramatic metabolic defect and the absence of any major phenotype during development when the inositol pyrophosphates accumulate, it is not clear what exactly these molecules are doing either in the vegetative state or during development. The extraordinarily high levels of the inositol pyrophosphates in *D. discoideum* are almost unmatched in any other model tested to date. So it is natural to expect that loss of the vast majority of

this pool would precipitate major changes in the physiology of these cells. However, these analyses failed to detect such changes.

In considering possible explanations for this lack of phenotypes it should be noted that it is far more common for the level of IP_7 to exist at a fraction of that of IP_6 and in the low μM range of concentrations, rather than the low mM range seen in *D. discoideum*. In yeast, where loss of IP_7 in the *kcs1Δ* strain, induces a wide range of phenotypes and has substantial effects on general fitness, the steady state level of IP_7 is barely 5% of the level of IP_6, itself a fraction of the level of IP_6 in the amoeba. Thus in other organisms very low steady state levels of inositol pyrophosphates are able to exert their influence on the physiology of a cell.

Whilst no attempt was made to quantify the abundance of residual IP_7 in either the *ip6k* or *ip6k/ppip5k* strains, IP_7 was detectable in the extracts made from ~2 $x10^6$ cells. Meanwhile, recent technological developments, including the use of Titanium dioxide (TiO_2) beads to enrich inositol pyrophosphates have allowed the use of PAGE to analysis mammalian inositol pyrophosphates (Wilson, Bulley et al. 2015). In this study, IP_7 could be detected by Toluidine in extracts made from 8 $x10^7$ cells, approximately 50 times more than required to detect IP_7 (by DAPI) in the *ip6k/ppip5k* strain. Clearly the added sensitivity of DAPI over Toluidine plays a role in this discrepancy. At the same time it should be noted that detection of IP_7 from barely 2 million cells still represents an abundance of IP_7 which may be comparable to yeast and mammalian cells. Thus, whilst inositol pyrophosphates are hugely diminished compared to WT amoeba, it is possible that the failure to detect any notable phenotype in *ip6k, ppip5k* or *ip6k/ppip5k* mutant strains, might be due to the residual levels of IP_7. It is possible that this residual pool might be sufficient to perform the many fundamental physiological roles of the inositol pyrophosphates.

This hypothesis has not been tested in this work since it would require the identification and deletion of the enzyme responsible for the synthesis of IP_7 in the *ip6k*/*ppip5k* strain. Whilst this hypothesis could explain the lack of phenotype observed in these mutants, it poses an additional question of why exactly the amoeba would accumulate such high levels of inositol pyrophosphates in the first place. Especially if the residual levels observed in the *ip6k*/*ppip5k* are sufficient for almost normal cell function.

At this point it is interesting to note a recent study postulating a possible explanation for the high abundance of IP_6 in these amoeba (Weber, Stirnimann et al. 2014). This work identified a cysteine phytase, termed Lppa, in the genome of the intracellular pathogen *Legionella pneumophila.* This bacteria, the causative agent of Legionnaire's disease, replicates in the "*Legionella*–containing vacuole" of free-living amoeba and mammalian phagocytes. During infection the bacteria secretes >300 proteins into the host cell. One such protein is Lppa. Lppa is able to degrade phytate *in vitro* and was shown to offer a growth advantage for bacteria when they infected *D. discoideum* amoeba pre-loaded with IP_6 (Weber, Stirnimann et al. 2014).

This study postulated that the degradation of intracellular IP_6 was beneficial for the infecting bacteria, possibly due to the release of ions chelated by IP_6. Thus the local degradation of IP_6 by bacterial proteins might release important micronutrients that are beneficial for the pathogen. This interesting hypothesis could be further extrapolated to suggest that exceptionally high levels of inositol phosphates in the amoeba might represent a protective measure to defend against pathogenic bacteria. The chelation of micronutrients by high concentrations of IP_6 might have been protective against pathogens, which have subsequently evolved phytase secretion as a means to counteract this measure. Whilst this work does not address the role of inositol pyrophosphates it does

offer interesting insight into the remarkably high concentrations of inositol phosphates in *D. discoideum*.

3.3.5 IPMK

The role of the IPMK was investigated by generating an *ipmk* null strain. *In vivo* evidence places this enzyme as primarily responsible for directly phosphorylating IP_3 to IP_5 (Saiardi, Sciambi et al. 2002), however, this enzyme has been shown to also synthesise inositol pyrophosphates (Saiardi, Nagata et al. 2001) and phosphoinositides (Resnick, Snowman et al. 2005) *in vitro*. Deletion of this gene was confirmed by Southern and Northern blot. Surprisingly, Northern blot analysis detected three bands hybridising to the IPMK probe in WT cells. All three were absent from the *ipmk* strain, suggesting that the two slower migrating bands may not be simply non-specific binding, but genuine IPMK transcripts. As discussed previously, the remarkably long 3' UTR of mammalian IPMK (Saiardi, Nagata et al. 2001) adds credence to this possibility.

Meanwhile, deletion of the Ipmk gene had no detectable effect on the synthesis of inositol pyrophosphates either in the vegetative state or during development. These results suggest that, as with the synthesis of inositol pyrophosphates, the synthetic pathway of inositol phosphates in *D. discoideum* is more complex than in yeast. Deletion of Arg82 ablates the presence of highly phosphorylated species of inositol phosphates above IP_3 (Saiardi, Sciambi et al. 2002). The *arg82Δ* also displays a range of phenotypes, including slow growth rate and inability to grow on non-fermentable carbon sources (Saiardi lab observation). Thus the lack of phenotype in *D. discoideum* is surprising.

The expansion in the number of inositol phosphate kinases encoded in the *D. discoideum* offers the most likely explanation for this difference from yeast. The presence of the ITPK1, which is also able to phosphorylate IP_3, may be of particular relevance. The expression levels of this gene are low (**Fig 3.4**),

however it is possible that its expression may be increased in response to deletion of Ipmk. This hypothesis was not tested.
Furthermore, the presence of two additional inositol phosphate kinase family members, named here IPKA and IPKB may be able to compensate for the deletion of IPMK. In fact IPKA was annotated as an IPMK and has been used to recue to overexpression of the phosphatase MIPPS (King, Keim et al. 2010). It is also possible that IPMK performs a slightly different function in *D. discoideum*, perhaps even acting as a phosphoinositide kinase rather than a soluble inositol phosphate kinase.

3.3.6 Concluding remarks

It is documented the deletion of phospholipase C has no effect on the levels of inositol phosphates in the amoeba (Drayer, Van der Kaay et al. 1994, Pisani, Livermore et al. 2014) and that inositol can be phosphorylated in a stepwise manner to form IP_6 (Stephens and Irvine 1990). When combined with the data described above it is evident that a large number of differences exist between the synthetic pathways of the inositol phosphates between *S. cerevisiae* and *D. discoideum.*

Moreover, there are divergences between the roles played by these molecules in the amoeba. Despite being far lower abundance in yeast, the loss of inositol pyrophosphates has a range of dramatic phenotypes. Whilst only a small number of these were investigated in this work, no dramatic alterations to growth rate or primary metabolism were observed in the *ip6k* or *ip6k*/*ppip5k* strains. It is possible that these molecules play an altogether different role in the *D. discoideum.*

The conservation in the function of inositol pyrophosphates between yeast and mammalian cells makes this conclusion a surprising one. An alternative explanation, as described above, could be the presence of residual levels of IP_7

in both the single *ip6k* and the double *ip6k*/*ppip5k* mutants. When compared to virtually all other cells this abundance of IP_7 reflects a substantial level of inositol pyrophosphates. Thus it is plausible that this apparently small residual pool is, nevertheless, functional and sufficient to protect the *ip6k* and *ip6k*/*ppip5k* strains from the phenotypes observed in other models.

In order to investigate this hypothesis and to develop the amoeba as a clean genetic model, it is necessary to identify the enzyme or enzymes capable of synthesising inositol pyrophosphates in the *ip6k*/*ppip5k* strain. The final experiment in this chapter offers a tempting methodology to investigate this. The ability to detect the activity of inositol phosphate kinases in cell extracts allowed the activity towards a range of IP_5 substrates to be tested (**Figure 3.17**). The availability of highly pure IP_7 isomers (courtesy of Prof Henning Jessen)(Capolicchio, Thakor et al. 2013) could be used to test for the presence of the additional IP_7 kinase activity identified in the *ppip5k* strain. If such an activity could be detected in the cell extract of *D. discoideum* it may allow the biochemical purification and identification of the enzyme responsible. Identifying this enzyme could ultimately help to develop a “clean” genetic model lacking all inositol pyrophosphates.

4. Identifying additional sources of inositol pyrophosphates

4.1 Introduction

The results discussed in **Chapter 3** demonstrate the presence of at least one additional enzyme capable of synthesising inositol pyrophosphates. The detection of residual IP_7 in the *ip6k*/*ppip5k* strain indicated that a further enzyme displays IP_6 kinase activity. Furthermore, there is a pool of IP_8 synthesised independently of PPIP5K, in a developmentally regulated way. It is possible that a single enzyme that is capable of phosphorylating both IP_6 and IP_7 catalyses both of these activities. If so, it would appear that the preferred substrate of this enzyme is IP_7 rather than IP_6 Alternatively, different enzymes may catalyse each reaction.

It has previously been described that WT *D. discoideum* cell extract possesses a kinase activity towards a particular isomer of IP_7 in which the pyrophosphate moiety is positioned on carbon 6 of the inositol ring (Laussmann, Reddy et al. 1997). The identification of this activity is consistent with the NMR characterisation of IP_8 in *D. discoideum* as either the (4,5)PP_2-IP_4 or (5,6)PP_2-IP_4 (Laussmann, Eujen et al. 1996, Laussmann, Reddy et al. 1997) with positions 4 and 6 being enantiomeric (**Figure 1.1**) and indistinguishable by NMR. In fact the identification of this activity allowed the distinction between the two possible isomeric forms, indicating that the IP_8 found in *D. discoideum* is (5,6)PP_2-IP_4, in contrast to the (1,5)PP_2-IP_4 thought to be present in both yeast and mammalian cells. In truth, the only inositol pyrophosphates extracted from cells to have been examined by NMR are those extracted from the amoeba *D. discoideum.*

The enzyme responsible for the unusual IP_7 kinase activity was partially purified, identifying an enzyme of ~40 kDa (Laussmann, Reddy et al. 1997). The precise

enzyme responsible for this activity was not cloned, however, the approximate size suggests that it is unlikely to be either IP6K or PPIP5K (**Table 3.1**).

The objective of the work described in this chapter, was therefore to identify the additional enzyme, or enzymes, capable of synthesising inositol pyrophosphates in *D. discoideum*. The previous description of an IP_7 kinase activity in WT extract, as well as the cell extract kinase assays performed in **Figure 3.17** offered an experimental design that could be followed. Testing for this activity in a panel of mutants could confirm that this activity is not attributable to either IP6K or PPIP5K.

4.2 Results

4.2.1 IP_6 and IP_7 kinase activity in cell extract

Isomeric forms of IP_7 were made available to the Saiardi lab courtesy of Dr Henning Jessen (Capolicchio, Thakor et al. 2013). These isomers facilitated cell-free assays to test for IP_7 kinase activity in WT and mutant *D. discoideum* extract as well as mouse (*Mus musculus*) brain extract. These assays were analogous to those described in **Chapter 3** (**Figure 3.17**). IP_6 was also provided as a substrate in order to test the presence of an IP6K activity in extract. The products of these cell-extract assays were analysed by 35.5% PAGE and stained with Toluidine (**Figure 4.1-4.2**).

Initial experiments compared the IP_7 kinase activities detected in WT *D. discoideum* extract (*Dd*) and *M. musculus* brain extract (*Mm*) (**Figure 4.1**) Extract alone was loaded in lanes 10 and 11 on both gel panels (**A** and **B**) for reference. *Dd* extract contained detectable endogenous levels of IP_6, IP_7 and IP_8 as seen in lane 10. Meanwhile, endogenous inositol phosphates could not be detected in *Mus musculus* extract. Furthermore, the IP_7 substrates provided in each reaction were not completely pure and contained some residual levels of IP_6 and IP_8. The

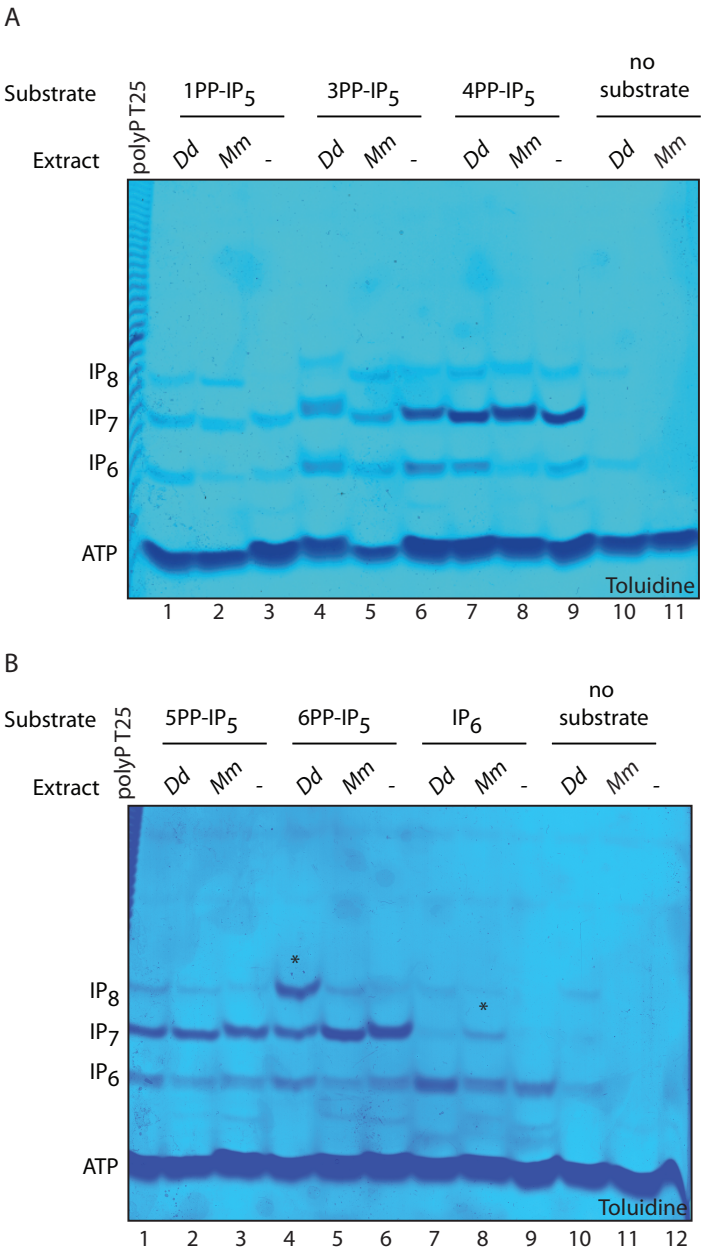

Figure 4.1 IP_6 and IP_7 kinase activity in *D. discoideum* (Dd) and *Mus musculus* (Mm) cell extract.

Cell extracts were prepared as described (**materials and methods, 2.3.11**) from WT vegetative *D. discoideum* culture (Dd) and mouse brain (Mm). Five isomers of IP_7 as well as IP_6 were treated with extract. Formation of IP_8 and IP_7 was detected by 35.5% PAGE analysis and Toluidine staining and indicated with (*).

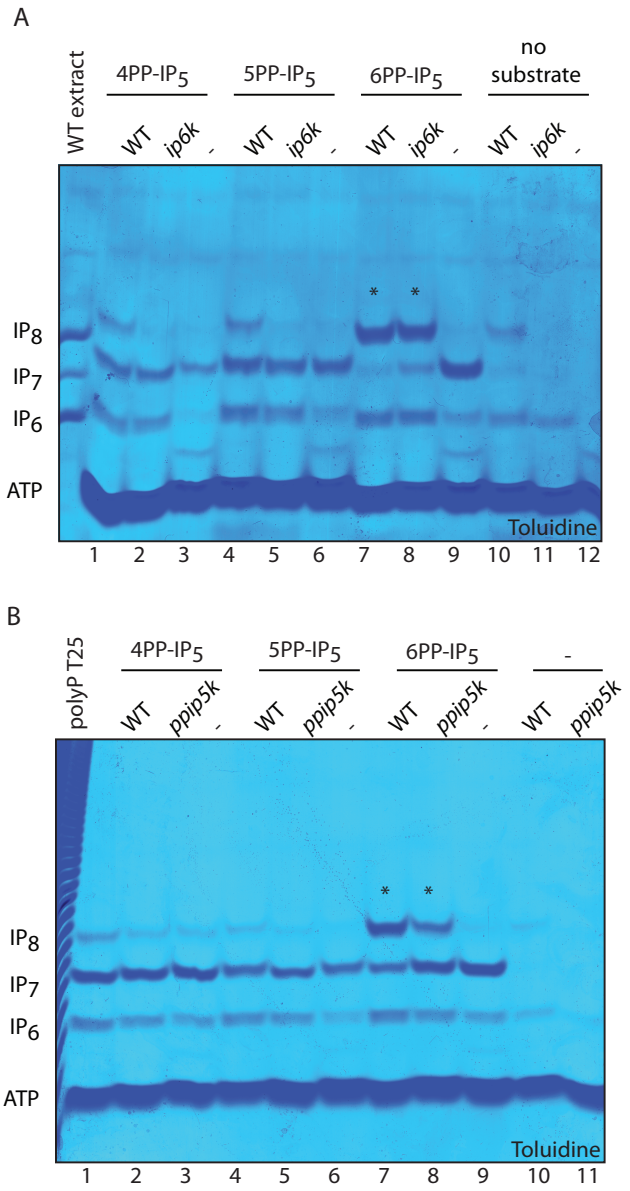

Figure 4.2 IP_7 kinase activity in ip6k and ppip5k *D. discoideum* (Dd) cell extract.

Cell extracts were prepared as described (**materials and methods, 2.3.11)** from vegetative *D. discoideum* culture as indicated. Three isomers of IP_7 were treated with extract prepared from WT, *ip6k* and *ppip5k*. Formation of IP_8 was detected by 35.5% PAGE analysis and Toluidine staining and indicated with (*)

substrates utilised in these assays were IP_6 and five isomers of IP_7, 2PP-IP_5 was not available and therefore not included.

Robust conversion of IP_7 to IP_8 by *Dd* extract could only be detected when the 6PP-IP_5 isomer was provided as a substrate (**Figure 4.1 A,** lane 4) marked with an asterix (*). Notably, IP_6 kinase activity could not be detected in *Dd* extract (**Figure 4.1 B,** lane 7). Conversely, in mouse brain extract, no IP_7 kinase activity could be detected, although IP_6 kinase activity was present (**Figure 4.1 B,** lane 8).

The kinase activity identified towards 6PP-IP_5 was consistent with the activity previously reported in *D. discoideum* extract (Laussmann, Reddy et al. 1997). The partial purification of this enzyme identified a protein of a ~40 kDa. However, its identity was not confirmed. To-date no inositol phosphate kinases have been found to be specific to 6PP-IP_5. However, to confirm that neither IP6K, nor PPIP5K were responsible for the phosphorylation of 6PP-IP_5, cell extracts from both *ip6k* and *ppip5k* were used in this assay (**Figure 4.2**). As in (**Figure 4.1**), extract alone was loaded in lanes 10 and 11 (**Figure 4.2 A and B**). It should be noted that whist IP_6, IP_7 and IP_8 were detectable in WT extract; only IP_6 was detected in *ip6k* (**Figure 4.2 A,** lane 11). However, despite the absence of IP6K, the conversion of 6PP-IP_5 to IP_8 was equally robust when treated with *ip6k* cell extract (**Figure 4.2 A,** lane 8). No other activity could be detected in either WT of *ip6k* extract. Similarly, *ppip5k* cell extract also retained the ability to phosphorylate 6PP-IP_5 to IP_8 (**Figure 4.2 B,** lane 8). The conversion of IP_7 to IP_8 appeared slightly reduced in the *ppip5k* strain, however this may be due to a reduced concentration of extract as shown by the weaker endogenous IP_6 band seen in extract alone (lanes 10 and 11).

These results suggested that neither IP6K, nor PPIP5K were the enzymes responsible for the conversion of 6PP-IP_5 to IP_8. To unambiguously confirm this

the extract of the *ip6k*/*ppip5k* double mutant was tested (**Figure 4.3)**. All extracts tested, including the previously generated *ip6k** mutant (Luo, Huang et al. 2003)(**Figure 4.3,** lane 9) and the double mutant *ip6k*/*ppip5k* (lane 7), demonstrated very robust conversion of 6PP-IP_5 to IP_8.

The identification of an IP_7 kinase activity in the *ip6k*/*ppip5k* mutant extract clearly demonstrated the presence of an alternative source of inositol pyrophosphates in *D. discoideum*. The next step was to identify the enzyme responsible for this activity. Two separate approaches were employed; the first was the biochemical purification of this activity following diverse enrichment procedures. In order for this approach to be successful the activity must be very robustly detectable after numerous processing steps, explored in **Figures 4.4** and **4.5**. The second approach was a candidate approach, described in **Figure 4.6** onwards.

4.2.2 Biochemical purification of 6PP-IP_5 kinase activity

Initially, the ability of *ip6k*/*ppip5k* extract to phosphorylate 6PP-IP_5 in a range of different conditions was tested (**Figure 4.4)** to study the stability of this activity and its suitability to purification.

1) Testing the effect of freezing. Extract was prepared from fresh *ip6k*/*ppip5k* cell pellets as well as those that had been frozen at -80°C. These extracts were then incubated with substrate for between 30 min and 3 h. Faint IP_6 bands were detectable in both fresh extract alone (**Figure 4.4 A,** lanes 1 and 4), as well a frozen extract alone (lanes 6 and 12), with a stronger IP_6 band in the frozen extract. This may be due to more complete lysis during preparation of extract due to freezing. Substrate alone contained some IP_6 contaminant, but no detectable IP_8 (lanes 14 and 15). IP_7 kinase activity could be observed in extract made from both fresh and frozen cell extract in reaction volumes of both 25 μl (lane 2, 7-10) and 40 μl lanes 3 and 11). Activity could be detected after

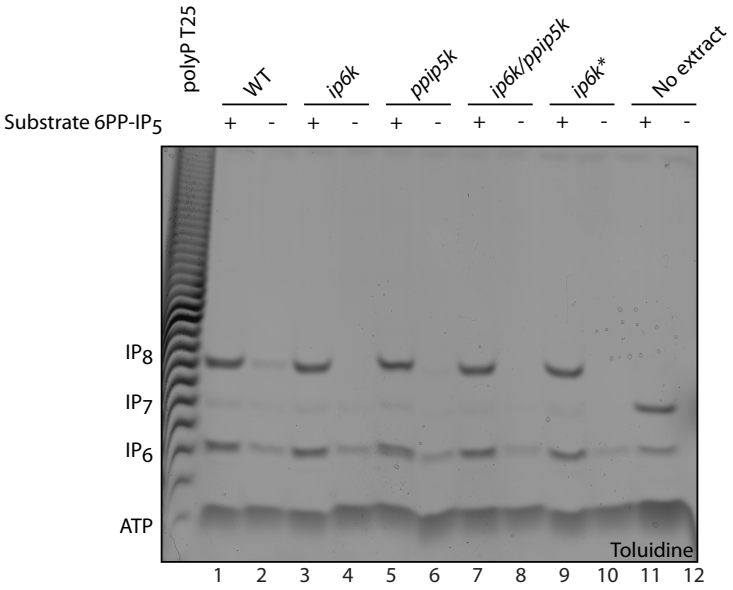

Figure 4.3 6PP-IP_5 kinase activity in mutant panel of *D. discoideum (Dd)* cell extracts.

Cell extracts were prepared as described in (**materials and methods, 2.3.11**) from vegetative *D. discoideum* culture as indicated. Three isomers of IP_7 were treated with extract WT, *ip6k, ppip5k, ip6k/ppip5k* and *ip6k**. Formation of IP_8 was detected by 35.5% PAGE analysis and Toluidine staining.

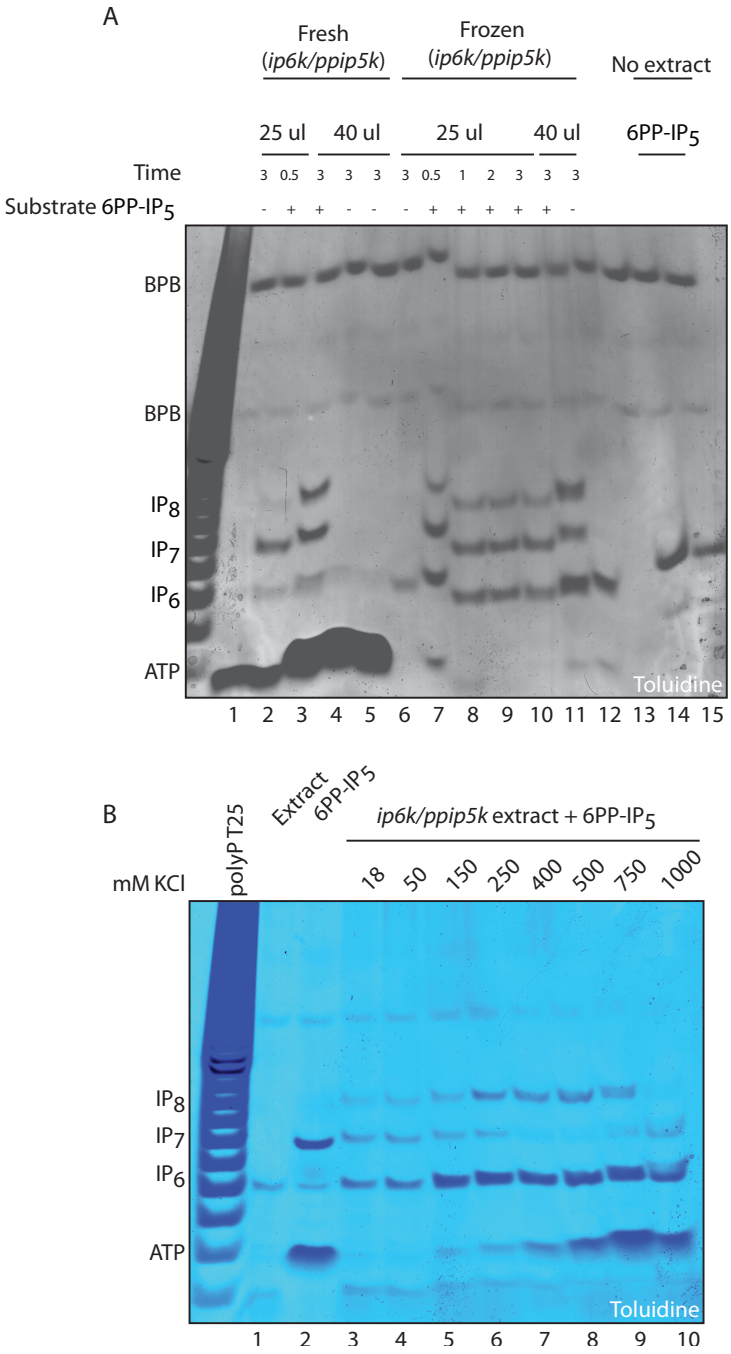

Figure 4.4 6PP-IP$_5$ kinase activity could be robust detected in a range of conditions.

Cell extracts were prepared as described (**materials and methods, 2.3.11**) from vegetative *ip6k/ppip5k* culture or from frozen pellets (as indicated) (A). The activity of these extracts in either 25 μl or 40 μl was assayed as were reaction incubations between 30 min and 3 h as indicated (A). Cell extracts were supplemented with between 18 and 1000 mM KCL. IP$_7$-kinase activity of extract was determined by conversion of substrate to IP$_8$ through 35.5% PAGE analysis and Toluidine staining (B).

incubation of only 30 min (lanes 2 and 7), although this was weak when using fresh extract (lane 2).

2) Testing the effect of salt. The effect of salt concentration on IP_7 kinase activity was then investigated by supplementing the reaction mix with concentrations between 18 mM KCl to 1 M KCl (**Figure 4.4 B**). IP_7 kinase activity could be detected in all fractions up to 750 mM KCl. The strongest activity appeared at relatively high concentrations of salt, between 400 mM and 750 mM (lanes 7-9). No IP_7 kinase activity could be detected in reactions containing 1 M KCl (lane 10). Another activity could also be detected in these samples, degrading IP_7 to IP_6. This activity also showed a similar increasing activity up to 750 mM KCl. Degradation of substrate to IP_6 could also be detected in conditions of 1 M KCl. These results indicated that the IP_7 kinase activity present in this extract was very robust and possibly amenable to purification by fractionation.

3) Identification of the appropriate chromatography substrate. Following these observations it was necessary to identify the appropriate chromatography to use in order to purify this activity. Three purification steps would be desirable to generate a fraction pure enough to be analysed by mass spectrometry. Biochemical purification can be achieved by several means, including selective precipitation, differential binding to chromatography substrates as well as size exclusion chromatography (also referred to as gel filtration). Preliminary experiments were performed by ion exchange chromatography using a DEAE column (GE Healthcare) (**Figure 4.5 A**) and a HiTrap Heparin column (GE Healthcare) (**Figure 4.5 B**). In both cases the activity could only be detected in the flow through (**Figure 4.5 A**, lanes 1-4 and **Figure 4.5 B**, lanes 4 and 5), indicating that the protein responsible for this activity did not bind to either column.

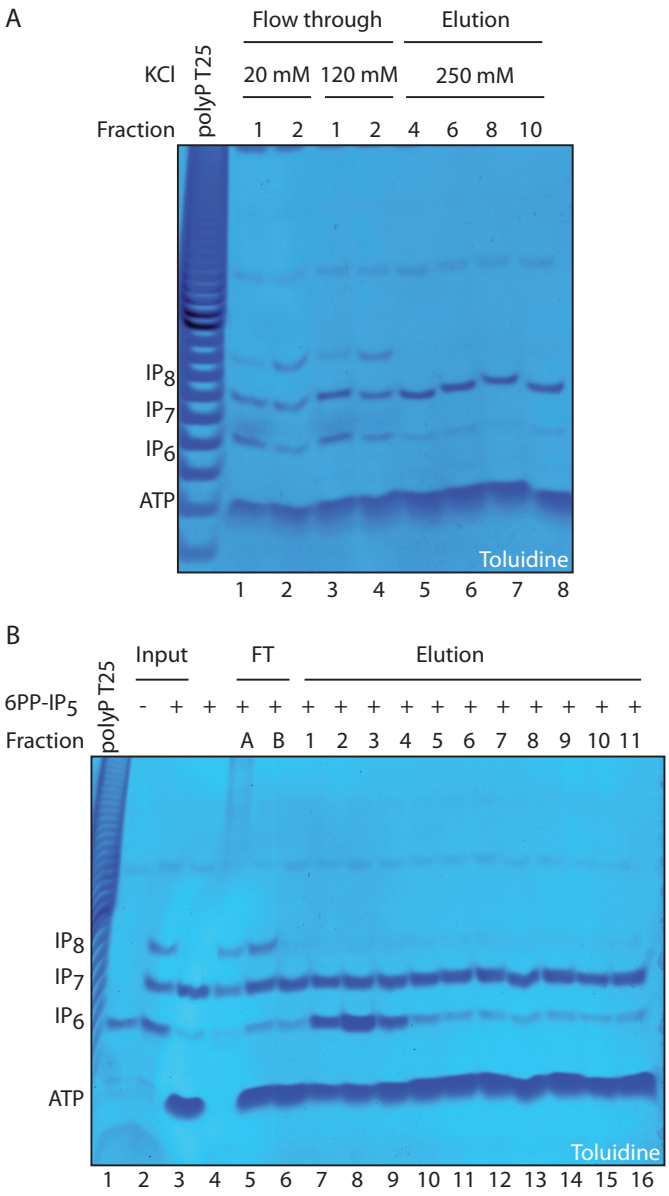

Figure 4.5 Biochemical purification of cell extract failed to identify a IP_7 kinase purification strategy

Cell extracts were prepared as described (**materials and methods, 2.3.11**) from vegetative *ip6k/ppip5k* culture and subjected to biochemical purification using either Heparin (A) or DEAE (B) columns. The activity eluted in flow through of both fractionation approaches indicating the enzyme did not bind to either column. Reactions were analysed by 35.5% PAGE and stained with Toluidine.

Interestingly an increase in the level of IP_6 could be detected in some fractions eluting from the Heparin column (**Figure 4.5 B**, lanes 7-9). There were two possible sources for this increase in IP_6; the first was the elution of the IP_7 phosphatase activity noted in **Figure 4.4 B**, the second was the elution of endogenous IP_6 that had bound to the column. Given that the level of IP_7 did not seem to decrease in these reactions (which would be indicative of a phosphatase) it seemed most likely that endogenous IP_6 bound to the Heparin column and eluted in these fractions. This was surprising due to strong negative charge of both heparin and IP_6, however, the early elution suggests that this interaction was relatively weak.

These preliminary purification procedures confirmed that it was possible to follow the kinase activity of this extract. However, the enzyme responsible for this activity did not bind to either column tested. Neither of these steps would therefore be appropriate for purificaion and identification of the enzyme by this approach. Whilst many other purification approaches and chromatography columns were available, a parallel, candidate approach was taken.

4.2.3 Identifying the 6PP-IP_5 kinase by a candidate approach

As noted previously (**Table 3.1**) two genes for uncharacterised inositol phosphate kinases have been identified in the *D. discoideum* genome. One of these enzymes has been described as an IPMK (King, Keim et al. 2010), whilst the other has been annotated to encode an IP6K. These genes will be hereafter referred to as Ipka and Ipkb respectively. The gene products (referred to here as IPKA and IPKB) have predicted sizes of 37 kDa and 70 kDa (**Table 3.1**).

Previous attempts to purify the 6PP-IP_5 activity were able to identify the enzyme responsible to have a size of ~40 kDa (Laussmann, Reddy et al. 1997). Therefore, despite previous characterisation as an IPMK, IPKA appeared a

strong candidate for this activity. Consequently, several attempts were made to delete the gene by homologous recombination. Two deletion constructs were designed (**Figure 4.6**) and each used several times to try and delete this gene. However, neither approach was successful. Unfortunately, one disadvantage of using the haploid *D. discoideum* amoeba as a model system is the difficulty in confirming whether a gene is essential. Deletion of an essential gene, as in any system will result in a lethal phenotype. However, unlike in yeast crossing of heterozygous mutants is not possible. Therefore, after several failed attempts at deletion, it was assumed that this gene is either essential, or the local genomic environment of the gene prohibited the homologous recombination required for deletion. Whilst it is possible to use RNA-mediated knock down approaches in the *D. discoideum* (Friedrich, Meier et al. 2015), these were not investigated in this work.

4.2.4 IPKA: cloning and expression in *S. cerevisiae*

Due to the inability to delete this gene, an alternative approach was employed and this enzyme was cloned from a cDNA library, (generated as described in **materials and methods, 2.2.9)**. Given its relatively small size (~900 bp) and high GC content it seemed possible that this gene could be expressed in the yeast, *S. cerevisiae*. The availability of a comprehensive panel of mutants in yeast allowed the enzymatic activity of this gene product to be probed according to its ability to rescue certain yeast strains. The disadvantage of this approach, aside from using a heterologous system, would be that the putative substrate for this enzyme, 6PP-IP_5 is not present in yeast. Yeast has just two enzymes capable of synthesising inositol pyrophosphates, Kcs1p and Vip1p, which phosphorylate positions 5 and 1 of the inositol ring, respectively.

In order to assess the activity of this enzyme and distinguish between action as an IPMK, as annotated, or an inositol-pyrophosphate synthesising enzyme, the

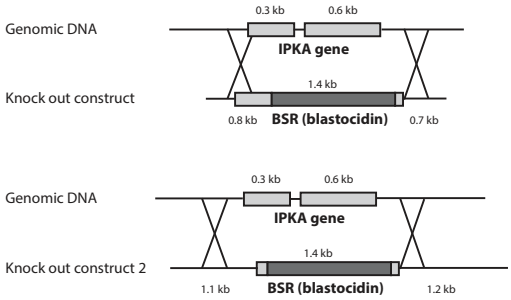

Figure 4.6 Deletion strategies for IPKA by Homologous Recombination.
Schematic of deletion strategies, deletion construct contained a 5' targeting arm of ~800 bp and a 3' targeting arm of ~700 bp (top) or a 5' targeting arm of ~1200 bp and a 3' targeting arm of ~1100 bp (bottom).

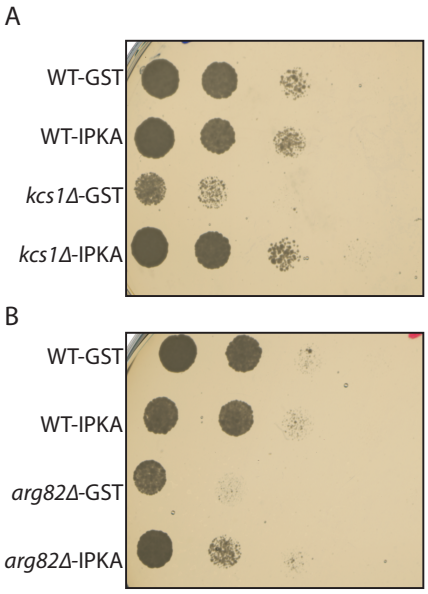

Figure 4.7 Overexpression of GST-IPKA rescues growth defect of *kcs1Δ* and *arg82Δ*.
WT, *kcs1Δ* and *arg82Δ* yeast overexpressing either GST or GST tagged IPKA were grown to an OD^{600} of 0.8, then serial dilutions were prepared and 10 μl dropped onto URA^- minimal media plates. Growth rescue could be observed in both *kcs1Δ* and *arg82Δ* after 3 days at 30°C.

gene was overexpressed in both *kcs1Δ* and *arg82Δ* yeast strains. Neither *kcs1Δ* nor *arg82Δ* possess detectable inositol pyrophosphates. However these strains are defective at different stages of the synthetic pathway (**Figure 1.4**), with *arg82Δ* deficient in the synthesis of IP_6 and *kcs1Δ* able to synthesise IP_6 as normal but lacking the inositol pyrophosphates (Saiardi, Sciambi et al. 2002). Both *kcs1Δ* and *arg82Δ* display a growth defect on glucose minimal media (**Figure 4.7**). The ability of IPKA to rescue the growth defect of these mutants was assayed as an indicator of its kinase activity.

Overexpression of a GST tagged IPKA was able to rescue the growth defect of both *kcs1Δ* and *arg82Δ* mutants (**Figure 4.7 A and B**). The defect observed in *kcs1Δ* could be almost completely rescued by overexpression of IPKA, returning these cells to almost WT growth (**Figure 4.7 A**). The ability of IPKA to complement the growth defect of in *arg82Δ* was not quite so complete (**Figure 4.7 B**).

These results indicated that IPKA may be able to act as both an IPMK and an IP6K. Such a hybrid kinase activity was reminiscent of the recently described *E. histolytica* IP6K crystalized in the Shears laboratory (Wang, DeRose et al. 2014). However, an alternative explanation could be that IPKA was able to use IP_3 as a substrate for IP_3-derived inositol pyrophosphates. Given the presence of IP_5-derived inositol pyrophosphates in *D. discoideum* (Pisani, Livermore et al. 2014), it is plausible that a promiscuous kinase may also be able to pyrophosphorylate IP_3. The observed rescue of *arg82Δ* could be due to either activity. In fact, the overexpression of Kcs1p in the *arg82Δ* strain is able to rescue a number of phenotypes including vacuole morphogenesis and growth defects (Dubois, Scherens et al. 2002). HPLC analysis of this strain reveals the formation higher inositol phosphates, including a range of “unconventional” inositol pyrophosphates, derived from IP_5 and possibly other species (Dubois, Scherens et al. 2002).

In order to confirm that this enzyme was that responsible for the observed 6PP-IP_5 kinase activity in cell extract, the enzyme was purified from yeast extract by GST pull down. Glutathione sepharose beads were used to purify tagged IPKA (**materials and methods, 2.5.3**), as confirmed by the presence of a ~65 kDa band by silver staining (**Figure 4.8**).

4.2.5 IPKA: *in vitro* activity

The activity of this purified protein was tested against a range of substrates, including I(1,4,5)P_3, I(1,3,4,5,6)P_5, IP_6 and 6PP-IP_5. This range of substrates was chosen given the previous annotation of IPKA as an IPMK, with predicted activity towards IP_3 (King, Keim et al. 2010). Furthermore, the ability of IPKA to rescue the growth defect in *arg82Δ* and *kcs1Δ* (**Figure 4.7**), suggested it might be able to utilise both IP_3 and IP_6 as substrates. These reactions, performed under the same conditions as the prior cell extract assays (**materials and methods,, 2.5.5**), revealed that GST-IPKA had very strong kinase activity towards 6PP-IP_5, resulting in the formation of IP_8 (**Figure 4.9, lane 12**). No activity towards any other substrate could be detected. However, it should be noted that PAGE technology and Toluidine staining, whilst excellent for detecting highly phosphorylated inositol species, is less effective for analysing less phosphorylated species such as IP_3 and IP_4.

Subsequently the activity of this enzyme against all isomeric forms of IP_7 was tested (**Figure 4.10**). Whilst each isomer contained different levels of contaminating IP_6 and IP_8 (particularly evident in lanes 7-10), clear activity towards 6PP-IP_5 could be detected in lane 14. This activity was not as strong as seen in previous enzyme preparations, but activity could not be detected in any other lanes.

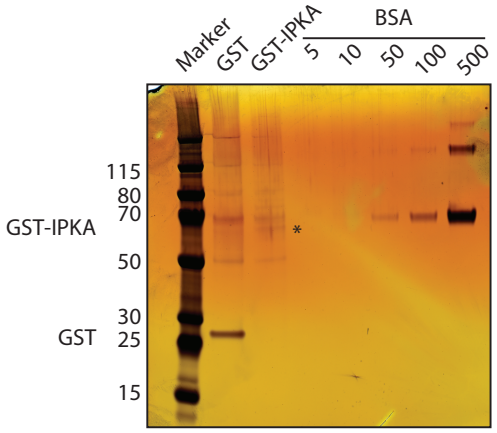

Figure 4.8 Silver stain of IPKA pull down.

GST-IPKA was pulled down with Glutathione sepharose beads. 15 μl of GST beads were analysed by a 4-12% PAGE and protein was visualised by silver staining (**materials and methods, 2.5.4**). A band corresponding to GST –IPKA was detected at approximately 65 kDa, marked with an (*). A dilution of BSA from 5 – 500 ng was added for reference.

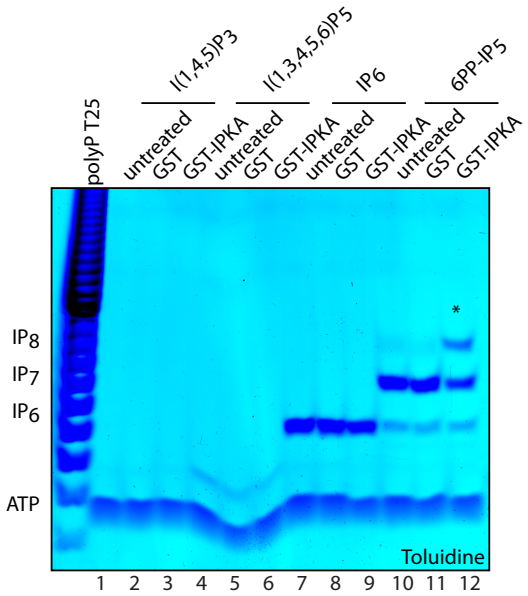

Figure 4.9 IPKA is an IP_7 kinase.

Purified GST-IPKA was incubated with indicated isomers of IP_3 IP_5, IP_6 and IP_7 for 3 h at 37°C (**materials and methods, 2.5.5**). IP_7 was robustly converted to IP_8 by GST-IPKA, whilst no other activity could be detected. Reaction products were analysed by 35.5% PAGE and stained with Toluidine. Representative result of an experiment performed more than three times.

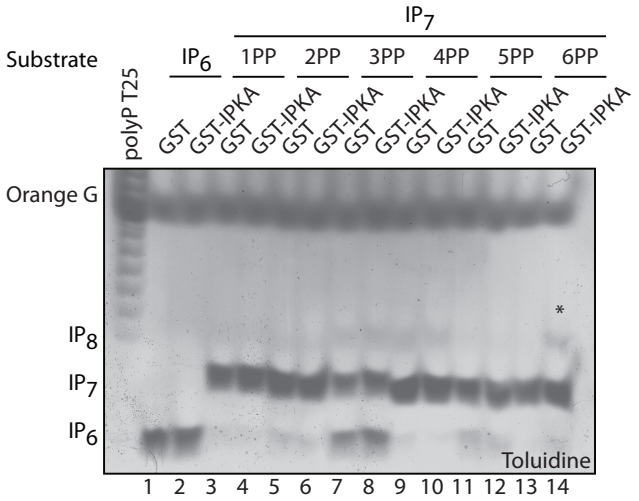

Figure 4.10 IPKA is specific to 6PP-IP_5

Purified GST-IPKA was incubated with indicated isomers of IP_7 for 3 h at 37°C (**materials and methods, 2.5.5)**. Only 6PP-IP_5 was converted to IP_8 by GST-IPKA, whilst no other activity could be detected. Reaction products were analysed by 35.5% PAGE and stained with Toluidine. Representative result of experiment performed twice.

These results provided very strong evidence that IPKA is, in fact, the enzyme responsible for the 6PP-IP_5 kinase activity detected in cell extract (**Figures 4.1-4.3**). *In vitro* evidence pointed towards IPKA being a very robust IP_7 kinase, possessing a very specific activity towards a single isomer of IP_7. This activity is consistent with both the previously identified isomeric arrangement of IP_8 (Laussmann, Eujen et al. 1996) and genetic evidence to suggest that an additional enzyme, alongside PPIP5K, is able to phosphorylate IP_7 to form IP_8 in *D. discoideum*. Furthermore, examination of the expression level (**Figure 3.4**) of this gene revealed a developmental increase, suggesting that this enzyme could be responsible for the developmental increase observed in *ppip5k* amoeba. However, these results did not offer insight into the rescue of either *arg82Δ* or *kcs1Δ.* In fact, they showed some inconsistencies with *in vivo* rescue data. *In vitro*, IPKA appears to be a very specific enzyme, with activity only detectable towards 6PP-IP_5, whilst the *in vivo* rescue of the growth defect of both *arg82Δ* and *kcs1Δ* indicated a far more promiscuous activity as neither strain should possess 6PP-IP_5.

It was reasoned that the inability to detect activity *in vitro* could be due to limitations in detection of less phosphorylated inositol species. Consequently, an alternative approach was employed to investigate the *in vivo* activity of IPKA. The catalytic flexibility of IPKA suggested by *in vivo* experiments offered the attractive hypothesis that this kinase may display other inositol phosphate kinase activities, including, perhaps the direct phosphorylation of *myo*-inositol described by Stephens, et al. (Stephens and Irvine 1990). Thus further experiments investigated this hypothesis by overexpressing IPKA in *plc1Δ* yeast strain.

Plc1Δ yeast lack any soluble inositol phosphates above IP_3 as well as lacking the second messenger DAG. Consequently, this strain displays diverse and very strong phenotypes, including a very severe growth defect (Yoko-o, Matsui et al.

1993), likely due to defects in the combined effect of lacking both soluble inositol phosphates and DAG signalling. Therefore, even complete rescue of levels of inositol pyrophosphates may not rescue the growth defect. Consequently, growth rescue was not assessed and an alternative approach was taken.

4.2.6 IPKA: polyP rescue in *S. cerevisiae*

Wild type *S. cerevisae* yeast possess high levels of inorganic polyphosphate (polyP). As outlined in **Chapter One**, the levels of polyP correlate with the levels of inositol pyrophosphates in yeast (Auesukaree, Tochio et al. 2005, Lonetti, Szijgyarto et al. 2011). Consequently, strains lacking inositol pyrophosphates, e.g. *kcs1Δ,* contain dramatically reduced levels of polyP (**Figure 4.11**). Thus the level of polyP can be used as an indirect measure of the level of inositol pyrophosphates in yeast cells. This method, whilst indirect, allowed the quick and easy assessment of a range of yeast to estimate the ability of IPKA overexpression to rescue levels of inositol pyrophosphates (**Figure 4.11**). PolyP was extracted from logarithmically growing WT, *kcs1Δ arg82Δ* and *plc1Δ* by phenol chloroform extraction (**materials and methods, 2.6.2**). As well as polyP, this method also extracted RNA, allowing RNA to be used as a loading control between samples. These extracts were analysed by 30% PAGE and stained with DAPI.

Expression of GST and GST-IPKA in these strains was confirmed by Western blot (**Figure 4.11, lower panel**). Blotting with an α-GST antibody revealed a band of around 65 kDa in strains overexpressing the GST tagged IPKA. A second non-specific band could be seen migrating slightly faster than the GST-IPKA. Expression levels of GST-IPKA were not uniform between strains, with the *arg82Δ* strain showing highest level of expression.

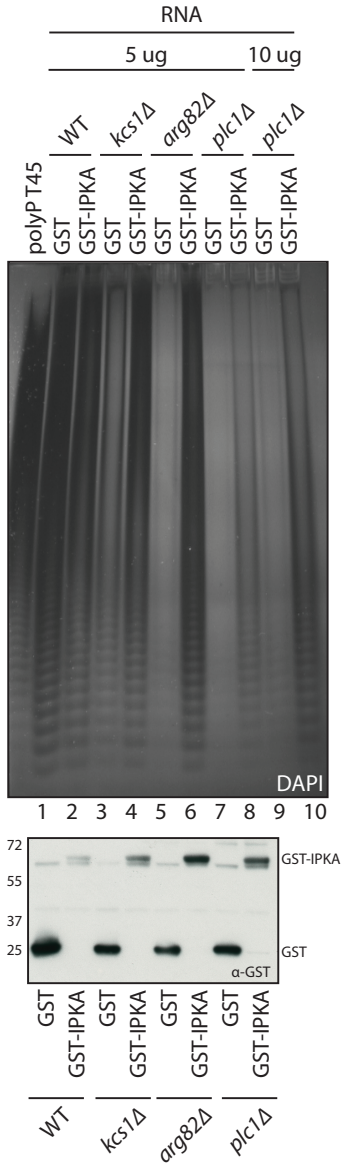

Figure 4.11 Overexpression of GST-IPKA rescues level of polyP in *kcs1Δ, arg82Δ* and *plc1Δ.*

Phenol chloroform extracts from logarithmic WT, *kcs1Δ, arg82Δ* and *plc1Δ* cultures expressing either GST or GST-IPKA were analysed by 30% PAGE and stained with DAPI. Samples were normalised by RNA with 5 μg of RNA loaded in all lanes except 9 & 10 in which 10 μg was loaded. Overexpression of GST IPKA increased the level of polyP in all strains except WT (Upper panel). Protein extracts were analysed by Western and probed with an α-GST antibody at a dilution 1:5000. GST-IPKA expression was not uniform in all strains and was highest in *arg82Δ* (Lower panel). Representative result of experiment performed twice.

As expected due to the ability of IPKA to rescue the growth defect of both *kcs1Δ* and *arg82Δ*, overexpression of GST-IPKA was able to restore the levels of polyP to levels comparable to WT (**Figure 4.11,** lanes 4 and 6). This further suggested that the ability of IPKA to rescue the growth defect (**Figure 4.7**) was due to the synthesis of inositol pyrophosphates in these strains. However, as before these experiments failed to distinguish between synthesis of IP_6-derived inositol pyrophosphates or those derived from less phosphorylated species.

The *plc1Δ* strain possessed the lowest level of polyP of all strains examined in this work (**Figure 4.11,** lane 7). Surprisingly, overexpression of IPKA in the *plc1Δ* strain was also able to partially restore the level of polyP in these cells. Whilst DAPI staining of polyP precludes quantitation of the absolute level of polyP in extract, these observations indicated that the rescue of polyP in the *plc1Δ* GST-IPKA strain was not complete. Even loading double the amount of material (10 μg RNA) failed to recapitulate the level of polyP detected in 5 μg of WT extract. It was also evident that the average length of polyP present in lane 8 and 10 was shorter than in WT. The speed of migration of polyP through a 30% polyacrylamide gel is proportional to polymer length. Thus a stronger staining towards the bottom of the gel, as seen in lanes 8 and 10 indicated a shorter average chain length than seen in lanes 1, 2, 4 and 6, where the staining was stronger towards the top of the gel.

The observed increase in polyP in the *plc1Δ* GST-IPKA strain was likely due to an increase in the level of inositol pyrophosphates in this strain. However, as with *arg82Δ* it was not possible to distinguish between IPKA restoring the levels of IP_6 or generating IP_2/IP_3-derived inositol pyrophosphates. Nevertheless, these results offered further evidence that IPKA was more flexible with its substrate *in vivo* than *in vitro.* Furthermore, the partial rescue of *plc1Δ* polyP suggested that this enzyme could indeed play role in the direct synthesis of inositol phosphates and pyrophosphates from *myo*-inositol.

4.2.7 IPKA: HPLC analysis of *S. cerevisiae* overexpressing IPKA

Further investigation of the inositol phosphate profile of these strains required their labelling with ^{3}H *myo*-inositol. This analysis was conducted as described previously (Azevedo and Saiardi 2006), with cells labelled overnight before preparation of a perchloric acid extract and analysis by HPLC. Analysis of *kcs1Δ* by HPLC was performed twice and a representative trace is shown in **Figure 4.12 A.** HPLC analysis was only performed once for *arg82Δ and plc1Δ* and samples were poorly labelled. Consequently the results for *plc1Δ* could not be interpreted and are not shown. Meanwhile the results of IPKA overexpression *arg82Δ,* whilst also afflicted by poor labelling, did offer insight into IPKA function (**Figure 4.12**). Nevertheless, repeats will be required to confirm these observations.

Despite the limitations described above, it was clear that overexpression of GST-IPKA altered the inositol phosphate profile of both *arg82Δ* and *kcs1Δ.* HPLC traces are shown on different scales due to the differing labelling efficiency between experiments.

Overexpression of IPKA in the *kcs1Δ* strain (**Figure 4.12 A,** blue line) resulted in the formation of a clear IP_7 peak after ~71 min. This peak was identified as IP_7 due to its elution approximately 10 min after IP_6 (~61 min), as identified by comparison to IP_6 standard (data not shown).

Meanwhile, overexpression of IPKA in the *arg82Δ* strain resulted in numerous alterations to the HPLC trace (**Figure 4.12 B** blue line). Peaks eluting before 30 min, representing the less phosphorylated inositol phosphates were altered, however interpretation of these peaks was not possible due to poor labelling. It can be noted, however that overexpression of IPKA induced the formation of a peak that at 61 minutes. As indicated above, this elution profile is consistent with formation of IP_6.

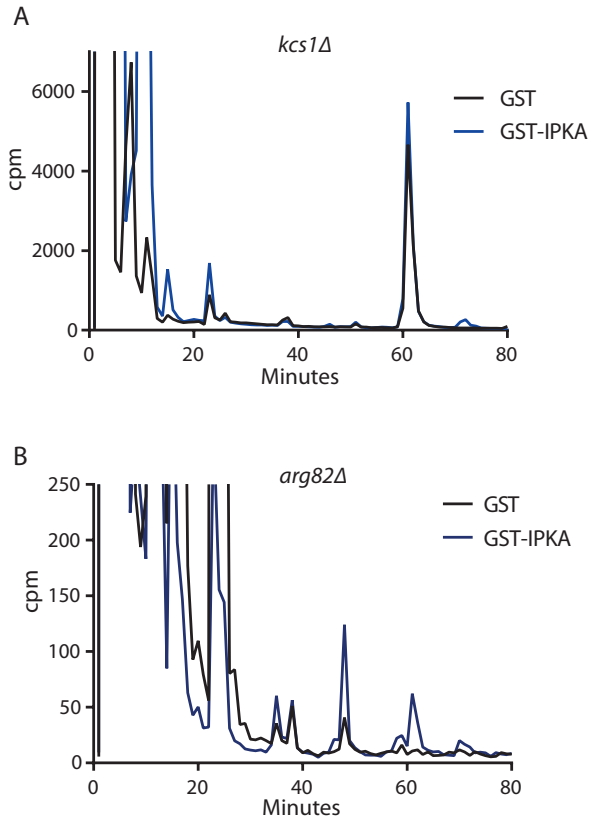

Figure 4.12 Overexpression of GST-IPKA alters the inositol phosphate profile in *kcs1Δ* and *arg82Δ*

HPLC analysis of perchloric acid extract prepared (**materials and methods, 2.6.4**). Overexpression of GST-IPKA (blue line) altered the inositol phosphate profile compared to strains overexpressing GST (black line).

These results suggested that whilst IPKA was an excellent IP_7 kinase, it did also appear to display some ability to synthesise inositol pyrophosphates from other substrates, particularly IP_6. Importantly it also appeared able to contribute to the synthesis of IP_6 in *arg82Δ*. Thus, IPKA appeared to be a hybrid-kinase, displaying ability to synthesis a range of inositol phosphate products from a range of substrates. Further experiments are required to fully untangle substrate specificity and product formation of this enzyme, particularly of the lower inositol phosphates.

4.2.8 IPKB: cloning

As noted above, a further inositol phosphate kinase is encoded in the *D. discoideum* genome, referred to here as Ipkb. Similarly, attempts to delete this gene (**Figure 4.13**) proved unsuccessful. Therefore an analogous approach to that described above was employed to explore the activity of this gene. Ipkb was slightly less amenable to expression in yeast due to its larger size (70 kDa), highly AT-rich coding sequence (>75%) and repetitive amino acid sequence, including a 56 amino acid stretch containing 52 arginines.

Overexpression of this GST-tagged fusion protein in WT yeast negatively affected growth rate, suggesting some toxicity was associated with expression of this enzyme (data not shown). Therefore, growth rescue experiments as performed in **Figure 4.7** were not conducted using IPKB.

4.2.9 IPKB: *in vitro* activity

GST-tagged IPKB was purified from WT yeast by GST pull down. Although GST-IPKB could not be detected by Western blot (data not shown), the activity of GST-IPKB was examined as described above, using the substrates I(1,4,5)P_3, I(1,3,4,5,6)P_5, IP_6, 5PP-IP_5 and 6PP-IP_5 (**Figure 4.14**). Despite annotation of IPKB as an IP6K, no activity towards IP_6 could be detected. In fact, the only activity that could be detected was the formation of IP_8 from IP_7. As with GST-IPKA, this activity also appeared to be specific to a particular isomer of IP_7, although in

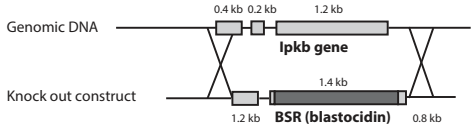

Figure 4.13 Deletion strategy for IPKB by Homologous Recombination.
Schematic of deletion strategy, deletion construct contained a 5' targeting arm of ~800 bp and a 3' targeting arm of ~1200 bp.

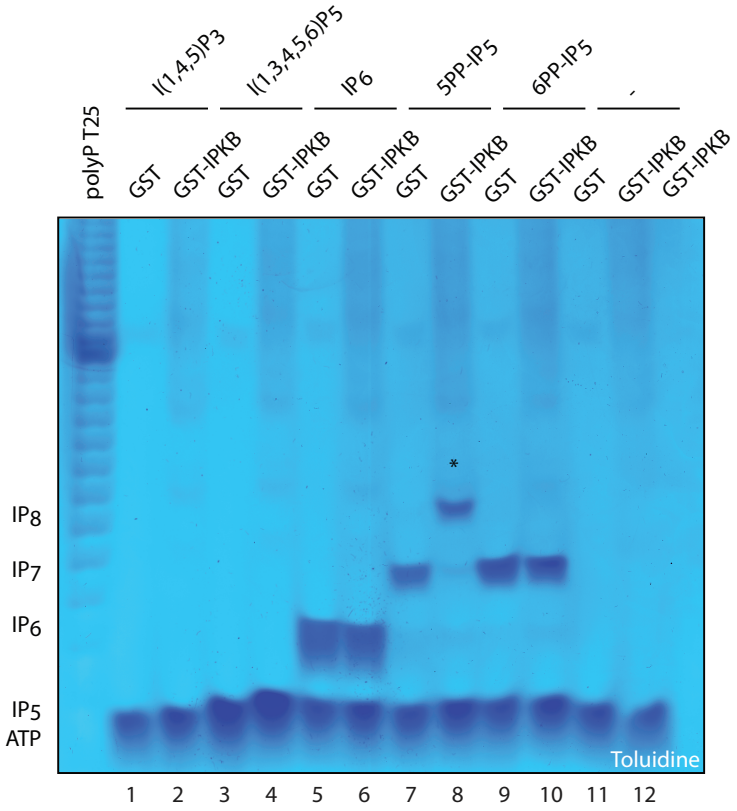

Figure 4.14 IPKB is an IP_7 kinase.
Purified GST-IPKB was incubated with indicated isomers of IP_3 IP_5, IP_6 and IP_7 for 3 h at 37°C as described in (**materials and methods, 2.5.5)**. Only 5PP-IP_5 was robustly converted to IP_8 by GST-IPKB, whilst no other activity could be detected. Reaction products analysed by 35.5% PAGE and stained with Toluidine. Representative result of an experiment performed twice.

this case it was 5PP-IP_5 (**Figure 4.14,** lane 8). This activity was surprising as 5PP-IP_5 is the predicted product of this enzyme, rather than its substrate.

Analysis of the gene expression pattern of IPKB during development also revealed a strong induction during the developmental response (**Figure 3.4**). Thus, *in vitro* activity suggested that IPKB might also be contributing to the increase in inositol pyrophosphates seen during development.

4.2.10 IPKA: polyP rescue in *S. cerevisiae*

The *in vitro* activity of IPKB appeared to be limited to phosphorylation of IP_7, however given the discrepancies observed between *in vitro* and *in vivo* activities displayed by IPKA, the *in vivo* activity of IPKB was also investigated. First, the ability of this enzyme to rescue the accumulation of polyP in a range of yeast strains was tested. As described above, polyP provided a rapid method to estimate the levels of inositol pyrophosphates in unlabelled yeast. Once again GST-IPKB could not be detected by Western blot, nevertheless, phenol chloroform extracts from logarithmically growing yeast were analysed by 30% PAGE and DAPI staining (**Figure 4.15**).

As noted with IPKA, overexpression of IPKB in *kcs1Δ* yeast was able to partially rescue the level of polyP (**Figure 4.15, lane 3 and 4**). Overexpression of IPKB in *arg82Δ* induced a very slight increase in the level of polyP (**Figure 4.15, lane 5 and 6**) in contrast to IPKA, which displayed a very strong rescue in this strain. Finally, GST-IPKB was also able to induce an increase in the level of polyP in the *plc1Δ* strain to a similar degree to IPKA (**Figure 4.15, lane 7-10**). As with IPKA, the chain length of polyP molecules extracted from *plc1Δ* overexpressing IPKB were shorter on average than those extracted from WT (**Figure 4.15**, lane 1).

These surprising results were, once again, in conflict with *in vitro* evidence, which suggested IPKB was a specific IP_7 kinase. The ability of IPKB to rescue,

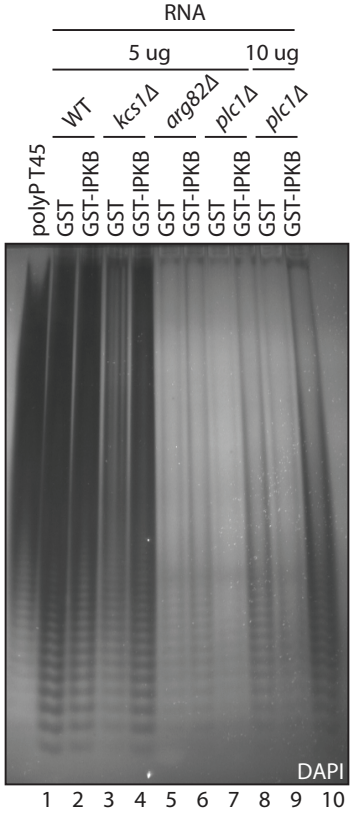

Figure 4.15 Overexpression of GST-IPKB rescues level of polyP in *kcs1Δ, arg82Δ* and *plc1Δ.*

Phenol chloroform extracts from vegetative cultures of WT, *kcs1Δ, arg82Δ* and *plc1Δ* expressing either GST or GST-IPKA were analysed by 20% PAGE and stained with DAPI. Samples were normalised by RNA with 5 μg of RNA loaded in all lanes, except 9 & 10 in which 10 μg was loaded. Overexpression of GST IPKA increased the level of polyP in all strains except WT. Representative result of an experiment performed twice.

to varying levels, the amount of polyP found in *kcs1Δ, arg82Δ* and *plc1Δ*, suggested it too could restore the level of inositol pyrophosphates in these strains. However, as discussed previously these experiments failed to distinguish between direct synthesis of inositol pyrophosphates from IP_6 precursors and contribution to synthesis of IP_6.

4.2.11 IPKB: HPLC analysis of *S. cerevisiae* overexpressing IPKB

The yeast strains: *kcs1Δ, arg82Δ* and *plc1* overexpressing IPKB were labelled with [^{3}H] *myo*-inositol as described above. Labelling of these cells was poor and HPLC analysis could not be interpreted. Consequently, the results of these experiments were excluded from this work and will require repetition to better characterise the effect of overexpression of IPKB

Although the HPLC data could not be interpreted, it was clear from polyP rescue and *in vitro* kinase assays that there were discrepancies between IPKB activity *in vitro* and *in vivo*. It should be noted that GST-IPKB could not be detected using standard Western blotting, suggesting that this enzyme was poorly expressed in these cells, possibly due to the larger size and repetitive sequence. As with IPKA, further experiments are required to fully appreciate the physiologic catalytic activities of IPKB. Nevertheless, *in vitro* data indicates that the annotation of this enzyme as an IP6K does not appear to be correct.

4.3 Discussion

The experiments described above confirm the presence of an additional IP_7 kinase activity in the extract of WT *D. discoideum*, as well as all mutants tested. As previously described (Laussmann, Reddy et al. 1997) and in accord with NMR data (Albert, Safrany et al. 1997), this robust activity is highly specific for the 6PP-IP_5 isomer.

4.3.1 IPKA activity

Initial attempts to purify this activity proved unsuccessful and thus an alternative candidate approach was employed. The cloning and expression of IPKA reveals an enzyme capable of rescuing the growth defects of both *kcs1Δ* and *arg82Δ.* These results suggest that this enzyme, whilst previously annotated as an IPMK, might in fact display the ability to synthesise inositol pyrophosphates. Meanwhile, purified IPKA shows very robust activity towards 6PP-IP_5, suggesting that it is the enzyme responsible for the activity detected in cell free assays (**Figures 4.1- 4.5**). The predicted molecular weight of IPKA at 37 kDa (**Table**) is also consistent with previous work which partially purified this activity to a protein with a molecular weight of ~40 kDa (Laussmann, Reddy et al. 1997).

These somewhat conflicting results suggest that at once this enzyme is highly selective for its substrate and yet also catalytically flexible. In addition, the strong activity towards 6PP-IP_5 *in vitro* begs the question, what enzyme synthesises this isomer *in vivo*?

Furthermore, the inability to delete IPKA, after numerous attempts with two constructs is notable. Local environments of the gene on a chromosome can influence the ability to knock a gene out, which may explain the problems encountered. However, an alternative explanation could be that this gene is in fact essential and deletion is lethal. If IPKA is simply an IP_7 kinase, as suggested by *in vitro* data, it seems unlikely that it is an essential gene, particularly given

the relative lack of phenotype observed for *ip6k*. However, if IPKA is essential, this might be due to an additional role, perhaps in synthesising the lower inositol phosphates. This hypothesis is supported by the ability of IPKA to rescue growth defects of both *kcs1Δ* and *arg82Δ*, indicating that at the very least it can act as more than simply an IP_7 kinase *in vivo.*

Further investigation of the effect of overexpression of IPKA in a range of yeast mutants focused on the possibility that this enzyme may be catalytically flexible. This included investigating a potential role for IPKA direct phosphorylation of inositol. Therefore, the ability of IPKA to rescue the *plc1Δ* yeast was investigated. In fact, IPKA is able to rescue the level of polyP (to a greater or lesser extent) in all mutants tested (*kcs1Δ, arg82Δ* and *plc1Δ*). This suggests that this enzyme is also restoring the level of inositol pyrophosphates in these strains.

As discussed above, this data can be explained by two potential hypotheses. The first is that IPKA catalyses the synthesis of inositol pyrophosphates derived from lower forms of inositol phosphate, such as IP_3 in the case of *arg82Δ* and even IP_2 in the case of *plc1Δ*. The second is that IPKA directly phosphorylates the inositol ring, catalysing the formation of IP_6. This IP_6 is then a substrate for the endogenous Kcs1p found in both *arg82Δ* and *plc1Δ*. The experiments using polyP as an indirect measure for inositol pyrophosphate synthesis fail to distinguish between these hypotheses. Therefore, HPLC was employed to further investigate the activity of IPKA.

As noted previously, the HPLC experiments conducted in this work showed very low labelling efficiency and so allow limited conclusions to be drawn. However, it is clear from the overexpression of IPKA in *arg82Δ* that a species resembling IP_6 is formed. However, it is also evident that IP_7 is formed by overexpression of the IPKA in the *kcs1Δ* strain. Whilst these data do not allow definitive

conclusions to be drawn about the activity of IPKA, they are consistent with both activity of IPKA as a hybrid kinase possessing the ability to synthesise, at the least, IP_6 and IP_7 when overexpressed in yeast. The ability of IPKA to directly phosphorylate *myo*-inositol will require further investigation.

Despite, the highly flexible catalytic activity of IPKA overexpressed in yeast, *in vitro* evidence and the very robust extract detected in cell extract assays favour IPKA being an IP_7 kinase. None of the yeast mutants tested possess the specific isomer of IP_7 towards which IPKA is active, 6PP-IP_5. Therefore, when overexpressed in yeast, IPKA is deprived of what seems to be its preferred substrate. Thus the catalytic flexibility seen here may be a reflection of a highly active enzyme exposed to a range of sub-optimal substrates.

In fact, catalytic flexibility of inositol phosphate kinases is not unprecedented, as demonstrated by the recent structural analysis of the *E. histolytica* IP6K. This study, discussed in **Chapter One**, offers support for the existence of inositol phosphate kinases displaying hybrid activities. The results described above suggest that IPKA may also be an exceptionally versatile kinase, with IP7K activity, IPMK activity and perhaps even the ability to phosphorylate inositol to IP_6. The latter activity is difficult to test using the methodologies described here and will require the use of radio-labelled inositol species for *in vitro* kinase assays to determine if IPKA can indeed catalyse the stepwise formation of IP_6.

4.3.2 IPKB activity

The final experiments described in this chapter focused on the remaining member of the inositol phosphate kinase family of genes in the *D. discoideum* genome, referred to here as Ipkb. The IPKB enzyme is larger than IPKA and shows greater sequence homology to IP6K, as seen by sequence alignment to HsIP6K (**Figure 7.5**). Similarly, attempts to knock out this enzyme were unsuccessful. Overexpression of the GST-tagged IPKB protein also revealed an

enzyme, which displays robust IP_7 kinase activity, but this time towards the 5PP-IP_5 isomer (**Figure 4.14**).

However, as with IPKA the results of overexpression of GST-IPKB in yeast mutants did not match those from *in vitro* experiments (**Figure 4.15**). Expression of IPKB was poor in yeast and recombinant protein could not be detected by Western blot. Nevertheless IPKB was able to rescue the level of polyP in *kcs1Δ* and to a lesser extent in *arg82Δ.* Surprisingly it was able to rescue the level of polyP in *plc1Δ* at least as well as IPKA (**Figure 4.11)**. Experiments with radiolabelled inositol analysed by HPLC also failed to give a clear answer regarding the activity of IPKB, although it can be noted that it was not possible to detect the formation of IP_6 in these experiments (data not shown).

These results again suggest that IPKB is not simply an IP_7 kinase. Rather, IPKB might also be a catalytically flexible enzyme. Discrepancies in the ability of IPKB to rescue yeast levels of polyP in *arg82Δ* could indicate that this enzyme is not as flexible as IPKA. Alternatively, the lower expression of IPKB, perhaps due to the larger size of IPKB and its repetitive sequence (**Figure 7.5**), may explain the reduced activity detected.

4.3.3 Why so many inositol phosphate kinases?

Taken together these results are somewhat counterintuitive, revealing two specific IP_7 kinases *in vitro*, but catalytically flexible kinases *in vivo*. Nevertheless, they do offer clues for the synthesis of inositol pyrophosphates in this amoeba. As discussed previously, the amoeba is highly unusual for its elevated levels of IP_8. The apparent presence of three IP_7 kinases, PPIP5K, IPKA and IPKB in these cells, goes some way towards explaining how this might be achieved. Cell extract experiments reveal that IP_7 kinase activity can be readily detected, whilst IP_6 kinase activity cannot. This is consistent with the higher abundance of IP_8 compared to IP_7 owing to rapid conversion of IP_7 directly to

IP_8. The enzyme responsible for the IP_7 kinase activity detected in cell extract was identified as IPKA

The activity of IPKB could not be detected in cell extract from vegetative cultures, however this developmentally regulated gene may play a more significant role during the onset of the starvation response, perhaps contributing the developmental accumulation of IP_8.

4.3.4 What is the source of 6PP-IP_5?

One interesting question to consider is the source of the substrate for IPKA. No enzymes have been described to phosphorylate IP_6 at position 6. It is possible that this activity is artefactual and simply represents an activity of the enzyme that is not physiologically relevant. This appears unlikely due to the presence of high levels of IP_8 in the *ppip5k* strain and previous NMR work identifying the isomer of IP_8 as either 4,5 or 5,6 (Albert, Safrany et al. 1997).

This work has identified 4 inositol phosphate kinases, which could be potential candidates, IP6K, PPIP5K, IPKA and IPKB. However, three of them appear to primarily be IP_7 kinases rather than IP_6 kinases (based on either genetic (PPIP5K) or biochemical (IPKA and IPKB) evidence). The genetic evidence suggests that in fact IP6K is the primary source of IP_7 in *D. discoideum*, raising the possibility that this enzyme is the one responsible for the synthesis of 6PP-IP_5. This would be unexpected, as *in vitro* both yeast and mammalian IP6K place a pyrophosphate moiety on position 5 (Draskovic, Saiardi et al. 2008). The divergence in sequence between *D. discoideum* IP6K and mammalian IP6K makes it difficult to predict whether the enzyme might have an altered catalytic specificity.

This difference could be indicative of further discrepancies between the synthesis of inositol pyrophosphates in *D. discoideum* and other models.

However, it is worth noting again that it is only the amoeba, where inositol pyrophosphates are sufficiently abundant, that NMR has been performed on molecules extracted from cells (Laussmann, Eujen et al. 1996). Whilst the weight of evidence suggests that mammalian IP6K phosphorylates position 5, this data is based on *in vitro* experiments using purified enzyme (Draskovic, Saiardi et al. 2008). The evidence presented here indicates that discrepancies can exist between the *in vivo* and *in vitro* specificities of certain inositol phosphate kinases.

In fact, it should also be noted that the *in vitro* specificity of purified IP6K2 towards IP_5 is dependent upon the choice of buffer; reactions performed in cacodylate buffer produce 5(PP)-IP_4, whilst those buffered with Tris generate 1(PP)-IP_4 (Draskovic, Saiardi et al. 2008). In light of these results it will be interesting to re-evaluate the isomeric nature of inositol pyrophosphates purified from *D. discoideum* using present day NMR techniques to confirm their isomeric arrangements. Moreover, it will be interesting to investigate whether the recently developed TiO_2 enrichment method (Wilson, Bulley et al. 2015) will allow sufficient quantities of mammalian inositol pyrophosphates to be subjected to NMR analysis.

4.3.5 Other functions of IPKA and IPKB?

Whilst many questions remain unanswered, it is clear that the synthetic pathway of inositol pyrophosphates in this amoeba is not as straightforward as may have been anticipated. Analysis of WT extract by PAGE and Toluidine reveals just three major bands, however it is evident that more species are present. DAPI staining reveals an additional IP_9 band, whilst the IP_7 band clearly consists of multiple species, including PPIP5K products (as discussed in **Chapter 3**). The enzymatic complexity suggests still more isomeric arrangements may exist in the amoeba.

In fact further characterisation of IPKA and IPKB may provide insight into the formation of the low-abundance IP_9 identified by Pisani et al. (Pisani, Livermore et al. 2014). It is possible that one, or both of these enzymes are responsible for the synthesis of this species. Unfortunately, isomers of IP_8 were not available for *in vitro* assays.

In addition to the possible role for IPKA and IPKB in the synthesis of inositol pyrophosphates, these enzymes both appear to display catalytic flexibility when overexpressed in yeast. Whether this catalytic flexibility represents a genuine activity in *D. discoideum* is not yet clear. Nevertheless, the inability to delete IPKA and IPKB, offers a hint that they may function as more than simply IP_7 kinases, particularly given the lack of phenotype of the *ip6k* strain. It is tempting to consider that these enzymes may act in concert to perform the stepwise phosphorylation of inositol described in these cells (Stephens and Irvine 1990). Whilst some work presented here supports this concept, additional work is required to explore this hypothesis.

It is evident that neither enzyme in isolation is able to offer full rescue of the inositol phosphate profile in yeast mutants, however it may be that these enzymes work in tandem to synthesise the lower inositol phosphates. Overexpression of both IPKA and IPKB in the same yeast strain would allow this hypothesis to be tested.

In addition, potential roles for these enzymes in *D. discoideum* should be explored as both *in vitro* and *in vivo* experiments using yeast have their limitations. Unfortunately, neither enzyme could be deleted, however methods to knock down mRNA in *D. discoideum* do exist (Friedrich, Meier et al. 2015). These methods were not tested in this work; however, transient knock down of IPKA and IPKB could provide insight into the true role of these enzymes in *D. discoideum.*

4.3.6 Concluding remarks

The evidence presented in this chapter point to both IPKA and IPKB displaying novel properties for inositol phosphate kinase family members. Despite their sequence similarities to IPMK and IP6K respectively (**Figure 7.4** and **7.5**), it seems that both display unique properties, not previously identified in this family of kinases. These unusual characteristics and catalytic flexibility are reminiscent of the IP6K/IPMK hybrid crystalised from *E. histolytica* (Wang, DeRose et al. 2014). It is possible that both IPKA and IPKB evolved divergently from an IP6K ancestor to generate this large family of inositol phosphate kinase activities in *D. discoideum.*

The characterisation of members of inositol phosphate kinase family in yeast and mammalian cells may suggest that these activities are unique to this amoeba, perhaps explaining why these cells accumulate such high levels of inositol pyrophosphates. The evolutionary pressure behind such a wide array of inositol phosphate kinases and high level of inositol pyrophosphates remains unclear. RNA-mediated knockdown of IPKA and IPKB in the *ip6k*/*ppip5k* strain may offer a potential route to generate a strain lacking any inositol pyrophosphates and thereby explore the true function enzymes and their products in *D. discoideum*.

5. PolyP in *D. discoideum*

5.1 Introduction

The social amoeba *D. discoideum* is one of the few eukaryotic organisms in which the polyphosphate kinase (PPK) has been identified. As previously noted the amoeba possesses a bacterial-like PPK1, as well as a heterotrimeric complex known as DdPPK2. PPK1 was likely acquired through a horizontal gene transfer event from the bacteria on which this amoeba feeds. This gene was identified due to homology to the *E. coli* PPK1 gene, with which it shares 30% identity and 51% similarity (Zhang, Gómez-García et al. 2007), although this is limited to the C terminal portion of the protein (**Figure 5.1**). Disruption of the PPK1 gene reveals a range of phenotypes, including aberrant fruiting body formation, impaired phagocytosis (Zhang, Gómez-García et al. 2005) and a defect in cytokinesis (Zhang, Gómez-García et al. 2007). This strain does, however, retain approximately 20-50 % of the level of polyP detected in WT (Zhang, Gómez-García et al. 2005). The residual polyP can be attributed to the activity of a second, and to-date unique, polyP kinase, the DdPPK2 complex of actin related proteins (Gómez-García and Kornberg 2004). It should be noted, however, that the deletion strategy employed to delete PPK1 (Zhang, Gómez-García et al. 2005) resulted in the removal of just 3% of the open reading frame of the gene. Consequently the residual polyP described in this strain could stem from the activity of a truncated PPK1. Nevertheless, the homology between components of DdPPK2 and a range of mammalian proteins has led to proposals that this enzyme complex might be a candidate for the mammalian polyphosphate kinase (Hooley, Whitehead et al. 2008).

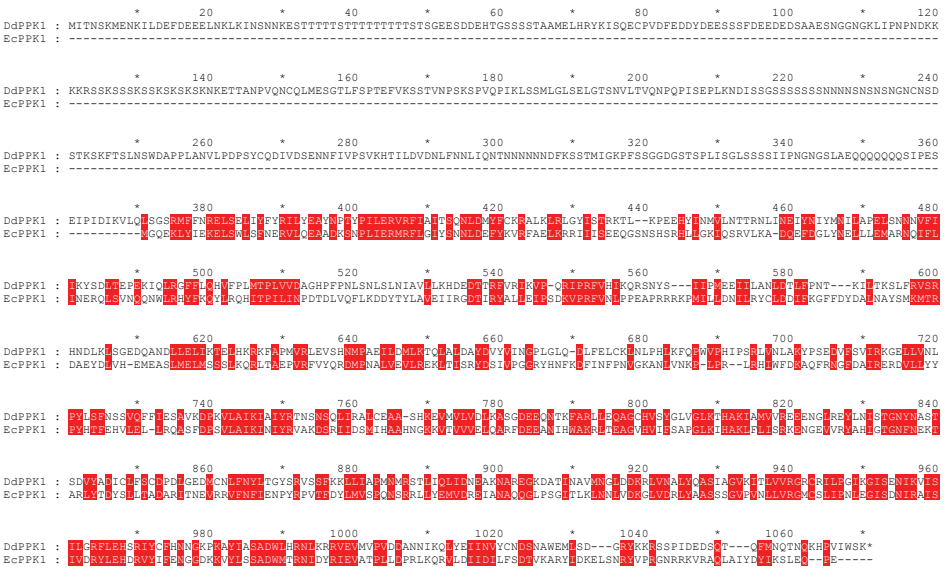

Figure 5.1 Sequence alignment of DdPPK1 and EcPPK1.

Protein sequence alignment of *D. discoideum* and *E. coli* PPK1 performed by CLUSTAL. Sequence similarity shown in red.

The work outlined above and in **Chapter One** laid the foundations for the study of polyP in this organism. The identification of polyP kinases in this organism provides the almost unique opportunity to develop a eukaryotic genetic model to study polyP function.

As noted in **Chapter One**, polyP has been localised to the acidocalcisome of *D. discoideum* (Marchesini, Ruiz et al. 2002). These experiments relied upon the use of DAPI to localise polyP. The fluorophore DAPI, when bound to DNA, can be excited at 360 nm, and emits at 460 nm. However, DAPI also binds to the negatively charged polyP and induces a shift in fluorescence, such that DAPI-polyP complexes can be excited with a wavelength of 410-420 nm and display an emission peak at 550 nm (Aschar-Sobbi, Abramov et al. 2008). Many groups have taken advantage of this fluorescence shift to localise polyP in cells from amoeba (Marchesini, Ruiz et al. 2002) to astrocytes (Holmström, Marina et al. 2013). However, the specificity of this method has recently been called into question by the observation that highly phosphorylated inositol species including IP_5, IP_6, IP_7 and IP_8 are also able to bind to DAPI and induce the same fluorescence shift described for polyP (Kolozsvari, Parisi et al. 2014). The fluorescence efficiency of DAPI when bound to inositol phosphates is comparable to when bound to polyP. Nevertheless, the scarcity of genetic models has precluded the *in vivo* control experiments required to validate this technique. The potential contaminating effect of inositol phosphates is of particular concern in *D. discoideum* due the exceptionally high levels of IP_6, IP_7 and IP_8 which seem likely to induce significant background fluorescence when using this method.

Whilst alternative methods to detect polyP do exist, including ^{32}P labelling and enzymatic assays utilising the PPK reverse reaction to drive ATP synthesis (Kornberg, Rao et al. 1999), these methods are not widely used. Instead, recent improvements in PAGE technology have allowed the reliable detection of polyP

from yeast extracts (Lonetti, Szijgyarto et al. 2011) (**Chapter 4**). This method, which can be coupled with either Toluidine Blue staining or DAPI, for added sensitivity, allows polyP to be resolved from co-purifying molecules such as RNA, inositol phosphates and nucleotides. In this way unlabelled polyP can be unambiguously detected. Therefore, the aim of the work described below was to utilise improvements in PAGE technology and develop the amoeba as a genetic model in which to study the synthesis, metabolism and function of polyP. In addition, the high levels of inositol pyrophosphates and strains generated in Chapter One place this amoeba as an ideal model in which to further investigate the metabolic relationship identified between inositol pyrophosphates and polyP (Auesukaree, Tochio et al. 2005, Lonetti, Szijgyarto et al. 2011, Ghosh, Shukla et al. 2013)

5.2 Results

Much of the work described in this chapter has been published in (Livermore, Chubb et al. 2016). Figures adapted from this publication are indicated accordingly.

5.2.1 Detecting *D. discoideum* polyP by PAGE

As described above, the presence of polyP in WT cells has been demonstrated by various methods, including [^{32}P] labelling, biochemical assays and microscopy (Marchesini, Ruiz et al. 2002, Zhang, Gómez-García et al. 2005). To further validate the presence of polyP in *D. discoideum* phenol chloroform extracts were prepared from WT cells. Numerous extraction procedures have been used to extract polyP, however experiments in the Saiardi lab have found the phenol chloroform extracts to be the most consistent. This method, which also co-purifies RNA and inositol pyrophosphates, was used in concert with 20% PAGE and DAPI staining to identify polyP in these amoeba (**Figure 5.2**) (**materials and methods, 2.6.4**).

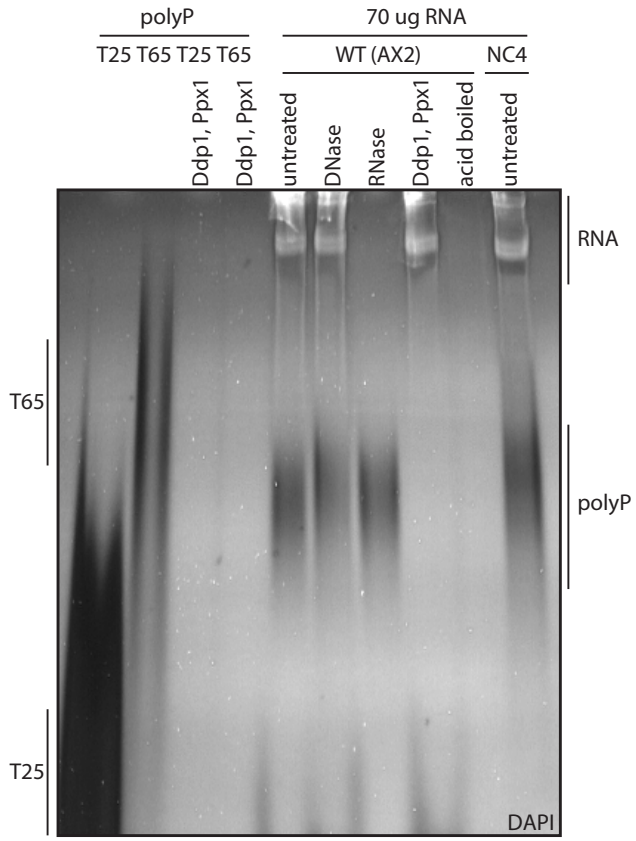

Figure 5.2 *D. discoideum* polyP detected by PAGE analysis.

Synthetic polyP standards with an average chain length of 25 (T25) and 65 (T65) were loaded, either untreated or after incubation with the exo- and endo-polyphosphatase (Ppx1, Ddp1). Equal amounts of vegetative AX2 *D. discoideum* phenol chloroform extract, as normalized by RNA (70 μg) were treated with DNase, RNase, exo- and endo-polyphosphatase (Ppx1, Ddp1) or treated in acid at high temperature (acid boiled). Samples were analysed by 20% PAGE and stained with DAPI. Phenol extract from wild isolate NC4 cells (right lane) was also analysed by PAGE. The figure shows the result of a representative experiment that was repeated more than three times. Figure and figure legend adapted from (Livermore, Chubb et al. 2016). .

This analysis revealed a negatively stained smear reminiscent of polyP. However, rather than displaying the characteristic laddering associated with polyP purified from yeast (**Figure 4.11**), this smear was comprised of species much more uniform in length, as shown by comparison to migration of standards (**Figure 5.2**). Furthermore visualisation of this smear required far more material to be loaded on the gel, 70 μg of RNA was loaded, compared to just 5 μg of yeast extract (**Figure 4.11**).

As noted, phenol chloroform extraction also purified a range of other molecules, including RNA, DNA, inositol phosphates and nucleotides. In order to confirm that the dark smear observed in WT extract was due to polyP and not due to these co-purifying molecules, the extract was subjected to a range of enzymatic and hydrolytic treatments. Treatment with either DNase or RNase had no effect on the smear, however, RNase treatment did ablate the slower migrating, positively staining RNA species visible at the top of the gel. Chemically synthesised polyP of average chain length or 25 and 65 phosphates (T25 and T65), as well as WT extract, were treated with a combination of polyphosphatases, Ddp1, the yeast endopolyphosphatase, and Ppx1 a yeast exopolyphosphatase. This treatment (Ddp1, Ppx1) was able to degrade both species of chemically synthesised polyP and the negatively staining smear in WT extract. Finally, the acidic extract was treated with acid at high temperature (acid boiled) causing the degradation of both the positively and negatively staining species. These treatments indicated that dark smear was indeed caused by photobleaching by DAPI-polyP complexes. Furthermore, the average chain length of this polyP could be estimated at approximately 50 residues due to its migration compared to synthetic standards of average length T25 and T65.

Finally, the presence of the polyP smear was also confirmed in the wild isolate NC4 strain. This polymeric species displayed similar characteristics to the polyP extracted from WT AX2.

These results demonstrated, for the first time, that unlabelled polyP could be detected in *D. discoideum* extract by PAGE and DAPI staining. It was notable that the abundance polyP in this amoeba was dramatically less than could be detected in yeast. This analysis also provided the first estimate of the average chain length of polyP found in *D. discoideum.* In fact, the polyP detected in both AX2 and NC4 extract was of a much more homogeneous length than detected in yeast extract (**Figure 4.11**), where the smear is comprised of a very mixed range of polymer lengths from few units to many hundreds units of phosphate groups.

5.2.2 Link between polyP and inositol pyrophosphates

Given that unlabelled polyP could be easily detected in WT phenol chloroform extract, the level of polyP present in the *ip6k* mutant described in **Chapter 3** was assessed. *Ip6k* mutants possess barely detectable levels of inositol pyrophosphates (**Figure 3.5**), providing an ideal model in which to assess the conservation of the correlation between levels of polyP and levels of inositol pyrophosphates. Therefore, 70 μg of RNA extracted from vegetative cultures of both WT and *ip6k* cultures were analysed by 20% PAGE (**Figure 5.3**). No difference could be detected between the levels of polyP in these strains, despite the clear difference in the level of inositol pyrophosphates (seen at bottom of the gel). PolyP extracted from both strains was of the same length and, crucially, of approximately the same abundance, suggesting that the correlation between the levels of inositol pyrophosphate and polyP was not conserved in the vegetative state of *D. discoideum.*

5.2.3 PolyP accumulation during development

As described in **Chapter 3**, the level of inositol pyrophosphates increases during development of *D. discoideum* (**Figure 3.10**), in addition earlier work suggested that polyP is highest in the spore (Gezelius 1974, Klein, Cotter et al. 1988, Zhang, Gómez-García et al. 2005). Since the expression of PPK1 is

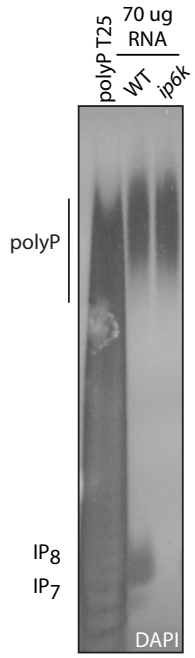

Figure 5.3 Vegetative levels of polyP do not correlate with inositol pyrophosphates.

Phenol chloroform extracts from vegetative cultures of WT and *ip6k* cells, normalized by 70 mg of co-purified RNA, were analysed by 20% PAGE and stained with DAPI. The figure shows the result of representative experiments that were repeated more than 3 times.

developmentally regulated, undergoing a dramatic increase in expression upon the onset of starvation (**Figure 5.4**) (https://dictyexpress.research.bcm.edu/landing/), it was investigated if there was any modulation in the level of polyP during *D. discoideum* development. WT cells were starved on 20 mM potassium phosphate (KK2) agar for up to 24 hours (as described in **materials and methods,, 2.3.10**). PolyP was extracted at five time points between the vegetative state and fruiting bodies. Extracts were analysed by 20% PAGE, with 70 μg of RNA loaded at each time point. Gels were stained with DAPI (**Figure 5.5 A**) and Toluidine (**Figure 5.5 B**).

Following the onset of the starvation response, the level of polyP underwent a dramatic accumulation, beginning very shortly after nutrient deprivation. The accumulation of polyP, observed by both staining methods, is at least two orders of magnitude, as calculated by densitometry of Toluidine stained gels (data not shown). Unfortunately this method is not sufficiently accurate to place a specific value on this accumulation as the signal becomes saturated in the fruiting bodies. Toluidine staining also confirmed that whilst the absolute level of polyP is dramatically increased, the average chain length appears unchanged. The broader smears observed by DAPI staining are most likely related to the increased abundance of polymers of all chain lengths, including those at the extremes.

This accumulation is consistent with previous observations that polyP is most abundant in the spores (Gezelius 1974, Klein, Cotter et al. 1988, Zhang, Gómez-García et al. 2005). However, the scale of this increase was not fully appreciated in previous work. In fact, the dramatic accumulation of polyP observed in these experiments was of a scale not previously seen in eukaryotic cells. It is interesting to note that the accumulation of polyP occurred in parallel with an increase in the level of inositol pyrophosphates, as seen in **Chapter 3**.

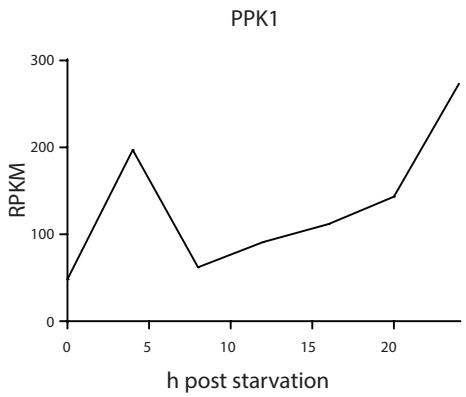

Figure 5.4 Developmental expression of PPK1.

Expression of PPK1 during development, source https://dictyexpress.research.bcm.edu/landing/

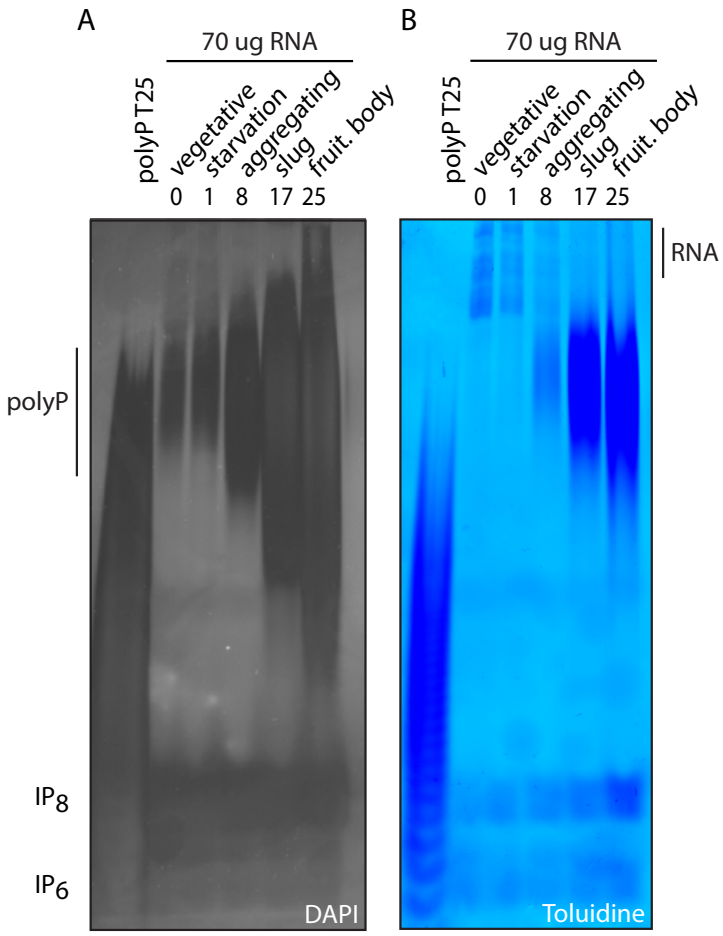

Figure 5.5 Developmental accumulation of polyP.

70 μg of RNA WT cell extracts from 5 developmental time points were analysed by 20% PAGE stained with Toluidine (A) and DAPI (B). Toluidine stained gels were analysed by densitometry using ImageJ. Figure and figure legend adapted from (Livermore, Chubb et al. 2016).

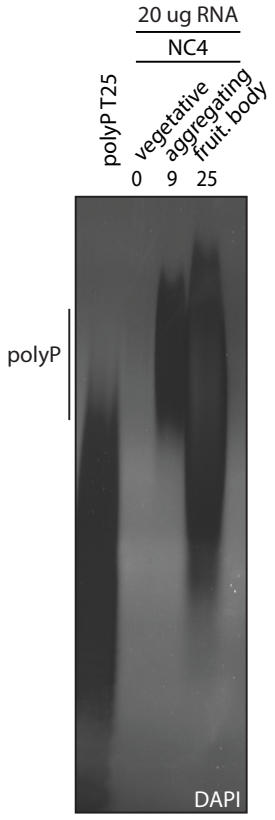

Figure 5.6 Developmental accumulation of polyP in NC4.

PolyP was extracted from NC4 cells at 3 time points during development, analysed by 20% PAGE and stained with DAPI. Figure and figure legend adapted from (Livermore, Chubb et al. 2016).

The accumulation of polyP during starvation was counterintuitive due to the substantial energetic investment required to synthesise polyP. Polyphosphate kinases utilise ATP to synthesise polyP, suggesting that this accumulation places a significant demand for ATP on starving cells. Therefore, to ensure that this was a physiological process, not an abnormality associated with AX2 lab strains, the level of polyP in developing NC4 cells was analysed. NC4 cells were starved as described above and polyP extracted at three time points, 20 μg of RNA was resolved by 20% PAGE and stained with DAPI (**Figure 5.6**). As in AX2 cells, the accumulation of polyP during this developmental response was dramatic.

In order to confirm that the results described above reflected a genuine increase in polyP, extract obtained from WT (AX2) fruiting bodies was subjected to enzymatic treatment (**Figure 5.7**). As observed previously (**Figure 5.2**), neither DNase, nor RNase affected the smear, whilst Ddp1, Ppx1 treatment and acid hydrolysis completely degraded the smear, confirming the identity of this smear as polyP. The increased abundance of polyP in the fruiting bodies made polyP detectable when just 1 μg of RNA was loaded per well. Thus no positive staining could be observed at the top of the gel.

The level of polyP during the vegetative state was unaffected by the level of inositol pyrophosphates (**Figure 5.3**), however as the inositol pyrophosphates increased during development in WT, so did polyP (**Figure 5.5**). Therefore, the correlation between these two phosphate rich species was examined during the development of a mutant strain displaying altered levels of inositol pyrophosphates, *ip6k* (**Figure 5.8**). The *ip6k** strain used in this experiment had been previously generated (Luo, Huang et al. 2003) and was the same as used in **Figure 4.3**. Experiments not shown here demonstrated that this strain also contained no detectable inositol pyrophosphates during development (Pisani, Livermore et al. 2014), as observed in the lower portion of

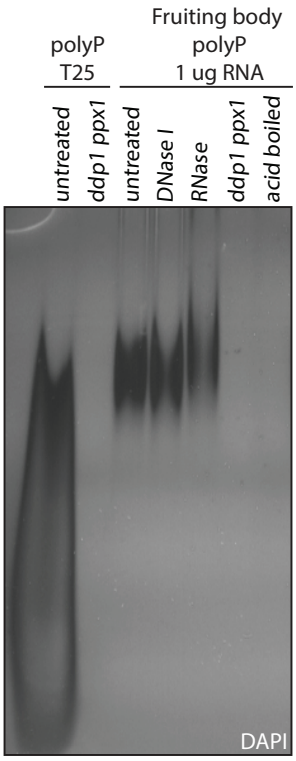

Figure 5.7 Enzymatic treatment of polyP from fruiting bodies.
Synthetic polyP standards with an average chain length of 25 (T25) was loaded, either untreated or after incubation with the exo- and endo-polyphosphatase (Ppx1, Ddp1). 1 μg samples of RNA phenol chloroform extract from fruiting bodies were treated with DNase, RNase, exo- and endo-polyphosphatase (Ppx1 and Ddp1) or treated in acid at high temperature (acid boiled). Samples were analysed by 20% PAGE and stained with DAPI.

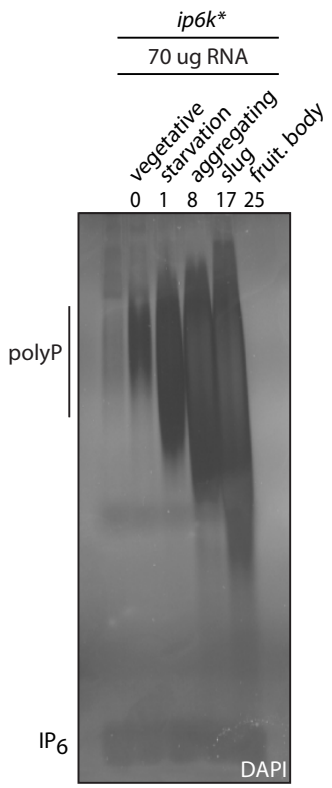

Figure 5.8 Developmental accumulation of polyP in *ip6k*.

PolyP was extracted from *ip6k** cells at 5 time points during development, analysed by 20% PAGE and stained with DAPI. Samples from were normalised by RNA with 70 μg RNA loaded.

Figure 5.8. Despite the failure to accumulate inositol pyrophosphates, this strain also underwent a dramatic accumulation of polyP during development.

These results indicated that although there was a correlation between the increases in inositol pyrophosphates and polyP during the development of WT cells, the increase in polyP was not dependent on an increase in inositol pyrophosphates. The observed increase in polyP in *ip6k* was comparable to that observed in WT, despite altered metabolism of inositol pyrophosphates. These results indicated once again that the correlation between inositol pyrophosphates and polyP present in yeast was not conserved in *D. discoideum*.

5.2.4 Deletion of PPK1

The scale of accumulation of polyP observed in **Figures 5.5** and **5.8** had never before been observed in eukaryotic cells. However the identity of the enzyme responsible for this accumulation was not clear. Two polyphosphate kinases have been described in *D. discoideum*, PPK1 and the DdPPK2 complex. The previously generated *ppk1* mutant generated by Zhang et al. (Zhang, Gómez-García et al. 2005) was not available and therefore could not be tested. Furthermore, the genes encoding DdPPK2 were not cloned. The *D. discoideum* genome encodes 41 actin or actin related genes, some with identical gene products (Joseph, Fey et al. 2008). The exact genes that encode the DdPPK2 gene were not unambiguously identified (Zhang, Gómez-García et al. 2007).

Consequently, the bacterial-like PPK1 gene was deleted. This strain will hereafter be referred to as *ppk1*. Unlike the previous *ppk1* strain, which deleted just 114 nucleotides, or ~3% of the coding sequence, the approach detailed in **Figure 5.9 A** deleted 69% of the Ppk1 ORF and >95% of the putative catalytic domain. This domain, identified by homology with the 688 amino acid *E. coli* Ppk1 (**Figure 5.1**), is found in the C-terminal portion of the larger (1050 amino

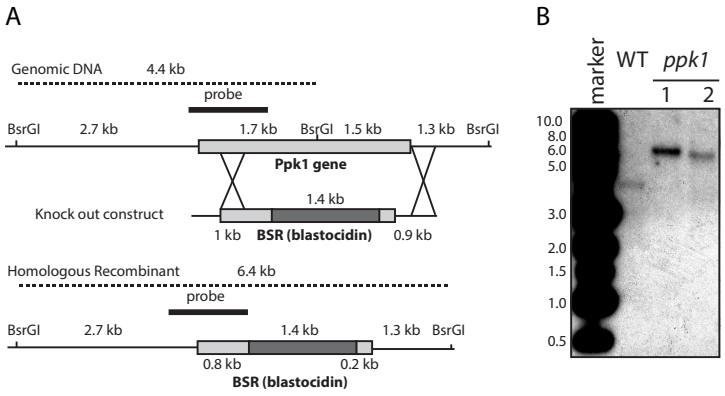

Figure 5.9 Deletion of PPK1.

Diagram showing the homologous recombination knockout strategy to generate *ppk1* amoeba (A). Southern blot of WT and *ppk1* genomic DNA (B). Genomic DNA was digested with BsrGI and probed for the 5' region, as indicated in (A). Figure and figure legend adapted from (Livermore, Chubb et al. 2016), .

acid) *D. discoideum* Ppk1. Deletion of this region was confirmed by Southern blot (**Figure 5.9 B**).

5.2.5 *ppk1* contains no detectable polyP

To investigate the presence of polyP in this strain, phenol chloroform extracts of vegetative WT and *ppk1* cells were analysed by 20% PAGE and DAPI staining (**Figure 5.10**). In this case 90 μg of RNA was loaded on the gel, the maximum possible without negatively affecting the migration of polyP in the gel, to ensure that any residual polyP could be detected. In fact, whilst the polyP in WT was clearly visible, no polyP smear could be detected in *ppk1* cells in the vegetative state. Equal loading of sample could be confirmed by the detection of RNA (above) and inositol phosphate species (below). This result provided further genetic evidence that the dark smear stained by DAPI was genuine polyP and that the *ppk1* strain contained no polyP.

Having confirmed the absence of polyP in the *ppk1* strain, the physiological effect on this strain was investigated. The growth rate of the *ppk1* strain in rich media was significantly reduced compared to WT (**Figure 5.11 A**), with a mean generation time of 11 h for WT and 15 h for the *ppk1* strain. The observed growth defect was also in contrast to previous findings, where no growth defect was reported in rich media (Zhang, Gómez-García et al. 2005).

5.2.6 PolyP and primary metabolism

It was reasoned that the poor growth of the *ppk1* strain might indicate an overall reduction in cellular fitness, perhaps due to altered phosphate metabolism and thus ATP synthesis. Therefore the cellular concentration of ATP was measured (**Figure 5.11 B**). Phenol chloroform extracts were analysed by ATP quantification luciferase assay (**materials and methods, 2.6.5**). This analysis revealed a striking and significant ($p<0.01$) decrease in the cellular concentration of ATP in *ppk1* cells (normalised by RNA). The concentration of ATP in vegetative WT cells was measured at approximately 2.5 nmoles/mg RNA. In contrast the

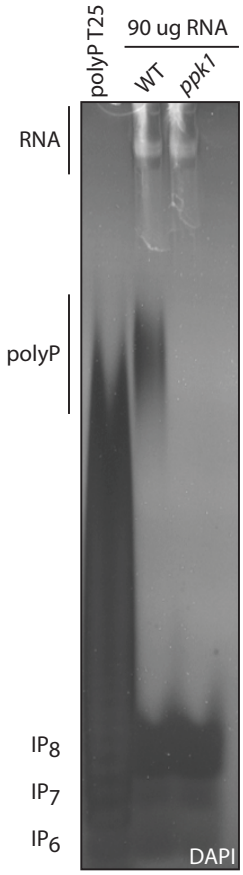

Figure 5.10 Ppk1 is the only polyphosphate kinase in D. Discoideum. Phenol chloroform extracts, normalized by loading 90 μg of co-purified RNA, from vegetative growing WT and *ppk1* cells were analysed by 20% PAGE and stained with DAPI. The figure shows the result of representative experiments that were repeated more than 3 times. Figure and figure legend adapted from (Livermore, Chubb et al. 2016).

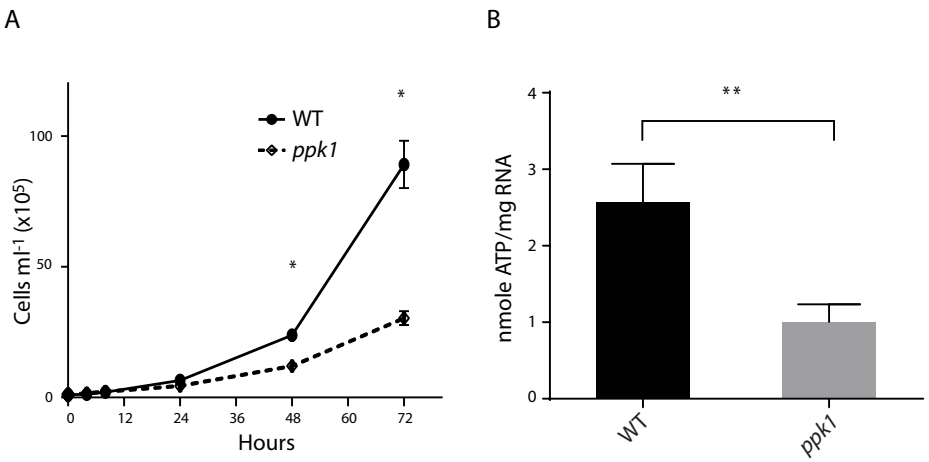

Figure 5.11 Ppk1 deletion affects growth and basic metabolism.
Cell growth curves in HL5 media. WT black line; *ppk1* dashed line. Average +/- SD of 3 experiments run in duplicate (*p < 0.05)(A). Quantification of ATP levels in vegetative growing WT and *ppk1* cells. Average +/- SD of 3 experiments run in duplicate (**p < 0.01)(B). Figure and figure legend adapted from (Livermore, Chubb et al. 2016).

concentration of ATP in vegetative *ppk1* cells was measured at just 1.0 nmoles/mg RNA. This dramatic decrease in cellular availability of ATP offered some explanation for the observed growth defect of *ppk1* and suggested a potential role for polyP in the control of primary metabolism.

This genetic evidence suggested a link between polyP and primary metabolism. Consequently, the effect of pharmacological inhibition of ATP production on polyP metabolism was investigated. Both WT and *ppk1* cells were treated with sublethal doses of KCN and benzohydroxamate (BHAM), to inhibit cytochrome oxidase and alternative oxidation respectively (Jarmuszkiewicz, Behrendt et al. 2002) (**Figure 5.12**). After two hours cells were visibly rounding (data not shown), but remained adherent. Treatment of WT cells for two hours induced an unexpected increase in polyP (**Figure 5.12 A**) despite significantly reducing the level of ATP by ~40% (**Figure 5.12 C**).

Unsurprisingly, the same treatment of *ppk1* cells (**Figure 5.12 B**) did not induce any accumulation of polyP. Nor did it result in a significant change in the level of ATP (**Figure 5.12 D**). The level of inositol pyrophosphates remained largely unchanged throughout this time course in both WT and *ppk1* cells (**Figure 5.12 A and B**). These unexpected results underscored the existence of a link between primary metabolism and polyP in these cells.

5.2.7 PPK1 responsible for developmental accumulation of polyP

Whilst the *ppk1* strain was demonstrated to possess no polyP in the vegetative state (**Figure 5.10**) or after inhibition of ATP synthesis (**Figure 5.12**), it was possible that the dramatic accumulation of polyP during the development of this amoeba (**Figure 5.5**) was due to the combined activity of PPK1 and DdPPK2. This possibility was assessed by starvation of the amoeba as previously described and analysis of extracts by 20% PAGE and DAPI staining (**Figure 5.13**).

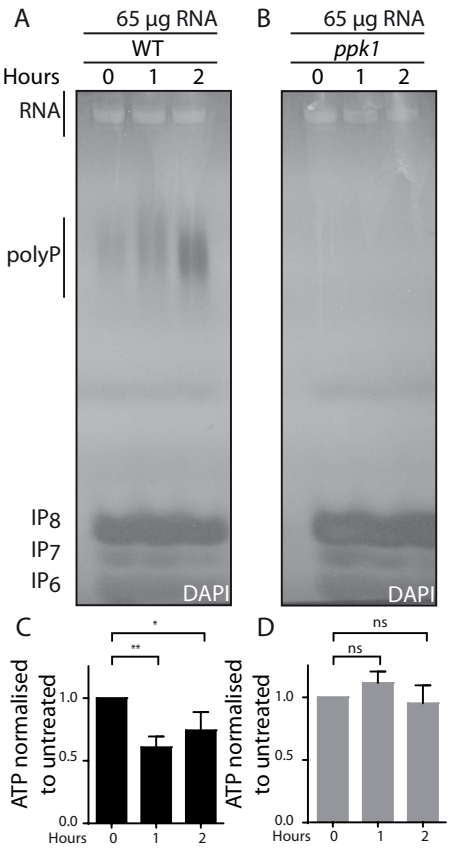

Figure 5.12 Inhibition of ATP synthesis induces an increase in polyP in WT cells.

Phenol chloroform extracts, normalized by loading 65 µg of co-purified RNA, from WT (A) and *ppk1* (B) cells treated with KCN and BHAM (see **materials and methods, 2.3.12**) for the indicated times were analysed by 20% PAGE and stained with DAPI. The figure shows the result of representative experiments that were repeated more than 3 times. Quantification of ATP levels in KCN and BHAM treated WT (C) and *ppk1* (D). Average +/- SD of 3 experiments run in duplicate (*$p < 0.05$, **$p < 0.01$). Figure and figure legend adapted from (Livermore, Chubb et al. 2016).

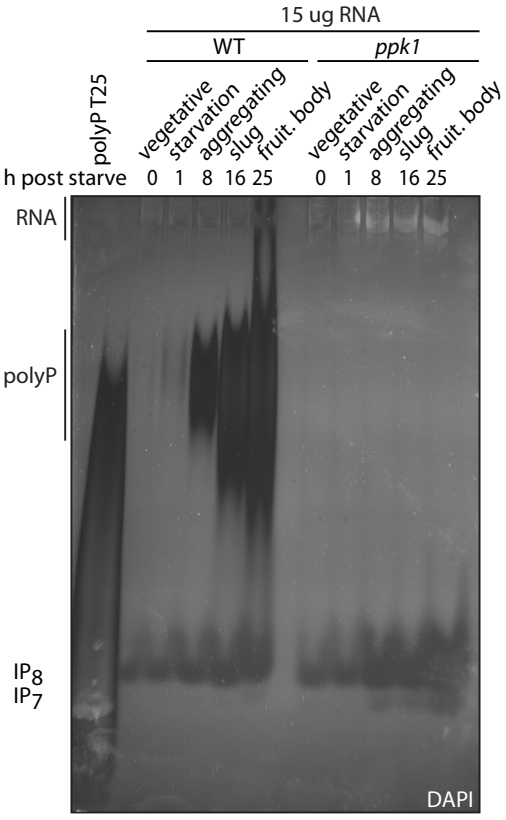

Figure 5.13 Ppk1 is the enzyme responsible for developmental accumulation of polyP in *D. Discoideum.*

WT and *ppk1* cells were developed on nutrient free agar and harvested at 5 time points. PolyP was extracted and 15 μg of RNA was analysed by 20% PAGE and stained with DAPI. Figure and figure legend adapted from (Livermore, Chubb et al. 2016).

As described above polyP dramatically accumulated during development in WT. However, no polyP could be detected at any stage of development in *ppk1* cells. This failure to accumulate any polyP in *ppk1* suggested that the synthesis of polyP during development was dependent upon the presence of the Ppk1 gene and the catalytic activity of the PPK1 enzyme. This offered further evidence that PPK1 was the only source of polyP in *D. discoideum.*

Interestingly, the co-purification of the inositol pyrophosphates during phenol chloroform extraction revealed the accumulation of inositol pyrophosphates in the latter stages of development. The increase in IP_8 in WT extract could be observed in the lower portion of the gel (**Figure 5.13**). Strikingly, the increase observed in the *ppk1* strain appeared to be greater. A very strong IP_8 band could be detected in this *ppk1* extract during the later stages of development (after 8 h or more). This band appeared to stain more strongly with DAPI than the corresponding band in WT extracts. Furthermore, an IP_7 band could also be detected in *ppk1* extracts beyond 8 h. The resolution of these bands was not as clear as when extracted with perchloric acid and analysed by 35.5% PAGE, however the difference was noticeable and reproducible and will be explored in more detail below.

5.2.8 *ppk1* defect in fruiting bodies formation

Despite the inability to identify morphological differences between WT and *ppk1* cells during the early stages of development by bright field microscopy (data not shown), a difference could be observed between the fruiting body structure (**Figure 5.14**), in accord with previously published results (Zhang, Gómez-García et al. 2005). In contrast to these previous reports, however, the speed of fruiting body formation was not dramatically altered (**Figure 5.13**). Fruiting bodies formed by *ppk1* cells did possess the basal disc, stalk and spore head, as found in WT fruiting bodies, however the size of the spore head was reduced (**Figure**

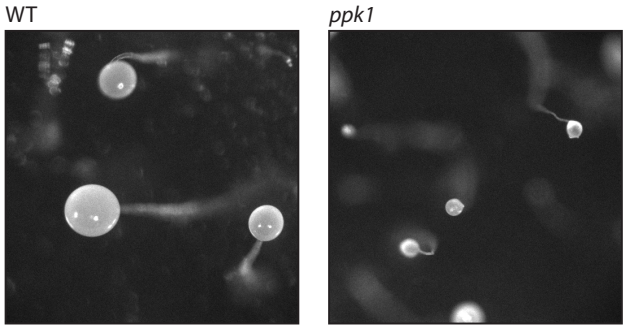

Figure 5.14 *ppk1* cells show impaired fruiting body formation.
Representative images of fruiting bodies from WT and *ppk1* cells. Images were taken after 48 h starvation at the same magnification. Figure and figure legend adapted from (Livermore, Chubb et al. 2016).

5.14). This striking phenotype in fruiting body formation correlated well with the developmental increase in polyP.

5.2.9 PolyP accumulates predominantly in spore cells

Fruiting body formation involves the differentiation of amoeboid cells first into prespore and prestalk cells and ultimately into the stalk and spore cells as seen in **Figure 5.14**. These cell types display different gene expression profiles (Williams 2006) and play dramatically different roles in the lifecycle of the amoeba. Stalk cells, which comprise approximately 20% of the cells in the structure, die during the formation of the fruiting body (Williams 2010). Meanwhile the spore cells enter into a dormant metabolic state until germination into unicellular amoeboid cells upon the restoration of a nutrient source. Given the differing expression profiles and roles of these cell types it was reasoned that identifying in which cell type polyP accumulated might provide clues to the physiological role of this accumulation of polyP. Interestingly the PPK1 gene expression profile displays no significant enrichment in either prespore or prestalk cells (https://dictyexpress.research.bcm.edu/landing/).

Therefore, spore cells were isolated from the fruiting bodies by vortexing and passing through Whatman No 114 filter paper via a method adapted from (Chiew, Reimers et al. 1985, Dynes, Clark et al. 1994)(**materials and methods, 2.3.14**). It was not possible to isolate pure preparations of stalk cells that were free of contaminant with spore cells. Consequently, polyP was extracted from pure spore preparations and compared to polyP extracted from whole fruiting bodies. Due to the relatively inert metabolic state of spore cells, RNA was not deemed to be the most accurate method for normalising. Therefore in this case the number of spore cells was counted after isolation and polyP was extracted from $5x10^6$ spores for both pure spores and fruiting bodies (comprised of both spore and stalk cells) of WT and *ppk1* strains. Analysis by 20% PAGE and DAPI revealed that polyP could be detected in both the fruiting bodies and the pure

spore preparation of WT cells (**Figure 5.15**). The level of polyP extracted from spores alone was broadly comparable to that extracted from whole fruiting bodies. No polyP was detected in either spores or whole fruiting bodies of *ppk1*.

These results indicated that polyP was present in WT spore cells. The inability to isolate pure stalk cells meant that it could not be concluded whether stalk cells contained any polyP, however, the similarity in the amount of polyP extracted from spores alone and from whole fruiting bodies suggested that the majority of polyP accumulated in spore cells.

5.2.10 PolyP plays a role in spore germination

The accumulation of polyP in the spores of *D. discoideum* was reminiscent of the accumulation of phytic acid (IP_6) in plant seeds. Germination of seeds containing low levels of phytic acid can be negatively affected (Pilu, Panzeri et al. 2003, Raboy 2007, Doria, Galleschi et al. 2009). Therefore the potential effect of a lack of polyP on spore germination was investigated by scoring the germination of WT and *ppk1*.

Spores were harvested from fruiting bodies 2-3 days after being plated on nutrient free agar. Fruiting bodies were washed in 0.5% NP40 to kill any remaining amoeboid cells. Spores were counted and then diluted to a density of 1.5 $x10^6$ spores per ml. Germination was then scored at indicated time points, with cells scored as ungerminated spores, swollen spores or amoeba. The percentage of cells remaining as ungerminated spores was calculated and plotted (**Figure 5.16,** average of three experiments).

WT spores germinated very rapidly in rich media (HL5) (**Figure 5.16 A,** solid line), with only ~15% remaining ungerminated after 4 h. Approximately 10% of spores remained ungerminated after 8 h and this was unchanged after 24 h. In contrast, *ppk1* spores showed a delay in germination (dashed line), after 4 h

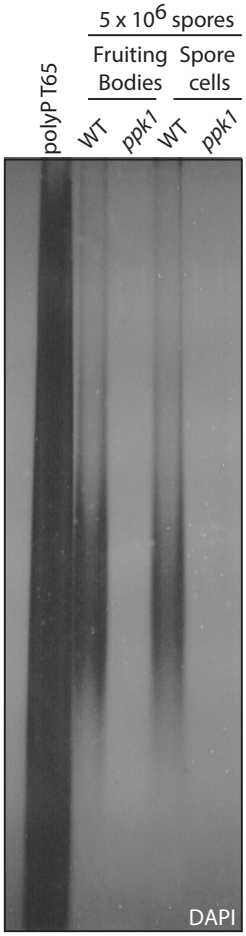

Figure 5.15 PolyP is predominantly present in the spores of fruiting bodies. Pure spore preparations were obtained (**materials and methods, 2.3.14**). 20% PAGE analysis of polyP extracted from whole fruiting bodies and pure spore preps, stained with DAPI. Figure and figure legend adapted from (Livermore, Chubb et al. 2016).

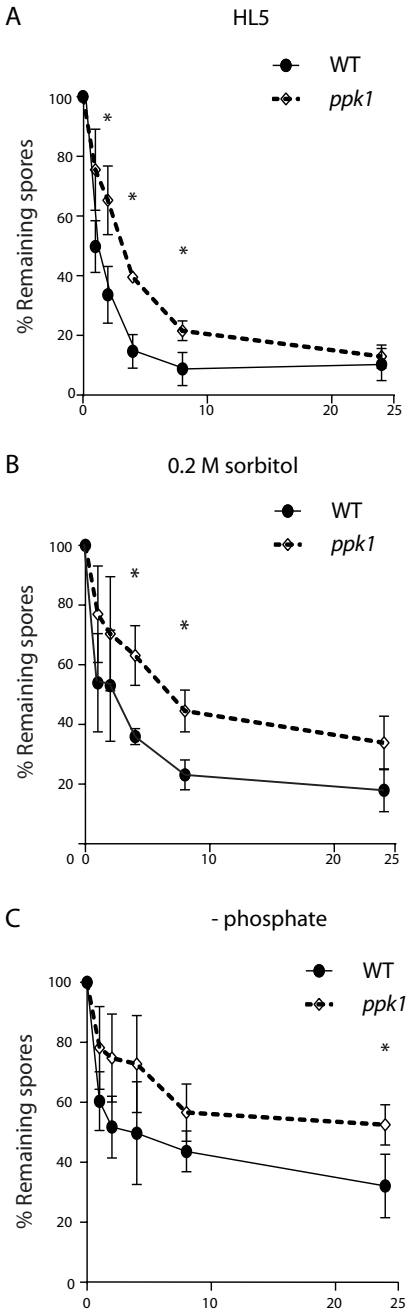

Figure 5.16 *ppk1* cells show delayed spore germination.

Spore germination in HL5 media (A), HL5 media supplemented with 0.2 M sorbitol (B) and SIH minus phosphate (C) over 24 hours. WT black line; *ppk1* dashed line. Average +/- SD of 3 experiments run in duplicate (*$p < 0.05$). Figure and figure legend adapted from (Livermore, Chubb et al. 2016).

approximately 40% of *ppk1* spores had failed to germinate. After 8 h there remained a significant difference ($p<0.05$) in the percentage germinated between WT and *ppk1* spores. However, only approximately 10% of spores remained ungerminated after 24 h, indicating that the defect in germination in rich media was a delay and not an absolute failure to germinate.

It was reasoned that the accumulation of polyP might indicate that the polymer acts as a storage molecule designed to aid germination in suboptimal conditions. Consequently the ability of *ppk1* spores to germinate in more challenging conditions was assayed. Both WT and *ppk1* spores were diluted in rich media supplemented with 0.2 M sorbitol (**Figure 5.16 B**) to determine the effect of osmotic stress on germination. In this case the germination of WT spores (solid line) was delayed, compared to rich media that had not been supplemented (**Figure 5.16 A**). Even after 24 h, approximately 20% of cells had not begun to germinate. The germination of *ppk1* cells (dashed line) was also delayed and was significantly different from WT germination after both 4 and 8 h. Whilst the difference was not significant after 24 h, almost 40% of spores had failed to germinate. This defect in germination under osmotic stress appeared to be slightly greater than in unsupplemented rich media.

To investigate the possibility that the accumulation of polyP in spores might represent a phosphate store this experiment was conducted in synthetic media deprived of phosphate. It was reasoned that the absence of phosphate in this experiment might exacerbate the difference seen between these strains. In fact the germination of both WT and *ppk1* was greatly impaired, with only ~60% of WT spores (solid line) germinating even after 24 h (**Figure 5.16 C**). Once again the germination of *ppk1* cells (dashed line) was slowed and significantly fewer *ppk1* spores had germinated after 24 h. Despite this significant reduction in germination compared to WT, >40% of *ppk1* spores were able to germinate after 24 h, even when deprived of any external phosphate. Once again it was not

possible to conclude whether the effect was simply a delay or an absolute failure to germinate in *ppk1* spores. However, very little change in germination was observed between 8 and 24 h in *ppk1* spores, perhaps suggesting that these spores might have failed to germinate had the experiment continued.

5.2.11 Electron microscopy to localise polyP in the spore

Given the failure to localise polyP in the vegetative state or during the first five hours of starvation (data not show), it was reasoned that spore cells, which contain the highest levels of polyP (Gezelius 1974, Klein, Cotter et al. 1988, Zhang, Gómez-García et al. 2005) (**Figure 5.5 and 5.15**), might represent the best cell type to localise polyP. However, spore cells are surrounded by a proteinaceous and polysaccharide coat, making them inappropriate for light microscopy studies. Consequently, the localisation of polyP in the spores was assayed by electron microscopy (**Figure 5.17**).

In the yeast *S. cerevisiae*, the majority of polyP is within the vacuole (Kornberg, Rao et al. 1999). It is possible to distinguish between yeast strains with different levels of polyP by electron microscopy. Yeast strains with high levels of polyP appear to have “dark-staining”, electron dense vacuoles by electron microscopy, whilst strains with low polyP have much “lighter-staining” less electron dense vacuoles (unpublished observation, Saiardi lab). Therefore, a similar approach was applied to WT and *ppk1* spores. Spores were embedded in an agarose pellet, sectioned and stained with lead citrate (**materials and methods, 2.3.17**). The integrity of structures appeared to be well conserved in this process, representative electron micrographs of WT and *ppk1* spores are shown in **Figure 5.17**. It was not possible to discern any electron dense organelle structures that were present in the WT spores but not the *ppk1* spores. This suggested that this method would not be appropriate to ascertain the subcellular localisation of polyP. In fact no gross morphological variations could be detected between the spores generated by WT and *ppk1* strains.

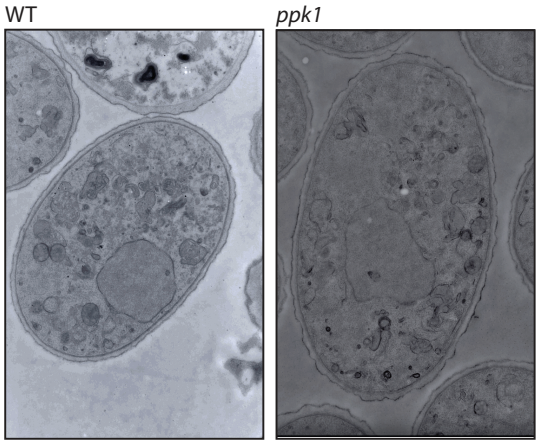

Figure 5.17 WT and *ppk1* spores indistinguishable by electron microscopy. Representative images taken by Transmission Electron Microscopy of pure spore preparations from WT (left) and *ppk1* (right). Spores were sectioned and stained with lead citrate and imaged (**materials and methods, 2.3.17**). Images are shown at the same scale and are representative of >20 spores analysed in this way.

5.2.12 PolyP and inositol pyrophosphates during development

As previously discussed the metabolism of inositol pyrophosphates and polyP are linked in yeast. However, the correlation between the levels of these two molecules in the vegetative state was not conserved in the *D. discoideum* (**Figure 5.3**). Nevertheless, it did appear that *ppk1* accumulated more inositol pyrophosphates during development than WT (**Figure 5.13**). This observation was further investigated by analysing perchloric acid extract of both WT and *ppk1* cells at different time points during development. Extracts were analysed by 35.5% PAGE and Toluidine staining (**Figure 5.18 A**). This analysis confirmed that the accumulation of inositol pyrophosphates during *ppk1* development was greater than in WT. This effect was most notable in the level of IP_7, which was dramatically increased in *ppk1* particularly after 16 h. The increase of total inositol pyrophosphates (IP_7 and IP_8) was quantified in comparison to IP_6 by densitometry as previously described. This quantification revealed that the total level of inositol pyrophosphates in *ppk1* fruiting bodies was double the level attained in WT fruiting bodies (when normalised by IP_6) (**Figure 5.18 B**).

The analyses thus far suggested that whilst the link between inositol pyrophosphates and polyP was not as seen in yeast (Lonetti, Szijgyarto et al. 2011), some metabolic link did exist in the amoeba. In the absence of polyP, it appeared that the level of high-energy phosphoanhydride bonds was partially compensated by an increase in the accumulation of another phosphate rich molecule, containing phosphoanhydride bonds, the inositol pyrophosphates. However, the nature of this link was not clear. Given that synthesis of polyP during the developmental process clearly requires large of energetic input in the form of ATP, it was reasoned that a strain lacking PPK1 might consume less ATP during development. Therefore the level of ATP in the *ppk1* strain was investigated.

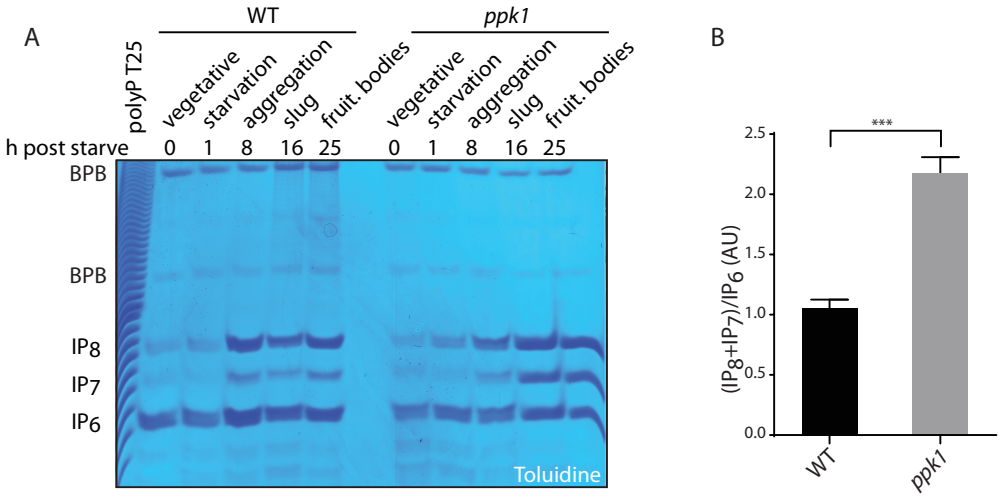

Figure 5.18 Developmental failure to accumulate polyP affects inositol pyrophosphate.

35.5% PAGE analysis of perchloric acid extract from WT and *ppk1* cells during development, stained with Toluidine (A). Quantification of the ratio between inositol pyrophosphates (IP_7 and IP_8) and their precursor, $InsP_6$ in fruiting bodies. Quantification by densitometry using ImageJ software, results represent the average +/- SD of 3 independent experiments (***$p < 0.0001$) (B). Figure and figure legend adapted from (Livermore, Chubb et al. 2016).

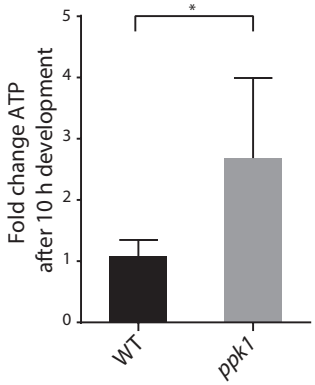

Figure 5.19 Developmental failure to accumulate polyP affects ATP metabolism.

Quantification of fold change in ATP between vegetative cells and “aggregating” cells starved for 10 hours. Average +/- SD of 6 experiments run in duplicate (*p < 0.05). Figure and figure legend adapted from (Livermore, Chubb et al. 2016).

Due to the technical difficulty in extracting ATP from multicellular stages of *D. discoideum* development, ATP was quantified at 0 h of starvation and at 10 h. The fold change of ATP was then calculated over this period (**Figure 5.19)**. Whilst the level of ATP did not change dramatically during the first 10 h of development in WT cells, the level of ATP in *ppk1* strains increased ~2.5 fold, rising to a level slightly exceeding WT. Thus, whilst *ppk1* cells failed to accumulate polyP during the developmental process, they accumulated both inositol pyrophosphates and ATP to a greater extent than WT cells. A common feature to all these molecules is the presence of high-energy phosphoanhydride bonds.

5.2.13 Investigating a molecular link between polyP and inositol pyrophosphates

Whilst the link between polyP and inositol pyrophosphates was not as described in yeast, these phosphate rich molecules did show some metabolic link in *D. discoideum*. A number of possible explanations for this metabolic link could be conceived, including a direct effect of inositol pyrophosphates on the polyP synthesising enzyme. Other explanations could include a direct linkage between these molecules, perhaps with inositol pyrophosphates “decorating” polyP and capping the ends of the polymer, potentially protecting it from degradation by exopolyphosphatases as has been proposed previously (Saiardi 2012). Alternatively a more general metabolic link could exist, exerted through the energetic status of the cell and the effect that both polyP and inositol pyrophosphates exert on ATP levels. The observed differences between yeast and *D. discoideum* does not allow one model to be favoured as universal.

It was reasoned that the different synthetic pathways of polyP in yeast and the amoeba made a direct effect on the synthetic enzyme (Vtc4 and PPK1 respectively) unlikely. The effect observed upon ATP levels was also not conserved between yeast and amoeba (**Figure 3.11 and Figure 5.11**).

Therefore, the most attractive model was reasoned to be a direct linkage between these molecules. It has previously been hypothesised that inositol pyrophosphates may act as a "cap" on the ends of the polyP polymer, possibly offering protection from degradation by exopolyphosphatases (Saiardi 2012). To explore this possibility an experimental procedure was devised in which polyP extracted by phenol chloroform was separated from co-purifying inositol pyrophosphates by gel filtration and then degraded by acid boiling. Complete hydrolysis of phosphoanhydride bonds would release any other attached molecules, including inositol species such as IP_6 (which is insensitive to acid hydrolysis). The potential release of IP_6 was then examined by PAGE and Toluidine staining. These experiments are detailed in **Figures 5.20 to 5.23**.

In order to obtain the high levels of polyP required, polyP was extracted from fruiting bodies. 6 $x10^8$ cells were allowed to develop for 2 days on KK2 agar. These cells were then used to prepare a phenol-chloroform extract that was spiked with 20 μl of 10 mM IP_6 and loaded on a Superdex peptide 10/300 gel filtration column (GE Healthcare Life Sciences). Eluted fractions were then pooled in pairs and 1/10 of fractions 11-30 were analysed by 30% PAGE and stained with DAPI (**Figure 5.20**). These experiments revealed that polyP extracted from fruiting bodies eluted in fractions 15-22. Spiked IP_6 (as well as small amounts of endogenous IP_7 and IP_8) could be detected in fractions 25-28. Thus this method allowed good separation of these two species based on their differing sizes. For future experiments polyP in fractions 15-19 were pooled and used for further analysis. Whilst polyP could still be detected in fractions 20-22, these were deemed to elute too close to inositol pyrophosphates and therefore discarded to avoid any potential contamination.

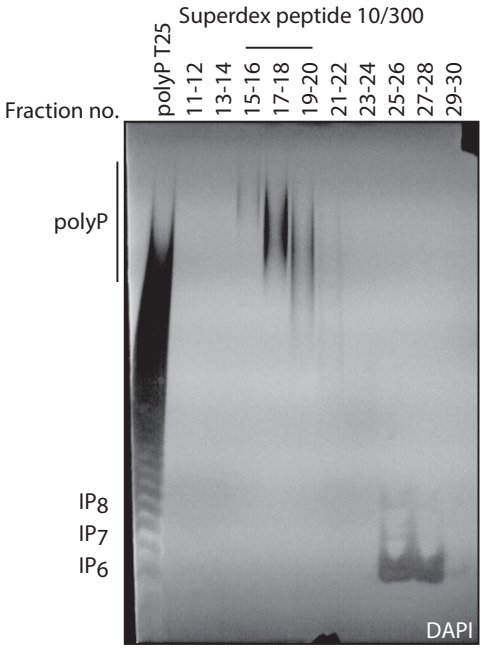

Figure 5.20 Fruiting body inorganic polyP can be separated according to size.

Phenol chloroform extracts from fruiting bodies were "spiked" with IP_6 were resolved by gel filtration (**materials and methods, 2.6.6**). Fractions were pooled as indicated, resolved by 30% PAGE and stained with DAPI.

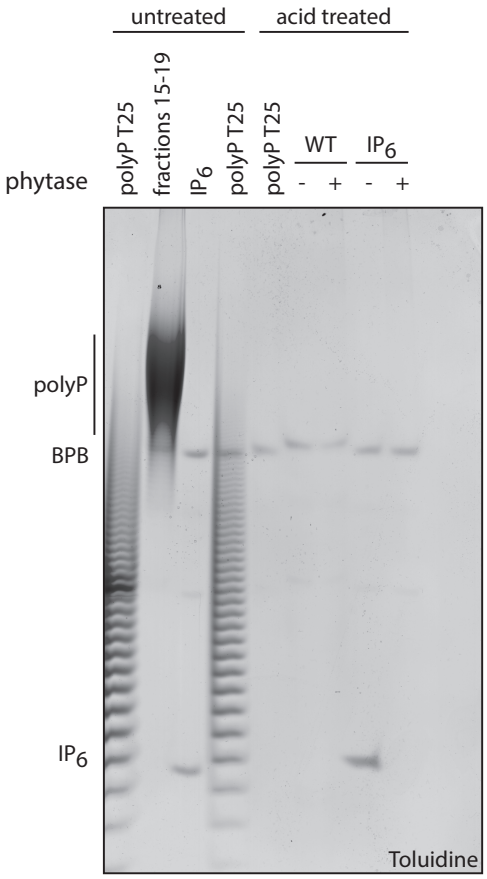

Figure 5.21 PAGE analysis of fruiting body polyP degraded by acid hydrolysis failed to detect inositol phosphates.

PolyP was resolved by gel filtration as shown in **Figure 5.20**. PolyP fractions were pooled as indicated and split into three, untreated, acid boiled for 1.5 h at 100°C and neutralised or acid boiled followed by phytase treatment. IP_6 samples were treated identically. Samples were concentrated in a vacuum evaporator and resolved by 30% PAGE and stained with Toluidine.

After pooling fractions 15-19, this sample was split into 3 equal volumes. One volume was stored on ice, whilst the other two were boiled in 1 M perchloric acid for 1.5 h. After acid treatment, these samples were neutralised with 1 M K_2CO_3 (supplemented with 3 mM EDTA). After neutralisation, one of the acid treated samples was treated with phytase. This step was designed to determine if any species that was released during acid boiling contained inositol. These experiments were performed in parallel with IP_6 (untreated; acid boiled; acid boiled then treated with phytase) to confirm that IP_6 was not degraded by acid boiling, but could be degraded by subsequent phytase treatment, as shown in lanes 2, 7 and 8 (**Figure 5.21**). Importantly, this analysis demonstrated that the polyP prepared by pooling of samples 15-19 from **Figure 5.20** was not contaminated with inositol pyrophosphates (lane 1). This smear was completely degraded by acid treatment (lane 5 and 6), however no band resembling IP_6 was released (lane 5).

This approach failed to demonstrate the release of any inositol phosphate containing species from fruiting body derived polyP. A similar approach was applied to polyP extracted from vegetative cells. Due to the lower abundance of polyP in the vegetative state, phenol chloroform extracts were prepared from 3 $x10^9$ cells. Prior to loading on a gel filtration column, these samples were then treated with RNase to degrade co-purifying RNA. This extract was then separated by Superdex peptide 10/300 gel filtration column (**Figure 5.22**). These species showed slightly different separation, with polyP eluting between fractions 13-20. In addition, much higher levels of endogenous inositol phosphates could be detected in fractions 21-28 (no IP_6 spike was included in these experiments). Fractions 16-20 were utilised in the following experiments.

As described above, pooled fractions were split into three and treated accordingly (**Figure 5.23**). Once again, IP_6 was unaffected by acid treatment (lane 7), but could be degraded by phytase (lane 8). Similarly, no inositol

phosphate contaminants could be detected in untreated, purified polyP (lane 3). Acid treatment once again degraded the polyP smear, however it also released three diffuse bands in the process (lane 4). These bands were not degraded by phytase treatment (lane 5), indicating that they were not inositol-containing species. This figure is representative of an experiment performed several times, where the three released bands could not be degraded by phytase. The identity of these bands was not thoroughly investigated. They could represent RNA degradation products, generated in the RNase step or be a non-inositol phosphate polyP-associated molecule.

This approach did not reveal the release of inositol species from either vegetative polyP or fruiting body polyP. Several attempts were made to refine this approach, including the use of TiO_2 beads to purify phosphate-rich species after acid hydrolysis (Wilson, Bulley et al. 2015), however the experiments described above gave the clearest results. Whilst this approach did not conclusively disprove the hypothesis that polyP and inositol phosphates are covalently linked or bound, however it failed to offer compelling evidence in support of this hypothesis.

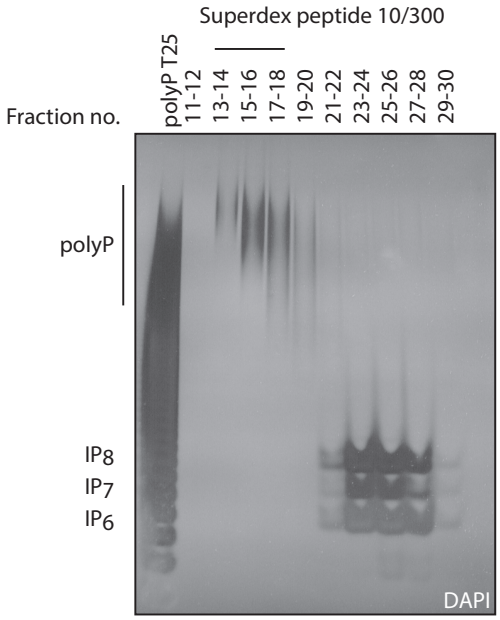

Figure 5.22 Vegetative inorganic polyP can be separated according to size. Phenol chloroform extracts from vegetative cells were resolved by gel filtration (**materials and methods, 2.6.6**). Fractions were pooled as indicated, resolved by 30% PAGE and stained with DAPI.

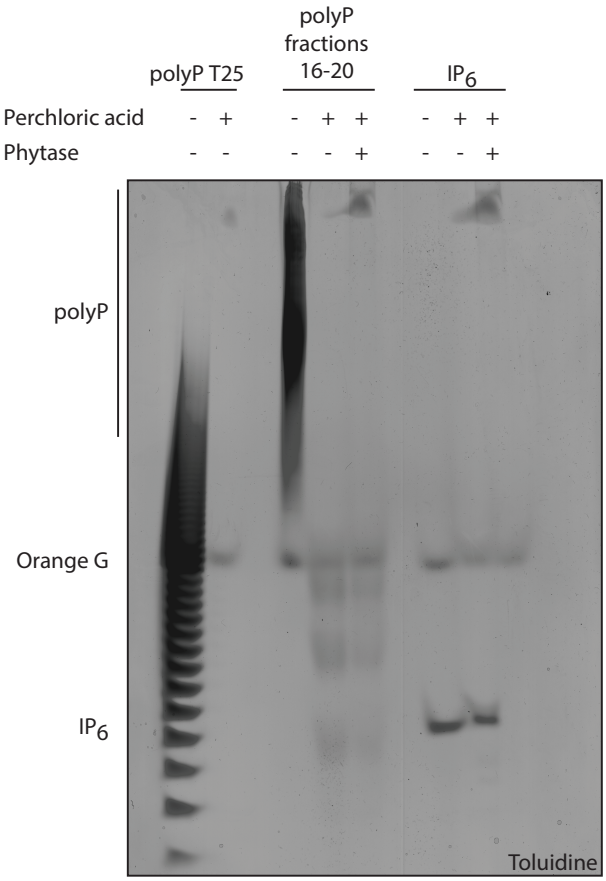

Figure 5.23 PAGE analysis of vegetative polyP degraded by acid hydrolysis failed to detect inositol phosphates.

PolyP samples were treated with RNase A and RNase T1 at 37°C for 1.5 h. PolyP was then resolved by gel filtration as shown in **Figure 5.22**. PolyP fractions were pooled as indicated and split into three, untreated, acid boiled for 2 h at 100°C for 2 h and neutralised or acid boiled followed by phytase treatment. IP_6 samples were treated identically (except RNase treatment). Samples were concentrated in a vacuum evaporator and resolved by 30% PAGE and stained with Toluidine.

5.3 Discussion

The experiments described above confirm that *D. discoideum* offers excellent potential as a model in which to study the role of inorganic polyphosphate on cellular metabolism. The application of PAGE technology, coupled with either Toluidine or DAPI staining allows the direct visualisation of unlabelled polyP extracted from *D. discoideum* for the first time (**Figure 5.2**). This method provides the most robust and reliable detection of polyP, allowing the polymer to be discerned from co-purifying molecules.

5.3.1 Detection of polyP in *D. discoideum*

Phenol chloroform extractions commonly used to purify polyP also co-extract a range of molecules, including RNA (**Figure 5.2**), inositol pyrophosphates (**Figure 5.5**), ATP (**Figure 3.13**) and perhaps even free phosphate. Traditional methods for polyP detection are indirect, requiring the degradation of polyP and quantification, by malachite green, or free phosphate released; use of polyP as a substrate to regenerate ATP using purified PPK; or the detection of a shift in DAPI fluorescence induced by polyP. All of these assays are influenced by co-purifying molecules, in particular the inositol pyrophosphates, which are degraded by both acid treatment and certain endopolyphosphatases (Lonetti, Szijgyarto et al. 2011). Furthermore, inositol phosphates are able to induce a fluorescence shift when bound to DAPI (Kolozsvari, Parisi et al. 2014). The methods used in these experiments are able to discern polyP from any other co-purifying molecules through both speed of migration and a range of biochemical treatments (**Figure 5.3**). An additional advantage of this technique is its ability the discern polyP chain length, something that other methods preclude. Thus, this work demonstrates the simple and reliable visualisation of unlabelled polyP extracted from a range of *D. discoideum* mutants at different stages of development.

In fact, these experiments surprisingly reveal that the nature of the link between polyP and inositol pyrophosphate metabolism seen in yeast is not conserved in *D. discoideum* (**Figure 5.4**). Nevertheless, the data described above does indicate a possible functional relationship, as shown by cells lacking polyP, which accumulate high levels of inositol pyrophosphates (**Figure 5.18**).

These results demonstrate, for the first time the true scale of the accumulation of polyP during the developmental time course. Whilst this unusual accumulation of polyP had been described before by a number of laboratories (Gezelius 1974, Klein, Cotter et al. 1988, Zhang, Gómez-García et al. 2005), previous estimates greatly underestimated the scale of the accumulation, which is at least two orders of magnitude (**Figure 5.5**). In accord with observations in the vegetative state, altered metabolism of inositol pyrophosphates does not affect the accumulation of polyP (**Figure 5.8**).

5.3.2 PPK1 is the only polyphosphate kinase in *D. discoideum*

Strikingly, these results also demonstrate that polyP cannot be detected in cells lacking the bacterial-like PPK1. This enzyme was previously deleted by Zhang et al., generating a mutant strain possessing 20-50% of WT polyP. In stark contrast, the experiments presented here describe the generation of a *ppk1* null strain in which >95% of the catalytic domain is deleted (**Figure 5.9**) and no polyP can be detected. Two possible explanations could account for this discrepancy, the first is the different methodologies used to detect polyP. It is possible that the signal obtained in the *ppk1* mutant by Zhang et al. was in fact due to co-purifying molecules. Alternatively, it is possible that a partially active, truncated PPK1 remained in this strain, as only ~3% of the coding sequence of this gene was deleted.

In fact, this discrepancy is significant as the presence of polyP in Zhang et al.'s mutant was presented as evidence for an additional polyP kinase activity in the

amoeba. This activity was attributed to the remarkable DdPPK2 complex (Gómez-García and Kornberg 2004). However, the experiments presented here failed to detect residual polyP in the *ppk1* strain, calling into question the physiological relevance of the DdPPK2 complex as a source of polyP either in the vegetative state or during development. Thus proposals that DdPPK2-like complexes might be the source of mammalian polyP (Hooley, Whitehead et al. 2008) must be reconsidered in light of this work. If, as seems to be the case, DdPPK2 is not a physiological polyP kinase, then the search for the true mammalian polyP kinase must continue.

5.3.3 PolyP is linked to primary metabolism in *D. discoideum*

Furthermore, the absence of detectable polyP in the *ppk1* strain offers an explanation for additional discrepancies between the results described here and those obtained by Zhang et al. The *ppk1* strain generated in this work has a defect in growth rate, causing an extension in doubling time from 11 h to 15 h compared to WT. No such defect was observed by Zhang et al., possibly due to the residual polyP present in their Ppk1 null strain.

The observed defect in growth is underpinned by a more than two-fold decrease in the level of ATP in the *ppk1* strain. This should perhaps not be surprising due to the ability of polyP to act as phosphate buffer and thus as a Pi donor for general metabolism. The consequences of which seem likely to affect the cell's ability to synthesise ATP. In fact, polyP has previously been linked to metabolic control. A genome-wide screen in yeast revealed a strong inter-dependence between polyP and primary metabolism (Freimoser, Hürlimann et al. 2006). As described above, this study demonstrated that deletion of genes involved in polyP metabolism was most frequently coincident with altered metabolism. The authors of this study postulated that the interdependence of polyP and basic

energetic metabolism positioned polyP as an indirect link between phosphate homeostasis and primary metabolism.

Furthermore, as described in **Chapter One**, polyP has been implicated in mitochondrial function in mammalian cells, including as a constituent of the mitochondrial permeability transition pore complex (Seidlmayer, Blatter et al. 2012). In contrast to the work presented in this chapter however, inhibition of mitochondrial function using the uncoupling agent FCCP, induced a decrease in polyP, as detected by DAPI fluorescence. Conversely, stimulation of mitochondrial activity by providing the substrate of complex II, methyl-succinate, prompted an increase in polyP. These results are in conflict to those described here and the exact role of polyP in mitochondrial functionality will require further investigation.

The interdependence between polyP and cellular ATP was demonstrated by both genetic means, through the dramatic decrease in ATP levels in the *ppk1* mutant, and also by pharmacological treatment with KCN and BHAM. Sublethal doses of inhibitors for both the electron transport chain and alternative oxidation pathway resulted in decrease in the cellular level of ATP in WT cells (**Figure 5.12**). Counterintuitively, this fall in ATP production was coupled with an increase in the level of polyP.

The failure of KCN and BHAM to induce significant reductions in the cellular ATP of *ppk1* cells raises the interesting question of how these cells generate ATP. The resistance of *ppk1* ATP levels to KCN and BHAM treatment, as well as the lower overall level of ATP in vegetative cells could indicate that the mitochondrial activity of the *ppk1* null cells is compromised. Whilst experimental evidence is lacking, these results could be consistent with a role for polyP in promoting efficient mitochondrial activity. Extending this hypothesis further, the observed increase in polyP in WT cells treated with mitochondrial inhibitors

might represent an adaptive measure to preserve mitochondrial function in the face of extreme stress.

Whilst this is an attractive hypothesis, the data presented here could also offer an alternative hypothesis for the accumulation of polyP upon inhibition of ATP production. As discussed above and demonstrated in **Figures 5.5-5.7** induction of the starvation response induces a rapid accumulation polyP. Inhibition of mitochondrial activity with KCN and BHAM could be considered as akin to the most acute starvation response, causing a dramatic reduction in the energetic currency of the cell. Thus the unexpected increase in polyP observed upon treatment with KCN and BHAM may represent a similar phenomenon to that observed upon starvation and during the developmental response.

The developmental response of the amoeba *D. discoideum* is a complex process involving the altered expression of a large network of genes (Loomis 2015). In fact, Ppk1 is one of the genes to be upregulated during development (**Figure 5.4**). The expression of Ppk1 during treatment with KCN or BHAM was not measured, but it seems unlikely that treatment with KCN and BHAM could mimic the effects of starvation and change expression of such a high number of genes. In fact, the role of cAMP as the key signalling molecule in this pathway, which is synthesised in a single catalytic step from ATP, suggests that any inhibition of ATP production might in fact preclude the starvation response. Thus, treatment with KCN and BHAM mimicking the starvation response seems unlikely. Instead, these results suggest a model in which the relationship between polyP and primary metabolism is a complex one. Further experiments are required to understand the precise nature of this link and the effect of polyP on mitochondrial function in these *D. discoideum*.

5.3.4 Why do spores accumulate polyP?

Whilst the accumulation of polyP in response to ATP depletion may not be related to the starvation induced increase, the scale of the increase of polyP during development is stark. It had been previously reported that the *ppk1* null strain show aberrant fruiting body formation (Zhang, Gómez-García et al. 2005). This observation is confirmed by this work (**Figure 5.14**). Therefore, the role of polyP in development was a focus of investigation. Separation of spore cells from stalks reveals that a large proportion of the polyP contained in fruiting bodies accumulates in the spores (**Figure 5.15**), leading to speculation that there may be a defect in sporulation.

Analysis of plaque formation failed to adequately distinguish between the growth defect shown by *ppk1* (**Figure 5.11**) and impaired sporulation (data not shown). Consequently an alternative method, adapted from van Dijken et al. (Van Dijken and Van Haastert 2001) was employed. This analysis identified a sporulation defect in *ppk1* spores (**Figure 5.16**). The germination delay in germination of *ppk1* could be caused by numerous factors, including the loss of polyP as an energy store. Considering polyP as an energy store to be utilised upon germination offers a potential explanation for the large investment of limited resources in polyP synthesis during the starvation response.

However, this germination defect is exacerbated by osmotic stress conditions in media supplemented with 0.2 M sorbitol. Given that synthesis and degradation of polyP affects not only the cellular abundance of free phosphate, but also the availability of the divalent cations such as Ca^{2+} and Mg^{2+} it is unsurprising that the loss of polyP might exert an osmotic effect. PolyP chelation of divalent cations may also have additional properties, acting as a sponge for these ions. Thus degradation of polyP during germination would allow the rapid release of these cations. The ability of *ppk1* to germinate in media depleted of divalent

cations was not tested, however, it would be interesting to explore this hypothesis further.

It was perhaps surprising that *ppk1* spores showed a less dramatic germination defect compared to WT in media lacking phosphate (**Figure 5.16**). It should be noted that both WT and *ppk1* spores were slower to germinate in media lacking phosphate, however the ability of over 40% of *ppk1* spores to germinate over the course of 24 hours was surprising. If the accumulation of polyP was simply considered a store of phosphate then it would be anticipated that failure to synthesise this store might have catastrophic effects on the ability of this strain to germinate in the absence of phosphate. This was not the case, suggesting that the role of polyP may be more complex, or that *ppk1* cells are able to compensate for the loss of polyP in other ways.

5.3.5 Inositol pyrophosphates compensating for loss of polyP?

This work also demonstrated that the *ppk1* strain accumulated significantly more inositol pyrophosphates than WT during development (**Figure 5.17**). Thus the accumulation of these phosphate rich and high-energy molecules may represent a partial compensation for the absence of polyP. In fact, the phosphate rich inositol pyrophosphates represent not only a store of phosphate, but also a store of phosphoanhydride bonds. It must be noted that the additional energy stored in the increase in IP_7 and IP_8 in *ppk1* spores is far less than that stored in the polyP pool of WT. Nevertheless, inositol pyrophosphates may offer some partial compensation for the lack of polyP both in phosphate storage, energy storage and in chelation of divalent cations; an additional property shared by polyP and inositol phosphates (Kornberg, Rao et al. 1999, Shears 2001).

These observations offer the attractive hypothesis, that whilst inositol pyrophosphates and polyP are not metabolically coupled as in yeast, there is a

more functional link between these molecules, particularly during the starvation and germination response.

It should also be noted that during the first 10 hours of development there is very little change observed in the level of ATP in WT cells. In contrast, *ppk1* cells increase their level of ATP by approximately 2.5 fold. This increase in ATP could be considered to be a consequence of the failure to accumulate polyP as ATP is not expended by PPK1 activity. In this context, the increase in inositol pyrophosphates in *ppk1* could simply be due to elevated cellular ATP (compared to vegetative growth). However, this seems to be an oversimplification as it implies a direct correlation between the level of inositol pyrophosphates and ATP. Numerous experiments, including the relatively unchanged level of inositol pyrophosphates in the vegetative state of *ppk1* despite low levels of ATP, suggest that the relationship is more complex than this. It is also worthy of note that the increase in ATP observed during development of *ppk1* cells brought the level of ATP to a value comparable to that of WT cells. Thus ATP was not raised to such aberrantly high levels to expect a total distortion of the synthesis of inositol pyrophosphates.

5.3.6 Capping things off?

Finally, one alternative hypothesis for the increase in inositol pyrophosphates during development of *ppk1* is that it might not represent increased synthesis at all. Rather it could be a result of failure to utilise these molecules. Whilst it is known that the PPK enzymes use ATP as a substrate (not IP_7 or IP_8) it is possible that synthesis of polyP may provide an alternative “sink” for inositol pyrophosphates. It has been postulated previously (Saiardi 2012) that polymers of polyP may be “capped” at their ends by molecules related to the inositol pyrophosphates. If this were true then a failure to accumulate polyP might manifest itself in an increase in the unused “capping molecules”, i.e. inositol pyrophosphates.

Indeed such a hypothesis could also offer a widely applicable model for the linkage between these molecules in divergent organisms from yeast (Auesukaree, Tochio et al. 2005, Lonetti, Szijgyarto et al. 2011) to mammals (Ghosh, Shukla et al. 2013). So-called, “capping” of polyP could confer protection against degradation by the exopolyphosphatases, which would not be able to access and cleave the terminal phosphate. Thus a decrease in inositol pyrophosphates would offer less protection to polyP and vice versa.

This attractive hypothesis is challenged by the normal levels of polyP observed in the *ip6k* strain of *D. discoideum* (**Figure 5.4**), but as discussed previously, this strain does contain residual levels of IP_7. It is possible this residual IP_7 might be sufficient to “protect” the low level of polyP present in the vegetative state.

Efforts to find experimental evidence for inositol pyrophosphates capping polyP failed to offer any support for this hypothesis (**Figures 5.20-5.23**). No inositol containing molecules could be detected upon degradation of either vegetative or fruiting body polyP. The absence of proof does not dispel this hypothesis completely, however it does suggest that it is not the cause of the observed increase of inositol pyrophosphates in *ppk1*. With this in mind, it is reasonable to conclude that the increase in inositol pyrophosphates noted in **Figure 5.17** is due to increased synthesis.

5.3.7 Concluding remarks

It is evident from the work described here that the amoeba *D. discoideum* can reveal much about the synthesis, regulation and function of the once overlooked polymer, polyP. This model represents only the second eukaryotic genetic model in which to study polyP. The yeast *vtc4Δ* represents the only other model in which the polyphosphate kinase has been identified and deleted. Remarkably, despite the very high levels of polyP found in yeast, this mutant displays a very

mild phenotype. In contrast the *ppk1* strain generated in this work shows a range of phenotypes, including slow growth, altered primary metabolism and defective fruiting body formation. The evidence presented here demonstrates that in the amoeba, polyP, primary metabolism and inositol pyrophosphates are linked. To elucidate the precise nature of these relationships will require further work, in particular assessing the mitochondrial activity in the *ppk1* strain and exploring the effect of mitochondrial inhibition on polyP synthesis in WT.

Furthermore, this clean genetic system will provide the ideal test bed for the development of fluorescent probes to detect polyP inside cells. This is particularly important as currently available methods fail to detect any differences between WT and *ppk1* cells (data not shown). Development and validation of improved polyP probes in *D. discoideum* would offer the invaluable opportunity to critically evaluate the available literature, as well as to facilitate future studies in the amoeba as well as in other models.

6. Conclusions and Perspectives

The work presented in this thesis has focused on the synthesis, metabolism and cellular function of the inositol pyrophosphates and inorganic polyphosphate, two of the most phosphate rich molecules in the cell. Using the social amoeba *D. discoideum*, this work has sought to develop a genetic model in which to study these molecules. It was demonstrated that recent improvements to PAGE technology allow the detection of both inositol pyrophosphates and polyP by either Toluidine or DAPI staining. This approach delivers the significant advantage that it allows the visualisation of both unlabelled inositol pyrophosphates and polyP. The straightforward detection of both of these molecules in the amoeba makes it an ideal model in which to study not only the synthesis and metabolism of each molecule, but also how they are related.

6.1 Inositol pyrophosphates

A genetic approach reveals that the synthesis of the inositol pyrophosphates is more complex than initially expected. A mutant lacking the only characterised IP_7 kinase (*ppip5k*) still possesses IP_8, whilst the double mutant lacking *ip6k*/*ppip5k* still possesses IP_7. In fact, this study, by either genetic or biochemical evidence, has identified at least four enzymes capable of synthesising inositol pyrophosphates. The novel inositol phosphate kinases IPKA and IPKB are both able to phosphorylate IP_7 to IP_8 *in vitro*, taking the number of IP_7 kinases encoded in the *D. discoideum* genome to three. This surprising abundance of IP_7 kinases, as well as the extremely robust activity of IPKA may offer insight into why *D. discoideum* possesses a higher level of IP_8 than IP_7 a property almost unique in models studied to date.

Whilst the presence of three IP_7 kinases might suggest an explanation for the source of such high levels of IP_8, it begs the question, why? The amoeba possesses by far the highest levels of inositol pyrophosphates identified in any

organism investigated. Deletion of both Ip6k and Ppip5k genes generates a strain lacking the majority of the inositol pyrophosphates. However, analysis of this strain failed to identify any major phenotype. Given the substantial energetic investment in synthesising and maintaining the inositol pyrophosphate pool this lack of phenotype is surprising.

As explored in **Chapter Three**, these results could be explained by the presence of a residual and potentially functional pool of IP_7 in the *ip6k/ppip5k* strain. Thus generation of a truly clean model system, in which no inositol pyrophosphates are present, will require the deletion, or depletion, of all four inositol phosphate kinases identified to date. As discussed above, numerous unsuccessful attempts were made to delete IPKA, suggesting lethality. Thus the generation of a "quadruple mutant" may not be practical. An alternative approach would be the depletion of both IPKA and IPKB by RNAi. Such an experimental approach may be required to shed further light on the role of these molecules in *D. discoideum*. This strategy is far more convoluted than originally anticipated and the value of pursuing this line of research should be critically evaluated.

Despite these limitations, the value of *D. discoideum* as a model for inositol pyrophosphates should not be underestimated. In **Chapter Four** of this work, the remarkable activities of two novel enzymes, IPKA and IPKB were investigated. Both enzymes show robust IP_7 kinase activities, however many questions remain unanswered regarding these two enzymes. The most prominent question of all is whether these catalytically flexible enzymes may operate in tandem to produce IP_6 in a stepwise manner, as was first described in 1990 (Stephens and Irvine 1990). Such a possibility is hinted at by the ability of both enzymes to partially rescue polyP in the *plcΔ* yeast as well as IPKA's synthesis of IP_6 in *arg82Δ* yeast. Further experiments are required to explore the physiological roles of these kinases.

Finally, the experiments in **Chapter Four** suggest that, in *D. discoideum* at least, IP6K may phosphorylate position 6 of the inositol ring, not position 5 as expected. It will be interesting to further investigate this possibility and to apply modern NMR techniques to inositol pyrophosphates extracted from *D. discoideum* mutants. It is possible that lessons learned in the amoeba might inform other models, which have to date relied on *in vitro* evidence to identify the precise products of IP6K and PPIP5K.

6.2 Inorganic polyphosphate

The work described in **Chapter Five** firmly establishes the amoeba as a powerful model in which to study the role of polyP. Whilst this work calls into question the physiological significance of the DdPPK2 enzyme, it identifies the true scale of polyP accumulation during spore formation and a role for this polymer in germination. Further investigation of this process might focus on the possibility that inositol pyrophosphates are able to partially compensate for the lack of polyP in *ppk1* spores. The generation of an *ip6k*/*ppk1* double mutant would be illuminating to test this nascent hypothesis.

The most striking observations in this work reveal a link between polyP and primary metabolism. The absence of polyP in the *ppk1* strain results in cells with dramatically reduced ATP, whilst the inhibition of ATP production in WT cells induces the accumulation of polyP. This is not the first time that polyP has been linked to primary metabolism (Freimoser, Hürlimann et al. 2006) and it is perhaps not surprising given the ability of polyP to buffer free phosphate concentration. Further investigation is required to understand the nature of this link. It will be particularly interesting to explore the possible link between polyP and mitochondrial function in both WT and *ppk1* cells.

Finally, the development of *D. discoideum* as a clean genetic model to study polyP represents a significant boost to the development of specific probes for

the *in vivo* detection of polyP. The relatively large size of the amoeba and lack of cell wall offer significant advantages for microscopy over the yeast model. Thus *D. discoideum* may represent the ideal model in which to develop much-needed tools for the study of polyP.

6.3 Concluding remarks

The experiments described in this work have revealed many unexpected and intriguing results. Developing the amoeba as a genetic model for both the inositol pyrophosphates and polyP has identified notable differences from the only other genetic model the yeast, *S. cerevisiae*.

In yeast the levels of inositol pyrophosphates are relatively low, however their absence causes a severe metabolic defect (Szijgyarto, Garedew et al. 2011). Meanwhile, polyP is highly abundant and yet complete loss of this polymer does not appear to induce major phenotypic effects. In the amoeba, almost the opposite appears to be true. The amoeba possesses very high levels of inositol pyrophosphates, however this work failed to identify a significant phenotype in cells lacking the vast majority of this pool. In contrast, the loss of the relatively low levels of polyP found in vegetative cells causes a substantial defect in the general fitness and primary metabolism of the amoeba.

Whilst this summary may represent an over simplification, it is important to note that there are clear differences between the phenotypes observed in these two genetic models. Nevertheless, it is evident that a link between the metabolism of inositol pyrophosphates and polyP exists in both organisms. These observations strengthen the hypothesis that phosphate, inositol and polyphosphates are intimately linked (Livermore, Azevedo et al. 2016). It will be fascinating to explore the nature of these relationships and how they regulate primary metabolism. For this, the development of *D. discoideum* as a parallel model to yeast will be invaluable.

D. discoideum has been a highly influential model in the study of both the inositol pyrophosphates and polyP. It was in this organism that the inositol pyrophosphates were first described (Stephens, Radenberg et al. 1993) and that the first eukaryotic PPK was identified (Zhang, Gómez-García et al. 2005). Returning to this organism as a model to study these fascinating and functionally related molecules has revealed some surprising results and posed many more interesting questions. It is clear that *D. discoideum* still has much to offer and will continue to influence both fields for years to come.

7. Appendix

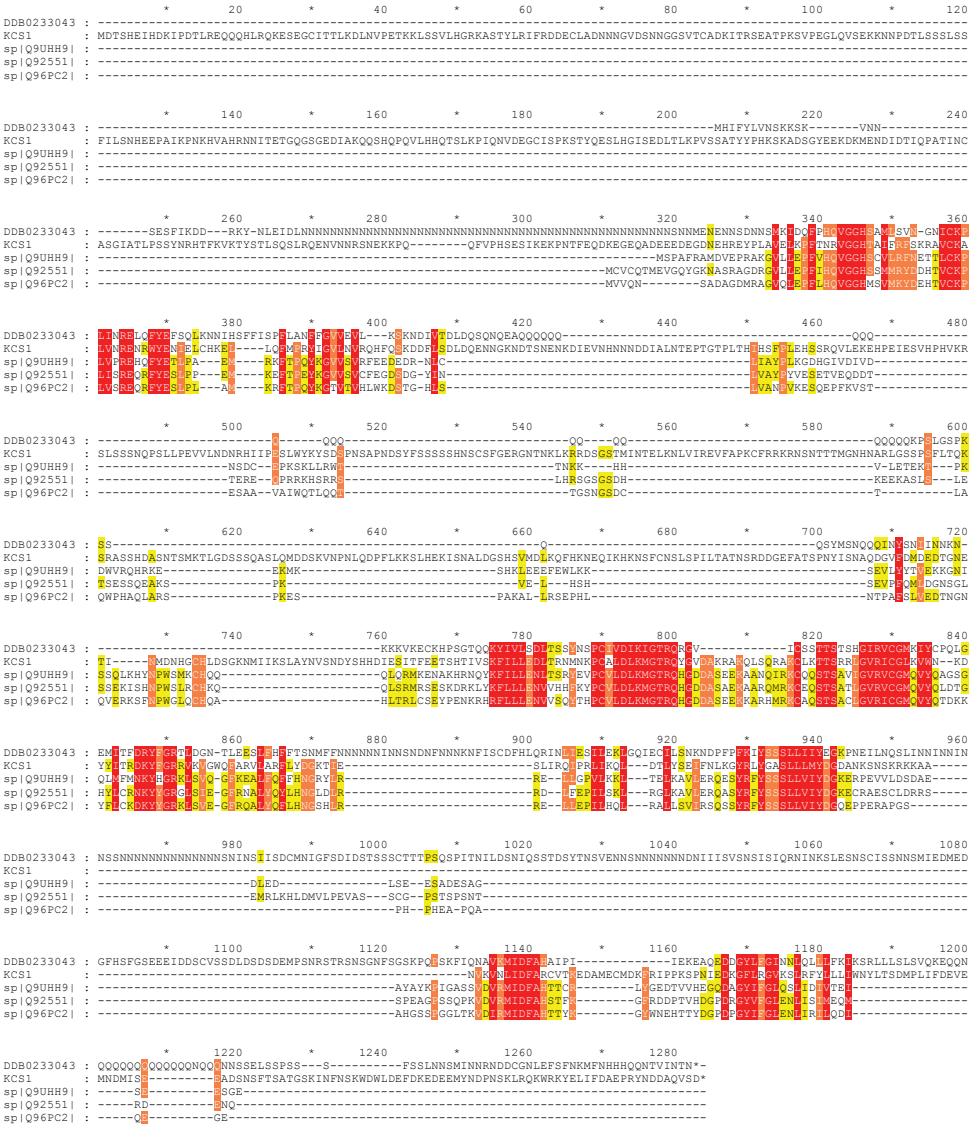

Figure 7.1 Sequence alignment of *D. discoideum* IP6K with *S. cerevisiae* KCS1 and *H. sapiens* IP6K1-3.

D. discoideum IP6K (top: DDB0233043), KCS1, *H. sapiens* IP6K1-3 (sp|Q9UHH9|, sp|Q92551| and sp|Q96PC2|). Protein sequence alignment performed by CLUSTAL, primary sequence similarity (across all sequences) shown in red, secondary similarity (between four sequences) shown in orange, tertiary similarity (between three sequences) shown in yellow.

Figure 7.2 Sequence alignment of *D. discoideum* PPIP5K with *S. cerevisiae* VIP and *H. sapiens* PPIP5K1-3.

Protein sequence alignment performed by CLUSTAL, primary sequence similarity (across all sequences) shown in red, secondary similarity (between three sequences) shown in orange, tertiary similarity (between two sequences) shown in yellow. The C terminal portion of the *S. cerevisiae* and *H. sapiens* proteins is absent from *D. discoideum* PPIP5K.

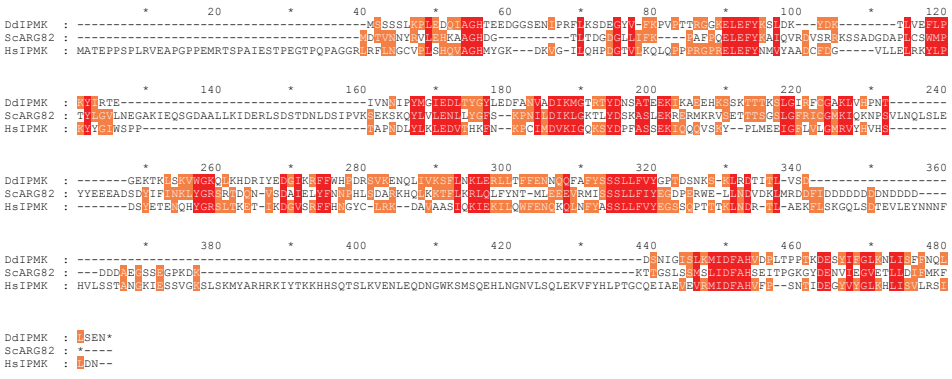

Figure 7.3 Sequence alignment of *D. discoideum* IPMK with *S. cerevisiae* ARG82 and *H. sapiens* IPMK.

Protein sequence alignment performed by CLUSTAL, primary sequence similarity (across all sequences) shown in red, secondary similarity (between two sequences) shown in orange.

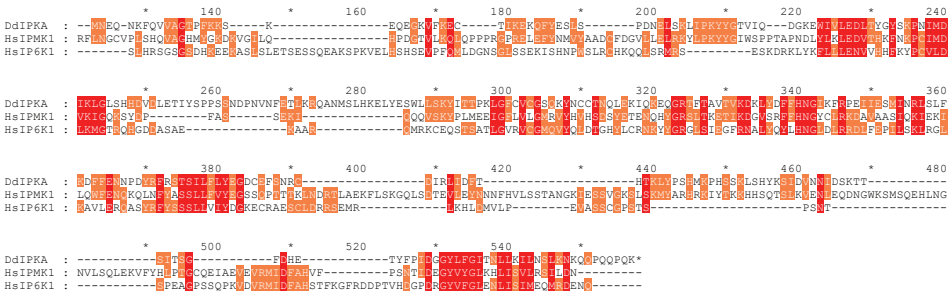

Figure 7.4 Sequence alignment of *D. discoideum* IPKA with *H. sapiens* IPMK and IP6K1.

Protein sequence alignment performed by CLUSTAL, primary sequence similarity (across all sequences) shown in red, secondary similarity (between two sequences) shown in orange.

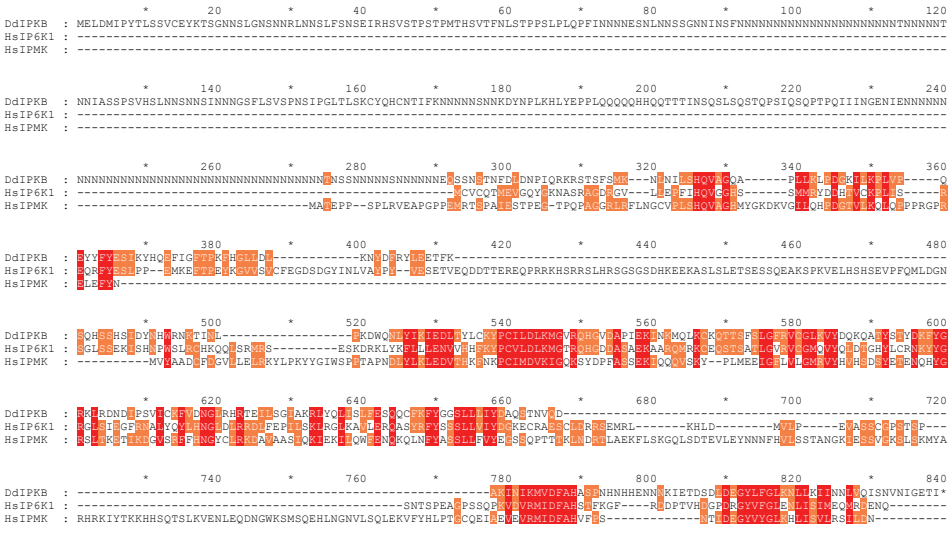

Figure 7.5 Sequence alignment of *D. discoideum* IPKB with *H. sapiens* IP6K1 and IPMK.

Protein sequence alignment performed by CLUSTAL, primary sequence similarity (across all sequences) shown in red, secondary similarity (between two sequences) shown in orange.

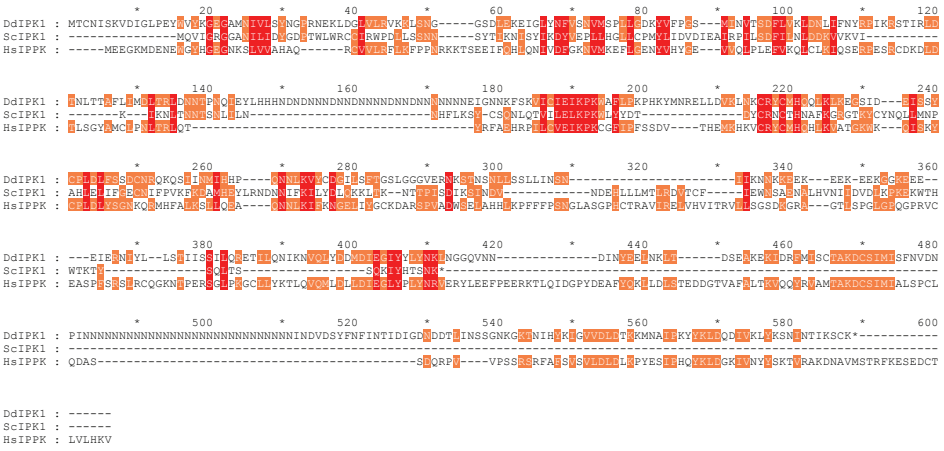

Figure 7.6 Sequence alignment of *D. discoideum* IPK1 with *S. cerevisiae* IPK1 and *H. sapiens* IPPK.

Protein sequence alignment performed by CLUSTAL, primary sequence similarity (across all sequences) shown in red, secondary similarity (between two sequences) shown in orange.

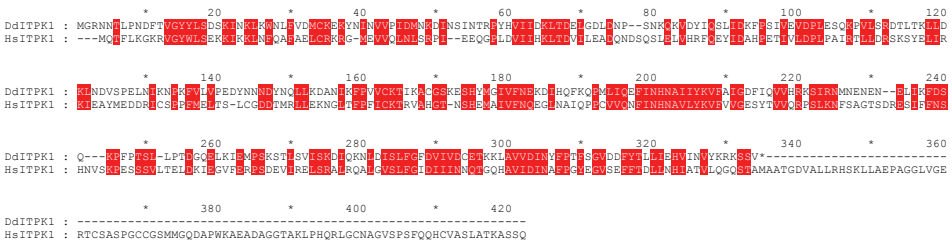

Figure 7.7 Sequence alignment of *D. discoideum* ITPK1 with *S. H. sapiens* ITPK1.

Protein sequence alignment performed by CLUSTAL, sequence similarity shown in red.

8. References

Abramov, A. Y., C. Fraley, C. T. Diao, R. Winkfein, M. A. Colicos, M. R. Duchen, R. J. French and E. Pavlov (2007). Targeted polyphosphatase expression alters mitochondrial metabolism and inhibits calcium-dependent cell death. Proc Natl Acad Sci USA. **104:** 18091-18096.

Ahn, K. and A. Kornberg (1990). Polyphosphate kinase from Escherichia coli. Purification and demonstration of a phosphoenzyme intermediate. J Biol Chem. **265:** 11734-11739.

Albert, C., S. T. Safrany, M. E. Bembenek, K. M. Reddy, K. Reddy, J. Falck, M. Bröcker, S. B. Shears and G. W. Mayr (1997). Biological variability in the structures of diphosphoinositol polyphosphates in Dictyostelium discoideum and mammalian cells. Biochem J. **327 (Pt 2):** 553-560.

Alessi, D. R., S. R. James, C. P. Downes, A. B. Holmes, P. R. Gaffney, C. B. Reese and P. Cohen (1997). Characterization of a 3-phosphoinositide-dependent protein kinase which phosphorylates and activates protein kinase Balpha. Curr Biol. **7:** 261-269.

Andreeva, N., L. Trilisenko, M. Eldarov and T. Kulakovskaya (2015). Polyphosphatase PPN1 of Saccharomyces cerevisiae: switching of exopolyphosphatase and endopolyphosphatase activities. PLoS ONE. **10:** e0119594.

Aschar-Sobbi, R., A. Y. Abramov, C. Diao, M. E. Kargacin, G. J. Kargacin, R. J. French and E. Pavlov (2008). High sensitivity, quantitative measurements of polyphosphate using a new DAPI-based approach. J Fluoresc. **18:** 859-866.

Auesukaree, C., H. Tochio, M. Shirakawa, Y. Kaneko and S. Harashima (2005). Plc1p, Arg82p, and Kcs1p, enzymes involved in inositol pyrophosphate synthesis, are essential for phosphate regulation and polyphosphate accumulation in Saccharomyces cerevisiae. J Biol Chem. **280:** 25127-25133.

Ault-Riché, D., C. D. Fraley, C. M. Tzeng and A. Kornberg (1998). Novel assay reveals multiple pathways regulating stress-induced accumulations of inorganic polyphosphate in Escherichia coli. J Bacteriol. **180:** 1841-1847.

Azevedo, C., A. Burton, E. Ruiz-Mateos, M. Marsh and A. Saiardi (2009). Inositol pyrophosphate mediated pyrophosphorylation of AP3B1 regulates HIV-1 Gag release. Proc Natl Acad Sci USA. **106:** 21161-21166.

Azevedo, C., T. Livermore and A. Saiardi (2015). Protein Polyphosphorylation of Lysine Residues by Inorganic Polyphosphate. Molecular cell.

Azevedo, C., T. Livermore and A. Saiardi (2015). "Protein polyphosphorylation of lysine residues by inorganic polyphosphate." Molecular cell **58**(1): 71-82.

Azevedo, C. and A. Saiardi (2006). Extraction and analysis of soluble inositol polyphosphates from yeast. Nature Protocols. **1:** 2416-2422.

Azevedo, C. and A. Saiardi (2014). Functions of inorganic polyphosphates in eukaryotic cells: a coat of many colours. Biochem Soc Trans. **42:** 98-102.

Balla, T. (2013). Phosphoinositides: tiny lipids with giant impact on cell regulation. Physiol Rev. **93:** 1019-1137.

Banfic, H., A. Bedalov, J. D. York and D. Visnjic (2012). Inositol pyrophosphates modulate S phase progression after pheromone-induced arrest in Saccharomyces cerevisiae. J Biol Chem.

Barker, C. J., J. Wright, P. J. Hughes, C. J. Kirk and R. H. Michell (2004). Complex changes in cellular inositol phosphate complement accompany transit through the cell cycle. Biochem J. **380:** 465-473.

Bennett, M., S. M. N. Onnebo, C. Azevedo and A. Saiardi (2006). Inositol pyrophosphates: metabolism and signaling. Cell Mol Life Sci. **63:** 552-564.

Berridge, M. J. (1993). Inositol trisphosphate and calcium signalling. Nature. **361:** 315-325.

Bhandari, R., K. R. Juluri, A. C. Resnick and S. H. Snyder (2008). Gene deletion of inositol hexakisphosphate kinase 1 reveals inositol pyrophosphate regulation of insulin secretion, growth, and spermiogenesis. Proc Natl Acad Sci USA. **105:** 2349-2353.

Bhandari, R., A. Saiardi, Y. Ahmadibeni, A. M. Snowman, A. C. Resnick, T. Z. Kristiansen, H. Molina, A. Pandey, J. K. Werner, K. R. Juluri, Y. Xu, G. D. Prestwich, K. Parang and S. H. Snyder (2007). Protein pyrophosphorylation by inositol pyrophosphates is a posttranslational event. Proc Natl Acad Sci USA. **104:** 15305-15310.

Blind, R. D., M. Suzawa and H. A. Ingraham (2012). Direct modification and activation of a nuclear receptor-PIP_2 complex by the inositol lipid kinase IPMK. Sci Signal. **5:** ra44.

Boer, V. M., C. A. Crutchfield, P. H. Bradley, D. Botstein and J. D. Rabinowitz (2010). Growth-limiting intracellular metabolites in yeast growing under diverse nutrient limitations. Molecular biology of the cell. **21:** 198-211.

Burton, A., C. Azevedo, C. Andreassi, A. Riccio and A. Saiardi (2013). Inositol pyrophosphates regulate JMJD2C-dependent histone demethylation. Proc Natl Acad Sci USA. **110:** 18970-18975.

Caffrey, J. J., S. T. Safrany, X. Yang and S. B. Shears (2000). Discovery of molecular and catalytic diversity among human diphosphoinositol-polyphosphate phosphohydrolases. An expanding Nudt family. J Biol Chem. **275:** 12730-12736.

Capolicchio, S., D. T. Thakor, A. Linden and H. J. Jessen (2013). Synthesis of unsymmetric diphospho-inositol polyphosphates. Angew Chem Int Ed Engl. **52:** 6912-6916.

Chakraborty, A., M. A. Koldobskiy, N. T. Bello, M. Maxwell, J. J. Potter, K. R. Juluri, D. Maag, S. Kim, A. S. Huang, M. J. Dailey, M. Saleh, A. M. Snowman, T. H. Moran, E. Mezey and S. H. Snyder (2010). Inositol pyrophosphates inhibit Akt signaling, thereby regulating insulin sensitivity and weight gain. Cell. **143:** 897-910.

Chiew, Y. Y., J. M. Reimers and B. E. Wright (1985). Steady state models of spore cell metabolism in Dictyostelium discoideum. J Biol Chem. **260:** 15325-15331.

Coates, M. L. (1975). Hemoglobin function in the vertebrates: an evolutionary model. Journal of molecular evolution. **6:** 285-307.

Corrigan, A. M. and J. R. Chubb (2014). Regulation of transcriptional bursting by a naturally oscillating signal. Curr Biol. **24:** 205-211.

de Boer, I. H., T. C. Rue and B. Kestenbaum (2009). Serum phosphorus concentrations in the third National Health and Nutrition Examination Survey (NHANES III). Am J Kidney Dis. **53:** 399-407.

Di Paolo, G. and P. De Camilli (2006). Phosphoinositides in cell regulation and membrane dynamics. Nature. **443:** 651-657.

Dick, C. F., A. L. A. Dos-Santos and J. R. Meyer-Fernandes (2014). Inorganic phosphate uptake in unicellular eukaryotes. Biochim Biophys Acta. **1840:** 2123-2127.

Dijken, P. V., J.-R. d. Haas, A. Craxton, C. Erneux, S. B. Shears and P. J. M. V. Haastert (1995). A novel, phospholipase C-independent pathway of inositol 1, 4, 5-trisphosphate formation in Dictyostelium and rat liver. Journal of Biological Chemistry. **270:** 29724-29731.

Docampo, R. and S. N. J. Moreno (2011). Acidocalcisomes. Cell Calcium. **50:** 113-119.

Doria, E., L. Galleschi, L. Calucci, C. Pinzino, R. Pilu, E. Cassani and E. Nielsen (2009). Phytic acid prevents oxidative stress in seeds: evidence from a maize (Zea mays L.) low phytic acid mutant. J Exp Bot. **60:** 967-978.

Draskovic, P., A. Saiardi, R. Bhandari, A. Burton, G. Ilc, M. Kovacevic, S. H. Snyder and M. Podobnik (2008). Inositol hexakisphosphate kinase products contain diphosphate and triphosphate groups. Chemistry & biology. **15:** 274-286.

Drayer, A. L., J. Van der Kaay, G. W. Mayr and P. J. Van Haastert (1994). Role of phospholipase C in Dictyostelium: formation of inositol 1,4,5-trisphosphate and normal development in cells lacking phospholipase C activity. EMBO J. **13:** 1601-1609.

Dubois, E., B. Scherens, F. Vierendeels, M. M. W. Ho, F. Messenguy and S. B. Shears (2002). In Saccharomyces cerevisiae, the inositol polyphosphate kinase activity of Kcs1p is required for resistance to salt stress, cell wall integrity, and vacuolar morphogenesis. J Biol Chem. **277:** 23755-23763.

Dynes, J. L., A. M. Clark, G. Shaulsky, A. Kuspa, W. F. Loomis and R. A. Firtel (1994). LagC is required for cell-cell interactions that are essential for cell-type differentiation in Dictyostelium. Genes Dev. **8:** 948-958.

Efanov, A. M., S. V. Zaitsev and P. O. Berggren (1997). Inositol hexakisphosphate stimulates non-Ca2+-mediated and primes Ca2+-mediated exocytosis of insulin by activation of protein kinase C. Proc Natl Acad Sci USA. **94:** 4435-4439.

Eichinger, L. and A. A. Noegel (2003). Crawling into a new era-the Dictyostelium genome project. The EMBO journal. **22:** 1941-1946.

Elias, M., A. Wellner, K. Goldin-Azulay, E. Chabriere, J. A. Vorholt, T. J. Erb and D. S. Tawfik (2012). The molecular basis of phosphate discrimination in arsenate-rich environments. Nature. **491:** 134-137.

Faix, J., L. Kreppel, G. Shaulsky, M. Schleicher and A. R. Kimmel (2004). A rapid and efficient method to generate multiple gene disruptions in Dictyostelium discoideum using a single selectable marker and the Cre-loxP system. Nucleic Acids Res. **32:** e143.

Fang, J., P. Rohloff, K. Miranda and R. Docampo (2007). Ablation of a small transmembrane protein of Trypanosoma brucei (TbVTC1) involved in the synthesis of polyphosphate alters acidocalcisome biogenesis and function, and leads to a cytokinesis defect. Biochem J. **407:** 161-170.

Feoktistova, A., D. McCollum, R. Ohi and K. L. Gould (1999). Identification and characterization of Schizosaccharomyces pombe asp1(+), a gene that interacts with mutations in the Arp2/3 complex and actin. Genetics. **152:** 895-908.

Freimoser, F. M., H. C. Hürlimann, C. A. Jakob, T. P. Werner and N. Amrhein (2006). Systematic screening of polyphosphate (poly P) levels in yeast mutant cells reveals strong interdependence with primary metabolism. Genome Biol. **7:** R109.

Friedrich, M., D. Meier, I. Schuster and W. Nellen (2015). A Simple Retroelement Based Knock-Down System in Dictyostelium: Further Insights into RNA Interference Mechanisms. PLoS ONE. **10:** e0131271.

Fu, C., J. Xu, R.-J. Li, J. A. Crawford, A. B. Khan, T. M. Ma, J. Y. Cha, A. M. Snowman, M. V. Pletnikov and S. H. Snyder (2015). Inositol Hexakisphosphate Kinase-3 Regulates the Morphology and Synapse Formation of Cerebellar Purkinje Cells via Spectrin/Adducin. J Neurosci. **35:** 11056-11067.

Gao, Y. and H.-y. Wang (2007). Inositol pentakisphosphate mediates Wnt/beta-catenin signaling. J Biol Chem. **282:** 26490-26502.

Gaudet, P., K. E. Pilcher, P. Fey and R. L. Chisholm (2007). Transformation of Dictyostelium discoideum with plasmid DNA. Nat Protoc. **2:** 1317-1324.

Gerasimaitė, R., S. Sharma, Y. Desfougères, A. Schmidt and A. Mayer (2014). Coupled synthesis and translocation restrains polyphosphate to acidocalcisome-like vacuoles and prevents its toxicity. J Cell Sci. **127:** 5093-5104.

Gezelius, K. (1974). Inorganic polyphosphates and enzymes of polyphosphate metabolism in the cellular slime mold Dictyostelium discoideum. Archives of microbiology. **98:** 311-329.

Ghosh, S., D. Shukla, K. Suman, B. J. Lakshmi, R. Manorama, S. Kumar and R. Bhandari (2013). Inositol hexakisphosphate kinase 1 maintains hemostasis in mice by regulating platelet polyphosphate levels. Blood. **122:** 1478-1486.

Glennon, M. C. and S. B. Shears (1993). Turnover of inositol pentakisphosphates, inositol hexakisphosphate and diphosphoinositol polyphosphates in primary cultured hepatocytes. Biochem J. **293 (Pt 2):** 583-590.

Godlee, C. and M. Kaksonen (2013). Review series: From uncertain beginnings: initiation mechanisms of clathrin-mediated endocytosis. The Journal of cell biology. **203:** 717-725.

Gómez-García, M. R. and A. Kornberg (2004). Formation of an actin-like filament concurrent with the enzymatic synthesis of inorganic polyphosphate. Proc Natl Acad Sci USA. **101:** 15876-15880.

Gray, M. J., W.-Y. Wholey, N. O. Wagner, C. M. Cremers, A. Mueller-Schickert, N. T. Hock, A. G. Krieger, E. M. Smith, R. A. Bender, J. C. A. Bardwell and U. Jakob (2014). Polyphosphate is a primordial chaperone. Mol Cell. **53:** 689-699.

Hanahan, D. (1983). Studies on transformation of Escherichia coli with plasmids. Journal of molecular biology. **166:** 557-580.

Hernández-Ruiz, L., A. Sáez-Benito, N. Pujol-Moix, J. Rodríguez-Martorell and F. A. Ruiz (2009). Platelet inorganic polyphosphate decreases in patients with delta storage pool disease. J Thromb Haemost. **7:** 361-363.

Hilgemann, D. W., S. Feng and C. Nasuhoglu (2001). The complex and intriguing lives of PIP2 with ion channels and transporters. Sci STKE. **2001:** re19.

Hoeller, O., P. Bolourani, J. Clark, L. R. Stephens, P. T. Hawkins, O. D. Weiner, G. Weeks and R. R. Kay (2013). Two distinct functions for PI3-kinases in macropinocytosis. J Cell Sci. **126:** 4296-4307.

Hoeller, O. and R. R. Kay (2007). Chemotaxis in the absence of PIP3 gradients. Curr Biol. **17:** 813-817.

Holmström, K. M., N. Marina, A. Y. Baev, N. W. Wood, A. V. Gourine and A. Y. Abramov (2013). Signalling properties of inorganic polyphosphate in the mammalian brain. Nat Commun. **4:** 1362.

Hooley, P., M. P. Whitehead and M. R. W. Brown (2008). Eukaryote polyphosphate kinases: is the 'Kornberg' complex ubiquitous? Trends Biochem Sci. **33:** 577-582.

Hothorn, M., H. Neumann, E. D. Lenherr, M. Wehner, V. Rybin, P. O. Hassa, A. Uttenweiler, M. Reinhardt, A. Schmidt, J. Seiler, A. G. Ladurner, C. Herrmann, K. Scheffzek and A. Mayer (2009). Catalytic core of a membrane-associated eukaryotic polyphosphate polymerase. Science. **324:** 513-516.

Hsieh, P. C., B. C. Shenoy, J. E. Jentoft and N. F. Phillips (1993). Purification of polyphosphate and ATP glucose phosphotransferase from Mycobacterium tuberculosis H37Ra: evidence that poly(P) and ATP glucokinase activities are catalyzed by the same enzyme. Protein Expr Purif. **4:** 76-84.

Hyvönen, M., M. J. Macias, M. Nilges, H. Oschkinat, M. Saraste and M. Wilmanns (1995). Structure of the binding site for inositol phosphates in a PH domain. EMBO J. **14:** 4676-4685.

Iijima, M., Y. E. Huang and P. Devreotes (2002). Temporal and spatial regulation of chemotaxis. Developmental cell. **3:** 469-478.

Illies, C., J. Gromada, R. Fiume, B. Leibiger, J. Yu, K. Juhl, S.-N. Yang, D. K. Barma, J. R. Falck, A. Saiardi, C. J. Barker and P.-O. Berggren (2007). Requirement of inositol pyrophosphates for full exocytotic capacity in pancreatic beta cells. Science. **318:** 1299-1302.

Irvine, R. F. and M. J. Schell (2001). Back in the water: the return of the inositol phosphates. Nat Rev Mol Cell Biol. **2:** 327-338.

Ishige, K., H. Zhang and A. Kornberg (2002). Polyphosphate kinase (PPK2), a potent, polyphosphate-driven generator of GTP. Proc Natl Acad Sci USA. **99:** 16684-16688.

Jarmuszkiewicz, W., M. Behrendt, R. Navet and F. E. Sluse (2002). Uncoupling protein and alternative oxidase of Dictyostelium discoideum: occurrence, properties and protein expression during vegetative life and starvation-induced early development. FEBS letters. **532:** 459-464.

Johnson, L. F. and M. E. Tate (1969). The structure of myo-inositol pentaphosphates. Annals of the New York Academy of Sciences. **165:** 526-532.

Joseph, J. M., P. Fey, N. Ramalingam, X. I. Liu, M. Rohlfs, A. A. Noegel, A. Müller-Taubenberger, G. Glöckner and M. Schleicher (2008). The actinome of Dictyostelium discoideum in comparison to actins and actin-related proteins from other organisms. PLoS ONE. **3:** e2654.

Kaffman, A., I. Herskowitz, R. Tjian and E. K. O'Shea (1994). Phosphorylation of the transcription factor PHO4 by a cyclin-CDK complex, PHO80-PHO85. Science. **263:** 1153-1156.

Kay, R. R., P. Flatman and C. R. Thompson (1999). DIF signalling and cell fate. Semin Cell Dev Biol. **10:** 577-585.

Kay, R. R., P. Langridge, D. Traynor and O. Hoeller (2008). Changing directions in the study of chemotaxis. Nat Rev Mol Cell Biol. **9:** 455-463.

King, J., M. Keim, R. Teo, K. E. Weening, M. Kapur, K. McQuillan, J. Ryves, B. Rogers, E. Dalton, R. S. B. Williams and A. J. Harwood (2010). Genetic control of lithium sensitivity and regulation of inositol biosynthetic genes. PLoS ONE. **5:** e11151.

Klein, G., D. Cotter, J. Martin, M. Bof and M. Satre (1988). Germination of Dictyostelium discoideum spores. A phosphorus-31 NMR analysis. Biochemistry**:** 8199-8203.

Kolozsvari, B., F. Parisi and A. Saiardi (2014). Inositol phosphates induce DAPI fluorescence shift. Biochem J. **460:** 377-385.

Komander, D., A. Fairservice, M. Deak, G. S. Kular, A. R. Prescott, C. Peter Downes, S. T. Safrany, D. R. Alessi and D. M. F. van Aalten (2004). Structural insights into the regulation of PDK1 by phosphoinositides and inositol phosphates. EMBO J. **23:** 3918-3928.

Kornberg, A. (1995). Inorganic polyphosphate: toward making a forgotten polymer unforgettable. J Bacteriol. **177:** 491-496.

Kornberg, A., N. N. Rao and D. Ault-Riché (1999). Inorganic polyphosphate: a molecule of many functions. Annu Rev Biochem. **68:** 89-125.

Kulaev, I. S. (1975). Biochemistry of inorganic polyphosphates. Rev Physiol Biochem Pharmacol. **73:** 131-158.

Kumble, K. D., K. Ahn and A. Kornberg (1996). Phosphohistidyl active sites in polyphosphate kinase of Escherichia coli. Proc Natl Acad Sci USA. **93:** 14391-14395.

Kumble, K. D. and A. Kornberg (1995). Inorganic polyphosphate in mammalian cells and tissues. J Biol Chem. **270:** 5818-5822.

Laha, D., P. Johnen, C. Azevedo, M. Dynowski, M. Weiß, S. Capolicchio, H. Mao, T. Iven, M. Steenbergen, M. Freyer, P. Gaugler, M. K. F. de Campos, N. Zheng, I. Feussner, H. J. Jessen, S. C. M. Van Wees, A. Saiardi and G. Schaaf (2015). VIH2 Regulates the Synthesis of Inositol Pyrophosphate InsP8 and Jasmonate-Dependent Defenses in Arabidopsis. Plant Cell. **27:** 1082-1097.

Laussmann, T., R. Eujen, C. M. Weisshuhn, U. Thiel and G. Vogel (1996). Structures of diphospho-myo-inositol pentakisphosphate and bisdiphospho-myo-inositol tetrakisphosphate from Dictyostelium resolved by NMR analysis. Biochem J. **315 (Pt 3):** 715-720.

Laussmann, T., C. Pikzack, U. Thiel, G. W. Mayr and G. Vogel (2000). Diphospho-myo-inositol phosphates during the life cycle of Dictyostelium and Polysphondylium. Eur J Biochem. **267:** 2447-2451.

Laussmann, T., K. M. Reddy, K. K. Reddy, J. R. Falck and G. Vogel (1997). Diphospho-myo-inositol phosphates from Dictyostelium identified as D-6-diphospho-myo-inositol pentakisphosphate and D-5,6-bisdiphospho-myo-inositol tetrakisphosphate. Biochem J. **322 (Pt 1):** 31-33.

Lee, Y.-S., S. Mulugu, J. D. York and E. K. O'Shea (2007). Regulation of a cyclin-CDK-CDK inhibitor complex by inositol pyrophosphates. Science. **316:** 109-112.

Letcher, A. J., M. J. Schell and R. F. Irvine (2008). Do mammals make all their own inositol hexakisphosphate? Biochem J. **416:** 263-270.

Lev, S., C. Li, D. Desmarini, A. Saiardi, N. L. Fewings, S. D. Schibeci, R. Sharma, T. C. Sorrell and J. T. Djordjevic (2015). Fungal Inositol Pyrophosphate IP7 Is Crucial for Metabolic Adaptation to the Host Environment and Pathogenicity. MBio. **6:** e00531-00515.

Livermore, T. M., C. Azevedo, B. Kolozsvari, M. S. C. Wilson and A. Saiardi (2016). Phosphate, inositol and polyphosphates. Biochem Soc Trans. **44:** 253-259.

Livermore, T. M., J. R. Chubb and A. Saiardi (2016). Developmental accumulation of inorganic polyphosphate affects germination and energetic metabolism in Dictyostelium discoideum. Proc Natl Acad Sci USA. **113:** 996-1001.

Lonetti, A., Z. Szijgyarto, D. Bosch, O. Loss, C. Azevedo and A. Saiardi (2011). Identification of an evolutionarily conserved family of inorganic polyphosphate endopolyphosphatases. J Biol Chem. **286:** 31966-31974.

Loomis, W. F. (2015). Genetic control of morphogenesis in Dictyostelium. Dev Biol. **402:** 146-161.

Losito, O., Z. Szijgyarto, A. C. Resnick and A. Saiardi (2009). Inositol Pyrophosphates and Their Unique Metabolic Complexity: Analysis by Gel Electrophoresis. PLoS ONE. **4:** e5580.

Loss, O., C. T. Wu, A. Riccio and A. Saiardi (2013). Modulation of inositol polyphosphate levels regulates neuronal differentiation. Molecular biology of the cell. **24:** 2981-2989.

Luo, H. R., Y. E. Huang, J. C. Chen, A. Saiardi, M. Iijima, K. Ye, Y. Huang, E. Nagata, P. Devreotes and S. H. Snyder (2003). Inositol pyrophosphates mediate chemotaxis in Dictyostelium via pleckstrin homology domain-PtdIns(3,4,5)P3 interactions. Cell. **114:** 559-572.

Macbeth, M. R., H. L. Schubert, A. P. Vandemark, A. T. Lingam, C. P. Hill and B. L. Bass (2005). Inositol hexakisphosphate is bound in the ADAR2 core and required for RNA editing. Science. **309:** 1534-1539.

Manning, G., D. B. Whyte, R. Martinez, T. Hunter and S. Sudarsanam (2002). The protein kinase complement of the human genome. Science. **298:** 1912-1934.

Marchesini, N., F. A. Ruiz, M. Vieira and R. Docampo (2002). Acidocalcisomes are functionally linked to the contractile vacuole of Dictyostelium discoideum. J Biol Chem. **277:** 8146-8153.

Menniti, F. S., R. N. Miller, J. W. Putney and S. B. Shears (1993). Turnover of inositol polyphosphate pyrophosphates in pancreatoma cells. J Biol Chem. **268:** 3850-3856.

Michell, R. H. (2011). Inositol and its derivatives: their evolution and functions. Adv Enzyme Regul. **51:** 84-90.

Mitchell, J., X. Wang, G. Zhang, M. Gentzsch, D. J. Nelson and S. B. Shears (2008). An expanded biological repertoire for Ins(3,4,5,6)P4 through its modulation of ClC-3 function. Curr Biol. **18:** 1600-1605.

Moreno, S. N. J. and R. Docampo (2013). Polyphosphate and its diverse functions in host cells and pathogens. PLoS Pathog. **9:** e1003230.

Morrison, B. H., R. Haney, E. Lamarre, J. Drazba, G. D. Prestwich and D. J. Lindner (2009). Gene deletion of inositol hexakisphosphate kinase 2 predisposes to aerodigestive tract carcinoma. Oncogene. **28:** 2383-2392.

Morrissey, J. H., S. H. Choi and S. A. Smith (2012). Polyphosphate: an ancient molecule that links platelets, coagulation, and inflammation. Blood. **119:** 5972-5979.

Müller, F., N. J. Mutch, W. A. Schenk, S. A. Smith, L. Esterl, H. M. Spronk, S. Schmidbauer, W. A. Gahl, J. H. Morrissey and T. Renné (2009). Platelet polyphosphates are proinflammatory and procoagulant mediators in vivo. Cell. **139:** 1143-1156.

Mulugu, S., W. Bai, P. C. Fridy, R. J. Bastidas, J. C. Otto, D. E. Dollins, T. A. Haystead, A. A. Ribeiro and J. D. York (2007). A conserved family of enzymes that phosphorylate inositol hexakisphosphate. Science. **316:** 106-109.

Muramoto, T., D. Cannon, M. Gierlinski, A. Corrigan, G. J. Barton and J. R. Chubb (2012). Live imaging of nascent RNA dynamics reveals distinct types of transcriptional pulse regulation. Proc Natl Acad Sci USA. **109:** 7350-7355.

Nagata, E., H. R. Luo, A. Saiardi, B.-I. Bae, N. Suzuki and S. H. Snyder (2005). Inositol hexakisphosphate kinase-2, a physiologic mediator of cell death. J Biol Chem. **280:** 1634-1640.

Nichols, J. M., D. Veltman and R. R. Kay (2015). Chemotaxis of a model organism: progress with Dictyostelium. Current opinion in cell biology. **36:** 7-12.

Norbis, F., M. Boll, G. Stange, D. Markovich, F. Verrey, J. Biber and H. Murer (1997). Identification of a cDNA/protein leading to an increased Pi-uptake in Xenopus laevis oocytes. J Membr Biol. **156:** 19-24.

O'Neill, E. M., A. Kaffman, E. R. Jolly and E. K. O'Shea (1996). Regulation of PHO4 nuclear localization by the PHO80-PHO85 cyclin-CDK complex. Science. **271:** 209-212.

Ohashi, K., S. Kawai and K. Murata (2012). Identification and characterization of a human mitochondrial NAD kinase. Nat Commun. **3:** 1248.

Onnebo, S. M. N. and A. Saiardi (2009). Inositol pyrophosphates modulate hydrogen peroxide signalling. Biochem J. **423:** 109-118.

Pilu, R., D. Panzeri, G. Gavazzi, S. K. Rasmussen, G. Consonni and E. Nielsen (2003). Phenotypic, genetic and molecular characterization of a maize low phytic acid mutant (lpa241). Theor Appl Genet. **107:** 980-987.

Pisani, F., T. Livermore, G. Rose, J. R. Chubb, M. Gaspari and A. Saiardi (2014). Analysis of Dictyostelium discoideum inositol pyrophosphate metabolism by gel electrophoresis. PLoS ONE. **9:** e85533.

Pollard, T. D. and G. G. Borisy (2003). Cellular motility driven by assembly and disassembly of actin filaments. Cell. **112:** 453-465.

Posternak, S. (1921). Sur la synthèse de l'acide inosito ‑ hexaphosphorique. Helvetica Chimica Acta.

Raboy, V. (2007). The ABCs of low-phytate crops. Nat Biotechnol. **25:** 874-875.

Rashid, M. H., K. Rumbaugh, L. Passador, D. G. Davies, A. N. Hamood, B. H. Iglewski and A. Kornberg (2000). Polyphosphate kinase is essential for biofilm development, quorum sensing, and virulence of Pseudomonas aeruginosa. Proc Natl Acad Sci USA. **97:** 9636-9641.

Resnick, A. C., A. M. Snowman, B. N. Kang, K. J. Hurt, S. H. Snyder and A. Saiardi (2005). Inositol polyphosphate multikinase is a nuclear PI3-kinase with transcriptional regulatory activity. Proc Natl Acad Sci USA. **102:** 12783-12788.

Reyland, M. E. (2009). Protein kinase C isoforms: Multi-functional regulators of cell life and death. Front Biosci (Landmark Ed). **14:** 2386-2399.

Rohatgi, R., H. Y. Ho and M. W. Kirschner (2000). Mechanism of N-WASP activation by CDC42 and phosphatidylinositol 4, 5-bisphosphate. J Cell Biol. **150:** 1299-1310.

Ruiz, F. A., C. R. Lea, E. Oldfield and R. Docampo (2004). Human platelet dense granules contain polyphosphate and are similar to acidocalcisomes of bacteria and unicellular eukaryotes. J Biol Chem. **279:** 44250-44257.

Saiardi, A. (2012). How inositol pyrophosphates control cellular phosphate homeostasis? Adv Biol Regul. **52:** 351-359.

Saiardi, A., R. Bhandari, A. C. Resnick, A. M. Snowman and S. H. Snyder (2004). Phosphorylation of proteins by inositol pyrophosphates. Science. **306:** 2101-2105.

Saiardi, A., J. J. Caffrey, S. H. Snyder and S. B. Shears (2000). The inositol hexakisphosphate kinase family. Catalytic flexibility and function in yeast vacuole biogenesis. J Biol Chem. **275:** 24686-24692.

Saiardi, A., H. Erdjument-Bromage, A. M. Snowman, P. Tempst and S. H. Snyder (1999). Synthesis of diphosphoinositol pentakisphosphate by a newly identified family of higher inositol polyphosphate kinases. Curr Biol. **9:** 1323-1326.

Saiardi, A., E. Nagata, H. R. Luo, A. Sawa, X. Luo, A. M. Snowman and S. H. Snyder (2001). Mammalian inositol polyphosphate multikinase synthesizes inositol 1,4,5-trisphosphate and an inositol pyrophosphate. Proc Natl Acad Sci USA. **98:** 2306-2311.

Saiardi, A., E. Nagata, H. R. Luo, A. M. Snowman and S. H. Snyder (2001). Identification and characterization of a novel inositol hexakisphosphate kinase. J Biol Chem. **276:** 39179-39185.

Saiardi, A., A. C. Resnick, A. M. Snowman, B. Wendland and S. H. Snyder (2005). Inositol pyrophosphates regulate cell death and telomere length through phosphoinositide 3-kinase-related protein kinases. Proc Natl Acad Sci USA. **102:** 1911-1914.

Saiardi, A., C. Sciambi, J. M. McCaffery, B. Wendland and S. H. Snyder (2002). Inositol pyrophosphates regulate endocytic trafficking. Proc Natl Acad Sci USA. **99:** 14206-14211.

Sarbassov, D. D., D. A. Guertin, S. M. Ali and D. M. Sabatini (2005). Phosphorylation and regulation of Akt/PKB by the rictor-mTOR complex. Science. **307:** 1098-1101.

Schell, M. J., A. J. Letcher, C. A. Brearley, J. Biber, H. Murer and R. F. Irvine (1999). PiUS (Pi uptake stimulator) is an inositol hexakisphosphate kinase. FEBS letters. **461:** 169-172.

Seeds, A. M., R. J. Bastidas and J. D. York (2005). Molecular definition of a novel inositol polyphosphate metabolic pathway initiated by inositol 1,4,5-trisphosphate 3-kinase activity in Saccharomyces cerevisiae. J Biol Chem. **280:** 27654-27661.

Seeds, A. M., J. C. Sandquist, E. P. Spana and J. D. York (2004). A molecular basis for inositol polyphosphate synthesis in Drosophila melanogaster. J Biol Chem. **279:** 47222-47232.

Seidlmayer, L. K., L. A. Blatter, E. Pavlov and E. N. Dedkova (2012). Inorganic polyphosphate--an unusual suspect of the mitochondrial permeability transition mystery. Channels (Austin). **6:** 463-467.

Shah, Z. H., D. R. Jones, L. Sommer, R. Foulger, Y. Bultsma, C. D'Santos and N. Divecha (2013). Nuclear phosphoinositides and their impact on nuclear functions. FEBS J. **280:** 6295-6310.

Shears, S. B. (2001). Assessing the omnipotence of inositol hexakisphosphate. Cell Signal. **13:** 151-158.

Shears, S. B. (2009). Diphosphoinositol polyphosphates: metabolic messengers? Mol Pharmacol. **76:** 236-252.

Shears, S. B. (2009). Molecular basis for the integration of inositol phosphate signaling pathways via human ITPK1. Adv Enzyme Regul. **49:** 87-96.

Shears, S. B., S. B. Ganapathi, N. A. Gokhale, T. M. H. Schenk, H. Wang, J. D. Weaver, A. Zaremba and Y. Zhou (2012). Defining signal transduction by inositol phosphates. Phosphoinositides II: The Diverse Biological Functions.

Shi, X. and A. Kornberg (2005). Endopolyphosphatase in Saccharomyces cerevisiae undergoes post-translational activations to produce short-chain polyphosphates. FEBS Lett. **579:** 2014-2018.

Skorko, R. (1989). Polyphosphate as a source of phosphoryl group in protein modification in the archaebacterium Sulfolobus acidocaldarius. Biochimie. **71:** 1089-1093.

Stephens, L., T. Radenberg, U. Thiel, G. Vogel, K. H. Khoo, A. Dell, T. R. Jackson, P. T. Hawkins and G. W. Mayr (1993). The detection, purification, structural characterization, and metabolism of diphosphoinositol pentakisphosphate(s) and bisdiphosphoinositol tetrakisphosphate(s). J Biol Chem. **268:** 4009-4015.

Stephens, L. R. and R. F. Irvine (1990). Stepwise phosphorylation of myo-inositol leading to myo-inositol hexakisphosphate in Dictyostelium. Nature. **346:** 580-583.

Stokoe, D., L. R. Stephens, T. Copeland, P. R. Gaffney, C. B. Reese, G. F. Painter, A. B. Holmes, F. McCormick and P. T. Hawkins (1997). Dual role of phosphatidylinositol-3,4,5-trisphosphate in the activation of protein kinase B. Science. **277:** 567-570.

Streb, H., R. F. Irvine, M. J. Berridge and I. Schulz (1983). Release of Ca2+ from a nonmitochondrial intracellular store in pancreatic acinar cells by inositol-1,4,5-trisphosphate. Nature. **306:** 67-69.

Suh, B.-C. and B. Hille (2005). Regulation of ion channels by phosphatidylinositol 4,5-bisphosphate. Curr Opin Neurobiol. **15:** 370-378.

Szijgyarto, Z., A. Garedew, C. Azevedo and A. Saiardi (2011). Influence of inositol pyrophosphates on cellular energy dynamics. Science. **334:** 802-805.

Trilisenko, L. V., N. A. Andreeva, T. V. Kulakovskaya, V. M. Vagabov and I. S. Kulaev (2003). Effect of inhibitors on polyphosphate metabolism in the yeast

Saccharomyces cerevisiae under hypercompensation conditions. Biochemistry Mosc. **68:** 577-581.

Van Dijken, P. and P. J. Van Haastert (2001). Phospholipase Cdelta regulates germination of Dictyostelium spores. BMC Cell Biol. **2:** 25.

Vanhaesebroeck, B., L. Stephens and P. Hawkins (2012). PI3K signalling: the path to discovery and understanding. Nat Rev Mol Cell Biol. **13:** 195-203.

Voglmaier, S. M., M. E. Bembenek, A. I. Kaplin, G. Dormán, J. D. Olszewski, G. D. Prestwich and S. H. Snyder (1996). Purified inositol hexakisphosphate kinase is an ATP synthase: diphosphoinositol pentakisphosphate as a high-energy phosphate donor. Proc Natl Acad Sci USA. **93:** 4305-4310.

Wang, H., E. F. DeRose, R. E. London and S. B. Shears (2014). IP6K structure and the molecular determinants of catalytic specificity in an inositol phosphate kinase family. Nat Commun. **5:** 4178.

Wang, H., J. R. Falck, T. M. T. Hall and S. B. Shears (2012). Structural basis for an inositol pyrophosphate kinase surmounting phosphate crowding. Nat Chem Biol. **8:** 111-116.

Wang, H., V. S. Nair, A. A. Holland, S. Capolicchio, H. J. Jessen, M. K. Johnson and S. B. Shears (2015). Asp1 from Schizosaccharomyces pombe Binds a [2Fe-2S](2+) Cluster Which Inhibits Inositol Pyrophosphate 1-Phosphatase Activity. Biochemistry. **54:** 6462-6474.

Watson, P. J., L. Fairall, G. M. Santos and J. W. R. Schwabe (2012). Structure of HDAC3 bound to co-repressor and inositol tetraphosphate. Nature. **481:** 335-340.

Weber, S., C. U. Stirnimann, M. Wieser, D. Frey, R. Meier, S. Engelhardt, X. Li, G. Capitani, R. A. Kammerer and H. Hilbi (2014). A type IV translocated Legionella cysteine phytase counteracts intracellular growth restriction by phytate. J Biol Chem. **289:** 34175-34188.

Williams, J. G. (2006). Transcriptional regulation of Dictyostelium pattern formation. EMBO Rep. **7:** 694-698.

Williams, J. G. (2010). Dictyostelium finds new roles to model. Genetics. **185:** 717-726.

Wilson, M. S. C., S. J. Bulley, F. Pisani, R. F. Irvine and A. Saiardi (2015). A novel method for the purification of inositol phosphates from biological samples reveals that no phytate is present in human plasma or urine. Open Biol. **5:** 150014.

Wilson, M. S. C., T. M. Livermore and A. Saiardi (2013). Inositol pyrophosphates: between signalling and metabolism. Biochem J. **452:** 369-379.

Worley, J., X. Luo and A. P. Capaldi (2013). Inositol pyrophosphates regulate cell growth and the environmental stress response by activating the HDAC Rpd3L. Cell Rep. **3:** 1476-1482.

Wundenberg, T. and G. W. Mayr (2012). Synthesis and biological actions of diphosphoinositol phosphates (inositol pyrophosphates), regulators of cell homeostasis. Biol Chem. **393:** 979-998.

Wurst, H. and A. Kornberg (1994). A soluble exopolyphosphatase of Saccharomyces cerevisiae. Purification and characterization. J Biol Chem. **269:** 10996-11001.

Yoko-o, T., Y. Matsui, H. Yagisawa, H. Nojima, I. Uno and A. Toh-e (1993). The putative phosphoinositide-specific phospholipase C gene, PLC1, of the yeast Saccharomyces cerevisiae is important for cell growth. Proc Natl Acad Sci USA. **90:** 1804-1808.

York, J. D., A. R. Odom, R. Murphy, E. B. Ives and S. R. Wente (1999). A phospholipase C-dependent inositol polyphosphate kinase pathway required for efficient messenger RNA export. Science. **285:** 96-100.

York, S. J., B. N. Armbruster, P. Greenwell, T. D. Petes and J. D. York (2005). Inositol diphosphate signaling regulates telomere length. J Biol Chem. **280:** 4264-4269.

Zhang, C., P. W. Majerus and M. P. Wilson (2012). Regulation of inositol 1,3,4-trisphosphate 5/6-kinase (ITPK1) by reversible lysine acetylation. Proc Natl Acad Sci USA. **109:** 2290-2295.

Zhang, H., M. R. Gómez-García, M. R. W. Brown and A. Kornberg (2005). Inorganic polyphosphate in Dictyostelium discoideum: influence on development, sporulation, and predation. Proc Natl Acad Sci USA. **102:** 2731-2735.

Zhang, H., M. R. Gómez-García, X. Shi, N. N. Rao and A. Kornberg (2007). Polyphosphate kinase 1, a conserved bacterial enzyme, in a eukaryote, Dictyostelium discoideum, with a role in cytokinesis. Proc Natl Acad Sci USA. **104:** 16486-16491.

Zhang, H., K. Ishige and A. Kornberg (2002). A polyphosphate kinase (PPK2) widely conserved in bacteria. Proc Natl Acad Sci USA. **99:** 16678-16683.

Zhu, Y., W. Huang, S. S. K. Lee and W. Xu (2005). Crystal structure of a polyphosphate kinase and its implications for polyphosphate synthesis. EMBO Rep. **6:** 681-687.